THE
PHYSICAL REVIEW

A journal of experimental and theoretical physics established by E. L. Nichols in 1893

SECOND SERIES, VOL. 72, No. 7 OCTOBER 1, 1947

Studies of the Delayed Neutrons[+]

I. The Decay Curve and the Intensity of the Delayed Neutrons

ARTHUR H. SNELL,* V. A. NEDZEL,** H. W. IBSER,† J. S. LEVINGER,†† R. G. WILKINSON,*** AND M. B. SAMPSON***
Metallurgical Laboratory, University of Chicago, Chicago, Illinois

(Received May 26, 1947)

The delayed neutrons resulting from slow neutron fission of uranium have been found to decay as a combination of exponentials with half-lives of 0.4, 1.8, 4.4, 23, and 56 seconds and respective initial relative intensities when activated to saturation of 0.4, 0.5, 1.1, 1.0, and 0.14. Under equilibrium conditions the delayed neutrons are 1.0±0.2 percent as abundant as the instantaneous fission neutrons.

MORE than a year before the first nuclear chain reaction was initiated on December 2, 1942, the importance of the delayed neutrons in controlling the reaction was foreseen. In a letter to S. K. Allison, E. Fermi pointed out the necessity of knowing how many of the fission neutrons were delayed, and suggested how this could be measured experimentally. The work was undertaken, using the University of Chicago cyclotron, and it culminated in a Metallurgical Laboratory report by Snell, Nedzel, and Ibser, the results of which have since been quoted in the Smyth report.[1] As a part of the intensity measurement, a study of the decay curve for the delayed neutrons was required. While this was accomplished in a manner adequate at the time, subsequent work in the same laboratory showed that the analysis of the short periods had been incomplete. It is the purpose of this paper to state the revised analysis of the delayed neutron decay curve, and to describe the intensity measurement more fully than was done by Smyth.

THE DECAY OF THE DELAYED NEUTRONS

The earlier work on this subject was that of Roberts, Mayer, Hafstad, and Wang[2] (decay period 12.5±3 sec.), of Booth, Dunning, and Slack[3] (10–15 seconds and 45 seconds), of Gibbs and Thomson[4] (no strong delayed neutron periods between 0.001 and 0.1 sec.), and of Brostrøm, Koch, and Lauritsen[5] (12.3 and 0.1–

[+] This document is based on work performed under Contract No. W-35-058-eng-71 for the Manhattan Project and the information covered therein will appear in Division IV of the Manhattan Project Technical Series as part of the contribution of the Clinton Laboratories.

* Now at Clinton Laboratories, Oak Ridge, Tennessee.
** Now at Los Alamos Laboratory, P. O. Box 1661, Santa Fe, New Mexico.
† Now at University of Wisconsin, Madison, Wisconsin.
†† Now at Physics Department, Cornell University, Ithaca, New York.
*** Now at Physics Department, Indiana University, Bloomington, Indiana.

[1] H. D. Smyth, *Atomic Energy for Military Purposes* (Princeton University Press, Princeton, New Jersey, 1945), Appendix III.

[2] R. B. Roberts, R. C. Meyer, and P. Wang, Phys. Rev. **55**, 510 (1939); R. B. Roberts, R. C. Meyer, L. R. Hafstad, and P. Wang, *ibid.* **55**, 664 (1939).

[3] E. T. Booth, J. R. Dunning, and F. G. Slack, Phys. Rev. **55**, 876 (1939).

[4] D. F. Gibbs and G. P. Thomson, Nature **144**, 202 (1939).

[5] K. J. Brostrøm, J. Koch, and T. Lauritsen, Nature **144**, 830 (1939).

0.3-second activities). Snell, Nedzel, and Ibser used 106 lb of U_3O_8 arranged in a hollow shell which was surrounded with paraffin and placed about a foot from the beryllium target of the cyclotron (see Fig. 1). A boron trifluoride proportional counter was placed inside the shell, and a thickness of $2\frac{1}{2}$ inches of paraffin filled the space between the counter and the U_3O_8. The maximum cyclotron beam on the target was 20 μA of 7.5-Mev deuterons. Readings were taken by photographing simultaneously the mechanical recorder actuated by the scaler, the scaler interpolation lights, a stopwatch which read to 1/100 second, and an electrical timer. The clearest result was the appearance of two well-defined activities with half-lives of 24 sec. and 57 sec., respectively. In relative saturation intensity, the 24-sec. activity was about eight times as strong as the 57-sec. activity. The earlier part of the decay curve could be accounted for by activities with half-lives of 7 sec. and 2.5 sec., but the analysis was not definite enough to enable one to have confidence in these as real activities.

In later work upon the shorter periods, activations of about 1 second were given, and the readings were taken without automatic recording. Instead, one man would call time intervals, while another would read the counts and a third would record them. With a little practice this method of operation seemed to work well. It had the advantage that the data could be taken and analyzed more rapidly than was possible with photographic film. By standardizing irradiation and counting times, repeated runs could be made which could be averaged simply. The main result of this work was the emergence of a fairly intense, well-defined activity with a half-life of 4.5 seconds. The shorter activity seemed to have a half-life of about 1.5 seconds, and the values of the half-lives of the previously discovered

TABLE I. Summary of results for the delayed neutron activities in fission of U^{235}.

Half-life	Relative saturation intensity
0.4 sec.	0.4
1.8 sec.	0.5
4.4 sec.	1.1
23 sec.	1.0
56 sec.	0.14

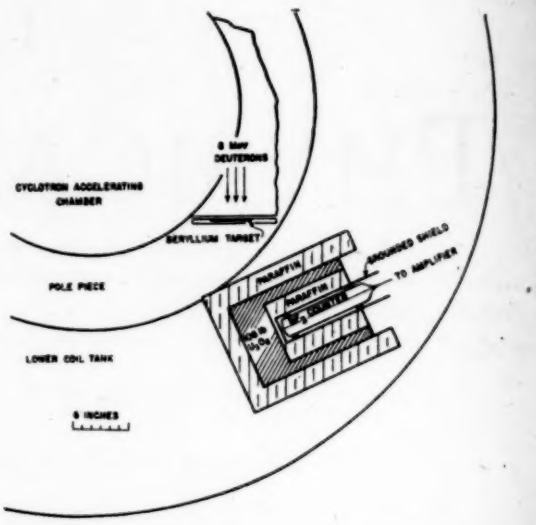

FIG. 1. Experimental arrangement used in initial measurement of delayed neutron decay by Snell, Nedzel, and Ibser.

longer periods were modified to 23 seconds and 56 seconds, respectively.

In a third phase of the experimentation, rapidly circulating uranyl nitrate solution was used. The stream passed from a reservoir through a two-stage turbine pump driven above its rated speed by a 5-hp motor, through an irradiation cell near the target of the cyclotron, and thence past two BF_3 counters in series and into a sump tank. The counters were surrounded with paraffin and massively shielded against direct cyclotron neutrons. The flow time between the two counters could be varied by altering the volume of tubing between them, or by by-passing some of the solution around the second counter. The first counter was a monitor; to a first approximation the flow time to it from the irradiation cell was constant. With this apparatus, timing was reduced to measurements of volume and rates of flow. Irradiation lasted 0.19 sec. and the first point on the decay curve was at a time 0.32 sec. after the liquid left the irradiation cell. At this and subsequent chosen points one could take as many counts as one desired. The results confirmed the presence of the 4.5-sec. period but gave the half-life the value 4.4 sec.; they indicated also an activity with a half-life of 1.8 sec. The first two points on the decay curve showed that a shorter period was also present; it could not be evaluated accurately, but had a half-life

of about 0.4 sec. and a moderate saturation intensity.

A summary of all of this work gives the results, shown in Table I, for the delayed neutron activities for fission of uranium 235.

No activities of longer half-life were observed. In looking for them, activations up to 30-minutes duration were given, and the decay of the delayed neutrons was followed for 15 minutes before their activity became indistinguishable from background.

It should be observed that the relative intensities of the various activities as given above may be slightly in error inasmuch as the energy dependence of their distribution in the paraffin surrounding the counters was not taken into account. The fact that the different activities have different energies has been established.[6,7] Hughes, Dabbs, and Cahn[6] have since resurveyed the delayed neutron activities, taking the energy dependence into account.

THE INTENSITY EXPERIMENT

The experimental arrangement is indicated in Fig. 2 and may be described as follows: Near the target of the cyclotron a movable graphite column was built, 26 in. × 30 in. in cross section, and 96 in. long. This column was supported in an aperture built into one of the water tanks with which the cyclotron was surrounded. It rode on roller chains so that for use it could be rolled toward the target, between the magnet coils of the cyclotron, until one end was a few inches from the target. Farther back it was completely surrounded by water or other effective shielding from fast neutrons. Five feet from the target end of this column a diaphragm of U_3O_8 was placed; it filled the whole cross section of the column, was 3 in. thick, and consisted of a sheet-iron box containing 291 lb of U_3O_8. Along the axis of the column, on the side of the diaphragm away from the target, a large BF_3 counter was placed. It was completely shielded with cadmium 0.020 in. thick.

The principle of the experiment is now apparent. When the cyclotron was on, the neutrons from the target which penetrated the 5 ft. of graphite to reach the U_3O_8 and the counter would be almost all of thermal energies. They, therefore, would cause fissions in the U_3O_8, but for the most part would not penetrate the cadmium surrounding the counter. On the other hand, many of the neutrons originating in the U_3O_8 would still have enough energy when reaching the counter nearby to escape capture in the cadmium and be counted. The experiment would, therefore, be to count the "instantaneous" fission neutrons emitted from the U_3O_8 diaphragm with the cyclotron on, then turn off the cyclotron and immediately count the delayed neutrons.

The delayed neutrons were so weak that only a few were registered even after counting instantaneous neutrons at the maximum trustworthy rate permitted by the apparatus. Since the shape of the decay curve was known with moderate precision, it was expedient to measure the intensity of the delayed neutrons by taking the integral number arriving during a certain time interval after turning off the cyclotron, rather than to attempt rate-of-counting measurements.

The start of counting was accomplished through a relay in the input of the scaler which closed when the radiofrequency power contactor of the cyclotron opened. This insured a uniform, short time interval between the stop of bombardment and the start of counting. The length of this time interval was estimated to be about a fiftieth of a second. A switch was provided which removed the relay from the circuit, thereby

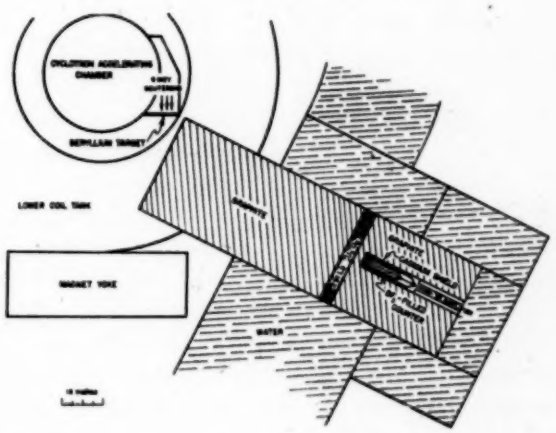

FIG. 2. Diagram of the apparatus used to measure the intensity of the delayed neutrons relative to that of the instantaneous fission neutrons.

[6] D. J. Hughes, J. Dabbs, and A. Cahn, CP-3094.
[7] M. Burgy, L. A. Pardue, H. B. Willard, and E. O. Wollan, MDDC 16, and Phys. Rev. **70**, 104 (1946).

making it possible to count when the cyclotron was on. One operator concentrated upon keeping the cyclotron beam steady, and after three minutes of bombardment the other operator went through the following procedure:

(a) Counted for one minute with the cyclotron on and noted the reading.

(b) Switched the relay into the circuit and reset the scaler to zero.

(c) Turned off the cyclotron (thereby automatically starting counting) and started a stopwatch.

(d) Counted for 2.0 minutes and noted the number of delayed counts.

The bombardment and counting were then repeated. The beam was kept at about 16 μA, which gave a counting rate with the cyclotron on of 15,000 to 20,000 counts per minute. A day's work yielded nineteen satisfactory runs, the main trouble being variability of the cyclotron beam. The delayed neutron counts of these nineteen runs were corrected for background, normalized to a counting rate with the cyclotron on of 10,000 per minute, and then averaged. The mean result was that if, during bombardment, neutrons were counting at a rate of 10,000 per minute, then in the interval 0.02 sec. to 2.0 min. after removing the source of primary neutrons, 22.4 ± 3.2 delayed neutrons were counted, where the 3.2 was the probable error of the mean of the nineteen observations. Now the result of the analysis of the decay curves can be expressed as

$$I(t)=C(0.4e^{-1.6t}+0.5e^{-0.38t}+1.1e^{-0.16t}+1.0e^{-0.031t}+0.14e^{-0.012t}), \quad (1)$$

so that at zero time $I(0)=3.14C$. The integral count of 22.4 from $t=0.02$ to $t=120$ seconds gives from (1) the value $C=0.46$. Thus $I(0)$ is 1.44 counts per second or 0.86 percent of the counting rate with the cyclotron on.

This result must be modified by two corrections. The more important of these is an upward correction in the delayed neutron intensity, arising from a blank experiment (i.e., with the U_3O_8 removed) in which it was found 365 counts per min. per μA were obtained under the same conditions as gave 1180 counts per min. per μA with the U_3O_8 present. The resulting factor 1.40 is clearly a considerable over-correction because it neglects the effect of the absorption of the cyclotron neutrons in the thick layer of U_3O_8. The other correction arises from missed counts, because of the high counting rates needed to give a reasonable number of delayed counts. It is a downward correction in the relative intensity of the delayed neutrons. The net effect of the two corrections may be estimated at an increase of about 15 percent, leading to the result that in a body of uranium emitting fission neutrons, at equilibrium (1.0 ± 0.2) percent of the neutrons are delayed by more than 0.02 second and have half-lives of 0.4 sec. or more. The error indicated here is a guess at the maximum uncertainty arising from the probable error of the counts and the vagueness in the corrections applied. No correction was attempted for a difference in the spatial distribution of the slowed-down fission and delayed neutrons arising from their possibly different initial energies, because of lack of knowledge of the energy spectra. The longitudinal arrangement of the counter would tend to reduce such a correction.

Studies of the Delayed Neutrons

II. Chemical Isolation of the 56-Second and the 23-Second Activities*

ARTHUR H. SNELL,** J. S. LEVINGER,*** E. P. MEINERS, JR.,† M. B. SAMPSON,†† AND R. G. WILKINSON††
Metallurgical Laboratory, University of Chicago, Chicago, Illinois

(Received May 26, 1947)

The 23-second delayed neutron activity is found to follow the chemistry of iodine, and the 56-second delayed neutron activity is found to follow the chemistry of bromine. Comparison with known beta-emitters of like half-lives suggests that the neutron-emitting nuclei may be Xe^{137} and Kr^{87}.

IN the preceding paper, resolution of the decay curve of the delayed neutrons resulting from the fission of uranium is described. Activities with half-lives of 0.4, 1.8, 4.4, 23, and 56 seconds were found. The fact that discrete decay periods are present is good evidence in favor of the interpretation put forward by Bohr and Wheeler[1] of the existence of delayed neutrons, namely, that they originate in the fission products and are emitted when the beta-decay of a fragment leaves the nucleus in a state of excitation higher than the binding energy of a neutron in that nucleus. The neutron is then immediately emitted, and the rate of decay of the neutron-emitting activity observed is just that of the preceding beta-activity. In this paper we shall describe successful chemical isolation of the 56-second and the 23-second activities in the fission products.

EXPERIMENTAL PROCEDURE AND RESULTS

Most of the irradiations were made with the University of Chicago cyclotron, using 7.3-Mev deuterons on beryllium as a neutron source. Beam currents ranged up to 100 micro amperes, giving in the paraffin-surrounded sample a slow neutron flux of about 10^9 neutrons per cm^2 per sec. The samples were usually a few hundred milliliters of aqueous solution of uranyl nitrate. The counting was done with a boron trifluoride proportional counter having a total boron cross section of about 2 cm^2, surrounded with several inches of paraffin. The counting was done by three workers; one called the time, the second read the scaler, and the third recorded the readings. During the early part of the decay the accumulating count was recorded every five seconds, but as the activity became weaker this interval was lengthened to 10 seconds and finally to 30 seconds.

The problem on first approach looked like a difficult one, namely, to identify, within the time limit for chemistry of about one minute, one or two of the thirty-odd fission product elements. With the idea of at least narrowing down the possibilities, we made a number of experiments which led to negative results. It seems nevertheless worth while to mention them briefly, because some of them rule out possibilities for the still unidentified shorter activities, and others give evidence against the odd chance of the presence in the elements concerned of activities with about the same decay periods as those which we have been able to extract.

(1) Sulphate precipitation: We irradiated 250-cc aqueous solution containing 40-g uranyl nitrate, fission product carrier, and barium nitrate. After irradiation we added sulphuric acid and filtered and examined the precipitate. Only a very weak neutron-emitting activity was found in the precipitate 30 seconds after the stop of the activation.

(2) Water extraction for ether solution: We irradiated 80 g of uranyl nitrate, dissolved in

* This document is based on work performed under Contract No. W-35-058-eng-71 for the Manhattan Project, and the information covered therein will appear in Division IV of the Manhattan Project Technical Series as part of the contribution of the Clinton Laboratories.

** Now at Clinton Laboratories, Oak Ridge, Tennessee.
*** Now at Physics Department, Cornell University, Ithaca, New York.
† Now at Physics Department, Washington University, St. Louis, Missouri.
†† Now at Physics Department, Indiana University, Bloomington, Indiana.

[1] N. Bohr and J. A. Wheeler, Phys. Rev. 56, 426 (1939).

500 cc ethyl ether in a separating funnel, with 10 cc water and fission product carrier. After irradiation the liquid was shaken, allowed to settle, and the water was drained off. Most of the neutron-emitting activity remained in the ether subsequent to 40 seconds after stop of activation.

(3) Barium: A barium chloride precipitate was taken from the water layer following an ether extraction. Only very weak activity was found in the precipitate 60 seconds after stop of activation. In other experiments aqueous solutions were activated, and barium chloride precipitates were taken out after irradiation. The precipitates had no neutron-emitting activity 40 seconds after the stop of activation.

(4) Rare gases: (a) A flask containing an aqueous solution of uranyl nitrate was boiled under reduced pressure while under irradiation. An air stream was led through the flask to a NaOH trap, and thence to a charcoal trap. A weak neutron-emitting activity built up in the NaOH trap, but none in the charcoal, although the latter became beta-active. (b) 1400 cc of uranyl nitrate solution containing 100 grams of the nitrate were irradiated, and after irradiation allowed to pour through a pipe into another vessel in which the boron trifluoride counter was set. A decay curve was taken. Then the experiment was repeated except that the solution was kept boiling during activation. The boiling should have greatly weakened any rare gas activities, but the decay curves were of the same shape and the activities were of about the same intensity subsequent to 10 seconds after stop of activation.

Experiments which gave positive results started after we tried a silver halide precipitation and found that both the 23-second and the 56-second activities came down very strongly. Since silver selenite and presumably tellurite also would have precipitated from the solution, we made separations from solutions which had been made strongly acid with HNO_3 under conditions such that (as we verified by trial) silver selenite would not precipitate. The 23-second and 56-second activities still came down with the silver halide. This evidence that these activities were distributed between bromine and iodine seemed not to be in disagreement with the results of experiments described in the preceding paragraphs.

THE IODINE ACTIVITY

About 150 cc of an aqueous solution of uranyl nitrate were irradiated for two minutes in a separating funnel. A few milligrams of KI and KBr were present to act as carrier, and a few cc of carbon tetrachloride were present. The concentration of the uranyl nitrate solution was held down so that the carbon tetrachloride would settle promptly after the funnel had been shaken. One cc of concentrated HCl was present in the solution, and after irradiation 10 cc of 5 percent sodium nitrite solution were added. Following shaking and settling, the carbon tetrachloride layer (colored violet by the iodine) was drawn off and counted. The result was a single exponential decay with a half-life of 24 seconds, covering the time interval 30 seconds to 200 seconds after stop of irradiation. Later we found that the sodium nitrite could just as well be present during the activation, and that repeated extractions could be made from one batch of solution. One added new carrier and new carbon tetrachloride before each activation, and did not shake until after the activation. By standardizing the procedure so that counts were always recorded at the same time after the stop of activation, we ran through eight extractions and by averaging the resulting readings we obtained the curve reproduced in Fig. 1 and labeled "Iodine." It will be noticed that the first point comes at 28 seconds after the stop of activation, that the curve is a simple exponential over an intensity factor of about 100, and that the half-life is 23.8 ± 0.7 seconds. The limits of error for this figure are those allowed by the scatter of the points.

THE BROMINE ACTIVITY

Since the 23-second delayed neutron activity appeared to follow the chemistry of iodine, it seemed very probable that the 56-second activity would follow that of bromine. A positive experiment required a specific separation for bromine in an attempt to get the longer-lived delayed neutron emitter clear of the others. This was accomplished at the Clinton Laboratories, and the experiment was as follows:

About 1 cc of uranyl nitrate solution was irradiated for two minutes in the Clinton pile. The transfer in and out of the pile was accomplished with the pneumatic tube arrangement. After irradiation the sample was allowed to stand for 16 seconds to permit decay to a moderately safe level of a strong 8-second nitrogen 16 activity which was induced in the Lucite container of the solution. Then the uranyl nitrate was poured into a separating funnel containing 30 ml of 8N nitric acid which was saturated with potassium chlorate. Br- and I-carriers were added and Br_2 and I_2 extracted with carbon tetrachloride. The carbon tetrachloride was run into a second separating funnel which contained a potassium nitrite solution made slightly acid with nitric acid. Here the bromine was reduced to bromide; the iodine at the same time was kept oxidized. The carbon tetrachloride was drained off and the water layer counted. As in the case of iodine, we standardized times and procedures so that five good runs could be averaged. The resulting decay curve is given in Fig. 1, labeled "bromine." For comparison, we took readings on samples of uranium nitrate irradiated for 2 min. but followed by no chemical extractions. These gave the curve labeled "unseparated." The presence in the bromine of a small amount of shorter activity, as indicated by the earliest two points on the bromine curve, is explicable on the basis of imperfect chemical separation in the somewhat hasty manipulations involved. The isolated bromine activity seems to have a half-life of 54 ± 1 seconds, where again the limits of error are those permitted by the scatter of the points.

To compare the decay of the separated bromine with that of an unseparated sample in which other activities have fully decayed, we activated several grams of uranyl nitrate, waiting six minutes before starting the count. The resulting curve is labeled "larger sample, unseparated" in the figure. Between 6 and 12 minutes after stop of irradiation the slope corresponds to a half-life of 57 ± 1 seconds. This is a little longer than that of the extracted bromine, but the difference is probably attributable to experimental effects such as the presence of a little iodine in the bromine samples.

DISCUSSION

Probably the bromine and iodine activities account for all of the 23-second and 56-second activity observed in the total delayed neutron decay curve. We are not able to set very low experimental limits on the presence in other fission products of activities having about the same decay periods, but in one set of experiments we compared the intensities of silver halide precipitates with those of their filtrates. The filtrates were 5 to 10 times weaker, and this residual activity is attributable to the imperfection of the fast filtering and to the probable presence of some activity in the form of bromates and iodates which did not precipitate. The

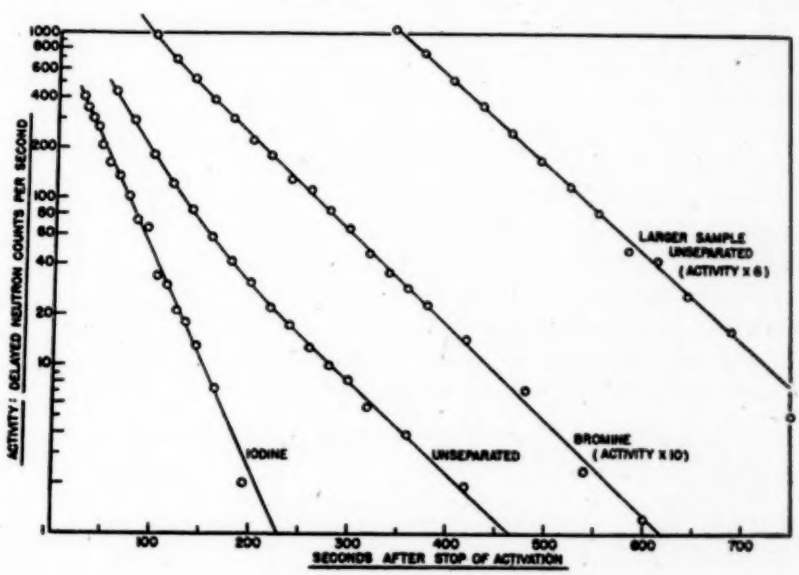

FIG. 1. Decay curves of the delayed neutrons emitted from uranium ("unseparated") and from the separated iodine and bromine fission products. The decay of the longest period in the unseparated sample is seen to be parallel to that of the bromine fraction. The relative intensities between the various curves are to be disregarded.

filtrate decay curves were rough but did not require new decay periods for their description.

It is tempting to identify these two delayed neutron activities, respectively, with the 30±6 second iodine beta-activity and the 50±10 second bromine beta-activity found by Strassmann and Hahn.[2] Seelmann-Eggebert and Born[3] subsequently found that a 3.8-minute xenon grows from the 30±6-second iodine, and a 75-minute krypton grows from the 50±10-second bromine. In other work,[4] the 75-minute krypton was identified as krypton 87, and the 3.8-minute xenon identified as probably xenon 137. If the possible existence of conflicting bromine and iodine beta-activities had been ruled out, it would seem that the mass assignments of the delayed neutron emitters would be settled. As it is, coincidences may exist whereby another isotope of bromine has a period close to that of bromine 87, or another isotope of iodine a period close to that of iodine 137. We did some work on the short-lived bromine and iodine beta- and gamma-emitters, but our results were not of direct assistance. They did indicate, however, that the 50-second bromine and the 30-second iodine are not the only short-lived halogen fission products; the situation is more complicated, both in bromine and in iodine.

A comparison of the fission product yield data with the intensity of the bromine and iodine delayed neutrons gives some information about their emission. The yields of the short-lived 87 and 137 chains have not been measured explicitly, but according to the fission product yields as determined chemically,[5] 2.5 percent of the fissions should lead to products of mass 87, and 6.2 percent should lead to products of mass 137. If there were one delayed neutron emitted for each of the mass 87 and 137 chains initiated, these figures would, of course, also give the percentages of fissions producing the 56-second and 23-second activities. Actually, one can see that such fissions are less frequent. If, on the average, 1 to 3 instantaneous neutrons are emitted per fission, there will be 0.01- to 0.03-delayed neutron

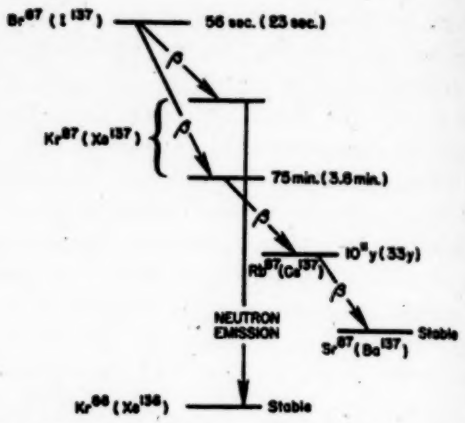

FIG. 2. Possible branching mechanism which would account for the low yield of the bromine and iodine delayed neutrons in comparison with the yields of fission products of mass 87 and 137. It is presumed that only a small proportion of the atoms choose the low energy beta-transition which is followed by neutron emission.

of all periods,[6] or 4.5×10^{-4} to 13×10^{-4} delayed neutron of the 56-second activity and 3.2×10^{-3} to 9.6×10^{-3} delayed neutron of the 23-second activity. In other words, 0.045 to 0.13 percent of the fissions actually produce the bromine activity instead of 2.5 percent, and 0.32 to 0.96 percent produce the iodine activity instead of 6.2 percent. Increasing the assigned masses does not bring closer agreement, and one must conclude that one or both of the following factors must be coming in: (1) a sharp drop in yield for the early members of the chain; (2) a branching decay process. Such a branching might be as indicated in Fig. 2, where the mass numbers 87 and 137 are provisionally written in. Here it is assumed that the decay of the bromine (iodine) leaves a few of the krypton (xenon) nuclei in one or more states which are excited highly enough to permit neutron evaporation, but that most of the decay passes through a lower state and eventually to strontium (barium) in the conventional manner.

Bohr and Wheeler give general theoretical arguments indicating how the energy of beta-transitions in some fission fragments can exceed the neutron-binding energy in the product nucleus and thus lead to delayed neutron emission. The identification of the neutron-emitting nuclei as isotopes of krypton and xenon now permits closer comparison with their theory, and one can see what the Bohr-Wheeler considera-

[2] O. Hahn and F. Strassmann, Naturwiss. **28**, 817 (1940).
[3] H. J. Born and W. Seelmann-Eggebert, Naturwiss. **31**, 59 (1943).
[4] H. J. Born and W. Seelmann-Eggebert, Naturwiss. **31**, 86 (1943). (See also V. Riezler, Naturwiss. **31**, 326 (1943)).
[5] Rev. Mod. Phys. **18**, 513 (1946), or J. Am. Chem. Soc. **68**, 2437 (1946).
[6] Snell, Nedzel, Ibser, Levinger, Wilkinson, and Lampson, Phys. Rev. **72**, 541 (1947).

tions predict with regard to the mass assignments of the activities. Table I we give the energies available for beta-transformation and the neutron-binding energies, as calculated according to the method of Bohr and Wheeler, for isotopes in the region with which we are concerned. It will be noticed that according to these figures delayed neutron emission would be energetically possible for bromine-krypton transitions of mass 88 or higher, and for the iodine-xenon transitions it would be possible for mass 140 or higher. Although the statistical theory probably cannot be forced to detail for individual isotopes, the figures illustrate the *a priori* probability that the delayed neutrons should come from nuclei heavier than 87 and 137.

Measurements have also been made in this laboratory upon the delayed neutrons from the fission of thorium.[7] For the most part the same decay periods were found, but the 56-second activity was about three times more intense relative to the 23-second activity than was the case for fission of uranium 235. This can be qualitatively understood from the fission yield curve[5] if the mass numbers 87 and 137 are approximately correct. A shift of the lower mass peak toward still lower masses would increase appreciably the relative yield at mass 87, while mass 137, being near the flattened top of the other peak, would be almost unaffected. Disregarding the possibilities of changes in yield along the chain and of changes in the branching ratio for the delayed neutron emission, the thorium results may be said to imply that the bromine activity should be ascribed to a mass number less than 90. The results of Jentschke[8] for uranium 238 and thorium fission seem to indicate that the lower mass peak is more sensitive than the higher mass peak with regard to changes in the mass of the fissioning nucleus.

TABLE I. Bohr-Wheeler beta-decay energies and neutron binding energies.

A	Beta-transition energy in bromine	Neutron-binding energy in krypton	A	Beta-transition energy in iodine	Neutron-binding energy in xenon
87	5.3 Mev	5.7 Mev	137	3.5 Mev	5.5 Mev
88	8.8	7.9	138	6.0	6.3
89	6.9	4.7	139	4.8	5.0
90	10.5	6.5	140	7.2	5.8
			141	6.0	4.6
			142	8.3	5.0

[7] J. E. Brolley, J. S. Levinger, M. B. Sampson, and R. G. Wilkinson, CP-787.
[8] W. Jentschke, Zeits. f. Physik **120**, 165 (1942).

ATTEMPTS AT RECOIL COLLECTION

An experiment which looks attractive from the point of view of obtaining unambiguous mass assignments, and also of identifying the shorter-lived emitters, is that of examining the radioactivity of the nuclei which recoil because of the emission of the delayed neutrons. These recoil nuclei might be expected, according to present knowledge, to have an energy of a few kilovolts. We attacked the problem as follows: Fission fragments, emitted from the inner surface of a uranium cylinder about 3 inches in diameter, were collected electrostatically upon the surface of a metal rod arranged axially in the cylinder. After irradiation, a paper or aluminum sleeve was slipped over (but not touching) the rod, and the cylinder was evacuated to a few millimeters pressure. The sleeve was supposed to pick up the delayed neutron recoils. Times of irradiation and times of waiting before placing the sleeve could be arranged so as to emphasize preferentially collection from any desired delayed neutron activity, and repeated collections could be made on one sleeve to build up intensity. We found that the sleeves always showed radioactivity—even when collection was started after the delayed neutrons had all decayed. This meant that activity was evaporating from the surface of the rod and blanketing the rather small effect which we sought. Variants of the experiment which we tried in attempts to reduce this effect included the application of retarding electrostatic fields, variation in pressure during the recoil collection, and cooling the rod bearing the fission fragments. Our results have been inconclusive, but the experiments might be worth pursuing under quite carefully controlled conditions. Incidental considerations in the case of the bromine and iodine activities are: (1) the recoiling rare gas atom might not stay on the sleeve, and (2), if the mass assignments of 87 and 137 are correct, the recoiling nuclei are probably stable.

We are indebted to Dr. N. Sugarman for early advice on the chemical separations, and to Dr. Katherine Way for consultations on the application of the Bohr-Wheeler theory.

Milne's Problem in Transport Theory

G. PLACZEK* AND W. SEIDEL**
*Montreal Laboratory, National Research Council of Canada,*** *Montreal, Canada*
(Received May 31, 1947)

A modified derivation of the Wiener-Hopf solution of Milne's problem is given in a form suitable for application to problems in the theory of neutron diffusion.

I. INTRODUCTION

We consider the following problem: A half-space $z>0$ bounded by the plane $z=0$ is filled by a non-capturing medium, which scatters neutrons isotropically without changing their velocity. No sources are present in the medium and no neutrons enter the plane $z=0$ from outside. A current density of magnitude j and direction $-z$ exists in the medium. We wish to determine the stationary neutron distribution in the medium and, in particular, the angular distribution of the neutrons leaving the plane $z=0$.

This problem, which represents an important standard case in the study of neutron diffusion, is completely identical with a problem known in astrophysical literature as "Milne's case." It has been extensively discussed in connection with the determination of the law of darkening at the sun's surface.[1] Its solution, explicit as far as the angular distribution of the emerging radiation is concerned, has been obtained by Wiener and Hopf.[2] Their method can also be used with advantage for the solution of other neutron diffusion problems, but their presentation is somewhat encumbered by generalizations in directions different from those of interest to us. We shall, therefore, in the following, give a somewhat modified derivation of Wiener and Hopf's results, in such a form as will most easily lend itself to generalizations to be discussed in later papers.

II. THE TRANSPORT EQUATION AND INTEGRAL RELATIONS FOLLOWING FROM IT

We denote by μ the cosine of the angle between the direction of the neutron and the positive z direction and by $\psi(z, \mu)d\mu$ the number of neutrons per unit volume at the point z with direction cosine between μ and $\mu+d\mu$. We call

$$\psi_0(z)=\int_{-1}^{1}\psi(z, \mu)d\mu$$

the neutron density.

Choosing as unit of length the mean free path and as unit of velocity the neutron velocity, we have the transport equation

$$\mu(\partial\psi/\partial z)+\psi=\tfrac{1}{2}\psi_0, \tag{1}$$

with the boundary condition

$$\psi(0, \mu)=0 \quad \text{for} \quad \mu>0, \tag{2}$$

since no neutrons enter the medium from outside.

Two important relations can be obtained at once from (1) and (2). Integrating (1) over the variable μ we obtain, with the notation

$$j=-\int_{-1}^{1}\mu\psi(z, \mu)d\mu, \tag{3}$$

$$\partial j/\partial z=0. \tag{4}$$

Equation (4) shows that the current density j is constant. We shall put

$$j=1 \tag{5}$$

and thus have $\psi(z, \mu)$ normalized for unit current density.

We now multiply (1) by μ and integrate over

* Now at General Electric Research Laboratory, Schenectady, New York.
** Department of Mathematics, University of Rochester, Rochester, New York.
*** Report issued June 24, 1943.
[1] For literature, see E. Milne, *Handbuch der Astrophysik*, Vol. 3, p. 1 and E. Hopf, "Mathematical problems of radiative equilibrium," *Cambridge Tracts No. 31* (1934).
[2] N. Wiener and E. Hopf, Berliner Ber. Math. Phys. Klasse 696 (1931); see also E. Hopf, *Cambridge Tracts No. 31*, (1934); R. E. A. C. Paley and N. Wiener, *Fourier Transforms in the Complex Domain* (American Mathematical Society Collection, New York, 1934), Vol. XIX, Chap. IV; E. C. Titchmarsh, *Introduction to the Theory of Fourier Integrals* (Oxford University Press, New York, 1937), Chap. XI.

the variable μ. Putting

$$K(z)=\int_{-1}^{1}\mu^2\psi(z,\mu)d\mu \tag{6}$$

we have

$$\partial K/\partial z=1, \tag{7}$$

and hence

$$K(z)=z+z_0, \tag{8}$$

where the constant z_0 is defined by (see Eq. (2))

$$z_0=K(0)=\int_{-1}^{0}\mu^2\psi(0,\mu)d\mu. \tag{9}$$

III. MILNE'S INTEGRAL EQUATION

On substitution of the transformation

$$\psi(z,\mu)=\chi(z,\mu)e^{-z/\mu} \tag{10}$$

into Eq. (1), integration of (1) over z with the boundary condition (2), and resubstitution from (10), we obtain

$$\psi(z,\mu)=\begin{cases}(2\mu)^{-1}\int_0^z\psi_0(z')\exp[(z'-z)/\mu]dz' & \text{if } \mu>0 \quad (11a)\\ -(2\mu)^{-1}\int_z^\infty\psi_0(z')\exp[(z'-z)/\mu]dz' & \text{if } \mu<0. \quad (11b)\end{cases}$$

Integration of Eqs. (11) over μ yields

$$\psi_0(z)=\tfrac{1}{2}\int_0^\infty\psi_0(z')\mathrm{E}(|z-z'|)dz' \tag{12}$$

with

$$\mathrm{E}(x)=-\mathrm{Ei}(-x)=\int_x^\infty(e^{-u}/u)du. \tag{13}$$

Equation (12) is known as Milne's integral equation. Its solution determines $\psi(z,\mu)$ by Eqs. (11). In particular, we have for the angular distribution of the neutrons emerging from the medium (Eq. (11b) for $z=0$)

$$\psi(0,\mu)=-(2\mu)^{-1}\int_0^\infty\psi_0(z')\exp(z'/\mu)dz', \qquad \mu<0. \tag{14}$$

Thus, $\psi(0,\mu)$ can be represented by the Laplace transform of $\psi_0(z)$. Equations (12) and (11) are an equivalent formulation of the problem stated by Eqs. (1) and (2), and it is customary to start the treatment of the problem from Eq. (12). In view of the fact that in the case of other problems with more complicated scattering laws the reduction of the transport equation to a homogeneous integral equation for the neutron density is in general not possible, here also we shall start directly from the transport Eq. (1) with condition (2) rather than from Milne's integral equation.

IV. AN INTEGRAL EQUATION FOR THE LAPLACE TRANSFORM OF THE NEUTRON DENSITY; ASYMPTOTIC FORM OF $\psi_0(z)$

We introduce the Laplace transforms of $\psi(z,\mu)$ and $\psi_0(z)$ by

$$\phi(s,\mu)=\int_0^\infty\psi(z,\mu)e^{-sz}dz, \tag{15a}$$

$$\phi_0(s)=\int_{-1}^{1}\phi(s,\mu)d\mu=\int_0^\infty\psi_0(z)e^{-sz}dz, \tag{15b}$$

where s is a complex variable $\Re(s)>0$. We multiply (1) by e^{-sz} and integrate over z from 0 to ∞. Noting that, by partial integration,

$$\int_0^\infty e^{-sz}\partial\psi/\partial z dz = |e^{-sz}\psi(z,\mu)|_0^\infty+s\int_0^\infty e^{-sz}\psi(z,\mu)dz = -\psi(0,\mu)+s\phi(s,\mu),$$

we obtain

$$\phi(s,\mu)=[\tfrac{1}{2}\phi_0(s)+\mu\psi(0,\mu)]/(1+s\mu). \tag{16}$$

By integration of (16) over μ we have

$$\phi_0(s)\left\{1-\tfrac{1}{2}\int_{-1}^{1}(1+s\mu)^{-1}d\mu\right\}=\int_{-1}^{0}\mu\psi(0,\mu)(1+s\mu)^{-1}d\mu$$

and, since[3]

$$\tfrac{1}{2}\int_{-1}^{1}(1+s\mu)^{-1}d\mu=\frac{1}{2s}\log[(1+s)/(1-s)]=s^{-1}\operatorname{arth}s, \tag{17}$$

[3] Here and in the following we use the notation arth for $\tanh^{-1}$ and art for $\tan^{-1}$.

$$\phi_0(s)=\frac{\int_{-1}^{0}(1+s\mu)^{-1}\mu\psi(0,\mu)d\mu}{1-s^{-1}\operatorname{arth}s}. \quad (18)$$

Comparison of (15b) and (14) yields

$$\mu\psi(0,\mu)=-\tfrac{1}{2}\phi_0(-1/\mu). \quad (19)$$

Hence we may write (18)

$$\phi_0(s)\{1-s^{-1}\operatorname{arth}s\}=-\tfrac{1}{2}\int_{-1}^{0}\frac{\phi_0(-1/\mu)}{1+s\mu}d\mu. \quad (20)$$

Before attempting to solve this integral equation for $\phi_0(s)$, we note that the asymptotic form of $\psi_0(z)$ for large z is determined by the behavior of $\phi_0(s)$ at $s=0$, which can be immediately ascertained by expanding (18) in a Laurent series about $s=0$. Noting that

$$\operatorname{arth}s=s+\tfrac{1}{3}s^3+\cdots \quad (21)$$

and using the relations (3), (5), and (9), we obtain

$$\phi_0(s)=3s^{-2}+3z_0s^{-1}+\cdots \quad (22)$$

and hence the asymptotic form[4] of $\psi_0(z)$ is given by

$$\psi_0(z)\sim 3(z+z_0) \quad \text{as} \quad z\to\infty. \quad (23)$$

TABLE I. Functional properties of $\phi_0(s)$, $s^{-1}\operatorname{arth}s$, $g(s)$.

Function	Domain of regularity*	Proof
$\phi_0(s)$	$\Re(s)>0$	Follows from definition (15b) and asymptotic form (23)
$s^{-1}\operatorname{arth}s$	$-1<\Re(s)<1$	Follows from definition (17)
$g(s)$	$\Re(s)<1$	Follows from definition (24)**

* One can actually show that the functions are analytic in domains wider than those indicated above, but we will not need to make use of this fact.

** From (24) it is seen that the only possible singularities of $g(s)$ can occur for those values of s for which the denominator of the integrand vanishes.

[4] That $\psi_0(z)$ has this asymptotic form follows also directly from (1) by noting that $\psi(z,\mu)$ must be almost isotropic for large z. It is therefore legitimate to write $\psi(z,\mu)$ for large z in the form

$$\psi(z,\mu)=\tfrac{1}{2}\psi_0(z)-\tfrac{3}{2}j\mu=\tfrac{1}{2}\psi_0(z)-\tfrac{3}{2}\mu. \quad (A)$$

Equation (A) can be considered as an expansion of $\psi(z,\mu)$ in Legendre polynomials neglecting all higher terms (diffusion approximation). Introduction of (A) into (1) yields

$$\psi_0(z)=3(z+\text{const.}).$$

V. SOLUTION OF THE INTEGRAL EQUATION FOR $\phi_0(s)$ BY THE METHOD OF WIENER AND HOPF

Setting

$$g(s)=\int_{-1}^{0}(1+s\mu)^{-1}\mu\psi(\mu,0)d\mu, \quad (24)$$

we may write (18) in the form

$$\phi_0(s)\{1-s^{-1}\operatorname{arth}s\}=g(s). \quad (25)$$

This integral equation can be solved by considering the domain in which the functions occurring in the equation are analytic. We shall form a certain function containing $\phi_0(s)$ and $(s^{-1}\operatorname{arth}s)$ which will have the property of being analytic and bounded in the whole complex s-plane. According to Liouville's theorem in the theory of complex variables, such a function must be a constant. From this, therefore, it will be possible to determine $\phi_0(s)$ in terms of the known function $(s^{-1}\operatorname{arth}s)$.

The functions occurring in Eq. (25) can immediately be shown to be analytic in the domains given in Table I.

In order to solve (25) we shall try to re-write it in such a manner that the left-hand side is analytic in a half-plane and the right-hand side in another half-plane overlapping the first so that both half-planes fill out the whole plane. Then the two sides of the equation can be considered as the analytical continuations of each other and therefore will represent the same function. This function will be analytic on the whole plane. If, in addition, it turns out to be bounded in the whole plane, it must be equal to a constant as mentioned above.

As it stands, Eq. (25) is not in the desired form, since the function $1-s^{-1}\operatorname{arth}s$ is analytic in a strip rather than a half-plane, namely, the strip $-1<\Re(s)<1$. Such a function can, however, be written as a quotient of two functions, each analytic in a half-plane, provided that the function (a) has no zeros in the strip and (b) that it tends to unity as $|s|\to\infty$ in the strip. The function $1-s^{-1}\operatorname{arth}s$ has, according to (21), a double zero at the origin and, as may easily be shown, no other zeros in the strip. We can satisfy condition (a) by replacing the function by $s^{-2}(1-s^{-1}\operatorname{arth}s)$. This function, however, will not satisfy condition (b). Hence, we form the

function

$$\tau(s)=s^{-2}(s^2-1)(1-s\,\mathrm{arth}s) \tag{26}$$

which satisfies both conditions. In terms of $\tau(s)$, Eq. (25) reads

$$[s^2/(s^2-1)]\phi_0(s)\tau(s)=g(s). \tag{27}$$

In order to decompose $\tau(s)$ in the desired manner we consider $\log\tau(s)$ which is single-valued in the strip $-1<\Re(s)<1$, provided we choose a particular determination of the logarithm. We shall choose it so that $\log 1=0$. Since $\tau(s)$ satisfies condition (b), $\log\tau(s)\to 0$ as $|s|\to\infty$ in the strip. Consequently, $\log\tau(s)$ can be represented by the Cauchy integral formula in the form

$$\log\tau(s)=(2\pi i)^{-1}\int_{\beta-i\infty}^{\beta+i\infty}(u-s)^{-1}\log\tau(u)du$$

$$-(2\pi i)^{-1}\int_{-\beta-i\infty}^{-\beta+i\infty}(u-s)^{-1}\log\tau(u)du$$

where $0<\beta<1$ and $-\beta<\Re(s)<\beta$. Defining

$$\tau_-(s)=\exp\left[(2\pi i)^{-1}\int_{-\beta-i\infty}^{-\beta+i\infty}(u-s)^{-1}\log\tau(u)du\right], \tag{28}$$

$$\tau_+(s)=\exp\left[(2\pi i)^{-1}\int_{\beta-i\infty}^{\beta+i\infty}(u-s)^{-1}\log\tau(u)du\right], \tag{29}$$

we obtain

$$\log\tau(s)=\log\tau_+(s)-\log\tau_-(s)$$

or

$$\tau(s)=\tau_+(s)/\tau_-(s), \tag{30}$$

where $\tau_-(s)$ is regular and different from zero in the half-plane $\Re(s)>-\beta$, while $\tau_+(s)$ is regular and different from zero in the half-plane $\Re(s)<\beta$. Putting Eq. (30) into (27), one may write it in the form

$$s^2\phi_0(s)/(s+1)\tau_-(s)=(s-1)g(s)/\tau_+(s). \tag{31}$$

Here, the left-hand side is regular in $\Re(s)>0$, while the right-hand side is regular in $\Re(s)<\beta$. Thus, each side of (31) represents the analytic continuation of the other, so that either side is regular in the whole finite s-plane. It is necessary now to investigate the order of magnitude of each side of (31). From (28) and (29) it follows (see appendix) that in any half-plane $\Re(s)>-\beta'>-\beta$, $\tau_-(s)$ is bounded away from zero, that is,

FIG. 1. Path of integration for $\tau_-(0)$.

$|\tau_-(s)|>C_1>0$ and similarly in any half-plane $\Re(s)<\beta'<\beta$, $|\tau_+(s)|>C_2>0$, where C_1 and C_2 are constants. Furthermore, the definitions (15b) and (24) imply that in their respective half-planes of regularity $\phi_0(s)$ and $g(s)$ are $0(1/|s|)$ at infinity. These conditions imply that each side of (31) is bounded at infinity. Since each side is regular elsewhere it must be bounded in the whole plane. Hence, it fulfills the conditions of Liouville's theorem and must be identically equal to a constant C. Therefore, from (31)

$$\phi_0(s)=C(s+1)\tau_-(s)/s^2. \tag{32}$$

In order to determine C we expand $\phi_0(s)$ in a Laurent series about $s=0$

$$\phi_0(s)=C\tau_-(0)s^{-2}$$

$$+C[\tau_-(0)+\tau_-'(0)]s^{-1}+\cdots. \tag{33}$$

Comparison with (22) yields

$$C=3/\tau_-(0). \tag{34}$$

We now evaluate $\tau_-(0)$. From (28) we have

$$1/\tau_-(0)=\exp\left[-(2\pi i)^{-1}\int_{-\beta-i\infty}^{-\beta+i\infty}u^{-1}\log\tau(u)du\right].$$

We deform the path of integration into the two segments $(-i\infty,\ -i\rho)$, $(i\rho,\ i\infty)$ of the imaginary axis and the semicircle S of radius ρ, as shown on Fig. 1, ρ being any positive number. The two integrals over the segments cancel since, according to (26), the integrand is odd so that

$$1/\tau_-(0)=\exp\left[-(2\pi i)^{-1}\int_S u^{-1}\log\tau(u)du\right].$$

On letting $\rho\to 0$ in the integral, we find

$$1/\tau_-(0)=\exp[\tfrac{1}{2}\log\tau(0)]=\sqrt{\tau(0)}.$$

From (26) and (21) we have $\tau(0)=\frac{1}{3}$, so that from (34)

$$C=\sqrt{3} \tag{35}$$

and thus from (32)

$$\phi_0(s)=\sqrt{3}(s+1)\tau_-(s)/s^2. \tag{36}$$

VI. DETERMINATION OF z_0 AND $\psi_0(0)$

Again comparing (33) with (22), we obtain

$$z_0=1+\tau_-'(0)/\tau_-(0).$$

From (28) we get

$$\tau_-'(0)/\tau_-(0)=(2\pi i)^{-1}\int_{-\beta-i\infty}^{-\beta+i\infty}u^{-2}\log\tau(u)du.$$

Integration by parts yields

$$\tau_-'(0)/\tau_-(0)=(2\pi i)^{-1}\int_{-\beta-i\infty}^{-\beta+i\infty}[\tau'(u)/u\tau(u)]du.$$

Since $\tau(u)$ is even, $\tau(0)\neq 0$, and $\tau'(0)=0$, the integrand does not have a singularity at $u=0$, and we may move the path of integration to the imaginary axis. Then, since the integrand is also even, we may write

$$\tau_-'(0)/\tau_-(0)=(\pi i)^{-1}\int_0^{i\infty}[\tau'(u)/u\tau(u)]du.$$

Introducing now the explicit form of τ as given by (26) and replacing the variable of integration by $s=it$, we obtain

$$z_0=\frac{1}{\pi}\int_0^\infty\left\{\frac{3}{t^2}-\frac{1}{(1+t^2)(1-t^{-1}\operatorname{ar}t)}\right\}dt \tag{37}$$

or, substituting $t=\tan x$,

$$z_0=\frac{1}{\pi}\int_0^{\pi/2}\left\{\frac{3}{\sin^2x}-\frac{1}{1-x\cot x}\right\}dx. \tag{38}$$

Each of the two parts of the integrand goes to infinity as $3/x^2$ as $x\to 0$. Writing

$$z_0=I_1+I_2$$

with

$$I_1=\frac{3}{\pi}\int_0^{\pi/2}\left(\frac{1}{\sin^2x}-\frac{1}{x^2}\right)dx=\frac{6}{\pi^2},$$

$$I_2=\frac{1}{\pi}\int_0^{\pi/2}\left(\frac{3}{x^2}-\frac{1}{1-x\cot x}\right)dx,$$

we have

$$z_0=\frac{6}{\pi^2}+\frac{1}{\pi}\int_0^{\pi/2}\left(\frac{3}{x^2}-\frac{1}{1-x\cot x}\right)dx. \tag{39}$$

The integrand in (39) can be expanded in a power series in x, which converges rapidly in the whole range of integration, and then integrated term by term, with the result[5]

$$z_0=0.71044609. \tag{40}$$

As seen from (23), the value of the neutron density at the boundary, extrapolated from the asymptotic solution, is $3z_0$. We now wish to determine the true neutron density at the boundary, $\psi_0(0)$. It is readily seen that

$$\psi_0(0)=\lim_{s\to\infty}s\phi_0(s). \tag{41}$$

Indeed, the relation follows formally from (15b) by introducing the new variable $u=sz$. Equation (15b) then becomes

$$s\phi_0(s)=\int_0^\infty\psi_0(u/s)e^{-u}du.$$

Here, letting $s\to\infty$ and interchanging the limit and integral sign,[6] we obtain

$$\lim_{s\to\infty}s\phi_0(s)=\int_0^\infty\psi_0(0)e^{-u}du=\psi_0(0).$$

Introducing (36) into (41) we now obtain

$$\psi_0(0)=\sqrt{3}\lim_{s\to\infty}\tau_-(s). \tag{42}$$

From (28) it is seen that $\tau_-(s)\to 1$ as $s\to\infty$ and hence[7]

$$\psi_0(0)=\sqrt{3}. \tag{43}$$

---

[5] The computation was carried out by Dr. P. R. Wallace and Mr. B. Carlson. As will be seen from later papers, very accurate knowledge of z_0 is necessary for various approximation methods.

[6] This step may readily be justified rigorously.

[7] For other derivations of this result, see M. Bronstein, Zeits. f. Physik **58**, 696, **59**, 144 (1929); E. Hopf, see reference 1.

VII. THE ANGULAR DISTRIBUTION OF THE EMERGING NEUTRONS

We wish to express the angular distribution of the emerging neutrons, as given by (19), (36), and (28), by a real integral. For this purpose, we have to transform $\tau_-(s)$. Again deforming the path of integration according to Fig. 1, we have:

$$\log\tau_-(s)=\frac{1}{2\pi i}\int_{-i\infty}^{-i\rho}\frac{\log\tau(u)}{u-s}du+\frac{1}{2\pi i}\int_{S_\rho}\frac{\log\tau(u)}{u-s}du+\frac{1}{2\pi i}\int_{i\rho}^{i\infty}\frac{\log\tau(u)}{u-s}du.$$

The first integral may be written as

$$\int_{-i\infty}^{-i\rho}(u-s)^{-1}\log\tau(u)du=-\int_{i\rho}^{i\infty}(u+s)^{-1}\log\tau(u)du.$$

As $\rho\to 0$, the middle integral approaches zero, for $s\neq 0$. Combining the first and third integrals we obtain

$$\log\tau_-(s)=\frac{s}{\pi i}\int_{i0}^{i\infty}\frac{\log\tau(u)}{u^2-s^2}du=-\frac{s}{\pi}\int_0^\infty\frac{\log\tau(it)}{t^2+s^2}dt$$

and, on substituting from (26),

$$\log\tau_-(s)=-\frac{s}{\pi}\int_0^\infty\frac{\log\left\{\frac{t^2+1}{t^2}\left(1-\frac{\operatorname{arc}t}{t}\right)\right\}}{t^2+s^2}dt. \quad (44)$$

Putting $t=\tan x$ we have finally

$$\log\tau_-(s)=\frac{s}{\pi}\int_0^{\pi/2}\frac{\log[\sin^2x/(1-x\cot x)]}{\sin^2x+s^2\cos^2x}dx \quad (45)$$

and, with (19) and (36):

$$\psi(0,\mu)=\tfrac{1}{2}\sqrt{3}(1-\mu)\tau_-(-1/\mu)=\tfrac{1}{2}\sqrt{3}(1-\mu)\times\exp\left[\frac{-\mu}{\pi}\int_0^{\pi/2}\frac{\log[\sin^2x/(1-x\cot x)]}{1-(1-\mu^2)\sin^2x}dx\right],\quad \mu<0. \quad (46)$$

The numerical evaluation of this expression is given in the following paper.[8]

APPENDIX

It remains to be shown that the functions $\tau_-(s)$ and $\tau_+(s)$, defined in (28) and (29), are such that $|\tau_-(s)|>C_1>0$ in any half-plane $\Re(s)>-\beta'>-\beta$ and $|\tau_+(s)|>C_2>0$ in any half-plane $\Re(s)<\beta'<\beta$. We shall confine ourselves to proving the assertion for $\tau_-(s)$. An entirely analogous argument holds for $\tau_+(s)$. From (28) it is evidently sufficient to prove that in any half-plane $\Re(s)>-\beta'>-\beta$ the integral

$$\int_{-\beta-i\infty}^{-\beta+i\infty}(u-s)^{-1}\log\tau(u)du$$

is bounded. Now for large values of u the function $\tau(u)$ is of the form

$$\tau(u)=1+O(1/|u^2|),$$

so that $\log\tau(u)$ is quadratically integrable. Hence, applying Schwarz's inequality to the integral,

$$\left|\int_{-\beta-i\infty}^{-\beta+i\infty}\frac{\log\tau(u)}{u-s}du\right|^2\leqslant\int_{-\beta-i\infty}^{-\beta+i\infty}|\log\tau(u)|^2du\times\int_{-\beta-i\infty}^{-\beta+i\infty}\frac{|du|}{|u-s|^2}.$$

The assertion follows at once since the denominator of the second integral stays uniformly away from zero whenever $\Re(s)>-\beta'>-\beta$.

[8] G. Placzek, Phys. Rev. **72**, 556 (1947).

The Angular Distribution of Neutrons Emerging from a Plane Surface

G. PLACZEK*
*Montreal Laboratory, National Research Council of Canada,** Montreal, Canada*
(Received May 31, 1947)

The Wiener-Hopf expression for the angular distribution in Milne's standard case is transformed into a form suitable for numerical evaluation. The results of the evaluation carried out by the Mathematical Tables Project are given.

1. INTRODUCTION

THE angular distribution of the neutrons emerging from a body of purely scattering material into a vacuum will in general depend upon the law of scattering and the source distribution in the body and, to a certain extent, also upon the size and shape of the body.

An important standard case, of interest in connection with fast as well as with slow neutron problems, is the following:

The body is infinite in two directions and is bounded by a plane. It contains no sources, and no neutrons enter the plane from the outside. A constant neutron current flows in the outward direction perpendicular to the plane. The law of scattering is isotropic without energy loss.

The problem of the determination of the angular distribution of the emerging neutrons for this case has been solved by Wiener and Hopf.[1] A simplified derivation of their expression has been given by Placzek and Seidel.[2] The present paper deals with a transformation of this expression into a more practical form and its numerical evaluation.[3]

2. THEORY

Let μ be the cosine of the angle between the direction of motion of the neutron and the outward normal, and $\varphi(\mu)d\mu$ the probability for the direction cosine of an emerging neutron to lie between μ and $\mu+d\mu$, so that

$$\int_0^1 \varphi(\mu)d\mu = 1. \tag{1}$$

The function $\varphi(\mu)$ is given by[4] Eq. (46) of Placzek and Seidel.

$$\varphi(\mu) = \tfrac{1}{2}(1+\mu) \times \exp\left[\frac{\mu}{\pi}\int_0^{\pi/2} \frac{\log[\sin^2 x/(1-x\cot x)]}{1-(1-\mu^2)\sin^2 x}dx\right]. \tag{2}$$

We integrate by parts, noting that

$$\mu\int dx/[1-(1-\mu^2)\sin^2 x] = \operatorname{art}(\mu \tan x)$$

and

$$\frac{d}{dx}\log\left[\frac{\sin^2 x}{1-x\cot x}\right] = 3\cot x - \frac{x}{1-x\cot x},$$

and obtain

$$\frac{\mu}{\pi}\int_0^{\pi/2} \frac{\log[\sin^2 x/(1-x\cot x)]}{1-(1-\mu^2)\sin^2 x}dx = \frac{1}{\pi}\int_0^{\pi/2}\left\{\frac{x}{1-x\cot x} - 3\cot x\right\}\operatorname{art}(\mu\tan x)dx, \tag{3}$$

since the integrated part vanishes.

The second part of this integral can be evaluated in closed form. Putting $\tan x = y$ and using

* Now at General Electric Research Laboratory, Schenectady, New York.
** Report issued September 30, 1943.
[1] N. Wiener and E. Hopf, Berliner Ber. Math. Phys. Klasse (1931), p. 696; see also E. Hopf, Cambridge Tracts No. 31 (1934).
[2] G. Placzek and W. Seidel, Phys. Rev. 72, 550 (1947).
[3] After the present work was done, results of a numerical evaluation of the original Wiener-Hopf expression have been published by S. Chandrasekhar (Astrophys. J. 99, 180 1944). The use of this function for numerical integrations, of which the following paper by Mark gives a significant example, requires the more accurate table given in the present paper.
[4] In G. Placzek and W. Seidel, Phys. Rev. 72, 550 (1947), the *inward* direction is counted positive, while for the purposes of the present paper it has been more convenient to define the *outward* direction as the positive one. Also, the function $\psi(0, \mu)$ in Placzek and Seidel is normalized to unit *current*, while we use here normalization to unit *density* (Eq. (1)). In order to express $\varphi(\mu)$ by $\psi(0, \mu)$ we have, therefore, to put

$$\varphi(\mu) = \psi(0, -\mu)/\sqrt{3}.$$

the fact that the integral from 0 to ∞ of the product of two even functions is equal to $1/2\pi$ times the integral from 0 to ∞ of the product of their Fourier transforms, we obtain:

$$\pi^{-1}\int_0^{\pi/2} \cot x \operatorname{art}(\mu \tan x)dx$$

$$=\pi^{-1}\int_0^{\infty} [\operatorname{art}(\mu y)/y(1+y^2)]dy$$

$$=\tfrac{1}{2}\int_0^{\infty} \mathrm{E}(z/\mu)e^{-z}dz=\tfrac{1}{2}\log(1+\mu), \quad (4)$$

where

$$\mathrm{E}(u)=\int_u^{\infty} v^{-1}e^{-v}dv$$

is the exponential integral.

From (4), (3), and (2) we obtain now

$$\varphi(\mu)=\frac{1}{2(1+\mu)^{\frac{1}{2}}}\exp\left[\frac{1}{\pi}\int_0^{\pi/2}\frac{x\operatorname{art}(\mu\tan x)}{1-x\cot x}dx\right] \quad (5)$$

From (5) it can be seen in a simpler way than from (2) that, for very small values of μ, $\varphi(\mu)$ is asymptotically given by

$$\varphi(\mu)=\tfrac{1}{2}(1-\tfrac{1}{2}\mu\log\mu), \quad \mu\ll 1. \quad (6)$$

Thus, the derivative of $\varphi(\mu)$ becomes logarithmically infinite for $\mu=0$. This is directly connected with the well-known fact that the spatial derivative of the neutron density has a logarithmic infinity at the surface.

The integral in (5) has been evaluated numerically by the Mathematical Tables Project. For 10 values of the argument accurate values of the integral were obtained by numerical integration, and from these the intermediate values were found by interpolation. Table I gives the results of the numerical integration at intervals of 0.1, while Table II gives the interpolated values at intervals of 0.01. The second table is in a suitable form for use in connection with the numerical integration of expressions containing the function φ, except that even for this close spacing linear interpolation is quite insufficient for small values of μ. In this region the difference

TABLE I. Values of $\varphi(\mu)$ at intervals of 0.1.

μ	$\varphi(\mu)$
0	0.5000000
0.1	0.6236751
0.2	0.7251757
0.3	0.8212611
0.4	0.9146378
0.5	1.0063894
0.6	1.0970665
0.7	1.1869875
0.8	1.2763522
0.9	1.3652938
1.0	1.4539053

TABLE II. Values of $\varphi(\mu)$ at intervals of 0.01.

μ	$\varphi(\mu)$	Δ	$-\Delta_2$	μ	$\varphi(\mu)$	Δ
0.00	0.50000	1713	312	0.50	1.00639	911
1	0.51713	1401	105	1	1.01550	910
2	0.53114	1296	64	2	1.02460	909
3	0.54410	1232	45	3	1.03369	908
4	0.55642	1187	34	4	1.04277	907
0.05	0.56829	1153	27	0.55	1.05184	906
6	0.57982	1126	22	6	1.06090	905
7	0.59108	1104	18	7	1.06995	905
8	0.60212	1086	16	8	1.07900	904
9	0.61298	1070	14	9	1.08804	903
0.10	0.62368	1056	12	0.60	1.09707	902
1	0.63424	1044	10	1	1.10609	901
2	0.64468	1034	10	2	1.11510	901
3	0.65502	1024	8	3	1.12411	900
4	0.66526	1016	8	4	1.13311	900
0.15	0.67542	1008	7	0.65	1.14211	899
6	0.68550	1001	7	6	1.15110	898
7	0.69551	994	5	7	1.16008	897
8	0.70545	989	5	8	1.16905	897
9	0.71534	984	6	9	1.17802	897
0.20	0.72518	978		0.70	1.18699	896
1	0.73496	974		1	1.19595	895
2	0.74470	969		2	1.20490	895
3	0.75439	966		3	1.21385	894
4	0.76405	961		4	1.22279	894
0.25	0.77366	958		0.75	1.23173	893
6	0.78324	955		6	1.24066	893
7	0.79279	952		7	1.24959	893
8	0.80231	949		8	1.25852	892
9	0.81180	946		9	1.26744	891
0.30	0.82126	944		0.80	1.27636	891
1	0.83070	941		1	1.28526	891
2	0.84011	938		2	1.29417	890
3	0.84949	937		3	1.30307	890
4	0.85886	934		4	1.31197	890
0.35	0.86820	933		0.85	1.32087	889
6	0.87753	930		6	1.32976	889
7	0.88683	929		7	1.33865	888
8	0.89612	927		8	1.34753	889
9	0.90539	925		9	1.35642	887
0.40	0.91464	923		0.90	1.36529	888
1	0.92387	923		1	1.37417	887
2	0.93310	920		2	1.38304	887
3	0.94230	920		3	1.39191	886
4	0.95150	917		4	1.40077	887
0.45	0.96067	917		0.95	1.40964	886
6	0.96984	916		6	1.41850	885
7	0.97900	914		7	1.42735	886
8	0.98814	913		8	1.43621	885
9	0.99727	912		9	1.44506	885
0.50	1.00639	911		1.00	1.45391	

of φ and the asymptotic expression (6) is best used for interpolation.

It is seen from the tables that $\varphi(\mu)$ is very close to a straight line except for small μ. Fermi's simple linear approximation[5]

$$\varphi(\mu)=(1+\sqrt{3}\mu)/(1+\sqrt{3}/2) \qquad (7)$$

has an error of 7.2 percent at $\mu=0$, but for $\mu>0.1$ its error is below one percent throughout. This has to be kept in mind when discussing the more complicated approximations.[6-9]

[5] E. Fermi, Ricerca Scient. **7** [2] 13 (1936).

[6] A. Unsoeld, *Physik der Sternatmosphaeren* (Julius Springer, Berlin, 1939).

[7] J. LeCaine, Phys. Rev. **72**, 564 (1947), Eq. (12).

[8] G. Placzek, Montreal Report MT 16, 1944; reissued by National Research Council of Canada, Chalk River 1947. See also Eq. (13) in LeCaine, l.c.

[9] S. Chandrasekhar, Astrophys. J. **99**, 180 (1944); **101**, 348 (1945).

PHYSICAL REVIEW VOLUME 72, NUMBER 7 OCTOBER 1, 1947

The Neutron Density Near a Plane Surface

C. MARK*
*Montreal Laboratory, National Research Council of Canada, Montreal, Canada***

(Received May 31, 1947)

The exact solution of Milne's integral equation is expressed as a real integral with non-oscillating integrand. This expression has been derived from the Wiener-Hopf solution for the Laplace transform of the density. The integrand involves the angular distribution of neutrons emerging from the surface, and the tabulation of this function by the Mathematical Tables Project given by Placzek has been used in the numerical evaluation of the integral. The values of the first three moments of the difference between the density and the asymptotic density, and an expansion of the density for points near the boundary are also given. Various authors have proposed or obtained approximations to the solution of this problem, and some of these approximations are referred to and compared with the exact solution.

1. INTRODUCTION

THE purpose of this paper is to determine the neutron density in Milne's problem as described by Placzek and Seidel.[1] We shall adopt the notation and definitions of their paper and make frequent references to its results.

The neutron density, $\psi_0(z)$, satisfies Milne's integral equation

$$\psi_0(z)=\tfrac{1}{2}\int_0^\infty \psi_0(z')E(|z-z'|)dz',$$

with $E(x)=-Ei(-x)$. An expression for the Laplace transform of the solution of this equation has been obtained by Wiener and Hopf.[2,3] A simplified derivation of their result is given in PS.

The angular distribution of the emerging neutrons is, except for a factor, equal to the Laplace transform of the density (PS, Eq. (19)), so that the problem of determining the emergent angular distribution is simply that of evaluating the expression for this Laplace transform; and an extensive and accurate tabulation of this is now available.[4] However, considerable difficulties have been encountered in attempts to invert the Laplace transform of the density in order to obtain the density itself, and an exact yet manageable integral for $\psi_0(z)$ does not seem to have been given heretofore. In this paper it is

* Now at Los Alamos Scientific Laboratory, Santa Fe, New Mexico.

** This paper, except for minor modifications, corrections, and improvements in some of the numerical work, was issued as a report of the Theoretical Division of the Montreal Laboratory on April 15, 1944.

[1] G. Placzek and W. Seidel, Phys. Rev. **72**, 550 (1947). Hereafter this paper will be referred to as PS.

[2] N. Wiener and E. Hopf, Berliner Ber. Math. Phys. Klasse (1931), p. 696.

[3] E. Hopf, *Mathematical Problems of Radiative Equilibrium*, Cambridge tracts No. 31, 1934.

[4] G. Placzek, Phys. Rev. **72**, 556 (1947).

shown that

$$\psi_0(z)=3\left\{z+z_0-\tfrac{1}{4}\int_0^1 (e^{-z/\mu}d\mu)/\psi(0,-\mu)[(1-\mu\,\mathrm{arth}\mu)^2+\pi^2\mu^2/4]\right\}, \quad (1)$$

where $z_0=0.710446$ (PS, Eq. (40)), and $\psi(0,-\mu)$, the angular distribution of emerging neutrons, is related to the function $\varphi(\mu)$ tabulated in the preceding paper[4] by

$$\varphi(\mu)=\psi(0,-\mu)/\sqrt{3}.$$

$\psi_0(z)$ has been evaluated by numerical integration of (1) with the help of the tabulation of $\varphi(\mu)$.

In addition to the tabulation of the exact neutron density for this standard problem, a few terms of an analytical expansion of the density function, valid for small z, have been included (Section 5). The first neglected term is $O(z^3\log^3 z)$, and the terms given represent the density with an error of less than 0.1 percent over the range $0\leq z<0.1$, where the mean free path is taken as the unit length.

There are also included (Section 4) the values of the zero, first, and second moments of the difference between the asymptotic density and the density itself: $3(z+z_0)-\psi_0(z)$.

In Section 3 note is made of the obvious fact that one may approach this semi-infinite medium problem through the formulae given by Placzek and Volkoff[5] which apply to an infinite medium.

2. AN EXPRESSION FOR $\psi_0(z)$

In PS the Laplace transform of the density,

$$\phi_0(s)=\int_0^\infty \psi_0(z)e^{-sz}dz, \quad (2)$$

is obtained in the explicit form (PS, Eq. (36))

$$\phi_0(s)=\sqrt{3}[(s+1)\tau_-(s)/s^2], \quad (3)$$

where $\tau_-(s)$ is defined in PS Eqs. (26) and (28). To obtain $\psi_0(z)$ we may write the inversion formula

$$\psi_0(z)=(1/2\pi i)\int_{c-i\infty}^{c+i\infty}\phi_0(s)e^{sz}dz, \quad 0<c; \quad (4)$$

but to substitute in this from Eq. (3) leads to an immediate impasse because of the complexity of the function $\tau_-(s)$. We therefore consider substituting in (4) from PS (18),

$$\phi_0(s)=\frac{\int_{-1}^0[\mu\psi(0,\mu)/(1+\mu s)]d\mu}{1-\frac{1}{2}\int_{-1}^1 d\mu/(1+\mu s)}. \quad (5)$$

On setting

$$\int_{-1}^0[\mu\psi(0,\mu)/(1+\mu s)]d\mu=g(s)$$

and

$$1-\tfrac{1}{2}\int_{-1}^1 d\mu/(1+\mu s)=K(s), \quad (6)$$

we have $\phi_0(s)=g(s)/K(s)$; and we now consider the properties of these two functions.

$$K(s)=1-\tfrac{1}{2}\int_{-1}^1 d\mu/(1+\mu s)=-s^2\int_0^1[\mu^2/(1-\mu^2s^2)]d\mu. \quad (7)$$

From this second form of $K(s)$ it is obvious that $K(s)$ has a double zero at $s=0$; and it may also be easily seen that $K(s)$ has no other zeros in the s-plane cut from $-\infty$ to -1 and from 1 to ∞. A proof of this is given by Placzek and Volkoff[6] (or one can show that the imaginary part of the second integral in (7) is unequal to zero unless s lies on one of the axes in the s-plane). $K(s)$ has branch points at $s=\pm 1$, and is regular in the cut plane. We use that branch of $K(s)$ which is real for $-1<s<1$.

For $g(s)$, we note that this function has a branch point at $s=+1$, and is regular in the plane cut from $+1$ to $+\infty$. We use that branch of $g(s)$ which is real for real $s<1$. We have

$$g(0)=\int_{-1}^0 \mu\psi(0,\mu)d\mu,$$

[5] G. Placzek and G. M. Volkoff, *Notes on Diffusion of Neutrons without Change in Energy*, M.T. 4, obtainable from Plans and Publications Branch, National Research Council of Canada, Ottawa, Canada.

[6] Appendix B of reference 5.

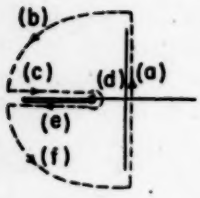

FIG. 1. Contour for the integration of Eq. (9).

which, as in PS, we take to be -1, thus normalizing the current.

We may now state that

$$\phi_0(s)=g(s)/K(s) \tag{8}$$

is regular in the s-plane cut from $-\infty$ to -1, except for a pole of the second order at $s=0$. (The regularity of $\phi_0(s)$ in the positive half-plane follows from the definition (2), and the fact that, as in reference 3, we are seeking solutions $\psi_0(z)$ of $O[\exp(az)]$, $a<1$.)

Now substituting from (8) in (4) we obtain

$$\psi_0(z)=(2\pi i)^{-1}\int_{c-i\infty}^{c+i\infty}[g(s)e^{sz}/K(s)]ds, \tag{9}$$

and to handle this integral we close the contour as in Fig. 1. It is shown in PS that for small values of s

$$\phi_0(s)=g(s)/K(s)=3s^{-2}+3z_0s^{-1}+\cdots \tag{10}$$

where z_0 is the number 0.710446. From Eqs. (10) and (9) we obtain

$$\psi_0(z)=(2\pi i)^{-1}\int_{(a)}[g(s)e^{sz}/K(s)]ds$$

$$=3(z+z_0)-(2\pi i)^{-1}\Big[\int_{(b)}+\int_{(c)}+\int_{(d)}$$

$$+\int_{(e)}+\int_{(f)}[g(s)e^{sz}/K(s)]ds\Big]. \tag{11}$$

In Eq. (11) we note first that

$$\int_{(d)}=0,$$

since the branch point at -1 is a zero of the integrand. We next consider

$$\int_{(b)}+\int_{(f)}.$$

From (6) it follows that $g(s)/K(s)=O(1/|s|)$ as $|s|\to\infty$ so that there is no contribution to these integrals from the small parts of paths (b) and (f) to the right of the imaginary axis. For the rest, we set $s=Re^{i\theta}(R\to\infty)$, so that $e^{sz}=e^{zR\cos\theta}\times e^{izR\sin\theta}$; and since, for the integrals considered, θ is in the 2nd and 3rd quadrants, $\cos\theta$ is negative and hence, for R infinite,

$$\int_{(b)}+\int_{(f)}=0.$$

Thus (11) reduces to

$$\psi_0(z)=3(z+z_0)-(2\pi i)^{-1}\Big[\int_{(c)}[g(s)e^{sz}/K(s)]$$

$$+\int_{(e)}[g(s)e^{sz}/K(s)]ds\Big]. \tag{12}$$

Along path (c), where $-\infty<s<-1$,

$$K(s)=1+(2s)^{-1}\log(s-1/s+1)-(i\pi/2s)$$
$$=1-s^{-1}\operatorname{cth}^{-1}s-i\pi/2s, \tag{13}$$

whereas, along path (e),

$$K(s)=1-s^{-1}\operatorname{cth}^{-1}s+i\pi/2s. \tag{14}$$

Using (13) and (14) in (12) and then setting $s=-t$ gives

$$\psi_0(z)=3(z+z_0)+\tfrac{1}{2}\int_1^\infty[g(-t)e^{-tz}dt]/$$

$$t[(1-t^{-1}\operatorname{cth}^{-1}t)^2+\pi^2/4t^2]. \tag{15}$$

To put (15) in a convenient form we use the result (not explicitly stated in PS but immediately available from PS Eqs. (31), (32), and (35)

$$g(-t)=-\sqrt{3}\,\tau_+(-t)/(1+t),$$

and the further fact, which may be verified from Eqs. (28) and (29) of PS, that

$$\tau_+(-t)=1/\tau_-(t).$$

Combining these with Eqs. (36) and (19) of PS we obtain

$$g(-t)=-3/[2t\psi(0,-1/t)]. \tag{16}$$

Substituting (16) in (15) and then setting $t=1/\mu$ gives relation (1) for $\psi_0(z)$.

The integral in (1) has been evaluated. The results are included in Section 6 where tables

of the function $\rho(z)=\frac{1}{3}\psi_0(z)$ and also of the quantity $z+z_0-\rho(z)$, which is the deviation from the asymptotic form, are given, and the method used for the integration is described.

The results of this evaluation of $\psi_0(z)$ may also be used to give the neutron density when the scattering is not isotropic but is represented by a linear expression in the cosine of the scattering angle. For, if b represent the average cosine of the scattering angle, the neutron density for such linear scattering differs from the neutron density for isotropic scattering only by a term linear in z[7]; in fact,

$$\psi_0^{(b)}(z)=\psi_0^{(is)}(z)-3bz.$$

3. AN ALTERNATIVE DERIVATIVE OF EQ. (15)

The Milne problem for a half-space may also be interpreted as a problem in an infinite medium. For this one would imagine an infinite non-capturing medium with a uniform current from infinity in a direction parallel to the z axis and with an anisotropic plane sink at $z=0$ which absorbs $\mu\psi(0,\mu)d\mu$ neutrons for negative μ between μ and $\mu+d\mu$.

Using the one-dimensional form of the formulae given by Placzek and Volkoff (reference 5, Section 5), taking $\mu'\psi(0,\mu')\delta(\mu-\mu')\delta(z)$, $\mu<0$, for the "source" term, and taking τ as Fourier transform variable, one gets

$$\phi_0(\tau)\{1-\tau^{-1}\operatorname{art}\tau\}=\int_{-1}^{0}\mu\psi(0,\mu)(1-i\tau\mu)^{-1}d\mu. \quad (17)$$

Now taking the Fourier inverse of this gives

$$\psi_0(z)=\frac{1}{2\pi}\int_{-\infty+ic}^{\infty+ic}\phi_0(\tau)e^{-i\tau z}d\tau$$

$$=\frac{1}{2\pi}\int_{-\infty+ic}^{\infty+ic}\frac{\int_{-1}^{0}\mu\psi(0,\mu)(1-i\tau\mu)^{-1}d\mu}{1-\tau^{-1}\operatorname{art}\tau}e^{-i\tau z}d\tau,$$

$$(c>0).$$

By the substitution $s=-i\tau$ this is reduced to (9) above; or the results of Placzek and Volkoff's Appendix B, may be applied to obtain (15) directly.

4. NOTE ON THE MOMENTS

$$\int_0^\infty z^n\{3(z+z_0)-\psi_0(z)\}dz=M_n$$

We give the values of M_0, M_1, M_2. These are obtained from the relation

$$\int_0^\infty e^{-sz}[3(z+z_0)-\psi_0(z)]dz=3s^{-2}+3z_0s^{-1}-\phi_0(s)$$

by expanding each side in powers of s and equating coefficients. Using (3) we have $\phi_0(s)=\sqrt{3}s^{-2}\times(s+1)[\tau_-(0)+s\tau_-'(0)+\frac{1}{2}s^2\tau_-''(0)+\cdots]$. If we define $c_n=(-1)^n\tau_-^{(n)}(0)/\tau_-(0)$, and recall (PS, Section 6) that $\tau_-(0)=\sqrt{3}$, then it follows from the statements above that

$$M_0=3(c_1-\tfrac{1}{2}c_2),\ M_1=\tfrac{3}{2}(c_2-\tfrac{1}{3}c_3),\ M_2=(c_3-\tfrac{1}{4}c_4).$$

To evaluate these we use the following relations, the first of which is given in Section 6 of PS and the rest of which may be obtained by a similar method:

$$c_1=1-z_0=0.289554;\ c_2=c_1^2+2/5=0.483842;$$

$c_3=c_1^3+16c_1/5+k$, with[8]

$$k=\int_0^1\frac{\mu d\mu}{(1-\mu\operatorname{arth}\mu)^2+\frac{1}{4}\pi^2\mu^2}=0.344708,$$

so that $c_3=1.29556$; and $c_4=612/175+4c_3c_1-3c_1^4-12c_1^2/5=4.77538$. The moments are now seen to have the values:

$$M_0=3(3-5z_0^2)/10=0.14290,$$
$$M_1=0.07798,\ M_2=0.10172.$$

Hence, at once, for the difference function,

$$z_M=0.546,\qquad (z^2)_M=0.712.$$

One may now, by expanding each side of (5) in powers of s, obtain the values of the current moments of the angular distribution:

$$\psi^{(n)}(0)=\int_{-1}^{0}\mu^n\psi(0,\mu)d\mu$$

for $n=3$, 4, and 5. From PS Eq. (14) we see also

[7] C. Mark, *Milne's Problem for Anisotropic Scattering* Eq. (42). MT-26, obtainable from Plans and Publications Branch, National Research Council of Canada, Ottawa.

[8] This results from a numerical integration by Bengt Carlson.

that

$$\psi^{(n)}(0)=\tfrac{1}{2}(-1)^n\int_0^\infty E_{n+1}(z)\psi_0(z)dz,$$

where

$$E_n(z)=\int_1^\infty u^{-n}e^{-zu}du.$$

The results are (in addition to $\psi^{(1)}(0)=-1$, $\psi^{(2)}(0)=z_0$), $\psi^{(3)}(0)=-(3+5z_0^2)/10=-0.55237$, $\psi^{(4)}(0)=0.45226$, $\psi^{(5)}(0)=-0.38304$.

5. NOTE ON AN EXPANSION OF $\psi_0(z)$ FOR SMALL VALUES OF z

Using Eq. (46) of PS and Eq. (5) of Placzek,[4] one can write

$$\log(s\phi_0(s)/\sqrt{3})=-\tfrac{1}{2}\log(1+s^{-1})+\pi^{-1}\int_0^{\pi/2}\frac{y\,\mathrm{art}(s^{-1}\tan y)}{1-y\cot y}dy. \quad (18)$$

It may be shown that the integral in (18) can, for large values of s, be expressed in the form

$$\frac{1}{2s}\log s+\frac{2a+1}{2s}+\frac{4-\pi^2}{16s^2}+O(s^{-3}\log s),$$

where

$$a=\frac{1}{\pi}\int_0^{\pi/2}\tan y\left\{\frac{y}{1-y\cot y}-\frac{\pi}{2}\right\}dy=1.0674.$$

From this asymptotic form of $\phi_0(s)$ for $s\to\infty$ we can deduce a from for $\psi_0(z)$ for small z. The expansion obtained is

$$\psi_0(z)=\sqrt{3}\{1-\tfrac{1}{2}z\log z+1.2788z+\tfrac{1}{16}z^2(\log z)^2-0.3822z^2\log z+0.7068z^2+O(z^3(\log z)^3)\}. \quad (19)$$

This expansion, as may be seen from the following tables, represents the density quite well for values of $z<0.1$ It could then be used to evaluate integrals containing $\psi_0(z)$ analytically over just that part of the range where $\psi_0(z)$ would give trouble in a numerical integration.

TABLE I. Evaluation of $q(z)=z+z_0-\rho(z)$, $\Delta=[q(z)-q_{\mathrm{app}}(z)]\times10^4$.

z	Correct	Lecaine[12]	Δ	Placzek[4]	Δ	Eddington[10]	Δ	Expansion (Section 5)	Δ
0	0.1331	0.1314	17	0.1331	0	0.1271	60	0.1331	0
0.01	0.1222	0.1213	9	0.1222	0	0.1193	29	0.1222	0
0.02	0.1150	0.1145	5	0.1151	−1	0.1076	74	0.1150	0
0.03	0.1092	0.1089	3	0.1094	−2	0.1016	76	0.1091	1
0.05	0.0997	0.0996	1	0.1001	−4	0.0921	76	0.0995	2
0.1	0.0825	0.0826	−1	0.0835	−10	0.0757	68	0.0817	8
0.2	0.0609	0.0609	0	0.0623	−14	0.0566	43	0.0582	27
0.3	0.0471	0.0470	1	0.0482	−11	0.0452	19		
0.4	0.0373	0.0371	2	0.0379	−6	0.0374	−1		
0.5	0.0301	0.0298	3	0.0301	0	0.0317	−16		
0.6	0.0246	0.0243	3	0.0240	6	0.0273	−27		
0.7	0.0203	0.0200	3	0.0191	12	0.0238	−35		
0.8	0.0169	0.0165	4	0.0153	16	0.0210	−41		
0.9	0.0141	0.0138	3	0.0122	19	0.0186	−45		
1.0	0.0119	0.0116	3	0.0097	22	0.0166	−47		
1.2	0.0085	0.0082	3	0.0061	24	0.0134	−49		
1.5	0.0053	0.0051	2	0.0030	23	0.0100	−47		
2.0	0.0025	0.0024	1	0.0008	17	0.0066	−41		
2.5	0.00125	0.00117	0.8	0.0001	11	0.0047	−35		
3.0	0.00064	0.00059	0.5	−0.0003	9	0.0036	−30		
3.5	0.00033	0.00030	0.3	−0.0001	4	0.0029	−26		
4.0	0.00018	0.00016	0.2						
5.0	0.000048	0.000046	0.02						

6. NUMERICAL RESULTS; DISCUSSION

If we define the function $q(z)=z+z_0-\rho(z)$, where $\rho(z)=\frac{1}{3}\psi_0(z)$, and set

$$1/h(\mu)=\varphi(\mu)[(1-\mu\,\mathrm{arth}\mu)^2+\pi^2\mu^2/4], \quad (20)$$

then from (1)

$$4\sqrt{3}q(z)=\int_0^1 h(\mu)e^{-z/\mu}d\mu. \quad (21)$$

Table I contains the results of the evaluation of $q(z)$. The last figure is considered to be reliable. The method used was as follows: The function $2+\mu\log\mu-h(\mu)$, which vanishes at $\mu=0$ and has a finite slope there, turned out to be almost straight from $\mu=0$ to $\mu=0.9$, so that it could be well approximated in that range by a polynomial $p(\mu)$ of the form $a\mu+b\mu^2+c\mu^3+d\mu^4$. Coefficients for $p(\mu)$ were chosen so that the function $k(\mu)=2+\mu\log\mu-h(\mu)-p(\mu)$, which vanishes at $\mu=0$, would also vanish at $\mu=0.1$, 0.2, and 0.9, and have $\int_0^1 k(\mu)d\mu=0$ ($\int_0^1 h(\mu)d\mu$, known from the value of $q(0)$). It then turned out that $k(\mu)$ also vanished between $\mu=0.5$ and $\mu=0.6$, and that from $\mu=0$ to 0.9, $k(\mu)$ is quite smooth and rather small (having a maximum ~0.028 near $\mu=0.8$). Relation (21) was then rewritten in the form

$$\begin{aligned}4\sqrt{3}q(z)&=\int_0^1[2-p(\mu)]e^{-z/\mu}d\mu\\&\quad+\int_0^1\mu\log\mu e^{-z/\mu}d\mu\\&\quad+\int_0^1(e^{-z}-e^{-z/\mu})k(\mu)du \quad (22)\\&=T_1+T_2+T_3.\end{aligned}$$

In Eq. (22) T_1 can be expressed in terms of the functions

$$E_n(z)=\int_1^\infty u^{-n}e^{-zu}du,$$

which are tabulated;

$$T_2=-\tfrac{1}{4}+z-\tfrac{1}{4}z^2\log^2 z+(\tfrac{3}{4}-\tfrac{1}{2}\gamma)z^2\log z$$
$$-(\tfrac{7}{8}-\tfrac{3}{4}\gamma+\tfrac{1}{4}\gamma^2+\pi^2/24)z^2$$
$$-\sum_3^\infty(-)^n z^n/(n-2)^2 n!;$$

and T_3 is the only term requiring numerical integration. Although $k(\mu)$ is appreciable and varies rapidly between $\mu=0.9$ and $\mu=1$, the integrand in T_3 is smooth and small, so that the maximum contribution of T_3 to the value of $q(z)$, which occurs near $z=1.5$, is only $7\cdot10^{-5}$. As a check on the evaluation, we may use the value of M_0 given in Section 4 by which we should have

$$\int_0^\infty q(z)dz=0.04763.$$

The contribution to this coming from T_1 and T_2, which may be obtained exactly, is 0.04777, and a numerical integration of the values obtained for T_3 (which is negative) gave a contribution from this term of -0.00017.

Table II gives the evaluation of $\rho(z)$.

Several of the numerous approximations to $q(z)$ are compared with the correct function. For the approximations, the differences: $[q(z)-q_{\text{app}}(z)]\times10^4$ are also given. In considering the approximations one must remember that the difference function in this problem is never very large and decreases rapidly, whereas $z+z_0$ increases, so that for large values of z one can tolerate very large relative errors in the difference function, and it is only for $z\ll1$ that it must be given to good accuracy. Furthermore, even the simple straight-line approximation to $\rho(z)$ which fits at the boundary,[9] $\rho(z)=z+1\sqrt{3}$, gives at the worst an error of 9 percent (for $z\doteq0.4$) in the value of $\rho(z)$. With this in mind, it is seen that the great complication (from an analytical point of view) of an approximation such as Eddington's[10] which still has errors up to 1.3 percent (for $z\doteq0.02$) is quite unnecessary.

[9] E. Fermi, Ricerca Scient. **7** [2], 13 (1936).

TABLE II. Evaluation of $\rho(z)$.

z	$z+z_0$	$\rho(z)$
0	0.7104	0.5773
0.01	0.7204	0.5982
0.02	0.7304	0.6154
0.03	0.7404	0.6312
0.05	0.7604	0.6607
0.1	0.8104	0.7279
0.2	0.9104	0.8495
0.3	1.0104	0.9633
0.4	1.1104	1.0731
0.5	1.2104	1.1803
0.6	1.3104	1.2858
0.7	1.4104	1.3901
0.8	1.5104	1.4935
0.9	1.6104	1.5963
1.0	1.7104	1.6985
1.2	1.9104	1.9019
1.5	2.2104	2.2051
2.0	2.7104	2.7079
2.5	3.2104	3.2092
3.0	3.7104	3.7098
3.5	4.2104	4.2101
4.0	4.7104	4.7102

In fact, the elementary approximation $\rho(z)$ $z+z_0-a_0e^{-\alpha_0 z}$ ($a_0=0.133096$, $\alpha_0=3.6986$) given by Placzek[11] gives at the worst an error of about 2 percent (for z between 0.05 and 0.1). The approximations of Lecaine[12] (errors ≤0.3 percent) and Placzek[11] (errors ≤0.16 percent) are, however, significant improvements over the simple exponential approximation. Lecaine's approximation,[12] obtained by a variational method, is

$$\rho(z)=z+0.710446$$
$$\times[1-0.342895E_2(z)+0.315870E_3(z)].$$

This has the advantage of a simple analytical form. The error of 0.3 percent at the boundary is quickly reduced, and for $z\geq0.05$ the error is less than 0.05 percent.

Placzek's approximation,[11] obtained by an iteration method, is

$$\rho(z)=z+z_0+\tfrac{1}{2}[E_3(z)-z_0E_2(z)]$$
$$-(a/2\alpha)\{[\log(\alpha+1/\alpha-1)$$
$$+E_i((a-1)z)]e^{-\alpha z}+E_1(z)\},$$

with $a=0.11354$, $\alpha=2.62032$. This approximation is devised so as to be correct at the boundary. For some purposes the region close to the boundary is that of greatest interest. The maximum error,

[10] A. S. Eddington, *Internal Constitution of the Stars* (Cambridge University Press, Teddington, England, 1926).

[11] G. Placzek, *The Neutron Density near a Plane Surface*, I. MT-16, obtainable from Plans and Publications Branch, National Research Council of Canada, Ottawa.

[12] J. Lecaine, Phys. Rev. **72**, 564 (1947).

which is about 0.16 percent, occurs for a value of z a little greater than 0.1.

Eddington's approximation,[10] is

$$\rho(z)=(z+17/24)\left[\frac{2+3z-\{E_2(z)-\frac{3}{2}E_3(z)\}}{2+3z-3\{E_4(z)-\frac{3}{2}E_5(z)\}}\right].$$

This seems to be the best approximation available in previously published literature, although it was done at a rather early stage. The error of 1 percent at the boundary, increases to 1.3 percent at $z=0.02$ and is less than 0.5 percent after $z=0.3$.

The expansion of Section 5 is also evaluated in Table I. This has the correct analytical form near the boundary and is a good approximation up to $z=0.05$. By combining this with Lecaine's approximation one would have a fairly simple and very accurate representation of the density over the entire range.

The author wishes to thank B. Carlson and M. Goldstein for performing the numerical calculations and preparing the tables in this paper.

Note. Since the first writing of this paper, Wick[13] and Chandrasekhar[14] have published applications to this problem of the method of expanding the angular distribution $\psi(z,\mu)$ in Legendre polynomials in μ. Chandrasekhar's highest approximation, in which three exponentials are used, still has a maximum error (near $z=0.1$) of more than 3.5 percent, while even the elementary approximation referred to above which uses only one exponential has a maximum error of about 1.6 percent. In the light of the criteria which should be applied to approximations here, and the other examples already given, it should be pointed out that the polynomial method does not seem to be well adapted to the problem we are considering. Of course, in more complicated problems where simple iteration and variation techniques are not available, the polynomial method has had many very successful applications.

[13] G. C. Wick, "Über ebene Diffusionsprobleme," Zeits. f. Physik **121**, 702 (1943).
[14] S. Chandrasekhar, Astrophys. J. **101**, 348 (1945).

PHYSICAL REVIEW VOLUME 72, NUMBER 7 OCTOBER 1, 1947

Application of a Variational Method to Milne's Problem

J. LECAINE
Montreal Laboratory, National Research Council of Canada, Montreal, Canada*
(Received May 31, 1947)

An approximate solution of Milne's integral equation for the neutron density is obtained by a variational method with high accuracy in simple analytical form. The extrapolated asymptotic density at the boundary is given by this method correct to 0.4 parts in a million. The density itself has a maximum error of 0.3 percent which occurs at the boundary and of less than 0.05 percent for all distances beyond 0.05 mean free paths. A simple expression for the angular distribution of emerging neutrons is also obtained.

THE exact solution of Milne's integral equation[1]

$$\psi_0(z)=\tfrac{1}{2}\int_0^\infty \psi_0(z')E_1(|z-z'|)dz' \qquad (1)$$

with

$$E_1(x)=-Ei(-x)=\int_1^\infty (e^{-xv}/v)dv$$

has been obtained by Mark[2] and evaluated by numerical integration.

We obtain here an approximate solution of this equation in simple analytical form by employing a variational technique.

From the integral equation it is seen that

$$\psi_0(z)=z+q(z), \qquad (2)$$

where $\lim_{z\to\infty}q(z)=z_0$. From Eqs. (9) and (14)

* Report issued May 15, 1944.
[1] For literature, see references 2 and 3.

[2] C. Mark, Phys. Rev. **72**, 558 (1947).

of the paper by Placzek and Seidel,[3] we have:

$$z_0=3\int_{-1}^{0}\mu^2\psi(0,\mu)d\mu$$
$$=\tfrac{3}{2}\int_0^\infty \psi_0(z')E_3(z')dz' \qquad (3)$$
$$=\tfrac{3}{2}\left[\tfrac{1}{4}+\int_0^\infty q(z')E_3(z')dz'\right],$$

where[4]

$$E_n(x)=\int^\infty e^{-xv}v^{-n}dv. \qquad (3')$$

From (1) and (2) we obtain

$$q(z)=\tfrac{1}{2}\int_0^\infty q(z')E_1(|z-z'|)dz'+\tfrac{1}{2}E_3(z). \qquad (4)$$

We then consider the functional[5]

$$F(\bar{q})=\frac{\int_0^\infty \bar{q}(z)\left[\bar{q}(z)-\tfrac{1}{2}\int^\infty \bar{q}(z')E_1(|z-z'|)dz'dz\right]}{\left[\int_0^\infty \bar{q}(z)E_3(z)dz\right]^2}. \qquad (5)$$

When $\bar{q}=q(z)$, $F(\bar{q})$ becomes, using (4) and (3),

$$F(q)=\left[2\int_0^\infty q(z)E_3(z)dz\right]^{-1}=(4z_0/3-\tfrac{1}{2})^{-1}. \qquad (6)$$

Also $F(q)$ is a minimum of $F(\bar{q})$.[6]

If we let $\bar{q}=$constant, $F(\bar{q})=9/4$ and from (6)

$$z_0=17/24. \qquad (7)$$

We now assume as an approximation to q, a function $\bar{q}$ of the form

$$\bar{q}=[1-AE_2(z)-BE_3(z)]z_0. \qquad (8)$$

This form is suggested by the fact that if the method of successive approximations is applied to Eq. (4), beginning with $q=z_0$ the next approximation is

$$q\doteq z_0-\tfrac{1}{2}z_0E_2(z)+\tfrac{1}{2}E_3(z).$$

We choose A and B such that $F(\bar{q})$ assumes an extreme value. In evaluating $F(\bar{q})$ with $\bar{q}$ given by (8) it is necessary to evaluate integrals of the form

$$\int_0^\infty E_m(z)dz\int_0^\infty E_n(z')E_1(|z-z'|)dz'$$
$$=\int_0^\infty E_m(z)dz\int_0^z E_n(z')E_1(z-z')dz'$$
$$+\int_0^\infty E_m(z)dz\int_0^\infty E_n(z+z')E_1(z')dz',$$

with m, $n=2$ or 3. By substituting from Eq. (3') and interchanging orders of integration, this can be reduced to

$$\int_1^\infty s^{-(m+1)}\log(1+s)ds\int_1^\infty v^{-n}(s+v)^{-1}dv$$
$$+\int_1^\infty v^{-(n+1)}\log(1+v)dv\int_1^\infty s^{-m}(s+v)^{-1}ds,$$

which can be evaluated for any m and n. Thus

$$\int_0^\infty E_2(z)dz\int_0^\infty E_2(z')E_1(|z-z'|)dz'$$
$$=\tfrac{1}{3}+\pi^2/12-(4/3)\log 2,$$
$$\int_0^\infty E_3(z)dz\int_0^\infty E_2(z')E_1(|z-z'|)dz'$$
$$=\tfrac{1}{3}\log 2-\tfrac{1}{12},$$
$$\int_0^\infty E_3(z)dz\int_0^\infty E_3(z')E_1(|z-z'|)dz'$$
$$=(56/45)\log 2-79/360-\pi^2/18,$$

and

$$F(q)=\frac{\tfrac{1}{4}+A\tfrac{2}{3}(\log 2-1)-\tfrac{1}{8}B+AB\tfrac{1}{3}(1-\log 2)+A^2\{\tfrac{1}{2}-\pi^2/24\}+B^2\{\pi^2/36-(2/9)\log 2-13/144\}}{\{\tfrac{1}{3}-\tfrac{1}{8}A-B\tfrac{1}{5}(2\log 2-1)\}^2}. \qquad (9)$$

[3] G. Placzek and W. Seidel, Phys. Rev. **72**, 550 (1947).
[4] For tables see G. Placzek, *The Functions* $E_n(x)$, MT-1, obtainable from Plans and Publications Branch, National Research Council of Canada, Ottawa, Canada.
[5] R. E. Marshak, Phys. Rev. **71**, 688 (1947).
[6] B. Davison, Phys. Rev. **71**, 694 (1947).

Now, solving the equations

$$\partial F/\partial A=0, \quad \partial F/\partial B=0,$$

we find

$$A=0.3428949, \quad B=-0.3158704,$$

and F for this value of A and B is 2.235831. From (6),

$$2.235831\doteqdot 1/(\tfrac{1}{3}4z_0-\tfrac{1}{2}),$$

whence

$$z_0\doteqdot 0.7104457. \tag{10}$$

The function of form (8) which best approximates $q(z)$ is

$$q_1(z)=0.7104457(1-0.3428949E_2 +0.3158704E_3). \tag{11}$$

This procedure is designed to give an approximation to the value of F. Since z_0 is related to F directly, whereas q is related only through an integral, the accuracy of the approximation to z_0 will be better than that of the approximation to $q(z)$. The true value of z_0 is 0.71044609,[3] the error in the approximation (10) being thus 4×10^{-5} percent. The approximation (11) has been tabulated and compared with the exact solution by Mark.[2] The maximum error in $z+q_1(z)$ is 0.3 percent and occurs at the boundary. Beyond $z=0.05$ the error is less than 0.05 percent.

Another method of approximation has been discussed by Placzek.[7] Although that approximation is better at the boundary, the present one is an improvement for $z\geqq0.05$, and has the further advantage of a simpler analytical form.

The emergent angular distribution implied by (11), normalized to unit density is

$$\varphi(\mu)=0.501362+0.671543\mu+[0.210927\mu +0.194303\mu^2]\log(1+1/\mu), \quad 0\leqslant\mu\leqslant1. \tag{12}$$

Comparison with the table of the exact function[8] shows that the maximum error of (12) is 0.3 percent at $\mu=0$ and decreases quickly as μ increases. The analytical form of (12) is however not much simpler than the form of Placzek's approximation (reference 7, Eq. (18)):

$$\varphi(\mu)=0.52414+0.43301\mu-0.02414(1+\alpha\mu)^{-1} +\{0.30763\mu+0.43301\mu^2 -0.04916\mu(1+\alpha\mu)^{-1}\}\log(1+1/\mu), \tag{13}$$

where $\alpha=2.62032$, which gives the correct value for $\mu=0$ and represents the true function through the whole range with an error of less than 0.1 percent.

The variational method has also been used for the treatment of a generalization of the present problem to capturing media. The results will be given in a separate paper.

[7] G. Placzek, *The Neutron Density Near a Plane Surface*, I. MT-16, obtainable from Plans and Publications Branch, National Research Council of Canada, Ottawa, Canada.

[8] G. Placzek, Phys. Rev. **72**, 556 (1947).

Delayed Neutrons from Pu^{239}*

F. DE HOFFMANN AND B. T. FELD**
University of California, Los Alamos Scientific Laboratory, Santa Fe, New Mexico
(Received June 23, 1947)

The shape of the decay curve of Pu^{239} delayed neutrons is found to be very nearly the same as that of U^{235}. The ratio of the relative number of delayed neutrons in Pu^{239} to that in U^{235} was found to be 0.47 for neutrons delayed over 2 seconds and 0.40 for neutrons delayed over 5 seconds. In the light of the experimental errors, it is questionable whether these numbers are significantly different.

1. INTRODUCTION

DELAYED neutrons emitted in the fission of U^{235} have been investigated extensively.[1] The delayed neutrons from Pu^{239} were investigated at Los Alamos and at Chicago[2] prior to our work. The experiments reported here made use of larger samples of Pu^{239} than had previously been used.

Our experiment divided itself into two parts:

A. The determination of the relative fraction of neutrons delayed in Pu^{239} to those in U^{235} and
B. The determination of the shape of the Pu^{239} delayed-neutron decay curve.

2. EXPERIMENTAL SET-UP

A. Determination of Relative Fraction

Metal samples of both Pu^{239} and U^{235} were available for this experiment. Irradiations were performed in the graphite thermal column of the Los Alamos "water boiler" (a chain-reacting assembly operating mainly on thermal neutrons). The ratio of activities of an indium foil without and with cadmium covering (cadmium ratio) at the position of irradiation was of the order of a thousand or better. Hence the neutron spectrum was predominately thermal. The Pu^{239} and U^{235} metal samples were each covered with cadmium save on one face. Thus both samples presented a known area to the neutron flux. The samples were sufficiently thick so that they could be considered essentially infinitely thick for thermal neutrons.

The experimental arrangement is sketched in Fig. 1. The sample was attached to a string and could be pulled out of the center of the thermal column into the paraffin geometry for counting. The sample was pulled through a 45° bend in a steel tube. The bend served to reduce background from the thermal column. The detector used was a flat parallel plate U^{235} fission chamber which was embedded in the paraffin. The paraffin arrangement served to increase the counting efficiency for fast neutrons and also tended to equalize the counting efficiency for neutrons of different initial energies. The detector was connected to a fast discriminator and amplifier, the output of which was fed into scaler units. A variable switching arrangement permitted use of scales of up to 2048 which could then be recorded on a mechanical "cyclotron" register.

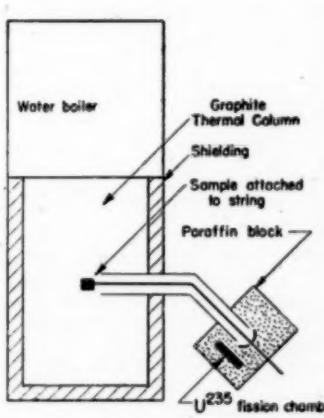

FIG. 1. Sketch of experimental arrangement for irradiation and counting (not to scale).

* This work was completed February 27, 1945. This paper is based on work performed under Contract No. W-7405-Eng-36 with the Manhattan Project at the Los Alamos Scientific Laboratory of the University of California. It will appear in Division V of the Manhattan Project Technical Series as part of the contribution of the Los Alamos Laboratory.
** Now at Massachusetts Institute of Technology.
[1] See, for instance, A. H. Snell, Phys. Rev. **70**, 111 (1946).
[2] R. R. Wilson, Phys. Rev. **71**, 560 (1947). C. Redman and D. Saxon, Phys. Rev. **72**, 570 (1947).

The over-all resolving time of the system was of the order of one microsecond.[3]

The length of time it took for the sample to be pulled from the thermal column into the paraffin geometry was just under 2 seconds. Counting was therefore started 2 seconds after the sample began to move (2-second runs). A second set of data was taken by starting the counter 5 seconds after the sample began to move (5-second runs).

The total number of counts registered in each run was recorded. Background was measured in each case just before pulling the sample, i.e., during irradiation. The entire procedure was performed alternately with the U^{235} and Pu^{239} samples.

B. Shape of the Delay Curve

In order to gain in intensity for this part of the experiment the Pu^{239} sample was irradiated at the center of the reactor rather than in the thermal column. This meant sacrificing the pure thermal-neutron spectrum previously attained in favor of a spectrum which contained a small fast neutron contribution.

The arrangement for pulling out and detecting the sample was the same as that described under *A*. In order to keep a permanent record of the decay curve the output of several of the scaler stages were fed into several channels of a 6-channel Heiland recording galvanometer. The use of several channels recording different scales permitted proper resolution at different

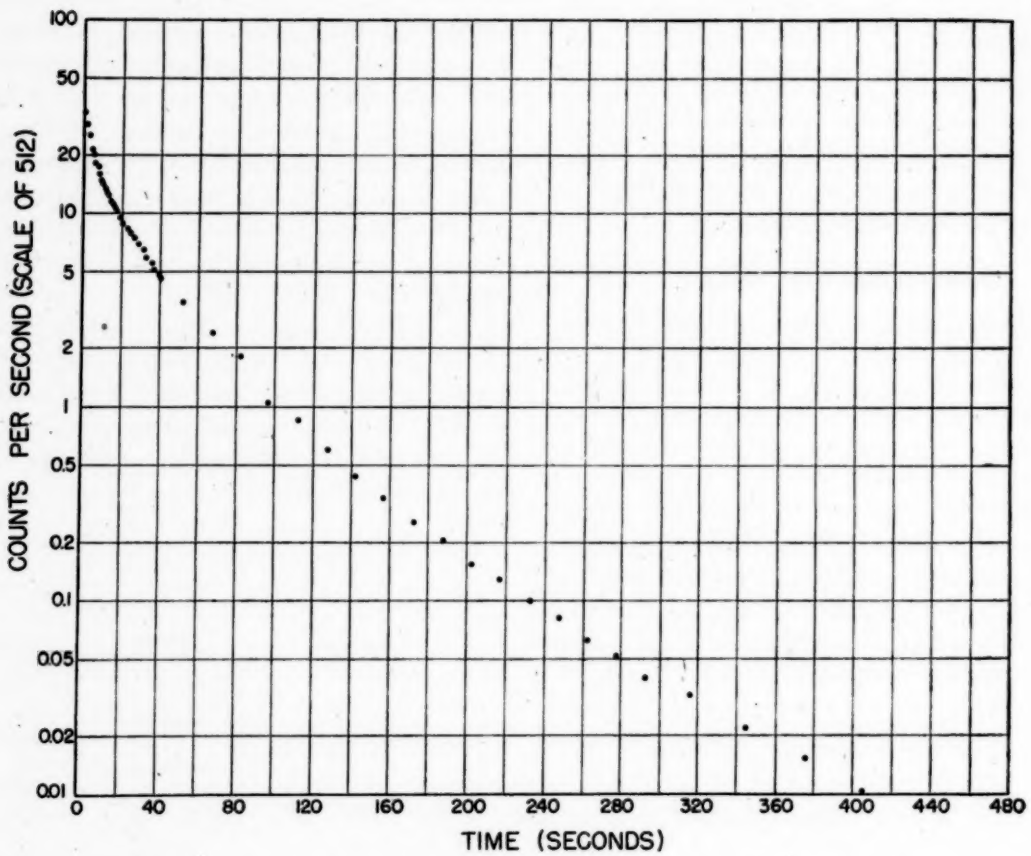

FIG. 2. Delayed neutron from Pu^{239} plotted against time after end of irradiation. The irradiation time was long compared to all of the periods.

[3] Our thanks are due the members of the Los Alamos Electronics Group and particularly to Matthew Sands for designing and building much of the equipment. Mr. J. W. Starner very kindly assisted in operating the "water boiler."

TABLE I. Relative numbers of counts from Pu^{239} and U^{235}.

Run No.	(U^{235}) Total counts minus background	(Pu^{239}) Total counts minus background
5-second runs		
1	1073×32	440×32
7	1062×32	528×32
8	441×32	214×32
9	475×32	207×32
10	396×32	201×32
Total counts	3447×32	1590×32
Ratio = x(5 seconds) = 0.46±0.07		
2-second runs		
3	1216×32	608×32
4	999×32	658×32
5	1152×32	662×32
6	1220×32	597×32
Total counts	4587×32	2525×32
Ratio = x(2 seconds) = 0.55±0.08		

times along the decay curve without sacrificing statistics. This recording instrument served to register the early portion of the decay curve, since it ran for only three minutes. From 15 seconds to 10 minutes after counting started the readings on the mechanical register and interpolation lights were directly observed at 15-second intervals.

3. RESULTS

A. Determination of Relative Fraction

Table I shows the experimental results obtained. Runs were performed at varying neutron intensity. However, the intensity was kept constant during any one run. In no case did the background exceed 10 percent of the total count. Errors indicated are conservative guesses based on the largest deviation observed.

The quantity of primary physical interest in this experiment is the ratio R of the relative number of delayed neutrons in Pu^{239} to that in U^{235}:

$$R=[\bar{\nu}_d(\mathrm{Pu})/\bar{\nu}(\mathrm{Pu})]/[\bar{\nu}_d(\mathrm{U})/\bar{\nu}(\mathrm{U})], \quad (1)$$

where $\bar{\nu}$ is the average total number of neutrons emitted per fission, and $\bar{\nu}_d$ is the average number of neutrons per fission which are emitted delayed. The quantity measured directly is x, the ratio of the number of delayed neutrons from the Pu^{239} sample to that from the U^{235} sample.

TABLE II. Intensities and periods of delayed neutrons.

Data of Fig. 2		Data of Redman and Saxon			
Pu^{239}		U^{235}		Pu^{239}	
A_i	τ_i	A_i	τ_i	A_i	τ_i
0.040	79.6 sec.	0.036	79.4 sec.	0.032	78.7 sec.
0.288	32.5	0.240	32.5	0.293	32.4
0.371	7.5	0.327	6.4	0.323	6.5
0.301	1.6	0.397	1.6	0.352	1.5

Since the samples were thick for thermal neutrons the relative areas essentially determined the relative number of neutrons absorbed. From the known areas and cross sections of the samples used, we derived the following relationship:

$$R=0.859x, \quad (2)$$

and hence

$$R\ (2\ \text{seconds})=0.47\pm0.07$$
$$R\ (5\ \text{seconds})=0.40\pm0.06.$$

It is believed that no conclusion is to be drawn from the difference of the results from the two- and five-second runs, although if the data were taken at face value one might conclude that there are more short period delayed neutrons from Pu^{239} than from U^{235}.

B. Shape of the Delay Curve

Figure 2 shows the delayed-neutron decay curve of Pu^{239} as obtained from the composite data of 2 runs.

Table II shows an analysis of this curve in terms of periods (e-folding time), τ_i, and initial activities, A_i. As a comparison, the data of Redman and Saxon for both Pu^{239} and U^{235} are given.[2] Because of the great difficulties in measuring short periods by both their methods and ours, the discrepancies between the three sets of data are not to be taken too seriously.[4]

[4] Since the time of this work the 1.6-second period in U^{235} has been resolved into two periods of ~0.5 and ~2.5 seconds (paper by the authors being prepared for publication, as well as unpublished work of D. J. Hughes *et al.* See also reference 1). This makes it not unlikely that the 1.6-second period in Pu^{239} is really a superposition of the same two periods.

Delayed Neutrons in Plutonium and Uranium Fission

W. C. REDMAN* AND D. SAXON
*Argonne Laboratory, University of Chicago, Chicago, Illinois***

(Received June 19, 1947)

Samples of Pu^{239} and U, enriched in the 235-isotope, were irradiated in the graphite pile at Argonne. The decay of the delayed neutrons following fission was recorded on a magnetic wire recorder. Analysis of the decay data, 18 runs with Pu^{239}, and 37 with U, gave the following expression for the decay curves:

$$A_t = C_{Pu}(1.2e^{-0.660t}+1.1e^{-0.154t}+1.0e^{-0.0309t}+0.10e^{-0.0127t}),$$

for Pu^{239}, and:

$$A_t = C_U(1.65e^{-0.613t}+1.36e^{-0.156t}+1.00e^{-0.0308t}+0.15e^{-0.0126t}),$$ for U^{235},

when all the periods are irradiated to saturation.

Within the limits of experimental error, the half-lives for Pu^{239} and U^{235} are identical, namely:

(55.0±0.4) sec., (22.5±0.3) sec., (4.45±0.15) sec., and (1.10±0.06) sec.

The error limits given were determined from the internal consistency of the various values of the periods, not from the statistical fluctuations in the counting procedure.

The change in the yield of the 55.0-sec. period relative to that of the 22.45-sec. period, in going from U^{235} to Pu^{239}, is of the proper sign but small in magnitude as compared to the change predicted from the fission yields for the known mass numbers of these delayed-neutron emitters. A comparison of the relative number of delayed neutrons per fission gives the ratio of the number from Pu^{239} to the number from U^{235} as 0.5.

1. INTRODUCTION

THIS study of delayed neutrons emitted from fission fragments was undertaken to determine the decay curve associated with Pu^{239} and to verify the reported values for U^{235}.

Previous work[1] gave the following analysis for the delayed neutrons from U^{235}:

$$A_t = C_U(1.2e^{-0.28t}+1.2e^{-0.099t}+1.0e^{-0.029t}+0.135e^{-0.012t}),$$

with the 57- and 24-sec. periods admittedly more accurate than the 7 and 2.5 sec. ones. Subsequent work[2] resulted in the following analysis, the result of a one-second irradiation to better resolve the shorter periods:

$$A_t = C_U(2.37e^{-1.38t}+1.67e^{-0.154t}+1.00e^{-0.030t}+0.083e^{-0.014t}),$$

representing periods of 50, 23, 4.5, and 0.5 seconds.

* Now at the Sloane Laboratory, Yale University.

** This document is based on work performed in 1944 (project publication on November 4, 1944) under Contract No. W-7405-eng-39 for the Manhattan Project, and the information covered here will appear in Division IV of the Manhattan Project Technical Series, as part of the contribution of the Argonne National Laboratory.

[1] A. H. Snell, A. V. Nedzel, and H. W. Ibser, C-81, May 16, 1942. *C*-numbers refer to reports in project files; unless otherwise indicated, they have not as yet been published elsewhere. Such references are included to indicate appropriate credit and chronology. See H. D. Smyth, Rev. Mod. Phys. 17, 459 (1945).

[2] A. H. Snell, M. B. Sampson, and J. S. Levinger, CP-1014, Oct. 28, 1943.

2. EXPERIMENTAL PROCEDURE

a. The Apparatus

Figure 1 indicates the experimental arrangement near the pile. A BF_3 proportional counter was mounted in a paraffin block 18×24×24 inches. The source was placed in an 8-in. lead cube, in such a position that there were 4 in. of lead between the source and BF_3 counter. Also, between the lead and counter there were 2 in. of paraffin. The lead served to reduce the intense γ-ray background, the paraffin to thermalize the neutrons for more efficient counting. An Armour (G.E.) magnetic wire recorder was used in determining the decay curves. It afforded two conveniences. In recording the scaler pulses, it made a permanent recording which could be used immediately for reduction; this is a distinct advantage over the photographic method of recording. Also, the record could be replayed at half-speed; this increased the accuracy in measuring the time interval between pulses.

The sources used in this experiment were contained in air-tight aluminum cylinders, one inch in diameter and height. The sample of U was considerably enriched in the 235-isotope.

b. The Taking of Data

The samples were irradiated in the graphite pile, five feet from the inner edge of the concrete

shield. For high intensity, long duration runs to determine the longer periods, the apparatus was set up about 40 yards from the pile and shielded from it by a number of concrete walls in order to reduce the background.

For measurement of the shorter periods, the apparatus was placed beside the pile as shown in Fig. 1. The samples were withdrawn from the pile by means of a falling-weight pulley system and guided through a bent aluminum pipe to their final position in the counting geometry. The bend in the aluminum guide pipe was necessary in order to shield the counting geometry from the intense radiation coming out of the hole used for irradiating the samples. Initially the sample was withdrawn in 1.0 sec. By allowing an initial free fall of the weight, this time was later reduced substantially, to 0.6 sec.

The scaler pulses, which usually operate a mechanical recorder, were recorded instead, on the magnetic wire apparatus. The sample was in counting position when the weight hit the floor, at which moment the scaler was started. In order to eliminate the neutron background and possible γ-ray effects, runs were taken with, and without, a cadmium shield covering the counter, and backgrounds for each case. The net curve was then the result of the subtractions.

[(Run without Cd) − (background without Cd)]
−[(Run with Cd) − (background with Cd)]

TABLE I. Longest period.

Date	Relative intensity	U^{235} Irradiation time	Half-life
5/19/44	1.00	6 min.	57.5 sec.
5/20/44	2.00	6	54.0
5/20/44	1.00	6	55.4
5/20/44	1.00	6	55.0
5/22/44	2.00	6	54.0
5/27/44	2.94	3	55.0
		Weighted mean:	55.1 sec.

Date	Relative intensity	Pu^{239} Irradiation time	Half-life
5/23/44	1.50	5	51.9
5/23/44	2.00	6	56.0
5/23/44	1.50	5	55.5
5/24/44	1.50	5	54.7
5/24/44	1.50	5	55.5
5/24/44	2.00	6	51.2
5/25/44	5.00	3	58.0
5/27/44	5.00	3	55.0
5/29/44	5.00	3	54.9
		Weighted mean:	54.9 sec.
		Deviation: $d/n^{\frac{1}{2}}=0.4$ sec.	

The cadmium correction was always less than 1.0 percent of the run without cadmium.

After the decay curves were recorded, the rate of decay was obtained by measurement of the time between successive recorded scaler pulses (or groups of pulses) with a 0.1-sec. stopwatch. The stopwatch was started with the first pulse, and the time noted for each succeeding pulse. Usually this replaying of the recorded data was made at half-speed to increase the accuracy of the timing procedure. In recording,

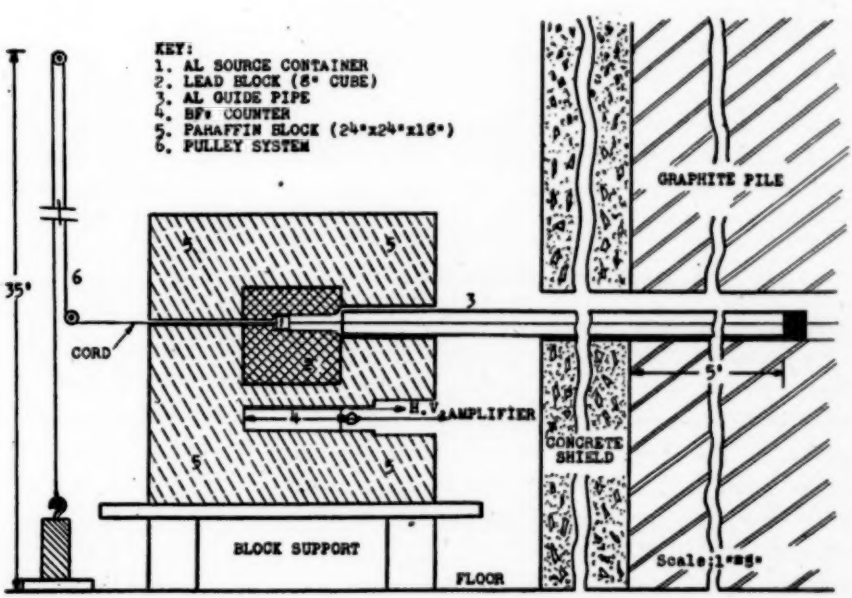

FIG. 1. Geometry of the apparatus for the measurement of the delayed neutrons (cross-sectional side view).

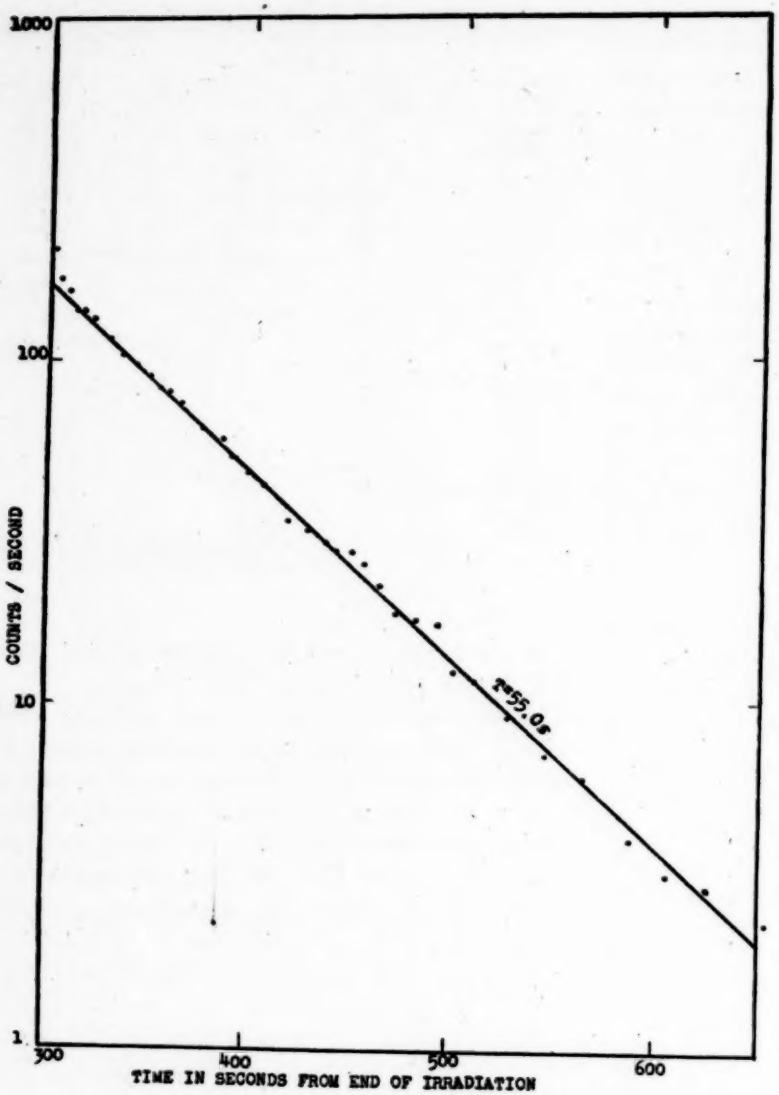

FIG. 2. Delayed neutrons from Pu^{239} (longest period only, with 3-min. irradation).

variable scaling was used to smooth out statistical fluctuations. Two independent reductions of each set of data were made, and any variation in results was re-examined.

3. DATA AND RESULTS

In these irradiations the intensity was varied by a factor of 1670 and the length of irradiation from two seconds to six minutes. The long and intense neutron bombardments were used in the study of the longer periods. For the longest period, counting was begun five to six minutes after removing the source from the pile in order that the contribution of the next longest period be less than 2 percent. (At $t=357$ sec. the contribution is 1 percent.) The data for one of these long period measurements are shown in Fig. 2, and the results for fifteen such runs are listed in Table I.

From these data the value of 55.0 sec. for the longest half-life was obtained and used in later reductions of the decay curves for determining the shorter periods. A second set of runs was made to determine the 22.5-sec. half-life. In these measurements the recorder was started 30 to 90 sec. after the end of irradiation. The medium intensity, shorter time irradiations were used to study the relative neutron yield of the various periods (Fig. 3 shows such a curve for Pu^{239}) and the least intense, shortest irradiations,

TABLE II. Half-lives in Pu^{239}.

Relative intensity	Irradiation time	T_1	T_2	T_3	T_4
2.5 (2 runs)	3 min.	55.0 sec.	22.2 sec.	3.9 sec.	1.07 sec.
2.5	30 sec.	55.0	20.6	4.4	1.16
2.5	13 sec.	55.0	24.3	4.5	1.03
1	1 min.	55.0	21.7	4.6	1.24
1	30 sec.	55.0	23.0	5.2	1.03
	Means:	55.0 sec.	22.5 sec.	4.5 sec.	1.10 sec.
	Deviations:	0.4 sec.	0.5 sec.	0.2 sec.	0.06 sec.

TABLE III. Saturated relative intensities for the half-lives in Pu^{239}

Relative intensities	Irradiation time	A_1	A_2	A_3	A_4
2.5	3 min.	0.101	1.00	0.955	0.78
2.5	3 min.	0.103	1.00	1.02	1.1
2.5	1 min.		1.00	1.07	1.1
2.5	30 sec.		1.00	1.06	1.6
1	1 min.		1.00	1.37	1.53
1	30 sec.		1.00	1.13	1.28
	Means:	0.10	1.00	1.09	1.2
	Deviations:	0.001		0.04	0.1
	Periods:	55.0 sec.	22.4 sec.	4.5 sec.	1.05 sec.

with the counting apparatus close by the pile, were used to best resolve the shortest periods.

Two methods were used in reducing the plotted decay curves. At first each run was reduced separately by the logarithmic "peeling off" process. Later, identical runs were made in groups of four or five, the curves plotted separately, and then the individual curves summed together. This composite curve was then used to determine the periods, again by the logarithmic "peeling off" procedure. The final results for the shorter periods are, for the most part, based on composite reductions. Such a reduction is shown in Fig. 4. The curve tailing off into a 22.4-second period is the sum of 9 individual curves after the 55.0-second half-life has been subtracted from each.

Because the Pu^{239} sample was available for only a short time, only nine runs were made on the short periods of Pu^{239}. Six of these runs were reduced individually, and the results are listed in Table II. The 55.0-sec. period was used with each. Next, the nine curves were added together and reduced compositely after applying to each the correction for the resolution time of the counting apparatus. The 55.0-sec. period was subtracted from each curve, and the curves were then added. From this composite curve the next period was determined and this value subtracted from the separate curves. The process was con-

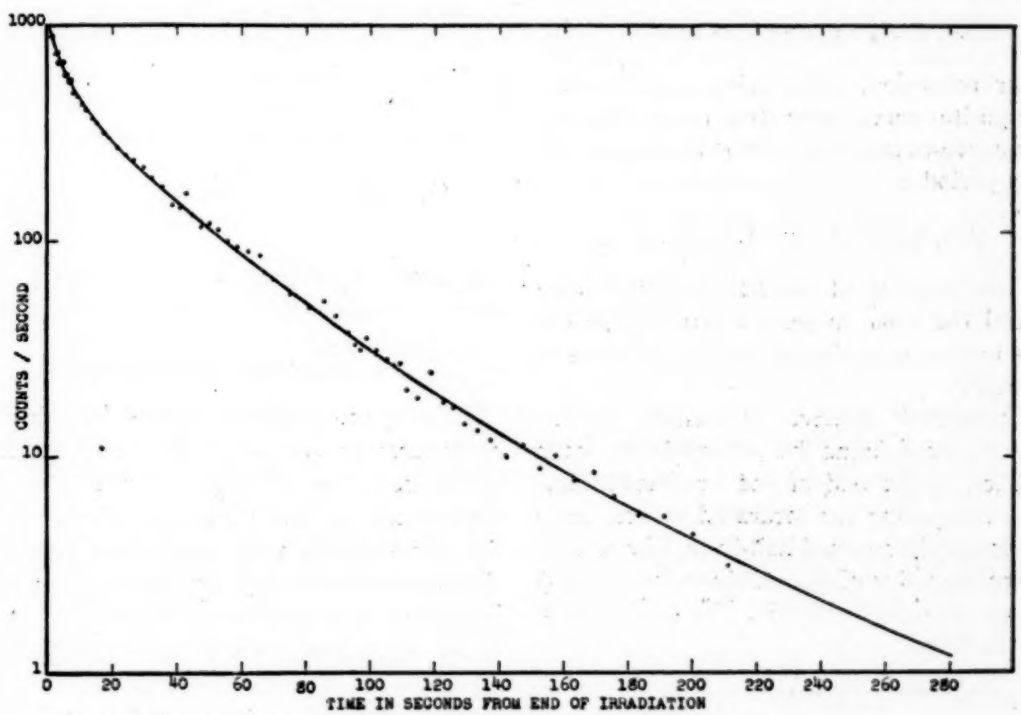

FIG. 3. Delayed neutrons from Pu^{239} (all periods present, 3-min. irradiation).

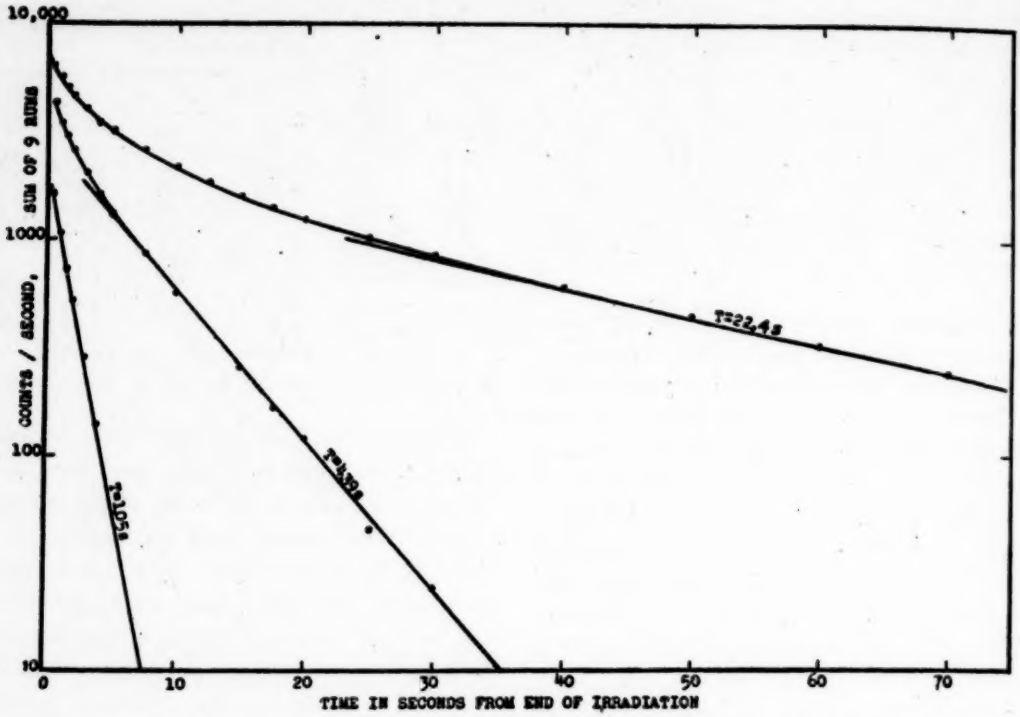

FIG. 4. Delayed neutrons from Pu^{239} (composite of 9 runs, showing the peeling-off procedure).

tinued until the final period was obtained. The resulting periods were:

55.0, 22.4, 4.6, and 1.04 sec.

A further reduction, subtracting periods from the composite curve only (no return to the separate curve to subtract each period) gave the following periods:

55.0, 22.4, 4.4, and 1.05 sec.

This last method of reduction should have introduced the least subjective error, since the data are treated a minimum number of times in this method.

The saturated relative intensities of the periods, A_i were found by extrapolating each period back to the end of the irradiation time and then computing the saturated values, using the previously determined half-lives. The results, relative to the value of $A_2=1.00$ for the 22.4-sec. period, are given in Table III. The final expression for Pu^{239} is:

$$A_t = C_{Pu}(1.2e^{-0.660t}+1.1e^{-0.154t} +1.0e^{-0.309}+0.10e^{-0.127t}).$$

Data on the shorter half-lives of U^{235} is more complete, since the U^{235} sample was available for a longer time. In Table IV are listed the values resulting from various reductions of 31 runs on U^{235}. For the most part, the various groups have been reduced compositely. The results for U^{235} are summarized in the expression:

$$A_t = C_U(1.65e^{-0.613t}+1.36e^{-0.156t} +1.00e^{-.0308t}+0.15e^{-0.0126t}).$$

The value of the constant C_U, the total delayed neutron yield for U^{235}, has been determined also.[3]

4. DISCUSSION OF RESULTS

In using the graphical method for reducing the gross decay curves, subjective errors are certainly introduced. For the values of the half-lives, as determined by the various methods for Pu^{239}, the agreement is very good. This internal consistency indicates that the composite method of reduction has adequately exploited the gross decay data. For a significant reduction of the

[3] D. E. Nagle, W. C. Redman, and D. Saxon, CP-2317, November 4, 1944.

errors, the statistics in the counting procedure itself must be improved.

One limitation of the experiment has been the resolving time of the counter system. This has been measured as 105 microseconds and corrected for, but the large magnitude of the corrections means that good resolution in the early part of the curve and statistical accuracy in the latter part were incompatible. Some of the Pu^{239} runs, in particular, have from 5 to 15 percent corrections in the early part of the curve; the early points on the U^{235} curves have corrections of the order of 5 percent. The apparatus was improved[4] and the resolving time decreased, but the Pu^{239} sample was not available for further measurements at that time.

Another shortcoming was the time required for removal of the irradiated source from the pile to the counting geometry. At first 1.0 seconds was required; later this value was reduced to 0.6 seconds. This removal time made detection of any half-life less than 0.5 seconds very difficult. It might be noted that recent reported values[5] substitute 1.8- and 0.44-second periods in place of the 1.10 second period. The longer periods are in good agreement with those reported here, but the removal time in this experiment prevented a confirmation of the shortest reported value.

These results indicate that the periods from both Pu^{239} and U^{235} are identical; hence, in all likelihood they are associated with the same fission fragments. A combination of the values of the half-lives for Pu^{239} and U^{235} gives:

(55.0 ± 0.4) sec., (22.5 ± 0.3) sec.,
(4.45 ± 0.15) sec., and (1.10 ± 0.06) sec.

The error limits given are those determined from the internal consistency of the various values of the periods, not from the statistical fluctuations in the counting procedure.

The chemical isolation of the two longest delayed-neutron periods,[6] together with the fission product yields of the associated mass numbers, leads one to expect a change in the delayed-neutron yield ratio of the two longest periods in going from U^{235} to Pu^{239}. The observed change in the yield of the 55.0-sec. period relative to that for the 22.5-sec. period has the proper sign but is smaller in magnitude than expected.

An approximate comparison of the relative number of delayed neutrons per fission for the two samples gives the ratio of the number from Pu^{239} to that from U^{235} as 0.5.

TABLE IV. Half-lives and saturated relative intensities for U^{235}.

T_1	A_1	T_2	A_2	T_3	A_3	T_4	A_4
6/13/44—4 runs, 3-min. irradiation							
55.0 sec.	0.153	23.8 sec.	1.00				
55.0	0.142	21.2	1.00	4.55 sec.	1.34	1.23 sec.	1.81
6/22/44—4 runs, 3-min. irradiation							
55.0	0.156	23.8	1.00	4.9	1.76		
55.0	0.146	21.2	1.00	4.43	1.33		
55.0	0.160	23.8	1.00				
6/23/44—5 runs, 3-min. irradiation							
55.0	0.171	23.6	1.00				
55.0	0.136	21.0	1.00	4.0	1.33		
55.0	0.120	22.0	1.00	5.35	1.42	0.92	2.36
6/29/44—4 runs, 3-min. irradiation							
55.0	0.133	21.5	1.00				
7/4/44—4 runs, 5-sec. irradiation							
		24.0	1.00	3.53	1.22	0.7	1.46
		22.4	1.00	4.0	1.38	1.08	0.95
		21.8	1.00	4.4	1.36	1.15	1.54
		22.0	1.00	4.1	1.38	0.97	1.57
		23.2	1.00	4.25	1.43	0.98	1.59
7/17/44—6 runs, 12-sec. irradiation							
		21.6	1.00	4.75	1.36	1.1	2.08
		23.0	1.00	4.7	1.34	1.5	1.47
		22.0	1.00	4.65	1.18	1.6	1.48
7/17/44—4 runs, 3-sec. irradiation							
		22.5	1.00	4.45	1.14	1.20	1.85
Means:							
55.0 sec.	0.146	22.47 sec.	1.00	4.43 sec.	1.36	1.13 sec.	1.65
Deviations:							
0.4 sec.	0.004	0.2 sec.		0.1 sec.	0.02	0.06 sec.	0.08

ACKNOWLEDGMENT

The authors wish to thank L. W. Alvarez for initial encouragement in the work, and H. L. Anderson and D. E. Nagle for helpful advice towards its completion.

[4] D. E. Nagle and D. Saxon, Monthly Report for October, 1944, CP-2301, November 4, 1944.
[5] M. T. Sampson and A. H. Snell, Monthly Report for July, 1944, CP-1934, August 3, 1944.
[6] A. H. Snell, J. S. Levinger, R. G. Wilkinson, E. P. Meiners, and M. B. Sampson, CP-1967, July 29, 1944. See Phys. Rev. 70, 111 (1946).

The Scattering of Slow Neutrons by Bound Protons. III. Intermediate Energies

P. R. ZILSEL, B. T. DARLING, AND G. BREIT
Yale University, New Haven, Connecticut*

(Received June 23, 1947)

The calculation of the cross section for scattering of neutrons by elastically bound protons is extended to energies up to the first excited state. As in the preceding papers the results are expressed in terms of a correction factor to be applied to Fermi's approximation. This factor [Eq. (5)] has been evaluated for a number of energies and angles of scattering. In all cases the correction is small and of the order 0.3 percent or less.

1. INTRODUCTION AND NOTATION

A PREVIOUSLY developed method[1] was applied in a preceding paper (II)[2] to calculate the scattering cross section for neutrons of zero energy from protons bound in molecules by simple harmonic oscillator forces. This calculation is extended in the present paper to neutrons of energy greater than zero but not sufficient to excite a molecular level. The calculation is carried out in detail only for isotropic molecular binding of the protons.

As in II, the results are expressed in the form of a correction to Fermi's approximation[3] which is found to be accurate to within a few tenths of a percent of the final result.

The notation is as in I and II; some of the most frequently used symbols are:

E = total energy,
$\mathbf{r}_\pi$ = proton coordinates; $\mathbf{r}_\nu$ = neutron coordinates,
$\mathbf{r}=\mathbf{r}_\nu-\mathbf{r}_\pi$ = relative coordinates,
a = intercept of r times radial wave function of neutron-proton relative motion,
E_n = energy of proton in a molecule in nth excited state.

For elastic binding

$$E_n=(\hbar^2/2M)\sum_{x,y,z}(2n_x+1)/\alpha_x^2,$$

where α_x, α_y, α_z = elastic binding constants,

$u_n(\mathbf{r}_\pi)$ = characteristic function of proton in state E_n,

$\kappa_s^2=(2M/\hbar^2)(E-E_s)$,
$q_x=\exp(-2\tau/\alpha_x^2)$ etc., $4T_x=4\tau+\alpha_x^2(1-q_x^2)$, etc.

The following new symbols are introduced:

$N=\pi^{-\frac{1}{2}}(\alpha_x\alpha_y\alpha_z)^{-\frac{1}{2}}$; $4S_x=4\tau+\alpha_x^2$, etc.,
$\epsilon=\frac{1}{2}\kappa_0^2\alpha^2=(E-E_0)/(E_1-E_0)$ = energy of incident neutron in units of molecular-level spacing,
θ = scattering angle, $\delta=\sin^2\frac{1}{2}\theta$.

The harmonic-oscillator potential energy representing the binding of the proton in the molecule is given by Eq. (II, 1) and the corresponding proton eigenfunctions by Eq. (II, 1.3). The complete wave function of the system is written in Eq. (I, 6) as the sum of the incident wave ψ_0 plus a modification representing the effect of the proton-neutron interaction. The latter term is expressed in the form of a generalized Green's function-type integral giving diverging neutron waves at large $|\mathbf{r}_\nu|$. The "source distribution" $f(\mathbf{r}_\pi)$ is given by the integral equation (I, 5), (I, 5′); in first approximation it is equal to $\psi_0(\mathbf{r}_\pi, \mathbf{r}_\pi)$. This approximation leads to Fermi's[3] results. The second approximation is obtained by iteration, that is, by evaluating the "background" $B(\mathbf{r}_\pi, \mathbf{r}_\nu)$ defined in Eq. (I, 5′) by using the first approximation for f.

2. EVALUATION OF THE BACKGROUND

As in II the background $B(\mathbf{r}_\pi, \mathbf{r}_\nu)$ defined by (I, 5′) can be evaluated by use of the transformation (I, 8.8), (I, 8.9) which expresses the kernel in the integral representation of the wave function as an infinite integral over the dummy variable τ. The transformation function F, occurring in (I, 8.8), is defined by (I, 8.6) and given in the case of harmonic binding by (II, 3). For the present calculation, with $E_0<E<E_1$, one must

* Assisted by Contract N6ori-44, Task Order XVI of the Office of Naval Research.

[1] G. Breit, Phys. Rev. **71**, 215 (1947).

[2] G. Breit and P. R. Zilsel, Phys. Rev. **71**, 232 (1947). References 1 and 2 will be referred to as I and II, respectively, in the text. Formulas occurring in these papers will be referred to by prefixing the roman numeral I or II ahead of the number of the formula.

[3] Enrico Fermi, Ricerca Scient. **7-2**, 15 (1936).

set $\sigma=0$ in (I, 8.8). Using the integral representation (I, 8.9′) for $1/r$ one obtains[4]

$$\sum_0^\infty u_s(\mathbf{r}_\tau)u_s^*(\mathbf{r}')\{2\exp(i\kappa_s|\mathbf{r}_\nu-\mathbf{r}'|)-1\}|\mathbf{r}_\nu-\mathbf{r}'|^{-1}$$
$$=\pi^{-\frac{1}{2}}\int_0^\infty N^2\tau^{-\frac{1}{2}}\exp(-|\mathbf{r}_\nu-\mathbf{r}'|^2/4\tau)$$
$$\times\Big\{\exp(\kappa_0^2\tau)\Big[-\exp\{-(\rho_\tau^2+\rho'^2)/2\}$$
$$+\Pi(1-q_z^2)^{-\frac{1}{2}}\exp\{-(\xi_\tau^2+\xi'^2)(1+q_z^2)/[2(1-q_z^2)]+2\xi_\tau\xi' q_z/(1-q_z^2)\}\Big]$$
$$-\tfrac{1}{2}\delta(\mathbf{r}_\tau-\mathbf{r}')\Big\}d\tau+2N^2|\mathbf{r}_\nu-\mathbf{r}'|^{-1}$$
$$\times\exp\{-\tfrac{1}{2}(\rho_\tau^2+\rho'^2)+i\kappa_0|\mathbf{r}_\nu-\mathbf{r}'|\}, \quad (1)$$

where

$$N=\pi^{-\frac{1}{4}}(\alpha_x\alpha_y\alpha_z)^{-\frac{1}{2}}.$$

Substituting (1) into the expression (I, 5′) for the background with the approximation

$$f(\mathbf{r})\cong\psi_0(\mathbf{r},\mathbf{r})=N\exp(i\kappa_0 z-\rho^2/2), \quad (1.1)$$

one obtains on carrying out the integration over $d\mathbf{r}'$ and letting $\mathbf{r}_\nu\to\mathbf{r}_\tau$

$$B(\mathbf{r}_\tau,\mathbf{r}_\tau)=B_1(\mathbf{r}_\tau)+B_2(\mathbf{r}_\tau) \quad (2)$$

with

$$B_1(\mathbf{r})=\pi^{-\frac{1}{2}}\psi_0(\mathbf{r},\mathbf{r})\int_0^\infty\Big\{-\exp\{(\kappa_0^2\tau^2-i\kappa_0\tau z)S_z^{-1}\}$$
$$\times\Pi\tau^{\frac{1}{2}}S_x^{-\frac{1}{2}}\exp(-x^2/4S_x)$$
$$+\exp\{[\kappa_0^2\tau^2-i\kappa_0\tau z(1-q_z)]T_z^{-1}\}$$
$$\times\Pi\exp\{-x^2(1-q_x)^2/4T_x\}\tau^{\frac{1}{2}}$$
$$\times T_z^{-\frac{1}{2}}-2^{-\frac{1}{2}}\Big\}\tau^{-\frac{1}{2}}d\tau, \quad (2.1)$$

and

$$B_2(\mathbf{r})=2N^2\int|\mathbf{r}-\mathbf{r}'|^{-1}\exp\{-\rho^2/2-\rho'^2+i\kappa_0 z'+i\kappa_0|\mathbf{r}-\mathbf{r}'|\}d\mathbf{r}'. \quad (2.2)$$

In Eq. (2.1)

$4S_x=4\tau+\alpha_x^2$, etc.; $4T_x=4\tau+\alpha_x^2(1-q_x^2)$, etc.

Equation (2.2) has been left in the form of an integral over $d\mathbf{r}'$, since it will be used in this form later. For $\kappa_0^2=0$, $(E=E_0)$, Eq. (2) reduces to the form (II, 3.2).

[4] The symbol II stands for the product over x, y, z throughout.

3. THE SCATTERING CROSS SECTION

By Eq. (I, 6) the wave function is

$$\psi(\mathbf{r}_\tau\mathbf{r}_\nu)=\psi_0(\mathbf{r}_\tau,\mathbf{r}_\nu)+2a\sum_s u_s(\mathbf{r}_\tau)\times\int u_s^*(\mathbf{r}')f(\mathbf{r}')|\mathbf{r}_\nu-\mathbf{r}'|^{-1}\times\exp(i\kappa_s|\mathbf{r}_\nu-\mathbf{r}'|)d\mathbf{r}' \quad (3)$$

with

$$f(\mathbf{r})\simeq\psi_0(\mathbf{r},\mathbf{r})+aB(\mathbf{r},\mathbf{r}). \quad (3.1)$$

In the present case, where $E_0<E<E_1$, all the κ_s except κ_0 are imaginary and give attenuated waves in the summation in Eq. (3). Only the term in κ_0 gives a diverging wave so that the scattered wave is

$$\psi_S=2au_0(\mathbf{r}_\tau)\int u_0^*(\mathbf{r}')f(\mathbf{r}')|\mathbf{r}_\nu-\mathbf{r}'|^{-1}\times\exp(i\kappa_0|\mathbf{r}_\nu-\mathbf{r}'|)d\mathbf{r}'. \quad (3.2)$$

At large r_ν, since $|\mathbf{r}_\nu-\mathbf{r}'|\simeq r_\nu-(\mathbf{r}'\cdot\mathbf{1}_\omega)$, with $\mathbf{1}_\omega=\mathbf{r}_\nu/r_\nu$, this becomes

$$\psi_S\simeq 2au_0(\mathbf{r}_\tau)\Big\{\int u_0^*(\mathbf{r}')f(\mathbf{r}')\exp[-i\kappa_0(\mathbf{r}'\cdot\mathbf{1}_\omega)]d\mathbf{r}'\Big\}\times[\exp(i\kappa_0 r_\nu)]r_\nu^{-1}. \quad (3.3)$$

The differential scattering cross section is

$$\sigma_\omega=r_\nu^2\int|\psi_S|^2d\mathbf{r}_\tau$$
$$\simeq 4a^2\left|\int u_0(\mathbf{r}')f(\mathbf{r}')\exp[-i\kappa_0(\mathbf{r}'\cdot\mathbf{1}_\omega)]d\mathbf{r}'\right|^2, \quad (3.4)$$

where $\mathbf{1}_\omega$ is the unit vector in the direction of the scattered neutron.

Substitution of (3.1) into (3.4) gives

$$\sigma_\omega\simeq\sigma_\omega^0\Big[1+2aR\Big\{\int u_0^*(\mathbf{r})B(\mathbf{r},\mathbf{r})\times\exp[-i\kappa_0(\mathbf{r}\cdot\mathbf{1}_\omega)]d\mathbf{r}\Big/\int|u_0(\mathbf{r})|^2\times\exp[-i\kappa_0\mathbf{r}\cdot(\mathbf{1}_z-\mathbf{1}_\omega)]d\mathbf{r}\Big\}\Big], \quad (4)$$

with $R\{\ \}$ denoting the real part of $\{\ \}$ and

$$\sigma_\omega^0=4a^2\left|\int|u_0(\mathbf{r})|^2\exp[-i\kappa_0\mathbf{r}(\mathbf{1}_z-\mathbf{1}_\omega)]d\mathbf{r}\right|^2. \quad (4.1)$$

σ_ω^0 is Fermi's approximation to which the bracket on the right side of Eq. (4) is a correction factor.

As in II, corrections in higher powers of the intercept a have been neglected.

The remainder of the calculation is carried out only for isotropic harmonic binding of the proton in the molecule, that is, for $\alpha_x=\alpha_y=\alpha_z=\alpha$. In this case Eq. (2.1) reduces to

$$B_1(\mathbf{r})=\pi^{-\frac{1}{2}}\psi_0(\mathbf{r},\mathbf{r})\int_0^\infty\Big\{-\exp\{(\kappa_0^2\tau^2-i\kappa_0\tau z)S^{-1}\}\times\tau^{\frac{1}{2}}S^{-\frac{1}{2}}\exp(-r^2/4S)+\exp\{[\kappa_0^2\tau^2-i\kappa_0\tau z(1-q)]T^{-1}\}\tau^{\frac{1}{2}}T^{-\frac{1}{2}}\times\exp\{-r^2(1-q)^2/4T\}-2^{-\frac{1}{2}}\Big\}\tau^{-\frac{1}{2}}d\tau. \quad (2.1')$$

S, T are obtained from S_z, T_z by omission of the subscript x from α_x and q_x.

When the integrals over $d\mathbf{r}$ occurring in Eq. (4) are evaluated by the method indicated in the Appendix, one obtains, setting $2\tau/\alpha^2=x$,

$$\int u_0^*(\mathbf{r})B_1(\mathbf{r})\exp[-i\kappa_0(\mathbf{r}\cdot\mathbf{1}_\omega)]d\mathbf{r}=(2/\pi)^{\frac{1}{2}}\alpha^{-1}\int_0^\infty\Big\{-(x+1)^{-\frac{1}{2}}\exp\{\epsilon(x^2-\delta)/(x+1)\}+(x+1-q)^{-\frac{1}{2}}\times\exp\{\epsilon[x^2-(2xq+1-q^2)\delta]/(x+1-q)\}-(2x)^{-\frac{1}{2}}e^{-2\epsilon\delta}\Big\}dx, \quad (4.2)$$

where

$$\epsilon=\tfrac{1}{2}\kappa_0^2\alpha^2=(E-E_0)/(E_1-E_0), \quad (4.3)$$

$q=e^{-x}$, and $\delta=\sin^2(\theta/2)$ with $\theta=$ scattering angle, that is the angle $(\mathbf{1}_z,\mathbf{1}_\omega)$; note that $0\leq\epsilon\leq1$. Similarly

$$\int u_0^*(\mathbf{r})B_2(\mathbf{r})\exp[-i\kappa_0(\mathbf{r}\cdot\mathbf{1}_\omega)]d\mathbf{r}=(2/\pi)^{\frac{1}{2}}\alpha^{-1}e^{-2\epsilon}[\epsilon^{\frac{1}{2}}\cos(\theta/2)]^{-1}\times\{e^{-2\epsilon\cos(\theta/2)}(I^++\pi^{\frac{1}{2}}/2i)-e^{2\epsilon\cos(\theta/2)}(I^-+\pi^{\frac{1}{2}}/2i)\} \quad (4.4)$$

with

$$I^+=\int_0^{\epsilon^{\frac{1}{2}}[1+\cos(\theta/2)]}\exp(u^2)du,$$

$$I^-=\int_0^{\epsilon^{\frac{1}{2}}[1-\cos(\theta/2)]}\exp(u^2)du.$$

Also

$$\int|u_0(\mathbf{r})|^2\exp[-i\kappa_0\mathbf{r}\cdot(\mathbf{1}_z-\mathbf{1}_\omega)]d\mathbf{r}=e^{-2\epsilon\delta}. \quad (4.5)$$

One thus obtains

$$\sigma_\omega\cong\sigma_\omega{}^0\{1+2a\alpha^{-1}(\pi/2)^{-\frac{1}{2}}\times[X_1(\epsilon,\theta/2)+X_2(\epsilon,\theta/2)]\} \quad (5)$$

with

$$X_1(\epsilon,\theta/2)=\int_0^\infty\Big\{-(x+1)^{-\frac{1}{2}}\exp\{\epsilon[x^2+(2x+1)\delta]/(x+1)\}+(x+1-q)^{-\frac{1}{2}}\exp\{\epsilon[x^2+(1-q)(2x+1-q)\delta]/(x+1-q)\}-(2x)^{-\frac{1}{2}}\Big\}dx, \quad (5.1)$$

$$X_2(\epsilon,\theta/2)=[\epsilon^{\frac{1}{2}}\cos(\theta/2)]^{-1}\exp[-2\epsilon\cos^2(\theta/2)]\{\exp[-2\epsilon\cos(\theta/2)]I^+-\exp[2\epsilon\cos(\theta/2)]I^-\}, \quad (5.2)$$

and

$$\sigma_\omega{}^0=4a^2e^{-4\epsilon\delta}. \quad (5.3)$$

Equation (5.3) is identical with Fermi's equation (103) for σ_ω. For $\theta=\pi$ the expression (5.2) for X_2 is indeterminate and must be replaced by its limit

$$\lim_{\theta\to\pi}X_2(\epsilon,\theta/2)\to2e^\epsilon-4\epsilon^{\frac{1}{2}}\int_0^{\epsilon^{\frac{1}{2}}}\exp(u^2)du. \quad (5.2')$$

4. NUMERICAL EVALUATION OF THE CORRECTION FACTOR

When the right side of Eq. (5.1) is expanded in a power series in ϵ the coefficients are powers of δ multiplied by definite integrals which can be evaluated by numerical quadrature. A similar expansion of (5.2) and (5.2') gives numerical coefficients. One obtains for small ϵ

$$X_1+X_2\simeq1.030-4.892\epsilon+3.606\epsilon\delta+\cdots. \quad (6)$$

Since the power series for X_1 and X_2 do not converge rapidly, Eq. (6) is useful only for determining the behavior of σ_ω at $\epsilon\simeq0$. Expressions (5.1) and (5.2) [(5.2') for $\theta=\pi$] have therefore been evaluated by numerical quadrature for $\epsilon=0.3,\ 0.5$; $\sin^2\theta/2=0,\ 0.25,\ 0.50,\ 0.75,\ 1.00$. The results are tabulated in Table I.

TABLE I. Numerical value of the correction factor for the scattering cross section.

$\sin^2\theta/2$	$\epsilon=0.3$ X_1	X_2	X_1+X_2	$\epsilon=0.5$ X_1	X_2	X_1+X_2
0	−0.862	0.962	0.100	−0.749	0.640	−0.109
0.25	−0.843	1.052	0.209	−0.710	0.710	0.000
0.50	−0.832	1.150	0.318	−0.699	0.782	0.083
0.75	−0.829	1.254	0.425	−0.712	0.869	0.157
1	−0.831	1.368	0.537	−0.760	0.910	0.150

These values of X_1+X_2 are plotted in Figs. 1 and 2 as functions of ϵ and θ, respectively. Curves are drawn through them with the values and slopes at $\epsilon=0$ obtained from Eq. (6). The broken lines in the figure are the linear approximations by (6).

The correction factor is seen to be of the same order of magnitude for $E_0<E<E_1$ as that for $E=E_0$ which was evaluated in II. It is small because of the smallness of the factor $2a\alpha^{-1}\times(\pi/2)^{-\frac{1}{2}}$ multiplying X_1+X_2 in the expression (5) for σ_ω. For scattering of neutrons by protons bound in water molecules it is no greater than ~0.3 percent (see II, Section 4).

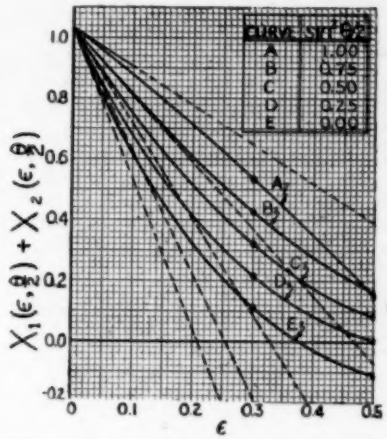

FIG. 1. Quantity X_1+X_2 of Eq. (5) as a function of the neutron energy in units of molecular-vibrational level spacing which is denoted by ϵ. To obtain correction factor to Fermi's approximation for scattering cross section the ordinate X_1+X_2 should be multiplied by $2a\alpha^{-1}(2/\pi)^{\frac{1}{2}}$ and added to unity. Solid curved lines represent X_1+X_2. The tangents to these graphs at $\epsilon=0$ represent approximation of Eq. (6) and are drawn in as broken straight lines. Curves *A*, *B*, *C*, *D*, *E* correspond respectively to such values of scattering angle θ that $\sin^2(\theta/2)=1.00$, 0.75, 0.50, 0.25, 0.00.

APPENDIX

The transformation of

$$\int u_0^*(\mathbf{r})B_1(\mathbf{r},\mathbf{r})\exp[-i\kappa_0(\mathbf{r}\cdot\mathbf{1}_\omega)]d\mathbf{r}$$

to formula (4.2) of the text can be achieved by carrying out the integrations over $d\mathbf{r}$ in appropriately chosen polar coordinates. The pole in this system of coordinates is chosen in each case in the direction of the vector which occurs in the scalar product with $\mathbf{r}$.

Thus the first summand in B_1 when multiplied by

$$u_0^*(\mathbf{r})\exp[-i\kappa_0(\mathbf{r}\cdot\mathbf{1}_\omega)]$$

and integrated with respect to $d\mathbf{r}$, may be written

$$-N^2\pi^{-\frac{1}{2}}\int_0^\infty S^{-\frac{1}{2}}\exp(\tau^2\kappa_0^2/S)\times\int\exp[-r^2/\alpha^2-r^2/4S+i\kappa_0\mathbf{r}\cdot\{(\alpha^2/4S)\mathbf{1}_z-\mathbf{1}_\omega\}]d\mathbf{r}d\tau. \quad (A1)$$

Choosing the polar axis in the direction of $\mathbf{u}=(\alpha^2/4S)\mathbf{1}_z-\mathbf{1}_\omega$ and denoting the average over the angles by $\langle\ \rangle$, one has

$$\langle\exp[i\kappa_0\mathbf{r}\cdot\{(\alpha^2/4S)\mathbf{1}_z-\mathbf{1}_\omega\}]\rangle$$
$$=\langle\exp[i\kappa_0 r\{16\tau^2+(8\tau\alpha^2+2\alpha^4)(1-\cos\theta)\}^{\frac{1}{2}}/(4S)\cdot\cos(\mathbf{r},\mathbf{u})]\rangle=[\sin(\beta r)]/\beta r,$$

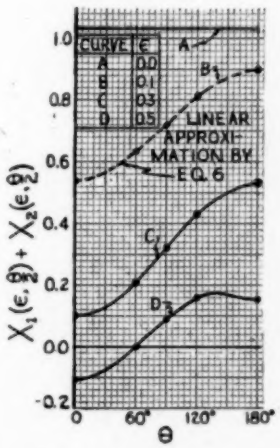

FIG. 2. Quantity X_1+X_2 of Fig. 1 and Eq. (5) as a function of the scattering angle θ. The four curves *A*, *B*, *C*, *D* correspond respectively to $\epsilon=0.0$, 0.1, 0.3, 0.5, where ϵ is the neutron energy in units of molecular-vibrational level spacing. Relation to Fermi's approximation has been explained in connection with Fig. 1.

in which (r, u) denotes the angle between r and u and

$$\beta=\kappa_0\{16\tau^2+(8\tau^2\alpha^2+2\alpha^4)(1-\cos\theta)\}^{\frac{1}{2}}/(4S).$$

The integral over $d\mathbf{r}$ in (A1) is then of the type

$$\int_0^\infty \sin(\beta r)\exp(-r^2/\gamma^2)rdr$$

$$=Im\left\{\int_0^\infty \exp(-r^2/\gamma^2+i\beta r)rdr\right\}$$

$$=Im\{(\gamma^2/2)\exp[-\beta^2\gamma^2/4+\beta^2/(4\gamma^2)]\}$$

$$+Im\left\{(i\gamma^2/2)\exp(-\beta^2\gamma^2/4)\times\int_0^\infty \exp[-(r-i\beta\gamma^2/2)/\gamma^2]dr\right\}.$$

The first term is zero. The integral of the second term may be evaluated by deforming the contour to go along the imaginary axis to $i\beta\gamma/2$ and from there to $+\infty$ along a line parallel to the real axis. The second term then gives

$$\pi^{\frac{1}{2}}(\beta\gamma^3/4)\exp(-\beta^2\gamma^2/4). \qquad \text{(A2)}$$

Using (A2) the expression (A1) becomes the first term of (4.2). Identical operations on the second and third summands give the second and third terms of (4.2).

To transform,

$$\int u_0^*(\mathbf{r}')B_2(\mathbf{r}',\mathbf{r}')\exp[-i\kappa_0(\mathbf{r}'\cdot\mathbf{1}_\omega)]d\mathbf{r}'$$

$$=2N^4\int\int \exp[-(\rho')^2-(\rho'')^2+i\kappa_0(\mathbf{r}'\cdot\mathbf{1}_z-\mathbf{r}''\cdot\mathbf{1}_\omega)+i\kappa_0|\mathbf{r}'-\mathbf{r}''|]\times|\mathbf{r}'-\mathbf{r}''|^{-1}d\mathbf{r}'d\mathbf{r}'' \qquad \text{(A3)}$$

make the change of variables,

$$\mathbf{r}=\mathbf{r}'-\mathbf{r}'', \qquad \mathbf{R}=\tfrac{1}{2}(\mathbf{r}'+\mathbf{r}'').$$

Introducing polar coordinates in each of the spaces $d\mathbf{r}$ and $d\mathbf{R}$ and averaging over the angles (A3) becomes,

$$2N^4\int_0^\infty [\sin(2\kappa_0\sin(\theta/2))R]/[2\kappa_0\sin(\theta/2)]\exp(-2R^2/\alpha^2)4\pi RdR$$

$$\cdot\int_0^\infty [\sin(\kappa_0\cos(\theta/2))r]/[\kappa_0\cos(\theta/2)]\exp[-r^2/2\alpha^2+i\kappa_0 r]\cdot 4\pi dr.$$

The first integral is of the previous type. The second integral is of the type

$$\int_0^\infty \sin\beta r\exp[-r^2/\gamma^2+i\kappa r]dr$$

$$=(\gamma/2i)\int_0^\infty \{\exp[-t^2+ir(\kappa+\beta)t]-\exp[-t^2+i\gamma(\kappa-\beta)t]\}dt,$$

where $t=r/\gamma$. Either integral may be treated similarly to the preceding case giving the final result

$$(\gamma\pi^{\frac{1}{2}}/4i)\{\exp[-\gamma^2(\kappa+\beta)^2/4]-\exp[-\gamma^2(\kappa-\beta)^2/4]\}$$
$$+(\gamma/2)\exp[-\gamma^2(\kappa+\beta)^2/4]\times\int_0^{\gamma(\kappa+\beta)/2}\exp(u^2)du$$
$$-(\gamma/2)\exp[-\gamma^2(\kappa-\beta)^2/4]\times\int_0^{\gamma(\kappa-\beta)/2}\exp(u^2)du. \qquad \text{(A4)}$$

By means of these integrals one finds that formula (A3) leads to (4.4).

Equation (4.5) is obtained by similar treatment.

Gamma-Radiation from Tantalum, Iridium, and Gold

J. M. CORK
Department of Physics, University of Michigan, Ann Arbor, Michigan
(Received June 16, 1947)

By using a photographic method in connection with semi-circular focusing magnetic spectrometers, the beta-spectra due to internal conversion have been evaluated for gold 198, iridium 194, and tantalum 182. For gold a simple spectrum of 3 lines with differences the same as between the *K-L-M* levels of mercury indicate a single gamma-ray of energy 0.408 Mev following beta-emission.

In iridium, a complicated spectrum of more than 26 lines is observed which may be identified from the *K-L-M* differences in platinum as due to 12 gamma-rays. These gamma-energies appear to fit well with a level scheme of six terms.

Tantalum yields a spectrum of about 34 lines from which about 16 gamma-rays may be derived by applying the *K-L-M* differences for tungsten. These gamma-energies fit satisfactorily on a level scheme of 9 terms.

IN preliminary reports[1] it has been shown that both tantalum and iridium yield beta-spectra with a multitude of superimposed lines due to internal conversion. In each of these cases it is now possible to associate the lines in *K*, *L*, and *M* groups and evaluate the discrete gamma-energies. It is then possible to construct energy-level schemes of relatively few terms from which the many gamma-rays may be derived by various transitions.

APPARATUS

This investigation makes use of the photographic method in magnetic spectrometers of the semi-circular focusing type. Three different instruments are in operation, one of which is excited by a stabilized electric current while the other two are of the permanent magnet type. In the latter, the "Alnico" component of the magnetic circuit is excited to any desired state by sending a momentary current through surrounding exciting coils. Figure 1 shows schematically the arrangement of the magnetic circuit.

The magnetic field is measured by an absolute method in which a rotor with commutator is driven at constant speed by a synchronous motor. The direct voltage output of the d.c. generator so formed is applied to a Leeds and Northrop K-2 potentiometer. Several spinners of this sort have been constructed with sensitivities varying from 10 to 100 microvolts per gauss. It is thus possible, with the high sensitivity of the potentiometer to measure the field very precisely provided the rotor can be driven at a constant speed.

Although some power companies do remarkably well at controlling the frequency, so that the net gain or loss in cycles over the interval of a week is negligible, sizable short-period fluctuations are impossible to avoid. To overcome this difficulty a thyrotron oscillator was constructed to drive the synchronous motors. The frequency of the output of this device is satisfactorily stable.

The radioactive samples were obtained through the Atomic Energy Commission from Oak Ridge, being produced in the pile by the (n, γ) reaction. Each specimen was mounted on a thread-like support on an aluminum frame. No metal was close to the source. The mass of the sample and support was made as small as possible, com-

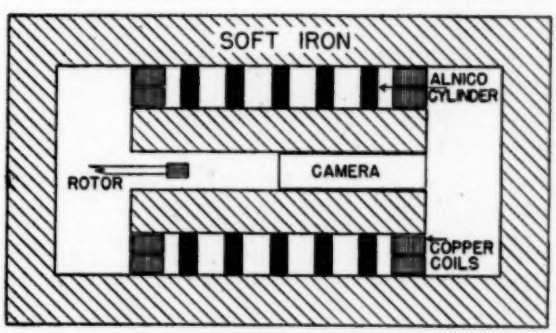

FIG. 1. Sketch of section of permanent magnet for spectrometer.

[1] J. M. Cork, R. G. Shreffler, A. D. Weaver, and F. B. Shull, Phys. Rev. 71, 467 (1947).

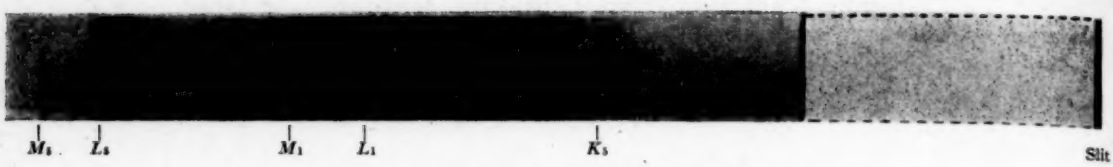

FIG. 2. Low energy portion of tantalum beta-spectrum.

patible with giving a satisfactory exposure in a reasonable time. In practice, a technique was developed in which a thin organic strip about 0.3 mm wide was uniformly coated with the sample on one side, so that the mass per cm was of the order of 0.10 mg. This geometry minimizes the broadening of the spectral lines by scattering or partial absorption in the source, and good exposures were obtained in from one to six days.

TABLE I. Gold beta-spectrum.

Observed energy	Identification	Gamma-energy
326 kev	K	406.5 kev
394 kev	L	408.4 kev
405 kev	M	408.4 kev

RESULTS

Each isotope was allowed to give several spectrograms under varied conditions. A typical plate showing a portion of the tantalum spectrum is reproduced in Fig. 2. It is apparent from the sharpness of the lines that partial energy loss within the sample is negligible. Iridium was used in the finely powdered metallic state and was not so favorable in this respect. Because of a lack of focusing in the vertical direction, the intensity of a line falls off with increased distance from the source so that a longer time is required for outlying lines.

Estimates of relative intensity can be made by covering half of the plate with an adjustable shutter during any fixed portion of the exposure.

Gold

The isotope of gold of mass 198 has been known,[2] since the early survey of Fermi, to be radioactive with a half-life of 2.7 days. It has been reported as emitting beta-radiation of maximum energy 0.78 Mev and gamma-rays of energy 0.28, 0.44, and 2.5 Mev. Only one of these gamma-rays appears to be strongly converted, and the spectrum in this case consists of only three lines. The differences in the energies of these lines agrees well with the differences between the K, L, and M levels in mercury. This indicates that the gamma-emission follows the loss of the beta-particle from the excited gold isotope. The observed average energies are presented in Table I. These values indicate for the

TABLE II. Beta-spectrum of iridium.

Observed energy	Identification	Gamma-energy	Observed energy	Identification	Gamma-energy
129.8	?	— kev	376	K_{13}	454.1 kev
162.5	?	—	387.3	K_7 or L_5	465.4 401.2
190.9	K_1	269.0	398.8	K_8	476.9
214.9	K_2	293.0	439.5	L_{13}	453.4
227.9	K_3	306.0	451.7	L_7	465.6
236.2	K_4	314.3	462.8	L_8 or M_7	476.7 466.1
254.5	L_1	268.4	507.5	K_9	585.6
280.5	L_2	294.4	524.0	K_{10}	602.1
292.5	L_3	306.4	531.0	K_{11}	609.1
301.5	L_4	315.4	572.8	L_9 or K_{12}	586.7 650.9
311.5	M_4	314.8	586.7	L_{10}	600.6
323.5	K_5	401.6(?)	597.0	L_{11}	610.9
330.3	K_6	408.0(?)	638.0	L_{12}	651.9

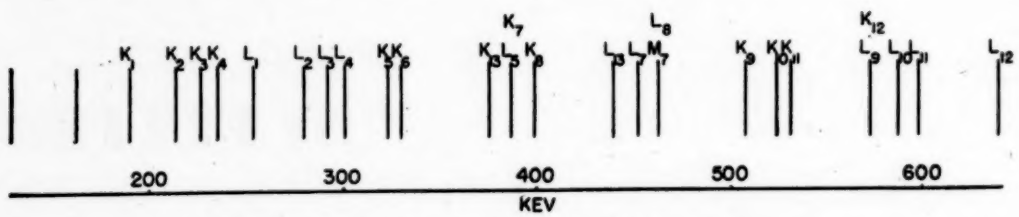

FIG. 3. The collected beta-spectrum of iridium on an energy scale.

[2] E. Amaldi, O. D'Agostino, E. Fermi, B. Pontecorvo, F. Rosetti, and E. Segrè, Proc. Roy. Soc. 149, 522 (1935).

energy of the gamma-ray an averaged value of 0.408 Mev.

Iridium

The isotope of iridium of mass 194 has previously been shown[3] to be radioactive with a half-life of 60 days. The beta-spectrum has not been studied but gamma-rays of energy 0.31, 0.47, and 0.60 Mev were reported. In the present investigation a sample of metallic iridium was activated, and because of the difficulty of getting it in solution the metal was pulverized in an agate mortar and applied to the specimen holder. When suitably exposed, many lines were obtained on the photographic plate. To cover completely the energy range, photographs were taken with several different magnetic fields.

The averaged values for the energies of the various lines obtained from the several plates are shown in Table II, and presented graphically in Fig. 3. By applying the known *K-L-M* differences for tungsten it becomes possible to detect certain groups among the lines, each group representing a single gamma-ray. From the 26 reasonably strong lines shown, 12 gamma-rays can be identified and are listed in Table III. In certain cases the interpretation of a line is not unique. Moreover, several additional lines are faintly apparent on the plates but because of low intensity are not included in the summary.

Having determined the gamma-energies, it becomes of interest to see if any relatively simple level scheme could be proposed, which would account for the numerous gamma-rays. The appearance of the lines in triplets of identical spacings offered encouragement in the search. It was soon evident that certain simple mathematical combinations could be formed. As a result, the scheme proposed in Fig. 4 seems reasonable. It is conceivable that some alternate plan may be equally good. With this scheme it is thus possible to account for 10 of the observed gamma-lines with 6 levels. In fact, almost every transition, except those at very low energies, that would be considered possible is actually observed, and the difference between the observed and expected values is less than 1 kev. However, many modifications of this scheme may ultimately be necessary when the weaker lines, not included here, are considered.

[3] E. McMillan, M. Kamen, and S. Ruben, Phys. Rev. 52, 375 (1937).

TABLE III. Summary of gamma-energies (averaged) for iridium.

Line	Energy	Line	Energy
1	269.0 kev	7	465.5 kev
2	293.7	8	476.8
3	306.2	9	586.2
4	314.8	10	601.4
5	401.4(?)	11	610.0
6	408.0(?)	12	651.4
		13	453.6(?)

Tantalum

The radioactive isotope of tantalum of mass 182 whose half-life is 97 days had been reported[4] to emit electrons of maximum energy 0.53 Mev. For the present investigation an oxide of the metal was irradiated in the pile. The small grain size of the oxide allowed excellent sources to be made. A typical photogram of the tantalum with a rather weak magnetic field is shown in Fig. 2. On this plate 1 kev corresponds to a distance of about 1 mm. To cover the entire spectrum additional exposures at higher magnetic fields were made. The averaged energies from the several photographic plates are collected in Table IV, and are shown graphically in Fig. 5. On treating these energies in a manner similar to that used

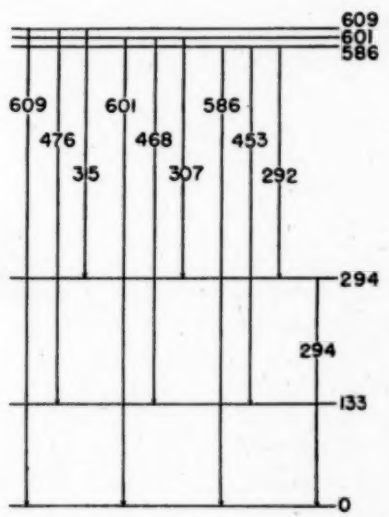

FIG. 4. A nuclear energy-level scheme for platinum* 194, following beta-emission from tantalum 194.

[4] O. Oldenberg, Phys. Rev. 53, 35 (1938); Science 103, 697 (1946).

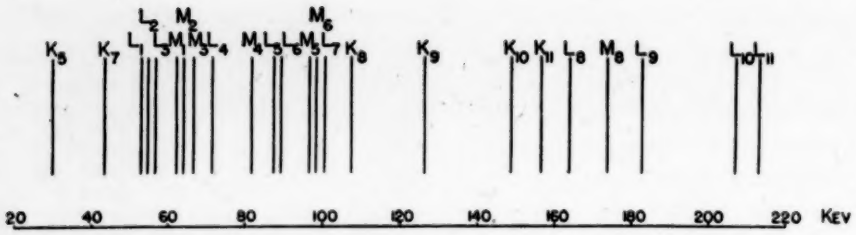

FIG. 5. The collected beta-spectrum of tantalum 182.

for the iridium an equally satisfactory solution was reached. Applying the *K-L-M* energy differences characteristic of tungsten to the 34 stronger lines 24 of which are shown in Fig. 5, it is possible to evaluate 16 gamma-rays as shown in Table V. Certain of the weaker lines are not used, and the interpretation of some of the lines may not be correct.

On inspecting the mathematical combinations existing between the various energies it becomes possible to arrive at an energy-level diagram as shown in Fig. 6. While some alternate scheme may work equally well it is rather amazing that so many of the observed lines are provided for, as transitions between levels, and in no case is the difference between observed and expected energy greater than one kev.

It would be desirable if the identification proposed could be substantiated by observing conversion ratios for the *K*, *L*, and *M* lines, compatible with a reasonable spin change, as predicted by theory. While this evidence is satisfactory in most cases, there is one notable exception. For many of the low energy gammas only the *L* and *M* lines appear, as the energy is not sufficient to eject a *K* electron. For the line

TABLE IV. Beta-spectrum of tantalum.

Observed energy	Identification	Gamma-energy	Observed energy	Identification	Gamma-energy
29.8 kev	K_5	99.1 kev	100.3 kev	L_7	112.4 kev
37.2	K ?	106.5	107.2	K_8	176.5
43.4	K_7	112.7	116.6	K_{15}	185.6
52.8	L_1	64.9	126.3	K_9	195.6
54.6	L_2	66.7	131.0	L_{14}	143.0
56.6	L_3	68.7	138.7	M_{14}	141.5
61.9	M_1	64.7	148.8	K_{10}	218.1
64.0	M_2	66.8	156.9	K_{11}	225.0
66.8	M_3	69.6	163.7	L_8	175.8
71.4	L_4	83.5	173.6	M_8 or L_{15}	176.4
73.5	K_{14}	142.8	182.4	L_9	194.6
81.6	M_4	83.8	190.0	K_{12}	259.3
87.2	L_5	99.3	206.2	L_{10}	218.6
89.2	L_6 or K_{13}	101.1 or 158.5	212.4	L_{11} or K_{13}	224.6 291.7
96.6	M_5	99.9	245.4	L_{12}	257.5
98.3	M_6	101.1	271.0	L_{13}	292.4

TABLE V. Summary of gamma-energies (averaged) for tantalum.

Line	Energy	Line	Energy
1	64.8 kev	9	195.1 kev
2	66.7	10	218.3
3	69.2	11	225.0
4	83.6	12	259.0
5	99.6	13	292.0
6	101.1 (?)	14	142.9
7	112.5	15	185.6
8	176.2	16	158.5 (?)

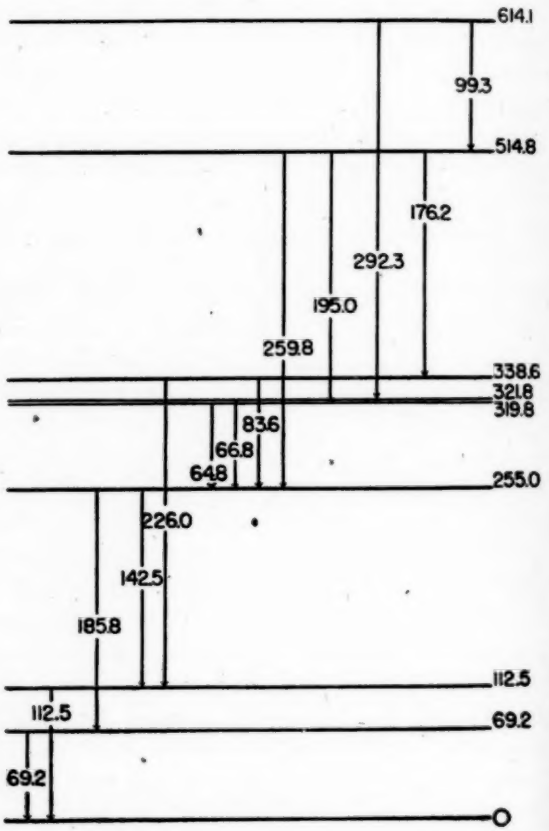

FIG. 6. Nuclear level scheme for tungsten* 182 following emission of beta-ray from tantalum 182.

designated as (5), however, the strongest line by far is the L_5, shown by legend in Fig. 2. The accompanying K line is very much weaker, although the gamma-energy is about 30 kev above the K threshold. Perhaps this energy difference is not sufficient to allow for maximum probability of K-electron emission.

Mr. R. G. Shreffler and Mr. A. D. Weaver assisted very materially in this investigation.

This investigation was initially aided by a grant from the Horace H. Rackham Fund. It is a pleasure to acknowledge the very valuable continuing support of the Office of Naval Research on this project.

PHYSICAL REVIEW VOLUME 72, NUMBER 7 OCTOBER 1, 1947

Neutron Cross-Section Studies with the Rotating Shutter Mechanism*

T. BRILL AND H. V. LICHTENBERGER
Argonne National Laboratory, Chicago, Illinois

(Received June 16, 1947)

It has been possible to extend the usefulness of the rotating shutter mechanism of Fermi, Marshall, and Marshall for velocity selection of neutrons by increasing the number of photo-electrically activated gate circuits. With the modifications here described data can be obtained simultaneously in six well-resolved velocity intervals. In this way the cross sections of gold, gadolinium, and dysprosium have been measured as a function of velocity for low energy neutrons.

1. INTRODUCTION

AN improved velocity-selector system for low energy neutrons, giving data for six energy intervals simultaneously, has been built around the rotating shutter used by Fermi, Marshall, and Marshall.[1] The shutter consists of a series of laminae, alternately 0.006-in. thick cadmium and 0.030-in. thick aluminum, mounted axially inside a thin cylindrical steel case. As this is rotated in a neutron beam (with its axis perpendicular to the beam), two bursts of neutrons are released per revolution. Neutrons reaching a detector some distance away are registered on different scaling circuits according to the time elapsed since the shutter was open (i.e., the time of flight of the neutron). The detector used in these experiments consisted of a suitably shielded proportional counter filled with BF_3 enriched in the B^{10} isotope. The general form of the apparatus is shown in Fig. 1.

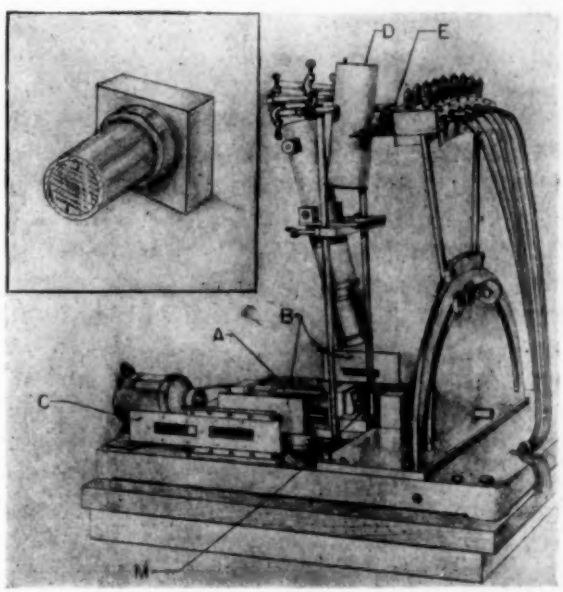

FIG. 1. Rotating shutter neutron-velocity selector. *A*—shutter; *B*—slits (cadmium); *C*—sample holder; *D*—light source; *E*—photo-cells; *M*—mirror. Insert—shutter, showing cross section. Dark areas—cadmium; crosses—aluminum; outer case—steel.

---

* This report is based on work done under the auspices of the Manhattan District at the Argonne National Laboratory, the University of Chicago in 1945–1946. The information contained in this document will appear in Division IV of the Manhattan Project Technical Series as a part of the contribution of the Argonne National Laboratory.

[1] E. Fermi, L. Marshall, and J. Marshall, Phys. Rev. 72, 193 (1947).

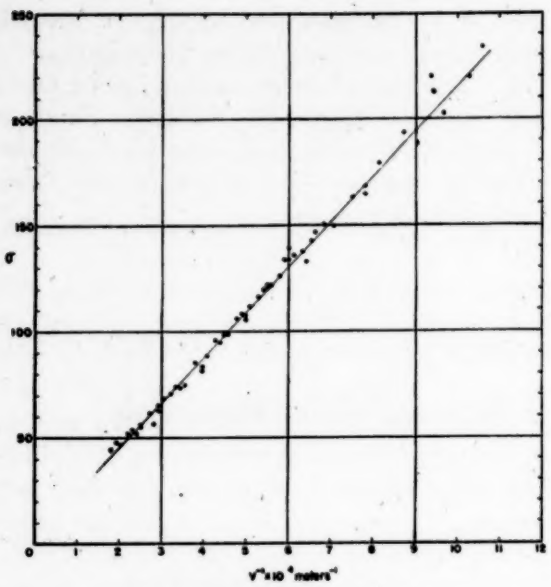

FIG. 2. Total slow-neutron cross section of gold as a function of energy.

To measure the rate of revolution and to actuate the gate circuits for registering the neutrons, a double mirror is mounted on the end of the rotating shutter at an angle of 45° to the laminae. The light beam reflected by this mirror from a strong tungsten source falls, successively, on seven photoelectric cells mounted 4° apart on a carrier whose position can be varied about the axis of the shutter. Six of these are used to open the gate circuits at known time intervals after the shutter is opened. The time intervals are determined by the angle through which the light beam rotates and its angular velocity, which is twice that of the shutter. The seventh photo-cell operates a special electronic tachometer to measure the rate of rotation of the shutter.[2] The rate used is 180 revolutions per second except for data for very slow neutrons, which are taken at 60 r.p.s. As the tachometer compares these rates to the line frequency it is possible to hold the shutter speed within 0.5 percent of the desired value and thus contribute no appreciable error to the measurement of neutron velocity. The gate circuits are each held open electronically for 31 microseconds (4° rotation of the light beam,

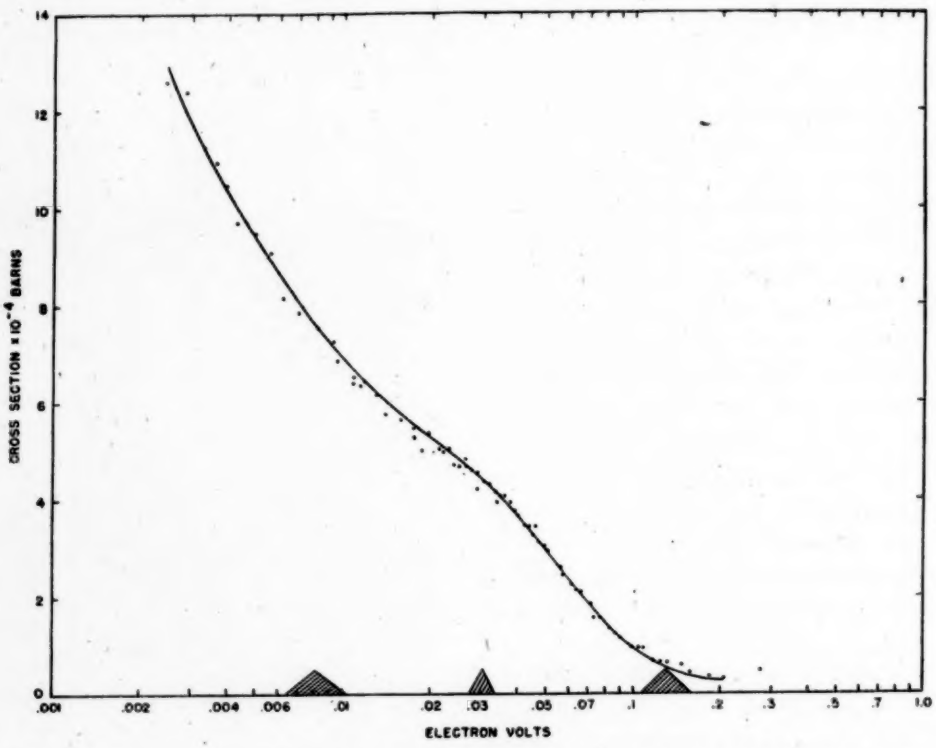

FIG. 3. Slow-neutron cross section of gadolinium. Plotted points are experimental values; solid curve, Breit-Wigner relation with $\sigma_0 = 45{,}000 \times 10^{-24}$ cm², $E_0 = 0.028$ ev, $\Gamma = 0.118$. Triangles show resolution width of instrument.

[2] A separate photo-cell is not necessary for this purpose —the signal from any of the others could be used.

or 2° rotation of the shutter at normal operating speed). The shutter itself is open (partially or completely) for about 3° of its rotation.

2. EXPERIMENTAL PROCEDURE AND RESULTS

In use, this instrument is set up before the thermal column of the Argonne heavy-water pile and a collimated beam of slow neutrons is allowed to fall upon the rotating shutter. The sample is placed in its holder with appropriate cadmium collimating slits. The counter, in a heavy boron shield, is set up with its axis parallel to that of the shutter and at a measured distance from it (usually 1.5 meters). A transmission measurement is then made for the particular energies as determined by the photo-cell position settings. The background is measured by stopping the shutter with the light beam striking the photo-cell corresponding to the desired energy and counting the total output of the detector (without the gate circuits). Knowing then the gate time, the background may be taken quite accurately in a short time. The photo-cell positions are then reset and the procedure repeated.

A. Gold

The transmission of a gold plate 1.674 g/cm² in thickness was measured over a range of neutron velocities of 900 to 5700 meters per second. Total cross sections (Fig. 2) calculated from these transmissions show a very slight departure from a 1/v behavior, possibly due to the wing of the resonance level[3] at 4.8 ev.

A measurement of the transmission of the gold sample, standardized in this manner and made in the flux of polyenergetic neutrons emitted by the thermal column, indicated a resultant cross section of 100×10^{-24} cm²/atom. This corresponds to an effective velocity of 2200 m/sec. for neutrons in equilibrium with graphite at room temperature.

B. Gadolinium[4]

Very accurate quartz cells were made up and filled with known heavy-water solutions containing various amounts of gadolinium. The transmission of the cell containing gadolinium was compared to that of a similar cell containing only the heavy water. These measurements were made in the region from 0.002 ev to 0.2 ev. The observed cross sections—the plotted points on Fig. 3—showed a resonance at about 0.028 ev. The Breit-Wigner relation with the constants $\sigma_0=45{,}000\times10^{-24}$ cm², $E_0=0.028$ ev, and $\Gamma=0.118$ ev is drawn in as a solid line. These values are not in agreement with those reported by Borst, Ulrich, Osborne, and Hasbrouck;[5] however, as has been pointed out[5,6] this energy lies in a region where second-order effects cause considerable difficulty in measurements made with the crystal spectrometer.

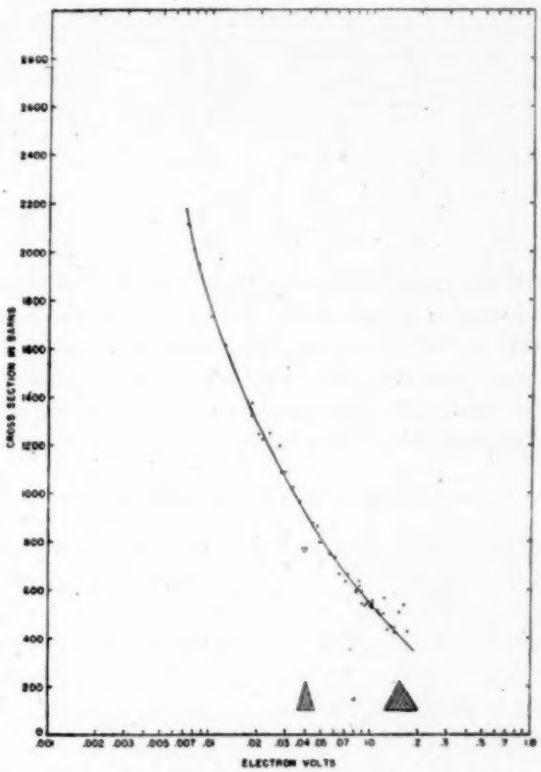

FIG. 4. Slow-neutron cross section of dysprosium. Triangles show resolution width of instrument.

C. Dysprosium[4]

The cells used in the measurement of the gadolinium cross section were cleaned and filled

[3] J. Rainwater and W. U. Havens Jr., Phys. Rev. **70**, 154 (1946).

[4] These elements had previously been studied in the energy region above 0.04 ev with the aid of the crystal spectrometer by W. J. Sturm. Paper to be published.

[5] L. B. Borst, A. J. Ulrich, C. L. Osborne, and B. Hasbrouck, Phys. Rev. **70**, 557 (1946).

[6] W. J. Sturm and S. Turkel, Phys. Rev. **70**, 103(A) (1946).

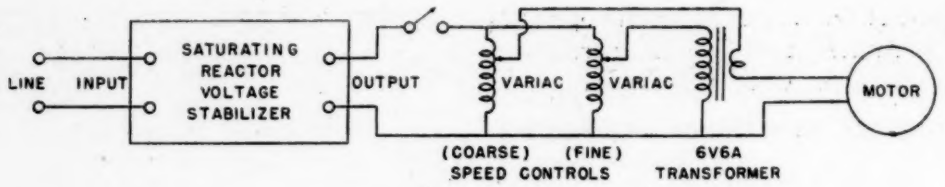

FIG. 5. Speed-control circuit.

with solutions containing dysprosium. This cross section was measured in the energy region from 0.007 to 0.15 ev (Fig. 4). No resonances were found; however, the cross section deviates somewhat from a 1/v behavior, indicating a resonance somewhere in the low energy region.

3. DETAILS OF THE INSTRUMENT

The shutter, mounted on ball bearings, is belt-driven by a high speed, series-wound grinder motor. The speed is controlled by varying the motor voltage, and a saturating, reactor-type voltage stabilizer minimizes the effects of varying line voltage upon speed. Vernier control is provided, as indicated in Fig. 5.

Type 925 vacuum photo-cells were used in this experiment. A type 6AK5 tube, mounted close to each photo-cell and used as a cathode follower with its screen by-passed to cathode, prevented capacitive loading of the photo-cell. This was followed by a type 6J6 cathode follower to drive the cable to the amplifier. As the photo-cell signal was only about 10–20 millivolts, a gain of about 500 was necessary in the amplifier used. The photo-cell and amplifier system for one channel is shown in Fig. 6.

The instrument has been simplified and improved since this experiment was performed by replacing the photo-cells with type 931-A multiplier cells. This eliminates the need for any voltage amplifier and for the double cathode-follower preamplifier—only the 6J6 is now used. In addition, excellent signal-to-noise ratio can be obtained with only a conventional galvanometer lamp as a light source instead of the much larger source previously used. A voltage of 450 volts—or 50 volts per stage—on the dynodes of the 931-A gives signals of 8–15 volts. This system is shown in Fig. 7.

Figure 8 shows one gate circuit. The first trigger pair, operated by the photo-cell signal, provides uniform pulses for the second, which is self-timed. This insures that the "on" time of the second is independent of the input signal. The gate tube itself is a twin cathode follower with separate inputs and a common output. As the cathodes essentially "follow" the more positive grid, a negative signal from the second trigger pair opens the gate by allowing the cathodes to follow the other grid, which receives negative pulses from the counter amplifier. A cathode follower prevents loading the gate tube,

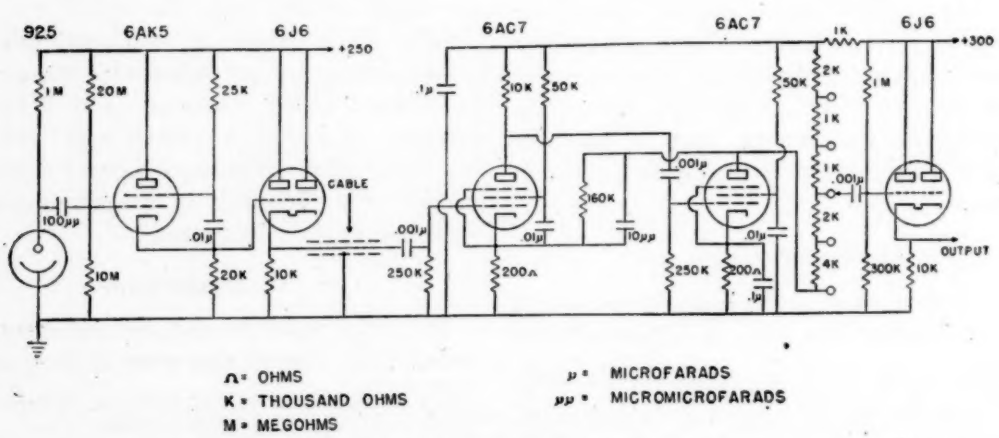

FIG. 6. Early photo-cell and amplifier system (one channel).

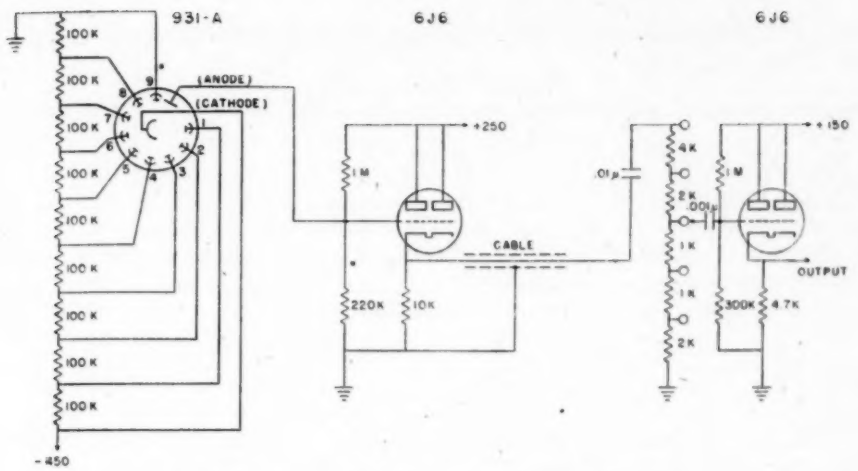

FIG. 7. Improved photo-cell and amplifier system.

and an output trigger pair provides a convenient signal for the scaler. To eliminate any dependence of the gate time upon line voltage, the power for the gate-determining trigger pairs is regulated—the plate supply electronically, and the heater supply by a 6.3-volt constant-voltage transformer.

The tachometer unit (Fig. 9) consists of a direct-reading electronic frequency meter and an oscilloscope tube having, on a 60-cycle circular sweep, a spot of light corresponding to each photo-cell pulse. Thus, if the shutter speed is a multiple of 30 revolutions per second (30 rather than 60 because the mirror has two faces) a set of spots appears to stand still on the face of the oscilloscope, one spot for 30 r.p.s., two for 60 r.p.s., and so on. If the shutter speed is not quite an exact multiple of 30 r.p.s., the ring of spots appears to rotate with a velocity proportional to the difference between the actual speed and the exact multiple. Thus, very accurate measurement of the shutter speed is possible.

The frequency meter is a trigger pair passing a fixed quantity of charge per photo-cell pulse. The resulting (averaged) current operates a meter, which registers the shutter speed directly

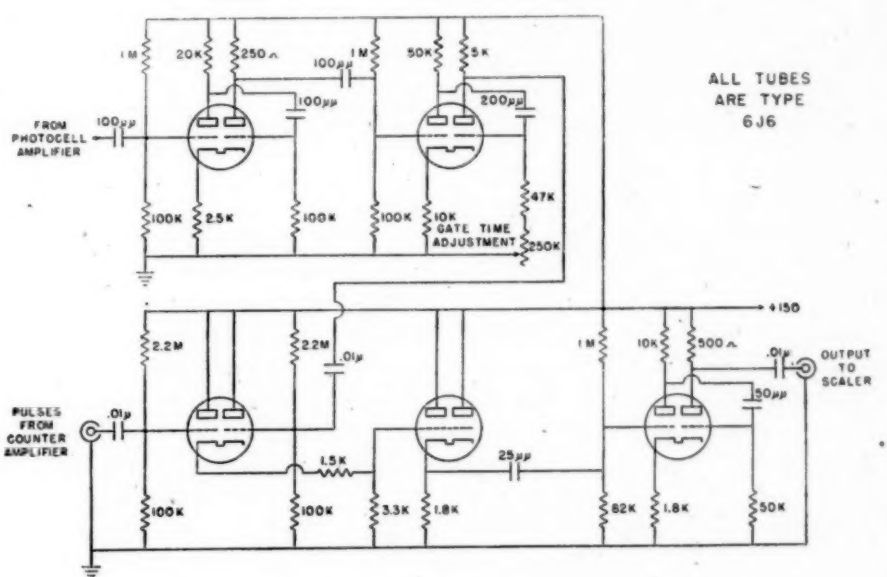

FIG. 8. Gate circuit.

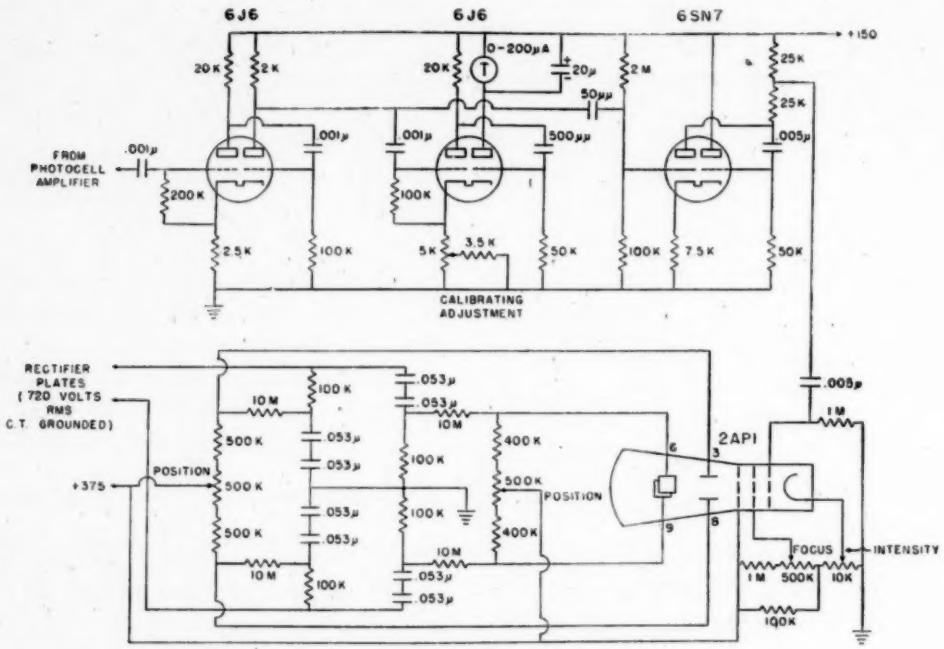

FIG. 9. Electronic tachometer.

in revolutions per second. Here, as in the gate circuits, an input trigger pair is used to eliminate any change in the pulse width of the self-timing trigger pair, and regulated supplies prevent dependence upon line voltage.

Another improvement (added since the experiments described were performed) is a synchronizer unit to "lock" the shutter to the line frequency. An iron bar on the end of the shutter rotates between the poles of an electromagnet fed with 60-cycle pulses. At present, the magnet coil is merely plugged into the line so that the synchronizer works only at 60 r.p.s. (and lower). It is planned to power this magnet with short duration pulses (1 or 2 milliseconds) synchronized with the line frequency so that the shutter speed can be locked to any multiple of 30 r.p.s.

The authors are indebted to the Ryerson Shop for its excellent machine shop work, to the Optical Shop for manufacture of the accurate quartz cells, and to the operating personnel of the Argonne pile for their cooperation and assistance in performing these experiments.

Energy and Half-Life of the Be^{10} Radioactivity*

EDWIN M. MCMILLAN
Radiation Laboratory, Department of Physics, University of California, Berkeley, California

(Received June 30, 1947)

The half-life and upper limit beta-ray energy of Be^{10} have been measured, using a sample prepared from a strongly deuteron-bombarded Be target. The upper limit energy, from the inspection end point of the absorption curve, is 560±10 kev. The half-life, from the specific activity (46 disintegrations per sec. per mg Be) and the directly measured isotopic abundance (one part in 18,600) is $(2.5\pm0.5)\times10^6$ years. A rough excitation curve and good evidence for the absence of a gamma-ray were also obtained.

1. INTRODUCTION

THE activity of Be^{10} is of special interest because of theoretical difficulties in explaining its very long half-life. Its existence has been shown by the work of McMillan and Ruben[1] and Levinger and Meiners,[2] the isotopic assignment has been confirmed directly by Pierce and Brown,[3] and the half-life measured by Hughes, Eggler, and Huddleston.[4] In this paper is reported some work made possible by the kindness of Professor A. L. Hughes of Washington University in sending the author a beryllium target that had received a very strong deuteron bombardment in the St. Louis cyclotron (about 200,000-microampere hours of 11-Mev deuterons at 45° incidence). The part of the surface struck by the intense central core of the beam had spalled off; the portion used consisted of a square inch of surface immediately adjacent to the spalled region.

Even though this target was about two years old when received, it still carried a total activity about 50 times as strong as the Be^{10} activity. The bulk of the contamination activity appeared in the filtrate from the NH_4OH precipitation and had an absorption curve identical with that of Na^{22}, so it probably was due to this substance made from traces of Mg in the target. The chemical procedure used was simpler than that used in reference 1, because of the relatively much weaker contamination and also the fact that experience has shown the simplified procedure to be quite adequate for purifying Be. The Be was dissolved in concentrated HCl, precipitated as hydroxide by NH_4OH, and converted to the basic acetate by dissolving the hydroxide in glacial acetic acid. The basic acetate was then dissolved in chloroform, washed several times by shaking with water, and then dissolved in diluted NHO_3. Finally, the nitrate was ignited to BeO. The activity measurements were made with a G-M counter having a mica window of 2.5 mg/cm² thickness.

2. EXCITATION CURVE

The surface of the target was milled off in 6 layers, each 0.005 in. thick, and the resulting samples were separately purified. Equal portions of these were taken by pipetting out equal volumes of the saturated chloroform solutions of the basic acetate, and the relative activities of these (counted in the form of the acetate) were measured. Nearly all the activity was found in the first three layers. The corresponding energies were computed by assuming the stopping power of Be per electron to be the same as that of air, and taking account of the 45° incidence. These energies are not highly accurate, particularly because of the uncertainty in the initial energy and the angle. The results were as given in

TABLE I.

No. of layer	Energy range	Relative activity
3	2.3–6.3 Mev	0.46
2	6.3–8.9 Mev	1.0
1	8.9–11.0 Mev	0.88

* This work was done under the auspices of the Atomic Energy Commission under contract No. W-7405-Eng-48.

[1] E. M. McMillan and S. Ruben, Phys. Rev. **70**, 123 (1946).
[2] J. Levinger and E. Meiners, Phys. Rev. **71**, 586 (1947).
[3] A. K. Pierce and F. W. Brown, III, Phys. Rev. **70**, 779 (1946).
[4] D. J. Hughes, C. Eggler, and C. M. Huddleston, Phys. Rev. **71**, 269 (1947).

Table I. A check was made with a second pair of pipetted samples, to show that the drop in activity of the first layer compared to the second is significant. A discussion of these results is given in a later paragraph.

3. ABSORPTION CURVE AND BETA-ENERGY

The material from the first three layers was combined and converted to BeO (360 mg were obtained). This was used for all the other measurements. Two absorption curves were taken. Figure 1 shows a curve taken with a thin layer of BeO (46.5 mg spread over a 2.5-cm diameter circle) mounted on paper to minimize backscattering. It was plotted without subtracting the counter background, in order to avoid running off the bottom of the logarithmic paper. On the same plot is shown a curve for Na^{22}, taken on the same apparatus, but with the background subtracted. Since the relative gamma-ray effect of the latter happens to be nearly equal to the background in the former, a good comparison of the shapes can be made. It is seen that the Be^{10} curve shows a slight upward convexity that is not exhibited by the Na^{22} curve. This is not pronounced enough to indicate a line of electrons, but shows that the shapes of the beta-ray energy distributions are slightly different.

The other absorption curve, taken to locate the end point, is shown in Fig. 2. This time a thick sample containing all the material was used. The residual counts beyond the end point, which amount to 1/10,000 of the initial beta-counts corresponding to the amount of material in the sample, are of the order to be expected from x-rays ("Bremsstrahlung") generated in the sample and absorbers by beta-impact. Therefore, there is good evidence against the occurrence of a gamma-ray in the decay of Be^{10}. The end point can be located rather accurately from Fig. 2; it can be given as 185 ± 5 mg/cm² Al. The corresponding upper limit energy, using the best present range-energy relation, is 560 ±10 kev which agrees with the rougher value of reference 1.

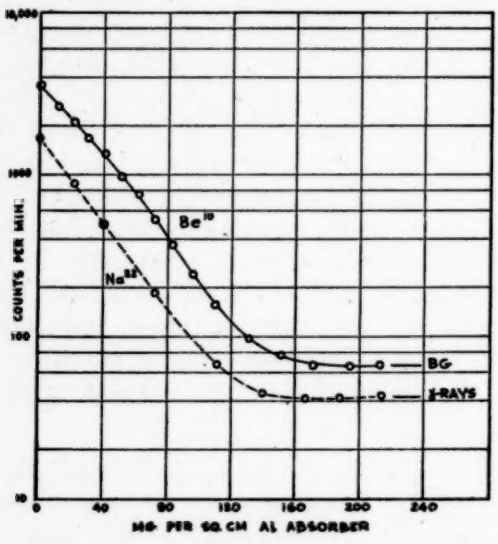

FIG. 1. Absorption of beta-particles in Al. Solid line: Be^{10} absorption data, plotted without subtracting counter background. Dashed line: Na^{22} absorption data, with background subtracted, for comparison of shape.

4. ISOTOPIC ABUNDANCE, SPECIFIC ACTIVITY, AND HALF-LIFE

Hughes *et al.*[4] found the half-life by comparing the specific activity with the isotopic abundance computed from the neutron flux, the time of exposure, and the cross section for the reaction Be^{9} (n, γ) Be^{10}. In our case the pertinent reaction is Be^{9} (d, p) Be^{10} whose cross section has not been measured, but on the other hand, the isotopic abundance was great enough that it could be measured directly on a Nier mass spectrometer. This measurement was made by A. K. Pierce under the direction of Dr. B. J. Moyer. The material was introduced into the spectrometer ion source in the form of the anhydrous chloride sealed in a glass capillary which was broken after evacuation. Good $(Be^{9})^{+}$ and $(Be^{10})^{+}$ peaks were obtained, separated by over ten times the total peak width; the galvanometer deflections at the mass 10 peak were around 2 cm. Since the ratio of the mass 9 to the mass 10 current was large, different galvanometer sensitivities had to be used, and the ratio of currents was determined by duplicating the deflections with known currents. Seven measurements with two different fillings of the source gave a mean 9/10 ratio of $15{,}700\pm2700$, the error being estimated from internal consistency only. To check against the possibility of the mass 10 peak being due to $(Be^{9}H^{1})^{+}$, $(B^{10})^{+}$, or $(Ne^{20})^{++}$, another run was made using a sample prepared in the same way from inactive Be, and this time the mass 10 peak was much smaller but still observable, with a 9/10 ratio of 100,000. If this is

taken as a correction on the value given above, the ratio Be^9/Be^{10} is 18,600±3000.

The specific activity was measured by comparing the counting rate of a uranium standard (calibrated by Dr. C. Tobias of the Medical Physics Department against an accurately prepared standard) with the counting rates of samples of the active BeO. Three samples were prepared, consisting of 12.0, 13.7, and 23.0 mg of the BeO spread over an area of 3 cm^2 on filter paper, and these were counted with no metal backing in order to minimize back-scattering. The absorption correction for the window plus the air path plus half the sample thickness, evaluated from the initial slope of the absorption curve, was about 20 percent. The mean value obtained for the specific activity was 16.6±1.7 disintegrations per second per mg BeO or 46±5 disintegrations per second per mg Be, the error given being considerably greater than the spread in the three values, in order to allow for the various uncertainties involved in all absolute beta-intensity measurements, particularly when the sample and the standard have different energies.

The half-life is easily computed from the above data. The decay constant λ is given by (disintegration rate per gram)/(number of active atoms per gram), or:

$$\lambda=(46{,}000\times9\times18{,}600)/(6.02\times10^{23})$$
$$=(1.28\pm0.24)\times10^{-14}\ \text{sec}^{-1}.$$

The half-life is then $(2.5\pm0.5)\times10^6$ years, in agreement with the value of 2.9×10^6 years given by Hughes *et al.*[4] within the accuracy of the determinations.

5. DISCUSSION OF YIELD

Dr. Serber has made an estimate of the yield expected in the reaction Be^9 (d, p) Be^{10}. First the total cross section for capture of the deuteron to form the intermediate nucleus was estimated from the classical expression: $\sigma=\pi R^2\times(1-E_B/E)$, where R=nuclear radius (taken as the sum of the beryllium and deuteron radii or 5.5×10^{-13} cm) and E_B=barrier height (taken as 1.67 Mev). Then the division between the (d, p) and (d, n) processes was computed, including a penetration factor for the former and otherwise supposing division in the ratio of available volumes in phase space; the (d, α) process was neglected as being probably less important. Finally, the competing reaction $(d, 2n)$ with an estimated threshold at 5 Mev was included, being given a probablity proportional to the volume in phase space and with a coefficient adjusted to match the data in paragraph 2. This process accounts for the decrease in cross section beyond 8 Mev.

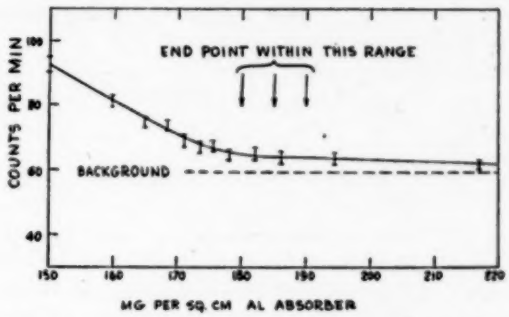

FIG. 2. Detail of Be^{10} absorption curve near the end point. Absorption of counter window plus air path included. Errors indicated are standard errors computed from counting statistics.

From this theory the absolute yield at 11 Mev is estimated to be 0.0016 active atoms per deuteron, and the observed yield of 21,000 dis./sec. or 1.6×10^{18} active atoms in the part of the target used would correspond to 46,000 microampere-hours bombardment of that part, which seems reasonable. Furthermore, the data of reference 1 combined with the measured half-life give an observed yield of 0.0039 active atoms per deuteron at 16 Mev, which can be compared with the value of 0.0026 computed from the above theory at this energy. The difference is well within the accuracy of the rather rough theory. It is interesting to note that the theory gives a neutron yield of 0.008 per deuteron at 16 Mev, in exact agreement with the value measured in the Crocker Radiation Laboratory by H. Yockey. This discussion of the excitation curve and the yield shows that there is no great peculiarity in the formation of Be^{10} to match its abnormal behavior in beta-decay.

The Photo-Conductivity of "Incomplete Phosphors"

RUDOLF FRERICHS
Technical University, Berlin-Charlottenburg, Germany

(Received June 4, 1947)

Synthetic single crystals of CdS, CdSe, and CdTe have been produced by the reaction of cadmium vapor with H_2S, H_2Se, and H_2Te, respectively. These "incomplete phosphors" show no phosphorescence but strongly developed photo-conductivity. Photo-cells made from these crystals are extremely sensitive in the whole region from the infra-red down to the ultraviolet, x-rays, and gamma-rays and for corpuscular rays, alpha- and beta-rays. Two different mechanisms of photo-conductivity occur. The normal photo-conductivity in the region of strong absorption from the blue to the ultraviolet, and the selective photo-conductivity in the region of weak absorption in the visible, x-rays, and corpuscular-rays region. The phenomena observed are in general accordance with the zonal theory of phosphorescence.

ONE of the most instructive examples of the zonal theory of solid structure is offered by the crystal phosphors. They combine the properties of isolators and electronic conductors, but unlike the metallic state, the number of conductive electrons in the crystal phosphor can be regulated by the process of light absorption and emission, and consequently a greater variety of conductive phenomena is to be expected in these substances.

The general idea of the coupling of motion of electrons with the optical properties of crystal phosphors has been already given in the early investigations of Lenard. Later, Gudden and Pohl, continuing and improving these researches, discovered the main laws and regularities of the electric conductivity connected with phosphorescence. Since these early researches, very little has been done in this particular field of research. Therefore, it might be worth while to give an account of some investigations of the author which deal in a rather extensive way with these hitherto neglected electric phenomena in crystal phosphors.[1] During the course of these investigations it has been found that it is quite possible to separate the electric and the optical properties of phosphors and to develop substances which show in a remarkable way the electric phenomena connected with phosphorescence but very little or no phosphorescence at all. The name "incomplete phosphors" might be proposed for such substances.

Gudden and Pohl[2] accomplished their investigations with commercial zinc sulfide phosphors and with natural crystals of zinc blende, greenockite, and cinnabar. As these crystals are rare—especially greenockite—it seemed to the author to be important to resume this work with artificially prepared phosphor crystals.

THE GROWING OF SINGLE CRYSTALS OF PHOSPHORS

Some preliminary experiments have been performed with a small condenser whose gap was filled with pulverized phosphors. In accordance with the results obtained by Gudden and Pohl, photo-conductivity could be easily measured at field strengths of some 10,000 volts/cm. The experiments carried on with different zinc-cadmium sulfides have shown that the photo-conductivity increases with increasing percentage of cadmium sulfide. By utilizing the best-known chemical methods of purifying, the late Dr. Schlegel in collaboration with the author succeeded in preparing very pure cadmium sulfide which showed remarkable photo-conductivity. As in the firing process involved, the phosphor easily dissociates; the cadmium sulfide was fired in thick-walled closed quartz tubes with the necessary sulfur added for producing a pressure of many atmospheres. But the difficulties of obtaining steady photo-currents with these phosphor powders were very large, as it was not

[1] The results of this investigation have been reported at the colloquium of the K. W. J. Dahlem of January 11, 1947. Dr. Rompe and Dr. Möglich, who have been engaged in the theoretical research on phosphorescence, some years ago in many discussions drew the attention of the author to this earlier work.

[2] B. Gudden and R. Pohl, Zeits. f. Physik 2, 181, 361 (1920).

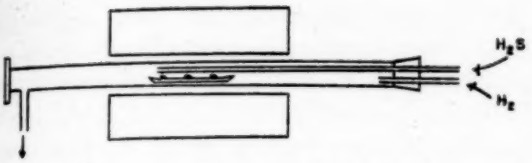

FIG. 1. Reaction tube for the production of CdS crystals.

possible to overcome the many troublesome contacts between the small particles. Later the author found a way of preparing rather large single crystals of these substances. Very little has been published up to now on the production and application of single crystal of phosphors.[3] According to Lorenz[4] artificial greenockite crystals of fairly large size are produced by the reaction of cadmium vapor and hydrogen sulfide. This method has been slightly modified (Fig. 1). Cadmium metal in a small porcelain boat was heated in a quartz tube to about 800 to 1000°C. The cadmium vapor was driven by a slow stream of hydrogen from the boat to the zone of the tube where it could react with a slow stream of hydrogen sulfide which passes there by a second quartz tube. By slowly cooling down, with the gases still flowing, crystals of very pure photoconductive cadmium sulfide are obtained. This method has two great advantages. As all impurities are separated by fractionate sublimation, it is not necessary to purify the cadmium; in fact ordinary technical cadmium yields as good results as the purest kind available. On the other hand, by cooling down in a steady stream of hydrogen sulfide, dissociation is entirely avoided. Crystals obtained by many hundred experiments show exactly the same photoelectric properties![5]

The size of the crystals obtained depends on the size of the reaction tube, as the crystals grow like thick bushes across the interior of the tube. With tubes of about 100 mm in diameter, crystals up to 1–2 cm^2 have been obtained. They consist of rather thin yellow or slightly yellow green ribbons of the size of about 2 to 3 by 10 to 20 by 0.1 to 0.2 mm, which are flat and optically clear or of somewhat larger crystals with a rippled surface caused by irregularities in the speed of crystal growing. Very often the crystals are twinned with a fishbone structure. The color of larger and thicker crystals is yellow orange. The structure of these crystals is dihexagonal pyramidal hemimorph according to some Debye-Scherrer diagrams.[6] This structure seems to be essential because only hexagonal cadmium sulfide—the beta-form—shows photoconductivity. Cadmium sulfide obtained at room temperature by passing H_2S through very pure cadmium sulfate solution, yielding the alpha-form of regular structure, shows no photo-conductivity at all.

THE OPTICAL ABSORPTION OF CADMIUM SULFIDE

With such clear and flat ribbons, the optical absorption, whose measurement is rather difficult when crystallized phosphor powder is used, can be easily measured (Fig. 2). The crystals are transparent in the infra-red and red. Thin crystals show at room temperature, absorption beginning at about 6000A. It rises slowly until it reaches a very steep absorption edge at 5200A. From there toward shorter wave-lengths the crystals are entirely opaque; ribbons as thin as 0.005 mm show no transmission at all of the very strong blue and violet lines of the high pressure mercury arc. While the absorption coefficient above 5200A amounts to 1 mm^{-1}, below 5200A it is some 10^4 to 10^5 times stronger. The absorption in this region is quite metallic, and the reflection

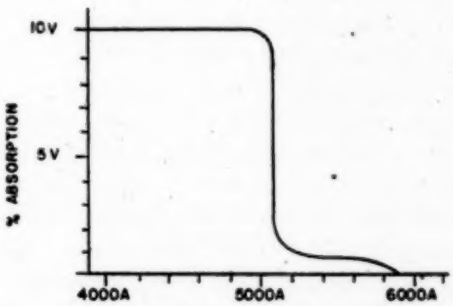

FIG. 2. Optical absorption of a CdS crystal 0.1 mm thick.

[3] Crystals of phosphorescent zinc sulfide which were accidentally obtained by N. Riehl have been mentioned by M. V. Ardenne as grainless screens for electron microscopes in his book on electron microscopy. Some methods of producing crystals of synthetic greenockite are mentioned in Gmelin, *Handbook of Inorganic Chemistry* (Verlag Chemie, Berlin, 1926), Vol. 33, "Cadmium."

[4] Lorenz, Chem. Ber. 24, 1509 (1891).

[5] This method of fractionate crystallization from the gaseous phase might be generally useful for the manufacturing of crystal phosphors.

[6] The author is indebted to Miss U. Martius for this structural analysis.

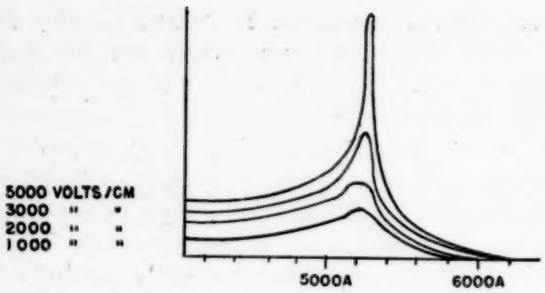

FIG. 3. Relative photo-conductivity of CdS crystals at different field strengths in arbitrary units.

power is accordingly high. Kroger[7] has observed that the absorption edge of the pulverized cadmium sulfide shifts rather strongly with changing temperature. The shift amounts to about 1A/°C between 90° and 298°K. Using these data, Rompe and Möglich have developed a theory which links this shift with the thermal expansion of the crystal lattice.[8]

THE PHOTO-CONDUCTIVITY OF SYNTHETIC GREENOCKITE

Using natural crystals, Gudden and Pohl[2] have measured the photo-conductivity of ZnS, CdS, and HgS in the region 7000 to 2500A. Their measurements cover a spectral region which contains the "selective" and the "normal" region of photo-conductivity. In the selective region the photo-conductivity depends very much on the field strength. Our measurements of the photo-conductivity of synthetic greenockite (Fig. 3) have been made with crystals on which two electrodes of aluminum, separated by a small gap of 0.2 to 0.3 mm, have been sputtered by evaporation in vacuum. The selective maximum is very sharp at field strengths of 5000 volts/cm, the width of the maximum being about 50A. With decreasing temperature the maximum still increases and shifts to the violet, and with increasing temperature it diminishes and shifts to the red. The position of the selective maximum at different temperatures is given by the position of the absorption edge. The maximum is situated on the long wave-length side of the edge. At 300°C the photo-conductivity becomes very small and hardly perceptible.

The photo-conductivity in the region of shorter wave-lengths has been investigated by Gudden and Pohl and by the author down to 2500A. Our measurements have been made with the lines of the high pressure mercury arc separated by a large Hilger-Müller double monochromator. The intensity of the spectral lines has been controlled by a thermocouple and the different lines have been reduced to one common intensity level by suitable platinum wedges sputtered on quartz plates. According to these measurements the photo-conductivity is constant over the whole region. As Gudden and Pohl[2] already pointed out, their measurements on HgS show some remarkable differences between these two effects. The photo-conductivity in the long wave region depends very much on the field strength and increases with it continuously until electric breakdown occurs. The photo-conductivity in the short wave region reaches saturation at higher field strengths and is on the whole much more stable and better defined than the former conductivity. The exact field strength at these measurements is not defined by the geometrical configuration of the electrodes. With strong illumination and high field strength the current slowly increases, indicating that probably conductive bridges are formed in the crystal. But, by suitable decreasing of the applied voltage, this effect can be entirely stopped and limited.

The currents obtained in these two effects are quite large. A photo-cell consisting of a crystal of the size $3\times10\times0.1$ mm, with a sensitive area between the electrodes of 0.2×10 mm, diminishes its resistance from more than 10^8 ohms to about 10^4 ohms, if the filament of a small incandescent lamp (10 watts) is projected by a lens 5 cm in diameter and 5-cm focal length on it. At an applied current of 10 volts, the current amounts to 1 ma. The energy effective on the small slit amounts in this case to 0.3×10^{-4} watt, and currents as high as 1 ma can be continuously passed through such crystals without destruction.

The photo-conductivity below 5200A is somewhat smaller if the same amount of energy is applied. For these measurements the energy of different spectral lines of the high pressure mercury arc has been adjusted by monochromatic filters and variation of distance with the aid of a

[7] F. A. Kroger, Physica 7, 1 (1940).
[8] F. Möglich and R. Rompe, Zeits. f. Physik 119, 472 (1942).

thermocouple to the constant value of 3.10^{-3} watt on the slit of the above-mentioned crystal. The resistance dropped to about 3×10^4 ohms. These measurements with filters could be extended to the strong group of mercury lines at 3650A. With the above-mentioned monochromator the relative sensitivity of the cadmium sulfide crystals has been followed down to 2536A. Spectroscopic apparatus for the shorter region (vacuum spectrographs) was not at our disposal. It might be worth while to extend these measurements to shorter wave-lengths as it is to be expected that the photo-conductivity extends still farther down in the Schuman-region.

THE PHOTO-CONDUCTIVITY BY X-RAYS AND CORPUSCULAR RAYS

The general parallelism between phosphorescence and photo-conductivity of incomplete phosphors suggests that the sensitivity of these crystals extends farther down to the region of x-rays and corpuscular rays. The results of some measurements with different sources are collected in Table I. A few remarks have to be made on these measurements. The crystals used had an effective area of 0.2×10 mm. The data on the energies are only approximate. There have been no calibrated ionization chambers for these measurements, which were made in the latter half of 1946, at the disposal of the author. Therefore, the data on distances, currents of tubes, and strengths of preparations have been given for additional information.

The measurements with x-rays were made with copper and iron tubes only. It is to be expected that cadmium sulfide will be still more effective in the region of the absorption edges of sulfur (5.00A) and cadmium (0.463A), respectively. The conductivities already obtained are very large. At a distance of 5 meters the photo-current in the above crystal amounted to about 1 microampere. In the case of more penetrating radiation it might be useful to use the small face of the crystals. This would reduce the effective area to about 0.2×0.1 mm, but, on the other hand, would increase the effective thickness to 10 mm. In the case of very hard radiation a number of such crystals might be lined up in the direction of the beam and connected either in parallel or in series. By connecting in series, the dark resistance, which is already very high and depends mainly on the mounting of these crystals, can be still further increased, Moreover, the density of cadmium sulfide compares very favorably with the absorption of air in ionization chambers.

TABLE I.

Radiation	Energy on crystal per second (effective area = 2 mm²)	Field strength	Current
x-rays: Fe-tube, 30 kv, 15 ma	1×10^4 quanta	2500 volts/cm	15×10^{-6} amp.
gamma-rays: 10-mg Ra at a distance of 25 mm from the crystal	2×10^4 quanta	2500 volts/cm	2×10^{-7} amp.
alpha-rays: Radium preparation emitting 10^3–10^4 alpha-particles per cm² per second	10^3 particles	2500 volts/cm	7.5×10^{-8} amp.
beta-rays: 10-mg Ra at a distance of 5 cm from the crystal	10^4 particles	2500 volts/cm	1×10^{-8} amp.

In the case of alpha-particles, the preparation consisted of a thin layer of some radium compound on a metal plate of 3×4 cm. The total number of alpha-rays emitted from this surface was known from some measurements of the ionization produced. The number of alpha-particles falling on the sensitive area of the crystal has been computed from the geometrical configuration.

The beta-radiation of a preparation of 10 mgs. of radium in a small, thin-walled glass tube has been computed.

The photo-conductivity of these crystals caused by irradiation with electrons of some 1000 volts had not previously been measured, but according to some unpublished results of Dr. E. Krautz obtained with plates sintered from cadmium sulfide powder, the incomplete phosphor shows a considerable amplification of the transverse current if it is irradiated by an electron beam of some thousand volts.

THE ZONAL PICTURE OF INCOMPLETE PHOSPHORS

During recent years the zonal theory of phosphorescence has been developed to a very elaborate description of the many processes involved. Therefore, one might expect that the phenomenon of photo-conductivity would fit

in the scheme of this theory, as incomplete phosphors are only a substantial part of ordinary phosphors.

Gudden and Pohl[2] investigated the photo-conductivity with zinc sulfide phosphors with different activators as well as with natural zinc blende which has to be considered as an incomplete phosphor. The observed phenomena of photo-conductivity are qualitatively identical in both cases. Quantitatively there are some slight differences depending on the activators used, but the general mechanism should be identical in both cases.

The zonal picture describes the phosphorescence by the assumptions shown in Fig. 4. Above the uppermost filled band *A* there is situated the normally empty conductive band *B*. In the intermediate space are located the trapping states *E* and the impurity states *C*. In some theories additional impurity states at *D* are assumed. The transition from the lower edge of the conductive band or—in the last mentioned theories—from the activator term *D* to the lower activator term *C* represents the light emission. The phosphorescence of longer duration is connected with electrons trapped in the states *E*. The trapped energy can be released either by thermal impacts or by infra-red irradiation. In both cases the electron is lifted up to the conductive band from which it might return to the above-mentioned transitions between the impurity states. This picture gives an adequate description of a great number of properties of crystal phosphorescence, and there are no essential objections to it. Considering this picture one has to attribute in the case of incomplete phosphors the absorption below 5200A to the transition of the electrons from *A* to *B*. Consequently, the conductivity in this region is connected with electrons moving in the conductivity band under the influence of the electric field applied. The selective absorption above 5200A corresponds to the transition *A*–*E*, and the selective conductivity should be attributed to the motion of electrons through the trapping states under the influence of the electric field applied. But, by assuming this picture it is difficult to understand why the conductivity at higher field strengths has such pronounced maximum at 5300A. It might be worth while to investigate this maximum very thoroughly, using highly selective radiation and very strong electric field up to the breakdown potential. By suitable reduction of the intensity of illumination the electric load on the crystal could be kept constant at these measurements. In accordance with the theory of phosphorescence, where the electrons in the conductive band show a very short life, the inertia of the photo-conductivity in the short wave region is small, at least much smaller than the inertia of the conduction in the trapping states.

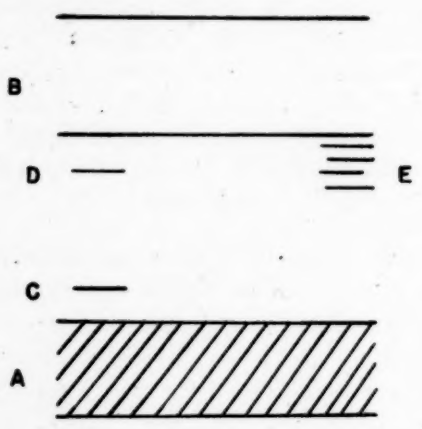

FIG. 4. The zonal picture of phosphorescence.

In the case of visible radiation less than or greater than 5200A, the attribution of the conductivity to either of these two mechanisms follows directly from the wave-length of excitation. The decision in the region of x-rays or in the field of corpuscular rays affords some additional experiments. In ordinary phosphors the trapping states are connected with the lasting phosphorescence, and electrons can be trapped at these states, especially at low temperatures. If they are lifted up to the conductive band by thermal impact, they might return to the impurity states under emission of phosphorescence bands. As these states are metastable, the electrons can be lifted to the conductive band by suitable infra-red radiation. In the case of incomplete phosphors the mean life of the electrons in the trapping states is quite long, while the mean life in the conductive band is shorter by some orders of magnitude. Any electron lifted up to the conductive state by thermal impact or by absorption of long wave-lengths should therefore reduce the total conductivity. This effect is very large and

can be quite easily observed. *Crystals illuminated with light >5200A reduce their photo-conductivity if additional infra-red illumination is falling on the effective areas.* The amount of reduction depends on the ratio of energies: visible light/infra-red light. The photo-conductivity due to weak visible radiation can be reduced to some 10 percent or less by a suitable amount of infra-red radiation. The exact shape of the coordinated absorption curve[9] has been measured with the double monochromator. At these measurements the crystals have been made conductive by weak illumination with green light filtered by a Schott-filter, and the reduction has been measured which takes place by additional illumination with a spectrum of constant energy.[10] The relative distribution is given by Fig. 5. The region of selective photo-conductivity extends very weakly but quite far in the red. At 8750A additional illumination neither increases nor decreases the conductivity. Beyond this wave-length the curve shows two maxima at 9300 and 11,400A. Above 13,000A no extinguishing effect can be observed. According to our knowledge of ordinary phosphors, the extinguishing effect at shorter and at longer wave-lengths of this distribution should be different. Phosphors illuminated with rather long wave-lengths show a sudden increase of their luminosity ("flash") with following decrease. If they are illuminated with shorter wave-lengths, red or near infra-red, the luminosity decreases at once without this increase ("quenching"). The electric analog to the second effect can be observed by suitable periodical illumination of these crystals. A few words have to be said about the inertia of the conductivity by illuminating with modulated light. The general shape of the increase and decrease of photo-conductivity by illumination, with rectangular pulses of about 200/sec. registered with a small oscillograph, is identical with similar curves for selenium photo-resistances and with the brightness curves of phosphors illuminated with pulsed electron beams.[11] With

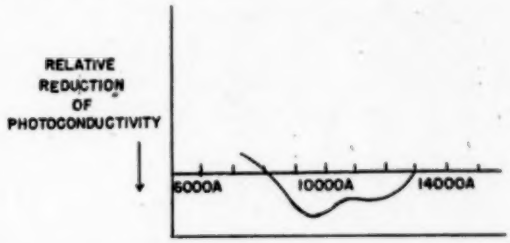

FIG. 5. The extinguishing of photo-conductivity of CdS crystals by additional illumination with infra-red radiation.

increasing intensity of illumination the curve becomes more and more rectangular (Fig. 6). On the other hand, if the crystals are illuminated with constant visible light and rectangular pulses of infra-red are superimposed, the general shape of these curves is given by Fig. 7.

If the crystal is excited by rectangular pulses of visible light and extinguished by short pulses of infra-red light, whose phase coincides with the "decreasing" part of the curve, curves of Fig. 8 are obtained. Such curves correspond to the "flash" of ordinary phosphors.

If one makes the assumption that the electrons are lifted up from the upper edge of the filled band to the trapping states, the state reached depends on the wave-length of the visible radiation. Therefore, one should expect that the conductivity in higher situated trapping states should be extinguished by correspondingly longer wave-lengths than the conductivity in lower states. By simultaneous variation of the exciting (V_1) and the extinguishing (V_2) wave-length by two monochromators, the exact state of the electron lifted up to the conductive band (V_1+V_2) can be measured. Such measurements should give valuable information on the return of the electrons from the different states of the conductive band to the lower band.

FIG. 6. General shape of the increasing and decreasing of photo-conductivity of CdS crystals by periodical illumination with pulses of 1/200-sec. duration. With higher intensity the current increases and decreases faster.

[9] In the nomenclature of Pohl, *f'*-center.

[10] The energy has been kept constant over the investigated region by previously measuring the necessary lamp current at different wave-lengths.

[11] For selenium see the book of G. P. Barnard, *The Selenium Photocell and Its Applications* (Constable, London, 1930).

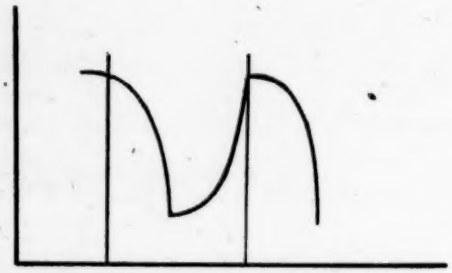

FIG. 7. General shape of the decreasing and increasing of photo-conductivity of CdS crystals by additional illumination with extinguishing infra-red light.

The conductivity excited by wave-lengths > 5200A cannot be extinguished by additional illumination. This is to be expected, since electrons cannot be transferred by strongly absorbed light to the trapping states which are sparsely distributed in the crystal lattice. The range of photo-conductivity due to the conductive band should extend over the whole ultraviolet down to the region of soft x-rays. On the other hand, in the region of x-rays, where the radiation penetrated deeper in the crystal, the selective photo-conductivity again prevails. The photo-conductivity caused by the $K\alpha$ line of iron can be easily extinguished by infra-red illumination. The following mechanism might be proposed. The radiation produces "cascades" of secondary, tertiary, and higher order process electrons,[12] and the slowest of these are trapped in the states and thus produce, under the influence of the electric field, the conductivity. In the same way alpha-rays and beta-rays give rise to the selective photo-conductivity which can be reduced to a very small amount by infra-red illumination.

A complete theory of the photo-conductivity would have to deal with the presence of electrons in the stationary states and their motion under the influence of electric fields. On the other hand, the theory of ordinary phosphors deals with the transitions between these stationary states. By comparing complete and incomplete phosphors the cadmium sulfide crystals can be transformed into a complete phosphor by tempering in metal vapors. A very extensive theory of quantum phenomena in solid state should be obtained.

[12] F. Möglich and R. Rompe, Zeits. f. tech. Physik 21, 304 (1940).

CADMIUM SELENIDE, CADMIUM TELLURIDE, AND MERCURY SULFIDE

The general regularities of similar incomplete phosphors can be deduced from the position of the elements involved in the periodical system. With increasing atomic number of the two components, the maximum of selective photo-conductivity and of the extinguishing curve shifts towards longer wave-lengths. Cadmium selenide has been prepared in rather small single crystals of 1–2 mm³ by passing a stream of hydrogen at first over the heated selenium and then through the above-mentioned reaction tube. The absorption and the considerable photo-conductivity are shifted to the red. The maximum of the selective conductivity is situated at 6000A.[13] Cadmium telluride crystals are made in an analogous way. The small crystals show a further shift of the absorption and of the selective conductivity towards the red. The maximum which is much flatter than in the case of CdS and CdSe is situated at 6200A. In addition, for CdTe the extinguishing by additional infra-red illumination has been observed. This curve is shifted towards longer wave-lengths and has one wide maximum. Single crystals of the analogous zinc compound have not yet been produced. But as the general shape of the curves of natural and of synthetic greenockite are identical, the properties of ZnS might be taken from the measurements of Gudden and Pohl on natural zinc blende. The maximum of the selective effect which is much smaller, as in the case of cadmium sulfide, is situated at 4200A.[14] According to their measure-

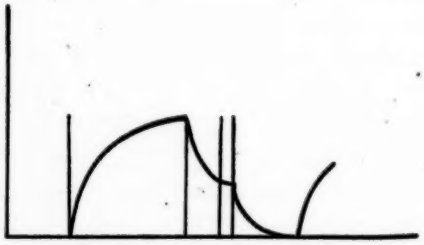

FIG. 8. General shape of the increasing and decreasing of photo-conductivity of CdS crystals by periodical illumination with long (1/200 sec.) pulses of exciting and short (1/2000) pulses of extinguishing light.

[13] The exact curves of CdSe and CdTe are at this time not at the disposal of the author.

[14] These crystals contain 1.6 percent Fe. The normal photo-conductivity below the absorption edge is about one order of magnitude less.

ments with ordinary phosphors with different activators, the maximum depends on the activator added. It shifts from 3700A for a phosphor with an unknown activator to 4250A for zinc sulfide with uranium activator.

According to Gudden and Pohl, natural cinnabar crystals show a very pronounced maximum of the selective conductivity at 6150A. In this case the difference between the current-voltage curves in the normal and in the selective photo-conductivity is very pronounced. The normal photo-conductivity shows saturation. The selective photo-conductivity increases continuously with increasing voltage. Curves of the extinguishing effect have not been published by these authors, inasmuch as they already mention the diminishing of the photo-conductivity by red light, added *after* the excitation of the photo-conductivity by visible light.

THE USE OF INCOMPLETE PHOSPHORS AS PHOTO-CELLS

A few words might be said about the possibilities of using such incomplete phosphors, especially cadmium sulfide, as photoelectric cells. It is one advantage of these crystals that the current obtained with ordinary illumination (daylight) is very high as compared with alkali photo-cells. Resistances of about 10^4 ohms can easily be obtained with effective areas of some mm^2. In contradistinction to the selenium photo-resistance, the dark current is extremely small; in fact, with careful mounting on perfect insulating bases, it can be neglected for all practical uses. As Gudden and Pohl have already shown in the case of natural zinc blende, the resistance depends on the previous history. By periodical illumination it diminishes, and the current increases very much, but according to our observations these crystals can be used for some years if the load on the crystals does not exceed about one milliwatt/mm^2 of the effective area between the electrodes. With frequencies up to 10,000 cycles the modulated part of the current decreases, but it is still much larger than in any other photo-cell known and can, therefore, be adjusted by suitable filters. The shape of the current curve is somewhat detrimental to the reproducing of sound tracks. The decrease of inertia by using normal photo-conductivity with wave-lengths below 5200A improves this curve considerably.

The possibilities offered by an effective photo-cell of such small dimensions in the region of x-rays hardly needs to be emphasized. From the great number of possible applications for registering x-ray spectrographs, registering structural analysis apparatus, dosimeters, and so on, one application might be mentioned which makes use of the possibility of reproducing x-ray pulses by such photo-resistances. The short wave-length shift of the continuous x-ray spectrum shifts periodically with the voltage curve of a half wave x-ray apparatus. A cadmium sulfide photo-resistance used with alternating current of the same frequency, but shifted in its phase 90° against the tube voltage, registers a nearly constant current on an oscillograph tube if it is irradiated by these pulsating x-rays. By inserting substances with selective absorption edges in the beam of x-rays, these edges are registered by small deflections in the oscillograms. Thus absorption spectroscopy can be performed without the use of a spectrograph.

In the x-ray region, as well as in the region of alpha-, beta-, and gamma-rays, the extinguishing effect might be used for intensity measurements.[15] If amplification is necessary, modulation of the photo-current can be obtained in two ways: first by modulation of the source by rotating sectors, and second by using the extinguishing effect of modulated infra-red radiation.

With symmetrical electrodes the photo-current is independent of the frequency of the current passing through the cell. Frequencies as high as 3×10^7 pass through such cells and follow the variation of the irradiating light in the same way as direct currents.

Thus the incomplete phosphors might prove to be a simple and useful instrument for measuring the different radiations connected with the development of nuclear physics.

[15] The reaction of slow neutrons (Cd) on these crystals has not yet been investigated.

The Discharge Mechanism of Self-Quenching Geiger-Mueller Counters

S. H. LIEBSON*
Naval Research Laboratory, Washington, D. C.
and
University of Maryland, College Park, Maryland
(Received May 21, 1947)

A split counter arrangement was used to investigate the absorption coefficient of the radiation which causes the discharge to spread along the wire of a counter after the triggering of a pulse. The counters used were filled with methylene bromide and argon at various pressures, and with ethyl alcohol and argon. The results indicate that the vapor dissipates electron energies, thereby reducing the number of photons produced during the discharge. It was also observed that the absorption coefficient is a function of the argon alone, from which it was concluded that photo-ionization of the argon is responsible for spreading the discharge along the wire. This behavior was also observed with helium and neon in combination with alcohol or methylene bromide.

1. INTRODUCTION

THE object of this investigation was to study the mechanism for the spread of the discharge along the length of the wire of a Geiger-Mueller counter. In proportional counting the pulses are localized and have amplitudes proportional to the primary ionization. The source of current amplification is ionization by electron impact leading to the formation of a Townsend avalanche.[1] The Geiger-Mueller region is characterized by the spread of the discharge along the length of the tube by a process previously shown to be photoelectric in nature.[2,3] The spreading of the discharge is supposed to depend on the excitation of certain spectral lines of the gas at a given field strength, corresponding to the threshold voltage.[4] Geiger-Mueller counting is also characterized by the self-quenching process resulting from the reduction of the field at the anode by the ion sheath.[5,6] At sufficiently high voltages a continuous corona discharge develops, which sets the limit to Geiger counting action.

Several experiments have been conducted to determine the mechanism for the spread of the discharge. Greiner's experiments[3] on slow counters came closest to the intent of this investigation. He used two counters facing each other, in a common envelope. The anodes were separated at a fixed distance of about 1 cm. Measurements were made of the number of counts that originated in one counter and spread across to the other, at different pressures. By means of these measurements he was able to deduce absorption coefficients for different gases. That the discharge depended on photon absorption was proven with the aid of ultraviolet absorbing films of Celluloid. The most plausible explanation for the spread of the discharge through the film was photoemission in the second counter produced by ultraviolet radiation penetrating the Celluloid. In another experiment, insulating beads of different thicknesses and diameters spaced on the anode localized the discharge between the beads.[7] In an experiment conducted by Ramsey,[8] two adjacent slow counters were triggered coincidentally when the discharge was initiated in one of the counters, but discharged randomly when a self-quenching gas mixture was used. Similar results were obtained by Curran and Strothers.[9] The arrangements in both experiments were such as to minimize the possibility that the discharge was being initiated by any mechanism other than photons. Another set of interesting experiments

* Extracted from thesis submitted to the faculty of the Graduate School of The University of Maryland in partial fulfillment of the requirements for the degree of Doctor of Philosophy, based on work done at the U. S. Naval Research Laboratory.

[1] M. E. Ross and S. A. Korff, Phys. Rev. **59**, 850 (1941).
[2] C. G. and D. D. Montgomery, J. Frank. Inst. **231**, 447 and 509 (1941).
[3] E. Greiner, Zeits. f. Physik **81**, 543 (1933).
[4] S. C. Brown, Phys. Rev. **62**, 244 (1942).
[5] C. G. and D. D. Montgomery, Phys. Rev. **57**, 1030 (1940).
[6] H. G. Stever, Phys. Rev. **61**, 38 (1942).
[7] M. H. Wilkening and W. R. Kanne, Phys. Rev. **62**, 534 (1942).
[8] W. E. Ramsey, J. Frank. Inst. **231**, 393 (1941).
[9] S. C. Curran and J. E. Strothers, Proc. Camb. Phil. Soc. **35**, 654 (1939).

was performed by Stever[6] following earlier work by R. Brode. Stever used counters with divided cylinders and beads on the wire. In one most suggestive experiment, a glass bead on a wire served to stop the discharge spread at low values of E/p, but did not hinder the discharge at large values of E/p, where E is the field strength and P is the pressure. This was interpreted to mean that the radius corresponding to the critical value of E/p was pushed out till the bead was well enclosed within it, and the discharge could then spread. The possibility of localization of the discharge at the surface of the wire was ruled out by these experiments which indicated a mechanism in the gas, starting at the critical value of E/p. In another paper, Stever[10] used the divided counters as a counter telescope where separate ionizing events were necessary in each segment to cause the segment to count. Other localization effects have been studied through the use of divided cathode cylinders with different voltages on each segment.[11] The effectiveness of insulating beads in stopping the discharge from spreading was attributed by Wilkening and Kanne[7] to a combination of reduction of field intensity by accumulation of charge on the insulators, and to photon absorption by the vapor. Their results were interpreted to mean that the photon absorption in the gas was complete within a few electron mean free paths.

2. THEORY OF THE EXPERIMENTS FOR DETERMINING ABSORPTION COEFFICIENT AND NUMBER OF PHOTONS

The following work was undertaken to determine the nature of the process responsible for the spreading of the discharge. In order to measure the absorption coefficient of the spreading radiation, a double counter arrangement was used. One of the counters could be moved along its axis with respect to the other, in the same glass enclosure (see Fig. 1). The electronic circuits were so designed that a count could be kept of all discharges which spread from one counter to the other. Since the charge per unit length of a counter is a constant, those discharges which spread across the intervening gap appeared as pulses twice the size of those which developed in one of the counters. Assuming an absorption to take place, the probability of discharge spread must be a function of the total amount of intervening gas, or what amounts to the same thing, the probability of spread must depend on the constitution of the gas mixture, the distance between the counters, and the pressure. The ratio of the number of large (double-sized) pulses to the total number of pulses determines w, the probability for spread of the discharge. In subsequent paragraphs it will be shown how this measurement can be used to derive both the absorption coefficient, μ, and the total number of photo-ionizations per unit length of the wire responsible for the spread of the discharge. Knowing the number of ions per unit length per discharge, the number of photo-ionizations produced per ion in the discharge may be computed.

The absorption coefficient may be determined directly from measurements of w. If $e^{-\mu z}$ is the

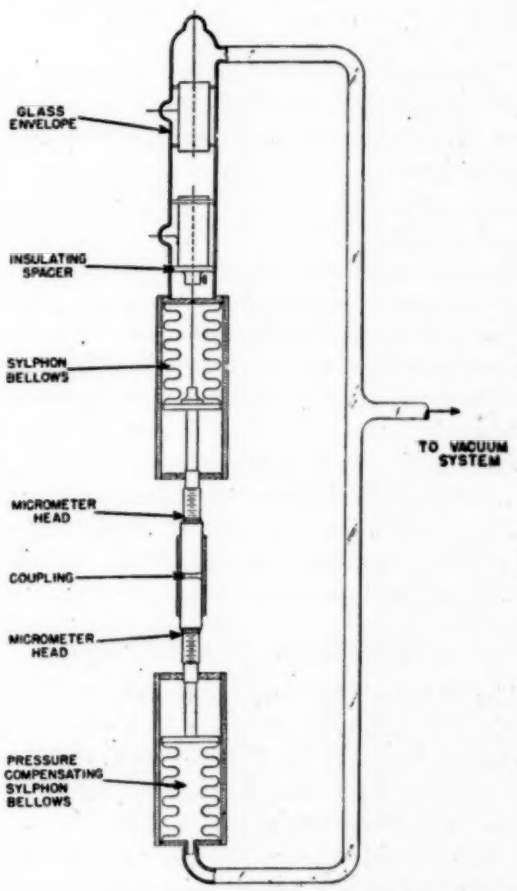

FIG. 1. The movable double counter.

[10] H. G. Stever, Phys. Rev. 59, 765 (1941).
[11] W. E. Ramsey, Phys. Rev. 61, 96 (1942).

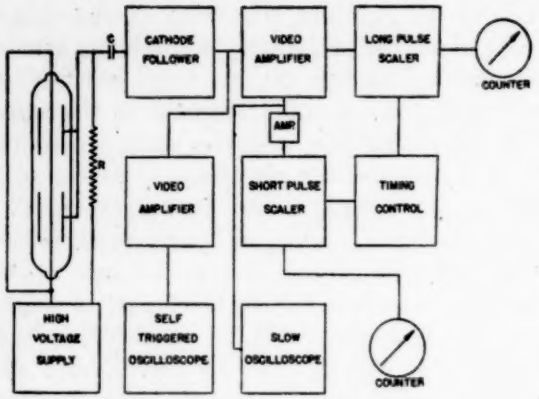

FIG. 2. Block diagram of measuring circuits.

probability that a quantum appearing at the end of one counter will not be absorbed within a distance x, then $1-e^{-\mu x}$ is the probability that it will be absorbed in that distance. The probability that all of N quanta will be absorbed is

$$(1-e^{-\mu x})^N, \tag{1}$$

or

$$w=1-e^{-N\exp(-\mu x)} \tag{2}$$

is the probability for a discharge to occur at large values of x. Taking the logarithm twice, the result is

$$\log[-\log(1-w)]=\log N-\mu x. \tag{3}$$

This is the equation of a straight line whose slope is given by μ, and the y intercept by $\log N$. To determine μ, the logarithm of $(1-w)$ was plotted on a logarithmic scale as a function of x, and the slope determined from the experimental curves.

The value of N used in the calculations represented the total number of photons capable of photo-ionization occurring at the end of the wire, and included the quantum efficiency, absorption, and related factors.

3. DESCRIPTION OF EQUIPMENT

The movable split counter was constructed of brass cylinders (Fig. 1) 5 cm long and 2.1-cm diameter, mounted in a Pyrex glass envelope. The anodes were tungsten wires 0.03 inch in diameter, one of which was sealed directly to the Pyrex envelope, and the other attached to a sylphon bellows and micrometer screw arrangement moving in a vacuum-tight brass housing to minimize side motion of the wire. The bottom cathode was movable through the same bellows. The brass housing was sealed to the Pyrex envelope with De Khotinsky cement. It was found necessary to provide another sylphon bellows system, coupled to that on the movable counter, in order to maintain the pressure constant, i.e., when the bellows in the counter was compressed, the compensating bellows expanded.

To correct for spurious effects in the determination of charge per pulse, such as the occurrence of point discharges and errors in resetting the micrometer, control measurements of plateau, charge per pulse, and photon production were made on a split-counter tube of the same general dimensions as the movable counter tube combination, except that a fixed distance between cathodes of 1.4 cm was employed, and the inner wire was continuous through the tube.

Figure 2 is a block diagram of the measuring circuits associated with counting the pulses for absorption determinations. The output-pulse voltage across resistance R was fed through a condenser to a cathode follower. A low value of grid leak (10,000 ohms) was used in conjunction with a 50-$\mu\mu$fd coupling condenser to differentiate the pulses, thereby accentuating changes in pulse shape. The purpose of the cathode follower was to isolate the counter tube from external circuits by virtue of the high input impedance typical of cathode followers, in addition to providing a low impedance output for the input circuits of the two video amplifiers. One of the video amplifiers was used to amplify the signals which were fed to a self-triggered oscilloscope with sweep times of 5, 25, 100, and 500 microseconds. This served as a monitoring oscilloscope to indicate the shape and characteristics of the Geiger-counter pulses. The band pass of the video amplifier was roughly 100 c.p.s. to 4 megacycles per second. The other amplifier output was connected to a conventional oscilloscope and to the input circuits of two scaler units. The scalers were conventional Eccles-Jordon type scale of two multi-vibrators, giving 1 output pulse to every 16 input pulses. Mechanical-impulse recorders were operated by a thyratron tube used as output stage from each scaler. One of the scalers was supplied with an additional amplifier tube with adjustable gain, so that all pulses

would register on its recorder, while the gain of the video amplifier was adjusted so that only the large pulses, those which propagated across the gap, could register on the other recorder. A mechanical timing control was connected to the scalers, so that the total number of large pulses, as well as the total number of all pulses, both large and small, could be recorded in the same time interval on the other recorder.

For each filling the data taken consisted of: the total number of counts per minute as a function of counter voltage for each counter, the average current flowing to the counter during the same time interval, and for the double counter, the number of double-sized pulses appearing per 16,000 total pulses.

Measurements of the current flowing through the counter were made in the ground return circuit of the counter anodes by means of a General Radio vacuum-tube d.c. amplifier, Model 715A, across whose input a 20-μfd condenser was placed to minimize fluctuations. During a given time interval the number of pulses occurring were counted, thus giving the necessary data for calculating the charge per pulse.

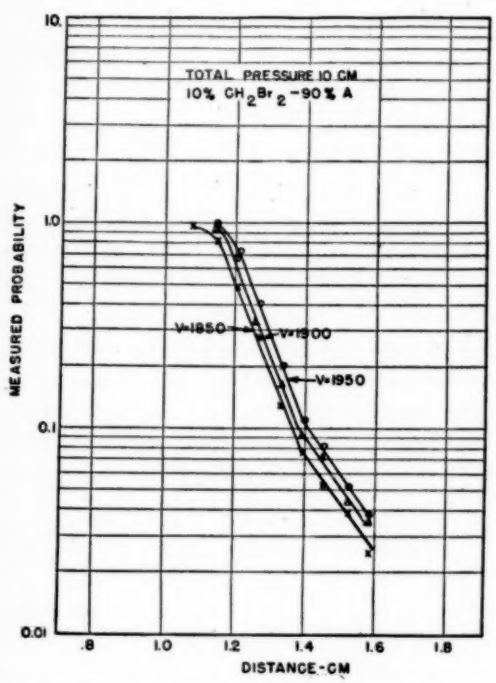

FIG. 3. Typical propagation probability curve.

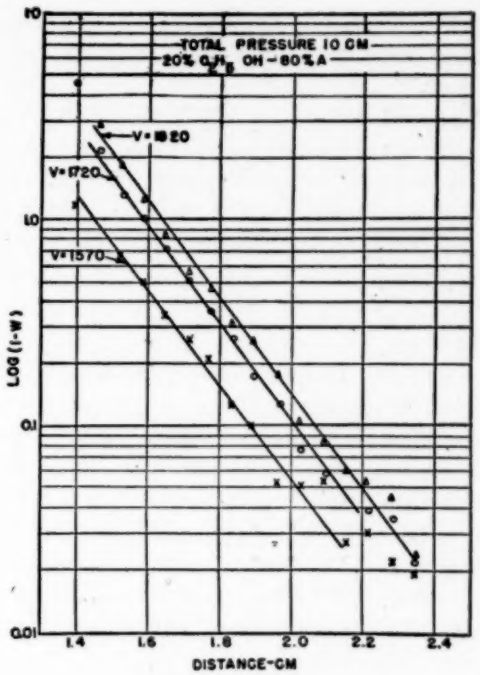

FIG. 4. Absorption curve.

4. MEASUREMENTS OF ABSORPTION COEFFICIENT

Figure 3 shows a typical curve of probability of propagation through the gas path between the cathodes of the movable double counter, filled with a mixture of 10 percent CH_2Br_2 and 90 percent argon at a total pressure of 10 cm Hg, for different voltages between anode and cathode. Figure 4 shows the values of $\log(1-w)$ plotted on semi-logarithmic graph paper as a function of distance between the cathodes of the movable counter system for an alcohol-argon filling. From Eq. (3) it is easily seen that the slope of these curves determines the absorption coefficient for the spreading mechanism.

Table I tabulates three sets of absorption coefficients computed from the curves. The first set lists measurements of the slope. The second set consists of absorption coefficients, corrected to one centimeter of pressure, assuming the absorption to be due only to the total amount of argon present. The third set consists of absorption coefficients, corrected to one centimeter of pressure, assuming the absorption to be due solely to the organic vapor.

For methylene bromide fillings, each absorption curve contained two slopes, one of which is

designated by μ_1 and the other by μ_2. For alcohol mixtures only the slope designated by μ_2 was observed.

The corrected values of the absorption coefficients shown in Table I were obtained by dividing the values of μ_1 and μ_2 obtained from the curves by the associated partial pressures of argon. The weighted values were obtained by estimating the accuracy of each set of readings, assigning relative weighting factors to each, and averaging the results.

It may be assumed that the various errors involved in counting, filling to the correct pressure, and measurement of slope, were sufficient to account for the minor variations observed in both the absorption coefficients listed in Table I. That the geometrical arrangement did not introduce appreciable errors in the measurements may be concluded from the fact that the data in general showed the same slope in spite of the different distances used, and that the slopes of the 5-cm, 10-cm, and 20-cm total pressure-absorption curves yielded the same values of the absorption coefficient.

Measurements made on methylene bromide were based on a counting rate of about 20 per second and a total count of about 16,000 counts, in order to minimize errors due to resolving time and to limit the standard deviation of counts per second to about one percent. Measurements made on the alcohol counters were not as accurate and, in general, were conducted only as a control experiment to support the results obtained with methylene bromide. The poor results obtained with the five percent alcohol mixtures are in accord with results of Wilkening and Kanne[7] who found that counters made with less than five percent alcohol showed almost no localization effects.

The absorption measurements were repeated with fillings of neon-methylene bromide and helium-methylene bromide. The results with these mixtures verified the conclusions that the absorption coefficient is a function of the rare gas alone. For a ten percent methylene bromide-neon mixture at 10-cm pressure, the coefficient of absorption was 0.93, corresponding to a coefficient of 0.1 per cm for neon at a pressure of one centimeter of mercury. For helium, the coefficient was so small that accurate determination of the slope was not feasible.

Certain conclusions may be drawn from these data:

1. The absorption per unit pressure is constant, depending only on the percent of argon present. These data are overwhelmingly in favor of the assumption that absorption is due to the argon alone.

2. There are two different absorption constants indicating two different types of photons. At various percentages of CH_2Br_2 at 10-cm total pressure, both coefficients showed clearly. In alcohol-argon mixtures only one coefficient was observed, from which it is concluded that the separation used during measurements was such that one type of photon had been almost completely absorbed when the separation was sufficient for readings to be taken. The larger value of the absorption coefficient is probably characteristic of the higher energy photon because it appeared more prominently as the voltage was increased.

3. From the shapes of the curves and their intersections with the $\log(1-w)$ axis, it appears that the number of effective photons increases with voltage. As will be shown later, the function of the vapor seems to be to inhibit the production of photons in the discharge.

The diameter of the atom, σ, for the absorption process may be defined by $\mu=N\pi(\sigma/2)^2$, where N is the number of atoms per cc. Inserting a value of $\mu=1.35$/cm for one absorption coefficient, and $\mu=0.65$/cm for the other absorption coefficient, the resulting values for the atomic

TABLE I. Absorption coefficients.

Pressure	Gas mixture %	Vapor	Slope measured from curves (cm^{-1}) μ_1	μ_2	Absorption coefficients Corrected for 1-cm argon (cm^{-1}) μ_1A	μ_2A	Corrected for 1-cm vapor (cm^{-1}) μ_1B	μ_2B
5 cm	10	CH_2BR_2	7.0		1.55		14	
5	20	CH_2BR_2	5.2		1.3		5.2	
10	4	CH_2BR_2	13.5	5.8	1.41	0.6	33.7	15
10	10	CH_2BR_2	11.5	6.4	1.28	0.71	11.5	6.4
10	20	CH_2BR_2	12.1	5.5	1.51	0.68	6.1	2.8
20	10	CH_2BR_2	23		1.28		11.5	
10	5	C_2H_5OH		3.83*				
10	10	C_2H_5OH		5.8		0.64		5.8
10	20	C_2H_5OH		5.4		0.67		2.7
10	30	C_2H_5OH		5.8		0.83		1.6
20	5	C_2H_5OH		3.5*				

*Low percentage of alcohol does not make counter with Geiger-Mueller characteristics.

Weighted average of $\mu_1A=1.35$
$\mu_2A=0.65$

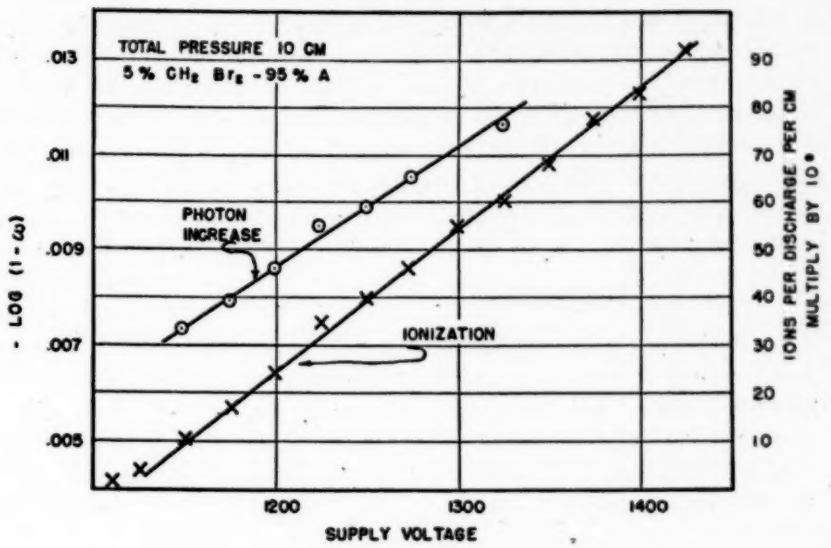

FIG. 5. Increase of photons and ions in the counting region.

cross section of argon for the two types of photons are: diameter $\sigma_{1.35}=0.23\times10^{-8}$ cm and $\sigma_{0.65}=0.16\times10^{-8}$ cm.

5. DETERMINATION OF THE RELATIVE NUMBER OF PHOTONS IN DIFFERENT MIXTURES

Equation (2) indicates that the experiment is well suited for the determination of N, the number of photons causing a photoelectric effect in the gas. Equation (2), rewritten as

$$\log(1-w)=-AN, \qquad (4)$$

shows that for a fixed separation between counter cathodes, $e^{-\mu x}$ is a constant, A, and $\log(1-w)$ is directly proportional to the number of effective photoelectrons. Accordingly, probability measurements were made on the double counter with fixed separation of 1.4 cm as the voltage was increased throughout the plateau region. Typical results are shown graphically in Fig. 5. The data in Table II clearly show the effect of the vapor on the number of photons available to propagate the discharge. The ionization data were obtained by measuring the average current flowing through the counter while the counts were being recorded, and converting to ions per cm per discharge by dividing the charge per count obtained on one counter by 5.5 cm (0.5-cm allowance being made for end effects). In this experiment, the separation of the counter was such that only the $\mu=0.65$ cm^{-1} type of photon was involved. More photons were produced in alcohol-argon mixtures than in equivalent proportions of methylene bromide-argon mixtures. If the transition from the proportional region to the plateau region depends on the number of photons available for propagating the discharge, then the results indicated that alcohol-argon counters should have lower thresholds, which is in agreement with observation. This was also borne out by the greater slope of photon increase in alcohol-argon counters. This greater increase of slope presumably is related to the fact that alcohol-argon counters have a smaller plateau before breaking into a continuous discharge. It was observed that the increase in rate of ion formation with voltage was almost a constant, independent of the type of vapor or percentage composition.

The data for alcohol-argon mixtures showed an increase in the number of photons relative to ions as the percentage of alcohol vapor was

TABLE II. Relative number of photons per discharge in different mixtures. Measured at over-voltage of 100 volts.

Pressure (cm)	Percent vapor (%)	Relative No. of photons		Relative No. of photons per ion	
		C_2H_5OH	CH_2Br_2	C_2H_5OH	CH_2Br_2
5	5		16.5		35
5	10		12.0		28
5	20		8.0		12
10	5		9.1		30
10	10	17.0	8.0	45	24
10	20	23.0	6.4	43	19
10	20	36.0		110	

increased. A possible explanation might be that in alcohol single ionization and dissociation occurs, with the electron by-product of the ionization contributing to the further production of photons. However, the data for alcohol would not be consistent with the fact that the discharge may be heavily quenched by the further addition of alcohol.

6. CONCLUSION

To understand the role of the organic vapor and its effect on the spread of the discharge, let us first consider the action taking place in the slow counter, i.e., a counter filled with monatomic gas. In the course of the discharge, several types of photons are created. The first type consists of photons derived primarily from excited neutral atoms. These photons lie in the visible and near ultraviolet region, and help perpetuate the discharge by the ejection of photoelectrons at the cathode. These photons do not cause ionization within the gas itself because of their low energy. The second type of photon is derived from the excited singly or doubly ionized gas atom, and may either eject photoelectrons from the cathode cylinder, or what is more probable, because of the opacity of the gas in the wave-length region involved, cause photoelectric emission in the gas itself. The emitted electrons then serve to trigger the formation of new Townsend avalanches. On the basis of previous hypotheses, it was assumed that the organic vapor served to absorb radiation in the ultraviolet, thus minimizing photoelectric action at the cathode and in the gas. The experiments conducted above invalidate this assumption.

Many of the photons from excited argon, originating in the avalanches, lie in the range of 11.5 to 15.7 ev, corresponding to 1070A to 790A. The photoelectric threshold of the cathode in most cases is about 4 ev. Thus, for localization of the discharge to the region in the immediate vicinity of the wire, either these photons must be strongly absorbed in the gas mixture, as hypothesized by Ramsey,[8] or the number of photons produced should be lowered to the point where photoelectric action at the cathode has a sufficiently low probability.

The results presented here show quite definitely that the mechanism of the spreading discharge, previously shown to be photoelectric in nature, is a function of the rare gas alone. The function of the vapor in the discharge is to poison the production of photons rather than contribute appreciably to photon absorption. Electrons in the avalanche tend to lose their energy through excitation and decomposition of the organic vapor molecules, as demonstrated by the experiments of Spatz[12] in which it is shown that the organic vapor is rapidly decomposed in the course of a discharge. That this process is so effective is primarily caused by the fact that the energy necessary for excitation and decomposition of the vapor is considerably less than the energy required for the production of suitable photons to spread the discharge.

ACKNOWLEDGMENT

I wish to express my appreciation to Professor R. D. Myers of The University of Maryland for his advice and encouragement during the investigation.

[12] W. D. B. Spatz, Phys. Rev. 64, 236 (1943).

Further Experiments on the Surplus Gamma-Radiation from Granite

VICTOR FRANCIS HESS
Fordham University, New York, New York

(Received June 17, 1947)

Field experiments in Massachusetts (1945) and laboratory experiments with a bulk sample of granite (300 lb.) from Quincy, Massachusetts, showed that the ionization produced by gamma-rays from this type of rock is about twice as great as the one computed from their content of uranium, thorium, and potassium. In order to find out the origin of this unexpected surplus radiation, new experiments were carried out, using essentially the same technique, but shielding the ionization chambers with lead cylinders about 1 cm thick. The radium content of the bulk sample of Quincy granite was re-checked in the National Bureau of Standards and found, on the average, only 7 percent above the figure given by Evans and Goodman.

These new experiments show again a surplus of penetrating radiation of about 100 percent above the computed value, exceeding by far all possible errors in the determination of the uranium, thorium, and potassium content of Quincy granite. It is shown that neither the production of photons in transmutations induced by alpha-rays within the granite, nor spontaneous fission of uranium and thorium in this rock by cosmic rays or by neutrons from cosmic rays could account for the observed effect.

Preliminary experiments with dunite (South Carolina), a mineral containing almost no uranium, thorium, or potassium showed a complete absence of any radiation from this type of rock.

It must be concluded that a hitherto unknown penetrating radiation is given off by granite. Further experiments are in progress.

IN May 1946, I found a very interesting discrepancy in the amount of observed ionization produced by gamma-rays from thick layers of granite, and the quantity computed from the known amounts of uranium, thorium, and potassium contained in it. The latter amounted to only about 50 percent of the total ionization actually found by measurements in a quarry (Quincy, Massachusetts), and in laboratory experiments with large quantities (300 lb.) of the same sort of granite. I reported on these experiments at the Annual Meeting of the American Geophysical Union in Washington, D. C. on May 30, 1946.[1]

A detailed description of the experiments and of the Gish-ionization meter used has been given in this paper (1946). It was concluded that it was very unlikely that the uranium, thorium, and potassium content given by R. D. Evans and Clark Goodman for the Quincy granite could be too low by such an extent. Therefore, it seemed necessary to investigate this discrepancy more rigorously by repeating all experiments with much heavier screening of the ionization chambers. These new experiments were carried out in the winter of 1946–47, and this paper presents the results.

I. EXPERIMENTAL PROCEDURE AND COMPUTATION OF THE IONIZATION IN THIS ARRANGEMENT

The Quincy granite was recommended to me by Robley D. Evans and Clark Goodman as one of the most homogeneous and best analyzed types of igneous rocks. These authors[2] give the following figures of uranium content: $M_1=(2.7\pm0.5)\cdot10^{-6}$ gu per g of granite (taken from Swingles quarry, Quincy, Massachusetts). This in equilibrium with radium corresponds to $0.95\cdot10^{-12}$ g Ra per g of rock. For the thorium content, they gave, $M_2=(8.1\pm2.0)\cdot10^{-6}$ g Th per g of rock. The potassium content is not given in their paper; however, it can be estimated to be between 3 and 4 percent. Warren's[3] figure (3.8 percent) is certainly reliable enough for this purpose.

If an ionization chamber is either placed directly above a large slab of the rock, or surrounded by a thick layer of crushed rock, the ionization produced by the hard gamma-rays from Ra (RaC″), Th (ThC″), and potassium in the rock can be computed by Eve's formulas. The formula for a point-shaped source of radiation is $q=Km/r^2e^{-\mu r}$. Here q is the number of pairs of ions produced per cm³ and per sec.; m is

[1] V. F. Hess, Trans. Am. Geophys. Union **27**, 670 (1946); V. F. Hess, Norsk Geologisk Tidsskrift **27** (Jan. 1947).

[2] Robley D. Evans and Clark Goodman, Bull. Geol. Soc. Am. **52**, 459 (1941).

[3] C. H. Warren, Proc. Am. Acad. **49**, 227 (1913).

the amount of radioactive material per cm³ of rock; and μ is the absorption coefficient of gamma-rays in the rock. This expression gives, when integrated for an infinite thickness of radioactive rock all around the ionization vessel, the total ionization $q=q_1+q_2+q_3$ where $q_1=(4\pi K_1 m_1/\mu_1)$, $q_2=(4\pi K_2 m_2/\mu_2)$, $q_3=(4\pi K_3 m_3/\mu_3)$ are the components of the ionization produced by the radium and thorium products and potassium (subscript 1 pertaining to radium, 2 to thorium, 3 to potassium). In these formulas, m_1, m_2, m_3, denote the amounts of radium, thorium, and potassium per cm³ of rock. Dividing by the density (ρ) of the rock, we obtain $M_1=m_1/\rho$, $M_2=m_2/\rho$, $M_3=m_3/\rho$, which are the figures for the radium, thorium, and potassium content per gram of rock listed above.

For an infinite layer of rock surrounding an ionization chamber, the formulas for the components of ionization to be expected in the chamber are, therefore: for radium $q_1=4\pi K M_1/(\mu_1/\rho)$, for thorium $q_2=4\pi K_2 M_2/(\mu_2/\rho)$, $q_3=4\pi K_3 M_3/(\mu_3/\rho)$. This way of writing the formulas has the further advantage that one needs only the mass absorption coefficients (μ_1/ρ), (μ_2/ρ), (μ_3/ρ) of the hard gamma-rays of Ra, Th, and potassium which are much better known than μ_1, μ_2, μ_3, and are practically constant for all materials.

The constants K_1, K_2, K_3 (Eve's constants) differing slightly for vessels of different size and materials, were redetermined by the author and Eva M. Balling[4] for the chambers actually used for the present study. For a brass vessel, filled with nitrogen at normal pressure, we obtained 4.9×10^9 I (ion pairs/cm³ sec.) per gram of radium, in a chamber of 4888-cm³ volume.

In a monograph[5] on the ionization balance of the atmosphere, I have shown that the gamma-ray effects of radium itself, of radium B, uranium X, etc., are negligible, and therefore a simplified treatment with only one significant absorption coefficient for each component is permissible.

It is obvious that μ_1/ρ, μ_2/ρ, μ_3/ρ must be known for the hardest component of gamma-rays in each case (RaC″, ThC″). The absorption coefficient of the gamma-rays from potassium is, according to L. H. Gray and C. T. P. Tarrant,[6] practically equal to the one of the gamma-rays from RaC″.

Consideration of the softer components of gamma-radiation (larger coefficients μ) would give only small and insignificant increases in the values of q_1 and q_2. However, in order to eliminate completely the possibility of interference from the softer gamma-radiation, the present experiments were carried out with the ionization chambers shielded with 0.98 cm of lead on all sides and on the bottom. This, in addition to the $\frac{1}{8}$-in. brass wall of the chamber, excludes all gamma-rays of less than 1-Mev energy. Eve's constant for this arrangement was found to be

$$K_1=4.9\times10^9\times\exp[-\mu_{Pb}d]=4.9\times10^9\times0.592=2.93\times10^9 \text{ I}$$

per gram of radium ($\mu_{Pb}=0.533$ cm^{-1}).

Eve's constant for thorium (K_2) has not as yet been determined because of the lack of a radium-free thorium standard old enough to be in equilibrium with mesothorium and radiothorium. Finally I decided to use a powdered sample of a thorium mineral, practically free of uranium (thorite) as a standard. This sample (102 grams of thorite) in a sealed glass tube, was put at my disposal by Dr. L. F. Curtiss, National Bureau of Standards and I reported on these determinations last year.[1]

For the heavily screened ionization chambers (9.8-mm Pb) Eve's constant for thorium was determined anew last winter and found to be $K_2=440$ I/g Th/cm behind 9.8-mm lead (without lead the value is 742 I). For potassium the value of Eve's constant (K_3) computed by two different methods (0.12) gives, after reduction to the present experimental conditions (filtered through 9.8-mm Pb), $K_3=0.071$ I/g K/cm.

The mass absorption coefficients used in the following computations are: for radium (RaC″) $\mu_1/\rho=0.045$ cm²/g (the same value holds for potassium); for thorium (ThC″): $\mu_2/\rho=0.041$ cm²/g.

The average radium content of a number of samples from the bulk sample of Quincy granite was recently re-determined by L. F. Curtiss in the National Bureau of Standards and given to

[4] V. F. Hess and Eva M. Balling, Trans. Am. Geophys. Union **26**, 237 (1945).

[5] V. F. Hess, "Jonisierungsbilans der Atmosphaere," Ergebn. Kosm. Physik **2**, 95 (1934).

[6] L. H. Gray and C. T. P. Tarrant, Proc. Roy. Soc., London **A145**, 681 (1934).

be 1.02×10^{-12} g radium per gram, corresponding to 2.9×10^{-6} g uranium per gram, in substantial agreement with Evans' and Goodman's value (0.95×10^{-12} g Ra/g). In the following computation I used Curtiss' value.

a. Radium component: $K_1=2.90\times10^9$, $M_1=1.02\times10^{-12}$, $\mu_1/\rho=0.045$

$$q_1=\frac{12.56\times2.90\times10^9\times1.02\times10^{-12}}{0.045}=0.832 \text{ I.}$$

b. Thorium component: $K_2=440$, $M_2=8.1\times10^{-6}$, $\mu_2/\rho=0.041$

$$q_2=\frac{12.56\times440\times8.1\times10^{-6}}{0.041}=1.094 \text{ I.}$$

c. Potassium component: $K_3=0.071$, $M_3=0.038$, $\mu_3/\rho=0.045$

$$q_3=\frac{12.56\times0.071\times0.038}{0.045}=0.753 \text{ I.}$$

The total ionization to be expected from (a), (b), and (c) is, therefore,

$$q=q_1+q_2+q_3=2.68 \text{ I.}$$

II. LABORATORY EXPERIMENTS WITH HEAVILY SCREENED IONIZATION CHAMBERS

For these experiments, a quantity of 300 lb. of crushed granite (grain size from $\frac{1}{4}$ to 1 in.) was shipped by Swingle Company quarries to Fordham University in bags. The "iron house" was built up from iron bars on the bottom and on all sides 10 cm thick, with the top left open. The medium or the small ionization chamber (4.9- and 1.6-liter volume, respectively) was placed in the center of the hollow space on a lead plate 1 cm thick, and the side wall of the chamber was surrounded with a lead cylinder of 0.98-cm thickness. The top of the iron house was left open so that the electrometer and its housing could be easily placed on or removed from the top of the ionization chambers. Local gamma-rays from the ceiling therefore had access to the system, but their intensity was cut down by placing a large half-cylinder of lead (1 cm thick) above the electrometer head.

In all experiments, alternate readings were taken first with the iron house empty and with the space between the lead cylinder and the inner wall of the iron house filled completely with the crushed granite. Each series of readings continued for several days.

The ionization in the empty iron house (observed with the medium chamber) was 3.345 I; with the granite, 5.61 I. Thus the difference 2.26 I corresponds to the effect of a layer of granite of 15.6 cm average thickness.

A graphical integration of the "open cone" on top of the chamber (i.e., for the part of the space which was not covered by granite) showed that about 82 percent of the full solid angle 4π was covered with granite. A complete concentric layer (spherical shell 15.6 cm thick) therefore would give $2.265/0.819=2.76_5$ I. Since the mean absorption coefficient of gamma-rays from radium and thorium (filtered through 15-mm lead) in crushed granite was directly determined by myself[1] ($\mu=0.0563$ cm^{-1}), one can now extrapolate to infinite thickness by using the formula[7]

$$q_d=q_\infty(1-\varepsilon^{-\mu d}),$$

and obtain

$$q_\infty=2.765/0.585=4.72 \text{ I.}$$

A final correction has to be made because the majority of the rays from the granite have to penetrate the lead cylinder and the wall of the chamber in an oblique direction. This correction was evaluated graphically and amounts to 3.5 percent. The final corrected value ($q_\infty=4.88$ I), therefore, is almost twice the value computed

TABLE I. Summary of results.

A. *Medium chamber:* (shielded with 0.98-cm lead)	
Ionization produced by a 15.6-cm layer of crushed granite	2.26_5 I
Corrected for open cone on top	2.76_5 I
Extrapolated for granite layer of infinite thickness	4.72 I
Corrected for oblique rays	4.88 I
B. *Small chamber:* (shielded with 0.98-cm lead)	
Ionization produced by a 15.6-cm layer of crushed granite	2.05 I
Corrected for open cone on top	2.44 I
Ionization extrapolated for infinite layer of granite	4.17 I
Corrected for oblique rays	4.32 I
C. *Value computed:* Taking uranium content of Quincy granite $(2.9\pm0.5)\times10^{-6}$ g/g; thorium, $(8.1\pm2.0)\times10^{-6}$ g/g; and potassium, 0.038 g/g	2.68 I

[7] V. F. Hess, Trans. Am. Electrochem. Soc. **41**, 287 (1922).

for this experiment from the uranium, thorium, and potassium content of the Quincy granite (2.68 I).

The experiments were repeated with the small (1.6-liter) ionization chamber, also screened with a 9.8-mm lead cylinder around. Table I gives a summary of the results with both chambers. It is evident that in both cases the ionization observed is almost twice as great as the computed value.

An independent, although only approximate, check on this discrepancy was made by another method: with the small chamber it was possible to perform an absorption experiment with the granite in place by inserting a second screen of lead (0.966-cm thickness) between the ionization chamber and the first lead screen. Taking a mean absorption coefficient $\mu/\rho=0.0433$ for the composite gamma-radiation of RaC″, ThC″, and potassium corresponding to $\mu=0.0563$ cm^{-1} in the crushed rock, and the thickness of the second lead screen, $d=0.966$ cm, we obtain for the transmitted fractions, $e^{-\mu d}=0.581$: the fraction of radiation absorbed in the second lead screen, therefore, is 0.419. This corresponds to the difference in the ionization actually observed with one and two lead screens, which was 1.10 I. This, therefore, is 41.9 percent of radiation which actually is emitted from the granite: $1.100/0.419=2.62$ I; the "open cone" correction in this case has to be doubled since the bottom of the chamber was not covered with a second lead plate. Therefore the open cone correction is accomplished by integrating the solid angle subtended by the contour of the second lead cylinder as seen from the center of the small chamber. This gives $2.62/(1-2\times0.0985)=3.26$ I and from a granite layer of infinite thickness $3.26/(1-e^{-\mu d})=3.26/0.585=5.6$ I, which again is about two times greater than the value computed from the uranium, thorium, and potassium content.

The experiments, previously reported upon[1] with the same material but without the 0.98-cm lead screen around the chambers, gave similar discrepancies: the "iron house" experiment with crushed granite surrounding the ionization chamber (brass wall $\frac{1}{8}$ in. thick) gave 9.5 I as compared with a value of 4.1 I computed from the value of the uranium, thorium, and potassium content. In an experiment in the quarry itself, where the apparatus was set up directly above a large block of solid granite, the observed ionization was 5 to 6 I, while for this case, the computed value was 2.06 I.

DISCUSSION

Since both the field experiments and the laboratory measurements show that the uranium, thorium, and potassium content of granite could account for only about one-half of the gamma-ray ionization observed in five independent experiments, one is now confronted with the existence of a "surplus penetrating radiation" of unknown origin.

At first one may be inclined to assume that the well-known "back scattering" of cosmic rays may be responsible for this surplus ionization. However, this effect would be expected to be of much smaller magnitude, since the total ionization produced by cosmic rays at sea level amounts to only 2 I. Furthermore, this intensity was considerably reduced in the case of all "iron house" experiments, since these were carried out in the basement of the Physics Building of Fordham University with four floors and ceilings above the iron house.

In addition, the most recent experiments carried out at Fordham where the iron house was filled with 340 lb. of dunite from North Carolina (a mineral containing only 0.02×10^{-6} g uranium, 0.06×10^{-6} g thorium, and 0.0002 g of potassium per gram), showed no trace of such an effect. The dunite experiments will be reported on later, quantitatively, in another publication.

The possibility that the uranium and thorium content of Quincy granite (as reported by R. D. Evans and C. Goodman), are much too low can be dismissed, in view of the great care and improved technique employed by these authors. Furthermore, the value of the radium content of the Quincy granite was confirmed recently by L. F. Curtiss by direct analysis of the crushed granite used in my experiments. There are only a few other possibilities of explanation left, some of which can be investigated by further experiments.

1. Nuclear Processes Produced by Alpha-Rays in Granite, and Accompanied by Photons

This possibility was suggested by the Swiss geologist H. Hirschi in a private communication. There are a few (α, p) and (α, n) reactions where photons of >1.5 Mev are also emitted, and some of the elements involved are present in granite. A rough quantitative estimate can be made as follows: assuming that the thorium and uranium products in granite are together equivalent to 2×10^{-12} g Ra/g in their alpha-ray emission, 1 g of granite would produce $3.7\times10^{10}\times2\times10^{-12}\times8=0.6$ alpha-particles per second, and the 300 lb. of granite in the iron house would give off 90,000 alpha-particles per second. Effective nuclear transmutations would certainly not be accomplished by alpha-rays of low range and energy. Furthermore, the yield would be less than 1 in 10^5, so that much less than one transmutation per second would occur in 300 lb. of granite. Photons may be produced perhaps in $\frac{1}{10}$ of these cases, and less than half of them could go through the ionization chamber. Thus the effect would amount to much less than 0.01 I (per cm³).

2. Nuclear Processes in the Granite Induced by Cosmic Rays

A. One might consider neutron-induced fission of uranium and thorium and the so-called spontaneous fission. G. N. Flerov and K. A. Petrshak[8] reported this first in 1940 and several authors have confirmed their findings.[9] The values of the "partial decay constant" for spontaneous fission can be taken as $\lambda_F=7$ to 9×10^{-24} sec.$^{-1}$ under the assumption that one neutron is emitted per fission, as compared with the "normal" alpha-ray decay of U_I with $\lambda_\alpha=5\times10^{-18}$ sec.$^{-1}$. The amount of uranium in 150 kg of Quincy granite $(2.9\times10^{-6}\times1.5\times10^{-5}=0.435$ g) corresponds to $0.44\times6.02\times10^{23}/238=1.1\times10^{21}$ atoms, and the number of spontaneous fissions in this material would be $n_f=8\times10^{-24}\times1.1\times10^{21}=8.8\times10^{-3}$ per sec. Doubling this amount because of the fissionable thorium in the granite, we would have about 18×10^{-3} fissions/sec. occurring in the bulk sample of 150-kg crushed granite. If the energy of photons in each fission is estimated as 10 Mev, we would have 18×10^4 ev of photon energy liberated, corresponding to a production of 5600 ion pairs/sec. for complete absorption all around. Taking the solid angle subtended by the cross section of the chamber as seen from an average point in the granite as $0.16/4\pi$ we would have an energy of 1×10^4 ev going through the chamber per second. Half of it will be absorbed in the granite before reaching the chamber. If now, the whole energy, arriving at the chamber (volume 1600 cm³) were absorbed in it and used for productions of ions (32 ev per ion pair), we could expect $(5\times10^3)/(32\times1.6\times10^3)=0.1$ I produced in the chamber. Actually, of course, only a very small fraction of this energy would be used up in producing ions within the chamber, and so we see that spontaneous or cosmic-ray induced fission of uranium and thorium in the granite cannot produce the surplus ionization actually observed. Mr. David Hill (Palmer Physical Laboratory, Princeton University) arrived independently at the same conclusion, using a different method of computation.*

B. One could also think of artificial radioactivity induced by cosmic radiations in the granite. There are so many elements contained in volcanic rocks like granite that it is almost impossible to speculate on it. P. J. G. deVos and S. J. duToit[10] found that penetrating ionizing particles are produced by cosmic-ray neutrons, although the effect in a triple coincidence-counter telescope, using a paraffin layer of 1.3 cm, was very small (3 percent of the total number of coincidences). The possibility of such an effect of cosmic rays on granite can be tested by performing the "iron house" experiment in a mine or in a tunnel deep enough to exclude cosmic rays completely. Such experiments are planned for the immediate future.

Since the dunite in the iron house experiment did not show any penetrating radiation, although exposed to cosmic rays, it is rather to be expected that other rocks, even granite, will behave similarly.

[8] G. N. Flerov and K. A. Petrshak, J. Phys. U.S.S.R. **3**, 275 (1940).

[9] Mauer and Pose, Zeits. f. Physik **121**, 285 (1940); G. Scharff-Goldhaber and G. S. Klaiber, Phys. Rev. **70**, 229 (1946).

* Private communication from Professor J. A. Wheeler.

[10] P. J. G. deVos and S. J. duToit, Phys. Rev. **70**, 229 (1946).

If the granite, protected from cosmic rays by thick layers of rock, shows the same ionizing effect as in the laboratory, we will have to assume that a hitherto unknown penetrating radiation is given off by the granite itself. It will be interesting to investigate other volcanic rocks of different uranium and thorium content in order to see whether this effect is correlated with the content of radioactive materials in the rocks.

The author is indebted to the American Philosophical Society for a grant (in 1947) which enabled him to improve his equipment, to get steel plates, iron bars, and other materials needed.

Grateful acknowledgment is also given to Dr. L. J. Adams, Dr. W. D. Urry, and Dr. W. Davis of the Geophysical Laboratory (Carnegie Institution of Washington, D. C.), Dr. M. A. Tuve, Department of Terrestrial Magnetism (Carnegie Institution of Washington, D. C.), and Dr. L. F. Curtiss (National Bureau of Standards) for their helpful cooperation.

The Rev. Dr. Edward M. Kovach assisted the author in many of the experiments.

PHYSICAL REVIEW VOLUME 72, NUMBER 7 OCTOBER 1, 1947

The Electric Resonance Method of Radiofrequency Spectroscopy The Moment of Inertia and Electric Dipole Moment of CsF*

HAROLD KENNETH HUGHES
*Pupin Physics Laboratories, Columbia University, New York, New York***

(Received June 19, 1947)

This paper describes a new method of radiofrequency spectroscopy in which transitions between the energy levels of a single rotational state of a linear rotator in an electric field are caused by a superimposed radiofrequency field. The method utilizes a molecular beam and has been applied to the measurement of the moment of inertia, I, and the electric dipole moment, μ, of CsF. Values for these quantities are: $I=(187\pm22)10^{-40}$ g cm^2 and $\mu=7.3\pm0.5$ Debye. The internuclear distance, derived from the moment of inertia, is 2.60 ± 0.16 angstroms.

1. INTRODUCTION

THE purpose of this paper is to describe some experiments[1] on CsF, a linear polar molecule which is convenient to handle, in which the molecular beam resonance method was applied to molecules in a single rotational state and in which the fields were all electric instead of magnetic. With the demonstrated high resolving power of this method, it is possible to evaluate the parameters which enter into the orientation polarizability of a molecule, namely, the moment of inertia and the electric dipole moment. In addition, it is expected that the resolving power will be so high that the variation of these quantities with vibrational quantum number will be observed. From the standpoint of nuclear physics it is also interesting that the resolving power should be ample to measure accurately the interaction of the nuclear electric quadrupole moment[2] with the electric field gradient of the electrons, and the interaction of the nuclear magnetic moment with the rotation of the molecule. These latter points will be developed in another paper from this laboratory.

The molecular transitions which have been observed are not of the ΔR type (transitions between different rotational states) since the microwave techniques required for their observation were not developed at the time that the apparatus was designed.[3] Rather, the transitions are between states with the same value of R but

* Publication assisted by the Ernest Kempton Adams Fund for Physical Research of Columbia University.

** Now at Socony-Vacuum Laboratories, Brooklyn, New York.

[1] H. Hughes, Phys. Rev. **70**, 570 and 909 (1946).

[2] Dr. U. Fano, National Bureau of Standards, private communication.

[3] Recently Dakin, Good, and Coles, Phys. Rev. **70**, 560 (1946), have observed a ΔR-type transition of OCS in a wave guide at 24,320 Mc. The frequency for the $R=1\rightarrow R=0$ transition of CsF is 8830 Mc. This is a wave-length of 3.4 cm.

different values of p, the electric quantum number. One can thus study the molecular transitions at frequencies in the ordinary radiofrequency range, and it is not necessary to stabilize a microwave oscillator in order to measure the small frequency differences which arise from the fine structure.

Shortly after the molecular beam technique was developed by Stern and others, it was applied to the measurement of electric moments. These moments were evaluated from deflection experiments[4–8] in which the transverse displacement of a beam of molecules depended upon their velocity, mass, effective electric moment, the deflecting field, and the geometry of the apparatus. Because of the distribution of velocities and effective electric moments in the beam, the field broadened the beam, the center deflected only a trifle, and the values of μ which were obtained by this method were only approximate.

The electric resonance method differs markedly from deflection experiments, since it is not necessary to evaluate the distribution of velocities, to calibrate the deflecting field, or to assume a constant intensity of the beam. In addition, the moment of inertia is obtained as well as the electric dipole moment. Experiments designed to measure the moment of inertia and the distortion polarizability by the deflection method have not been reported, though in principle they are possible. It is unlikely that the results would be very precise.

In the molecular beam electric resonance method transitions are induced between energy levels of a linear rotator in an *electric* field by a superimposed radiofrequency electric field. From a knowledge of the d.c. field and the frequency at which the transition occurs, one can compute the electric moment, μ, and the moment of inertia, I.

The first molecule to which this method was applied was cesium fluoride, because it is readily handled by standard molecular beam methods and its spectrum has no isotope effects. Another attractive property is its low moment of inertia compared with other alkali halides. This simplifies the intensity problem for reasons described below.

This method is closely analogous to the magnetic resonance method[9] which has been applied previously to atoms and molecules. It is an advance over previous methods in that a single rotational state of the molecule is studied even though it is present to only one part in ten thousand as a component of the beam.

While the theory and techniques presented in this paper relate only to linear molecules, it would appear a fruitful undertaking to examine the broad field of electric resonances in non-linear molecules. For these there is a first-order Stark effect and such molecules should be easier to deflect. The theory, however, will probably be considerably more complicated than that for linear molecules.

Definitions of the symbols are given in Table I.

2. METHOD

The beam of molecules can be formed and detected by any of the well-known molecular beam techniques. In this case the CsF molecules evaporate from a hot oven, are collimated by slits, and pass through two inhomogeneous electric fields which refocus one, or at most two, rotational states upon a surface ionization detector. Between these two fields is a short homogeneous electric field upon which is superimposed a radiofrequency electric field at right angles to the d.c. field. Here molecules may undergo transitions between different energy levels.

TABLE I. Definitions of letter symbols.

A_{R,p^2}	$[(R+1)^2-p^2]/(2R+1)(2R+3)$
E	Electric field strength in volts per cm except where stated otherwise
f	Frequency in cycles per second
I	Moment of inertia in g cm^2
p	Electric quantum number
R	Rotational quantum number
V	Electric potential difference
W	Energy
ϵ	$W/(h^2/2I)$
λ	$\mu E/(h^2/2I)$
μ	Permanent electric moment in e.s.u.
μ_e	Effective electric moment ($=-\partial W/\partial E$), in e.s.u.

[4] For a general discussion of the field, see R. G. J. Fraser, *Molecular Beams* (Chemical Publishing Company, New York, 1938) and R. G. J. Fraser, *Molecular Rays* (The Macmillan Company, New York, 1931).

[5] Erwin Wrede, Zeits. f. Physik **44**, 261 (1927).

[6] Max Wohlwill, Zeits. f. Physik **80**, 67 (1932).

[7] H. Scheffers, Physik. Zeits. **41**, 89 and 98 (1940); Rodebush, Murray, and Bixler, J. Chem. Phys. **4**, 372 (1936).

[8] Estermann, Zeits f. physik. Chemie B1, 161 (1928) and 2, 287 (1929); Leipziger Vorträge (1929), pp. 17 ff.

[9] Rabi, Millman, Kusch, and Zacharias, Phys. Rev. **55**, 526 (1939).

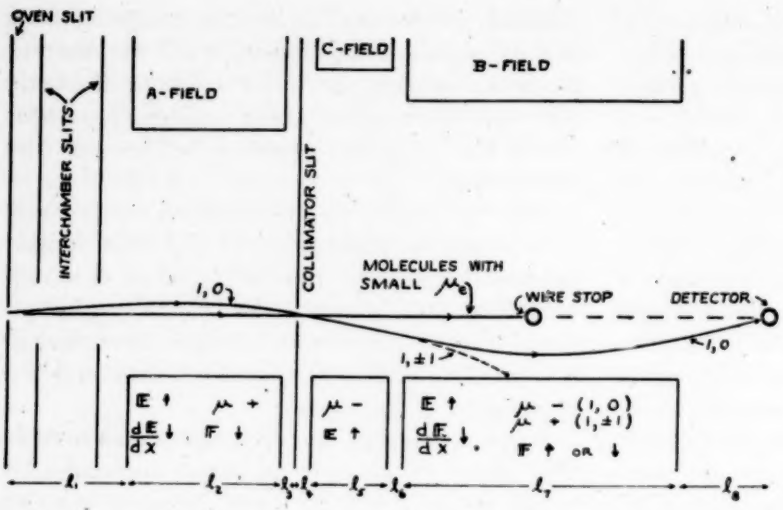

FIG. 1. Schematic diagram of the apparatus and paths of the molecules.

The selection of the particular electric state for study is accomplished by two inhomogeneous electric fields, named the A- and B-fields, which together cause molecules in the desired state to follow a sigmoid path around a wire stop and to fall upon the detector, as is shown in Fig. 1. Figure 2 shows the energy levels of a rotating polar linear molecule in an electric field. Only those molecules are refocused for which the electric moment has the correct sign and magnitude in the two fields. As shown in Fig. 3, at low fields molecules in state (1, 0) have a negative moment, while at high fields their moment is positive. If, then, $\mathbf{E}$ and $d\mathbf{E}/dx$ point in the same direction in both the A- and B-fields, and if the values of λ_A and λ_B are, respectively, greater and less than about 5 (at which $\mu_e=0$), (1, 0) molecules (and also some (2, ±1) molecules) will be refocused, but all others will hit either the wire stop or some other part of the apparatus. This is diagrammed in Fig. 1 where also are shown the directions of the various vectors and the signs of μ_e in all three fields. There are (1, 0) molecules streaming from the oven in all directions, but only those are refocused which start with just the correct angle.

The detected beam shows a decrease when the frequency of the oscillating field equals the difference in the energy of the two levels divided by Planck's constant. For CsF, transitions involving changes in the electric quantum number, p, are possible in the radiofrequency region in the presence of a static electric field. The rotational spectrum, for which the rotational quantum number changes, lies in the microwave region[3] and was not investigated. The matrix element for electric dipole radiation of the $\Delta R=0$, $\Delta p=\pm1$ type is different from zero only when the constant homogeneous field and the oscillating field are at right angles.

To reduce the general background against which these transitions are observed, a wire stop is placed in the path of the beam and the molecules in the beam are refocused around it.

Zero Moments

In this experiment, $\mu^2 I$ is calculated from the frequency and the field for a Δp transition (constant R), while by observing the departure of the frequency from a quadratic dependence on the field, it is possible to obtain a value of μI. By combining these two values, it is thus possible to obtain μ and I separately. The value of μI may also be obtained by the zero-moment method which, in analogous magnetic experiments, was used so often prior to the development of radiofrequency spectroscopy. All rotational states beyond $R=0$ possess at least one zero moment, two of which appear clearly in Fig. 3. For example, the 1, 0 state effective electric moment is zero near $\lambda=5$, while the 2, ±1 moment is zero at about $\lambda=5.6$. It is relatively simple to locate these points, and this experiment was done in order to establish the values of μ and I in a preliminary fashion. The precision of the final

result depends upon a knowledge of the deflecting field, E, at the exact position of the beam, a quantity which is somewhat difficult to obtain. The line-up of the beam changes as the oven is heated, yet values determined optically while the can is open must be used. Better values of the deflecting field E can be obtained by observing the effect of a calibrated shift of the oven, the collimator slit, and the detector, but this technique has not been perfected. Clearly, the electric resonance method is superior to the zero-moment method.

3. THEORY

Energy Levels of a Linear Rotator

The solution to Schroedinger's equation for the energy levels of a linear, rigid rotator in an electric field is generally obtained by the perturbation method from the well-known solution for the zero-field case. Because there is no time-average electric moment in a zero field, the first-order perturbation term is zero. Kronig[10] and others have given the second-order solution as follows:

$$W=\frac{h^2}{2I}\left[R(R+1)+\tfrac{1}{2}\lambda^2\left\{\frac{R(R+1)-3p^2}{R(R+1)(2R-1)(2R+3)}\right\}\right]. \quad (1)$$

This equation gives the oscillator frequency for a transition by application of the usual Bohr relation. It is customary to designate the stationary states by two numbers which give the rotational and electric quantum numbers. For the $(1,0)\rightarrow(1,\pm1)$ and the $(2,\pm1)\rightarrow(2,\pm2)$ transitions observed in this experiment, Eq. (1) yields Eqs. (19) and (20) below.

The next non-zero perturbation term is the fourth which Brouwer[11] found and, since his thesis is not readily available in the United States, his Eqs. (2) through (7) for the first three rotational states are reproduced below. By the use of the parameters λ and ϵ, generalized equations are obtained which are independent of the particular values of μ and I of any single molecule.

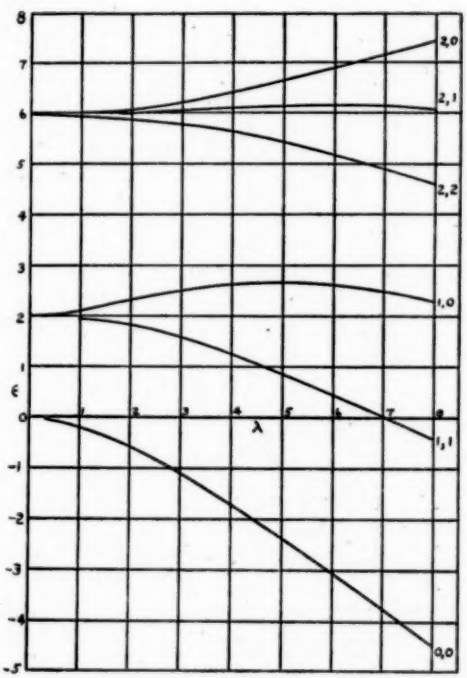

FIG. 2. Energy levels of a rotating polar linear molecule in an electric field.

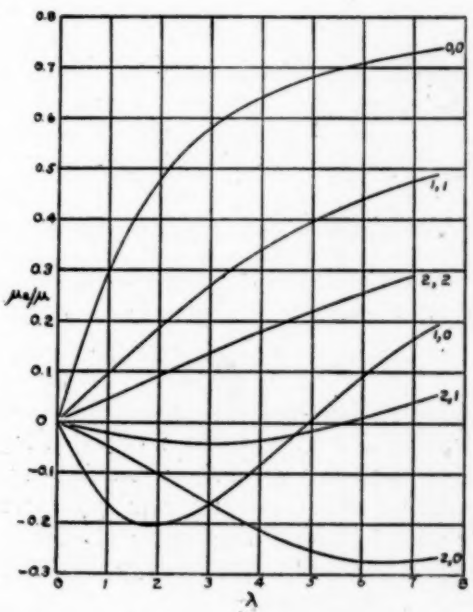

FIG. 3. Effective electric moments of a rotating polar linear molecule in an electric field.

[10] Kronig, Proc. Nat. Acad. Wash. **12**, 608 (1926).

[11] F. Brouwer, Dissertation, Amsterdam, 1930.

$R=0,\ p=0$:

$$\epsilon=-\frac{1}{6}\lambda^2+\frac{11}{1080}\lambda^4-\frac{1}{725}\lambda^6+\cdots, \tag{2}$$

$R=1,\ p=0$:

$$\epsilon=2+\frac{1}{10}\lambda^2-\frac{73}{7900}\lambda^4+\cdots, \tag{3}$$

$R=1,\ p=\pm1$:

$$\epsilon=2-\frac{1}{20}\lambda^2+\frac{19}{56{,}000}\lambda^4+\cdots, \tag{4}$$

$R=2,\ p=0$:

$$\epsilon=6+\frac{1}{42}\lambda^2+\left(\infty\frac{1}{3000}\right)\lambda^4+\cdots, \tag{5}$$

$R=2,\ p=\pm1$:

$$\epsilon=6+\frac{1}{84}\lambda^2-\frac{1}{3000}\lambda^4+\cdots, \tag{6}$$

$R=2,\ p=\pm2$:

$$\epsilon=6-\frac{1}{42}\lambda^2+\left(\frac{1}{25{,}000}\right)\lambda^4+\cdots. \tag{7}$$

The value of λ to which these equations are useful is determined by the desired accuracy and may be found by comparison with Lamb's exact Eq. (18) below. At $\lambda=1$ for the 1,0→1, ±1 transition, the two equations agree to better than 0.1 percent.

Fraction of Molecules Available

As calculated from the partition function, the fraction of molecules in the state $R=1$ is

$$\sigma_1=N_1/N=3(\hbar^2/2I)/kT. \tag{8}$$

The fraction of molecules in the $R=0$ state, σ_0, is $\frac{1}{3}$ of σ_1. For purposes of exploring the electric resonance method where the amount of refocused beam is an important consideration, it is obviously desirable to work with a high value of σ_1 and hence to employ molecules with a low value of I. Substituting the known values of the constants (see Section 6 below), we find that

$$\sigma_0=0.21/T, \tag{9}$$

$$\sigma_1=0.63/T. \tag{10}$$

Since the first rotational level is threefold degenerate and the fields are only 50 percent effective in selecting the desired molecules, this experiment has been performed with only about one ten-thousandth of the total beam.

Transition Probability

At zero field, a Δp transition in which $\Delta R=0$ is forbidden, but this selection rule is broken by the constant field, and both theory and experiment show that only a small field is needed to induce the (1,0)→(1, ±1) change. A negligible amount of power is required, and even a small oscillator is adequate, provided only that its output is a few volts.

The optimum condition for producing a transition is

$$M\tau\sim h, \tag{11}$$

where τ is the transit time of the molecule in the C-field and the matrix element, M, is given by

$$M=\int_V \psi_{1,0}{}^* E_{rf}\mu_e\psi_{1,\pm1}dV. \tag{12}$$

E_{rf} is $\frac{1}{2}$ of the peak value of the perturbing r-f field, and the ψ's are the perturbed wave functions. This matrix element has been calculated using the wave functions for a rotating dipole, and the final result is

$$M=\frac{\mu^2 E_{rf}E_{dc}3\sqrt{2}}{40(\hbar^2/2I)}. \tag{13}$$

On substituting the equation for the frequency of this transition

$$f=\frac{3\mu^2E_{dc}{}^2}{20h(\hbar^2/2I)}. \tag{14}$$

Eq. (13) simplifies to

$$E_{rf}/E_{dc}\approx\sqrt{2}/2\pi\tau f\doteq 1/4.5\tau f. \tag{15}$$

The transit time τ is of the order of 10^{-4} seconds, so that the theoretical ratio of the r-f field to the d.c. field is much less than unity for all frequencies in the megacycle range.

For an ideally uniform C-field, the probability of a transition, P, is related to this same ratio and to the ratio of the frequency f and the

resonance frequency f_0 by the relation[12]

$$P=\frac{0.5}{1+(E_{dc}/E_{rms})^2(1-f/f_0)^2}. \quad (16)$$

This relation takes into account the v^3-type velocity distribution of molecules in the beam.

For a $\Delta p=\pm 1$ transition, the oscillating field must be perpendicular to the d.c. field. When they are parallel, Δp must be equal to 0.

4. APPARATUS

General

The broad features of the apparatus are similar to those previously described[9] for the magnetic resonance method. The outer envelope of the apparatus is a 7-in. O.D. brass pipe, $24\frac{11}{16}$ in. long, crossed by an $8\frac{3}{4}$-in. O.D. brass pipe of length $10\frac{1}{2}$ in. The cross pipe provided convenient access to the fields. The apparatus is divided into three chambers by two plates on which are mounted slits just large enough to pass the beam. Each chamber is pumped separately. The first contains the oven, the second or "interchamber" isolates the oven chamber with its relatively poor vacuum ($\sim 10^{-5}$ mm Hg) from the third or "observation" chamber ($p<10^{-6}$ mm Hg) which contains all the fields and the detector. There are liquid nitrogen traps in all chambers.

In traveling to the surface ionization detector approximately 50 cm from the oven slit, a molecule passes first through a 10-cm inhomogeneous electric field (A-field), then through a 5-cm homogeneous electric field on which is superimposed a radiofrequency field normal to the d.c. component (C-field), and finally through another inhomogeneous field (B-field), 18 cm long, in which is placed the stop wire previously mentioned. The stop is 0.023 cm in diameter. Its function is described further below. Figure 1 depicts schematically the trajectory of molecules which are refocused and molecules which hit the stop.

Oven

The beam is produced by evaporation of CsF molecules in an iron oven heated to about 575°C and collimated by slits to a height of 0.3 cm and a width of 0.0075 cm. The oven, approximately a one-inch cube, is heated by coils of 0.010-in. tungsten wire which are insulated from the oven by short lengths of quartz tubing. As the oven gassing increases with temperature, a best "signal-to-noise" ratio was found, at 850°K. At this temperature $\sigma_0=0.00025$, $\sigma_1=0.00074$, and there are 200 rotational states populated up to the point where the Boltzmann exponent equals one.

A- and B-Fields

As previously described, the function of the deflecting fields is to select certain of the molecules for study. The general method of accomplishing this is well known.[4]

To apply the equations for the deflection of a molecule in an inhomogeneous field, it is necessary to know the force, F, in the direction, s. This is, in general,

$$F_s=\mu_e\partial E/\partial s. \quad (17)$$

TABLE II. The energy levels of a rotating polar linear molecule as a function of the electric field strength, calculated from Lamb's equation, and the effective electric moment calculated by first differences. $\mu_e/\mu=-d\epsilon/d\lambda$.

λ	ϵ	μ_e/μ	ϵ	μ_e/μ	ϵ	μ_e/μ
	$(R=0, p=0)$		$(R=1, p=0)$		$(R=1, p=1)$	
0.0	0.00000	0.000	2.000000	0.000	2.000000	0.000
0.5		+0.158		−0.091		+0.050
1.0	−0.15766		2.090758		1.95033	
1.5		0.400		−0.196		0.145
2.0	−0.55728		2.287173		1.805104	
2.5		0.535		−0.191		0.231
3.0	−1.09266		2.477962		1.57410	
3.5		0.612		−0.124		0.304
4.0	−1.70485		2.602378		1.26985	
4.5		0.661		−0.036		0.365
5.0	−2.36560		2.638730		0.904751	
5.5		0.695		+0.051		0.415
6.0	−3.06022		2.587276		0.48954	
6.5		0.720		+0.129		0.457
7.0	−3.78014		2.458169		+0.032949	
7.5		0.740		+0.194		0.491
8.0	−4.51990		2.263945		−0.458136	
	$(R=2, p=0)$		$(R=2, p=1)$		$(R=2, p=2)$	
0.0	6.000000	0.000	6.000000	0.000	6.00000	0.0000
0.5		−0.024		−0.012		+0.0238
1.0	6.024033		6.011578		5.97623	
1.5		−0.074		−0.031		0.0708
2.0	6.098452		6.042636		5.90540	
2.5		−0.129		−0.041		
3.0	6.227791		6.083712			0.138
3.5		−0.185		−0.039		
4.0	6.412842		6.122985		5.62877	
4.5		−0.233		−0.026		
5.0	6.645478		6.149323			0.220
5.5		−0.263		−0.005		
6.0	6.908774		6.153928		5.18863	
6.5		−0.273		+0.023		
7.0	7.181753		6.130768			0.290
7.5		−0.263		0.054		
8.0	7.444437		6.076336		4.60850	
8.5				0.087		
9.0			5.989152			

[12] Dr. Willis Lamb, private communication.

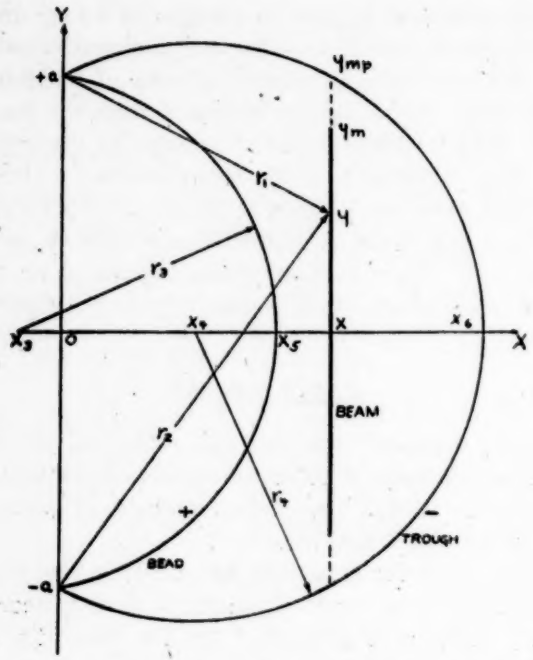

FIG. 4. Cross section of the A-field as viewed from the detector.

E and $\partial E/\partial s$ are well known[13,14] for the type of field used. μ_e is not a constant but must be calculated from the energy by differentiation. In this experiment, the deflecting field E is so large that the energy cannot be calculated from the perturbation solutions to Schroedinger's equation given above but must be derived from the exact solution. This yields a three-term recursion formula, and the energy eigenvalues are best determined through the continued fraction method.[12] The values of the parameter ϵ listed in Table II were determined by successive approximations in the implicit Eq. (18).

$$\epsilon = p(p+1) - \cfrac{\lambda^2 A_{p,p}{}^2}{(p+1)(p+2) - \epsilon - \cfrac{\lambda^2 A^2{}_{p+1,p}}{(p+2)(p+3) - \epsilon - \text{etc.}}}. \quad (18)$$

This equation neglects the distortion polarizability of the molecule,[4] which is quite small, the magnetic moments of the nuclei, and the quadrupole moment of the cesium nucleus. Fluorine with a spin of $\frac{1}{2}$ is not expected to possess a nuclear quadrupole moment.

To maintain the resolution of the apparatus, the beam should not spread or warp as it passes through the deflecting fields, and consequently F should be as constant as possible over the beam. As Eq. (17) shows, this does not mean that the gradient of the field should be constant. Figure 4 is a cross section of the field which meets these requirements. It consists of parts of two cylindrical surfaces with parallel axes. The design constants of the deflecting fields are listed in Table III.

Two independent half-wave rectifiers supply the A- and B-fields. Even with voltmeters connected, the output current is very small so that R-C filters provide excellent direct current. Small neon transformers with the primaries connected to 10,000-ohm potentiometers and the secondaries to 879's are used. Power is taken from the same Raytheon voltage regulator which supplies the oven. All three electric fields point in the same direction in order to maintain the quantization unchanged in the absence of a transition. This is essential to good refocusing. For the same reason, the collimating slit is quartz, not metal.

C-Field

One of the C-field plates is split horizontally. One of the halves is grounded while the other is

TABLE III. Design constants of the A- and B-fields.

Quantity	A-field	B-field	Units
x/a	1.05	1.50	—
y_m/a	0.8	1.2	—
λ	~6.6	~2.0	—
R	2.0	3.5	cm^{-1}
E	~8000	~2400	v/cm
dE/dx	~16,000	~8400	v/cm^2
s_{adjust}		0.012	cm
a	0.500	0.264	cm
y_m	0.400	0.317	cm
x	0.525	0.396	cm
y_{mp}/a	1.0	1.5	—
y_{mp}	0.500	0.396	cm
Good to	1.5	2.0	%
l	10.0	18.0	cm
r_3	0.507	0.266	cm
x_3	−0.082	0.030	cm
r_4	0.565	0.406	cm
x_4	0.263	0.308	cm
Gap	0.402	0.418	cm
V_4	~2500	~770	v
$-F_A/F_B$	1.27	1.27	—
$x-x_5$	0.1	0.1	cm
μ_e	~+0.10	~−0.15	debye

[13] Sidney Millman, Phys. Rev. **47**, 739 (1935).
[14] Rabi, Kellogg, and Zacharias, Phys. Rev. **46**, 157 (1934).

connected to a tap on the tank coil which is at d.c. ground potential. The other C-field plate is at r-f ground but at a d.c. potential which can be varied by means of potentiometers. The gap is somewhat under 5 mm. In parallel with the potentiometers is a Leeds and Northrup voltage divider connected to a Type K-3 Leeds and Northrup potentiometer. The C-field gap was measured accurately on a dividing engine.

The r-f source is a Hartley oscillator, parallel fed, with the tank at d.c. ground.

Wire Stop

Hanging from an extension of a ground joint in the top of the apparatus and passing through the slot in the B-field is a 0.009-in. wire. This stops all molecules of low effective electric moment which are not subject to the refocusing operations. It can be moved under vacuum and is damped by an eddy-current copper plate hanging between four U-shaped Alnico magnets. About 50 percent of the (1,0) molecules get around the stop and hit the detector.

Detector

The beam falls on a 0.003-in. tungsten wire exactly in line with the oven and collimator slits and maintained at approximately 475°C by a current of from 260 to 280 ma. After evaporating, the ionized molecules are attracted to a near-by negative plate and the current amplified by an FP-54 tube feeding a galvanometer. To clean the detector wire, it is flashed for two seconds at approximately 950°C by a current of 700 ma.

Constants of the Apparatus

Other important dimensions of the apparatus which have not previously been given follow. All dimensions are in cm.

$l_1=8$	$l_5=5$	start of B-field to stop = 8.72
$l_2=10$	$l_6=1$	total beam = 50
$l_3=1$	$l_7=18$	slits = 0.0075
$l_4=1$	$l_8=6$	

These distances are shown in Fig. 1.

5. PROCEDURE

With the end plates off, the oven slit, collimator slit, and detector are aligned optically using a telescope with a micrometer microscope head. The system is then pumped down and the final alignment made with the beam as indicator. A typical value for the beam during a run is 50,000 cm of galvanometer deflection. After the stop is centered the galvanometer deflection is about 7 cm which is a residual beam of 0.015 percent; this is caused by scattering. The B-field is then turned on and the A-field adjusted for a maximum refocused beam. This is about 10 cm of which an estimated 6 cm is in the (1,0) state and the remaining in the (2, ±1) state. This actual fraction of the beam in the useful (1,0) state, 0.00012, is to be compared with the partition-function value calculated with Eq. (10) above, $\sigma_1/3=0.00025$. As a means of selecting the (1,0) state, the fields are thus about 50 percent effective.

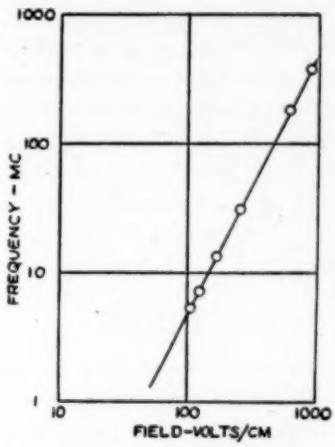

FIG. 5. Plot of frequency *vs.* field for the (1,0)→(1, ±1) transition of CsF.

From 10 cm of refocused beam in a typical run, 4 cm undergo transitions from the (1,0) state and 3 cm from the (2, ±1) state. This is an actual transition probability of 70 percent at resonance. These are only approximate figures, for the background may be a function of the field.

Identification of Transitions

The (1,0)→(1, ±1) transition was picked up first in a sweep of the C-field at fixed frequency. Complete identification could not be made merely by establishing a quadratic relationship between the frequency and the field. From the values of the A- and B-fields, it was fairly certain

that only three transitions could be observed. These were: $(1,0)\rightarrow(1,\pm1)$, $(2,\pm1)\rightarrow(2,0)$, and $(2,\pm1)\rightarrow(2,\pm2)$. In a further sweep of the C-field, a transition with a different value of f/E^2 was found and, by comparing the ratios of these two values of f/E^2 with the theoretical values which may be derived from Eq. (1), the identity of both of the transitions was established unambiguously.

6. RESULTS

Figure 5 shows the frequency *vs.* field plot for the $(1,0)\rightarrow(1,\pm1)$ transitions on log-log coordinates. The equations for the $(1,0)\rightarrow(1,\pm1)$ and the $(2,\pm1)\rightarrow(2,\pm2)$ transitions are:

$$(1,0)\rightarrow(1,\pm1)\quad f=\frac{3\mu^2IE^2}{10\hbar^2h(300)^2}=448E^2, \tag{19}$$

$$(2,\pm1)\rightarrow(2,\pm2)\quad f=\frac{3\mu^2IE^2}{42\hbar^2h(300)^2}=107E^2. \tag{20}$$

Here f is in cycles per second and E in volts per cm. For CsF, $\mu^2I=9.89\cdot10^{-73}\pm1.2$ percent electrostatic units.

At low C-fields, the frequency, f, is proportional to the square of the field, E. At higher fields there is an important deviation from this quadratic relation which permits the separate determination of μ and I. Subtracting Eqs. (3) and (4), we find for the $(1,0)\rightarrow(1,\pm1)$ transition frequency:

$$f=\frac{3\mu^2E_{\text{e.s.u.}}^2}{20h(\hbar^2/2I)}-\frac{0.00959\mu^4E_{\text{e.s.u.}}^4}{h(\hbar^2/2I)^3}, \tag{21}$$

where E is in e.s.u.'s. Let us define two experimentally determined constants, α and β, by the relation

$$f/E^2=\alpha-\beta E^2, \tag{22}$$

where E is in volts per cm. Then

$$\alpha=\frac{3\mu^2}{20h(\hbar^2/2I)(300)^2}, \tag{23}$$

$$\beta=\frac{0.00959\mu^4}{(300)^4h(\hbar^2/2I)^3}, \tag{24}$$

$$I=\frac{9\beta\hbar}{2\pi800(0.00959)\alpha^2}=(1.97)10^{-28}\frac{\beta}{\alpha^2}, \tag{25}$$

$$\mu^2=\frac{8(0.00959)10^7\hbar^2\alpha^3}{3\beta}=(1.12)10^{-47}\frac{\alpha^3}{\beta}. \tag{26}$$

It is interesting to note from Eqs. (22) and (25) that the value of E does not enter into the calculation of I but only into μ.

A least-square analysis of the data was made assuming the validity of Eq. (22). The following values were obtained for the two experimental constants: $\alpha=448\pm5.4$ and $\beta=(1.91\pm0.23)10^{-5}$. Even at 500 Mc the deviation from the quadratic relation is still very small so that a small error in f/E^2 causes a large error in β. The error in f/E^2 is a function of the width of the resonance curve and this, in turn, depends in part upon the homogeneity of the C-field. The present limitation in the accuracy with which β can be measured is largely instrumental and can be eliminated. The method is capable, therefore, of yielding very good results.

Inserting the values for α and β in Eqs. (25) and (26) we obtain: $I=(187\pm22)10^{-40}$ g cm^2 and $\mu=7.3\pm0.5$ Debye. A Debye is 10^{-18} e.s.u. From the value of I, we may calculate the internuclear distance, r, as 2.60 ± 0.16 angstroms. In m.k.s. units, the values of these quantities are: $I=(187\pm22)10^{-47}$ kg m^2, $\mu=(2.4\pm0.2)10^{-29}$ coul-m and $r=(2.60\pm0.16)10^{-10}$ m.

For CsF the parameter λ is related to the field by the equation

$$\lambda=(8.3)10^{-4}E, \tag{27}$$

where E is in volts/cm. The quantity $(\hbar^2/2I)$ which occurs frequently in the theory is equal to $(2.92)\ 10^{-17}$ g cm^2 sec.$^{-2}$. The rotational constant, B, is:

$$B=(1/hc)(\hbar^2/2I)=0.147\ \text{cm}^{-1}. \tag{28}$$

7. DISCUSSION

As a means of making a preliminary estimate of I, one can use the observed internuclear distance obtained from x-ray diffraction data for crystals and assume some reasonable percentage reduction in going over to the gaseous state. Various tables of x-ray crystallographic data exist[15] while Herzberg[16] gives an excellent table

[15] See for example Albright, *Handbook of Chemistry and Physics* (Chemical Rubber Publishing Company, Cleveland, 1942), 26 ed., p. 1911.

[16] Gerhard Herzberg, *Molecular Spectra and Molecular Structure* (Prentice-Hall, Inc., New York, 1939), p. 482.

of molecular constants for gases derived from band spectra which is complete as of July of 1939. CsF is not listed, but the percent reduction for similar molecules can be calculated. In a private communication, Professor Gerhard Herzberg very kindly estimated the internuclear distance by this method as 2.68A. If one uses the average reduction of 14 percent found by Maxwell, Hendricks, and Mosley[17] for other Cs compounds then $r=2.58$A.

Some years ago, Pauling[18] and others introduced the idea of ionic radii of atoms, the simple addition of which yields the internuclear distance for a wide variety of compounds in the solid state. The values for Cs and F are, respectively, 1.65 to 1.69 and 1.33 to 1.36. These total 2.98 to 3.05 which is in excellent agreement with the observed value of 3.00A. Later Pauling extended this method to gases. The most recent values are in a paper by Schomaker and Stevenson[19] who give the following equation:

$$r_{AB}=r_A+r_B-0.09|X_A-X_B| \qquad (29)$$

in which the sum of the covalent radii of the two atomic species is reduced by a fraction of the absolute difference of their "electronegativities."[20] The authors list the following values for Cs and F: $r_{Cs}=2.25$, $r_F=0.72$, $X_{Cs}=0.7$ and $X_F=4.0$. In a private communication, Professor Charles P. Smyth very kindly calculated r for CsF by this method as 2.67A. Other theoretical calculations by Rice[21] vary between 2.60 and 2.66A.

Less is known concerning the distribution of charge around the molecule than about the internuclear distance, and so theoretical values for μ are still in a rudimentary state. Hannay and Smyth[22] define a term which they call the "amount of ionic character" as (μ/re) and Professor Smyth in a letter has estimated this as 0.91 and $\mu=11.6$ Debye. He stated that the error might be at least 10 percent and μ was more likely to be high than low. The observed value reported here is 7.3 ± 0.5 Debye which is an "amount of ionic character" of only 59 percent. Since CsF has the greatest electronegativity difference of any possible pair of elements, barring 87, an accurate value for μ is obviously of interest in establishing the values of the electronegativities of the elements since these vary in a regular manner through the periodic table.

The advent of the electric resonance method now promises that gaps in our knowledge of the distribution of electric charge about a molecule will be filled with the help of precision measurements of the electric dipole moment and the moment of inertia. Because this new method can also probe the interactions of the nuclei of atoms with external fields, it would appear that it will become an important tool in further investigations of nuclear and molecular structure.

This problem was proposed to me by Professor I. I. Rabi and executed under his direction. It is a pleasure to thank Professor P. Kusch who gave me considerable help in the last stages of the work and, with Dr. John Trischka, made several runs on the apparatus. I have had many helpful discussions with Professor Willis Lamb on the theory of the experiment, while Professor J. M. B. Kellogg, Dr. S. Millman, and several other members of the Molecular Beam Laboratory have offered suggestions and helped during runs. Mr. S. Cooey of the Physics Department Shop displayed expert workmanship and unusual ingenuity in constructing much of the apparatus.

[17] Maxwell, Hendricks, and Mosley, Phys. Rev. **52**, 968 (1937).
[18] Internationale Tabellen zur Bestimmung von Kristallstrukturen, Vol. II, p. 611.
[19] Schomaker and Stevenson, J. Am. Chem. Soc. **63**, 37 (1941).
[20] For a discussion of this quantity see W. Gordy, Phys. Rev. **69**, 604 (1946).
[21] Oscar K. Rice, *Electronic Structure and Chemical Binding* (McGraw-Hill Book Company, Inc., New York, 1940), p. 253.
[22] Hannay and Smyth, J. Am. Chem. Soc. **68**, 171 (1946).

On the Lorentz Transformation of Charge and Current Densities

BORIS PODOLSKY
Graduate School, University of Cincinnati, Cincinnati, Ohio

(Received June 16, 1947)

The components of $\rho\mathbf{v}/c$ and $i\rho$ must transform as components of a four-vector, so that if measured in one coordinate system they are known in all coordinate systems. On the other hand, any operational definition of $\rho(\mathbf{r}, t)$ must take account of the positions of all particles at the same time t, that of the s-th particle being $\mathbf{r}_s(t)$. Upon performing the Lorentz transformation these will be $\mathbf{r}_s'(t_s')$, and the transformed time t_s' will be different for each particle. Another observer, in measuring ρ', would use $\mathbf{r}_s'(t')$, t' being the same for all particles. As particles are in motion $\mathbf{r}_s'(t_s') \neq \mathbf{r}_s'(t')$, and there appears to be no necessary relation between $\rho(\mathbf{r}, t)$ and $\rho'(\mathbf{r}', t')$, operationally defined in each coordinate system. It turns out, however, that if in each coordinate system the charge density is defined by $\rho(\mathbf{r}, t) = \sum_s e_s \delta(\mathbf{r} - \mathbf{r}_s(t))$, then relativistic equations of transformation hold.

1. INTRODUCTION

IN classical electrodynamics one introduces the *charge density* and the three-dimensional *current density vector* $\mathbf{j} = \mathbf{u}/c$, where $\mathbf{u}$ is the local velocity of the charges, both ρ and $\mathbf{j}$ being functions of position vector $\mathbf{r}$ and time t. It is then shown that the general theory requires that the four quantities

$$s_\alpha = (j_x, j_y, j_z, i\rho), \quad \alpha = 1, 2, 3, 4 \tag{1}$$

must form a four-dimensional vector, i.e., that the four components of s_α must transform as the four quantities

$$x_\alpha = (x, y, z, ict), \tag{2}$$

respectively.

The question now arises as to how one must define ρ and $\mathbf{j}$ in order that s_α may indeed transform in this way.[1] The problem may be stated more precisely as follows: How can each observer write down ρ and $\mathbf{j}$ for his own coordinate system, in such a way that they would then be connected by the Lorentz transformation with the corresponding quantities for other observers?

I intend to show that, if a charge distribution consists of a system of point charges e_s ($s = 1, 2, \cdots n$; n = number of charges present), located at points $\mathbf{r}_s(t)$, and having velocities $\mathbf{u}_s(t) = d\mathbf{r}_s(t)/dt$, then we may take

$$\mathbf{j} = \mathbf{j}(\mathbf{r}, t) = \sum_s (e_s/c)\mathbf{u}_s(t)\delta(\mathbf{r} - \mathbf{r}_s(t)) \tag{3}$$

and

$$\rho = \rho(\mathbf{r}, t) = \sum_s e_s \delta(\mathbf{r} - \mathbf{r}_s(t)) \tag{4}$$

as satisfactory definitions of the current and charge densities, respectively.

[1] The difficulty involved in formulating this definition was called to my attention by Professor Carl Eckart.

2. THEORY

We shall use the vector form of the Lorentz transformation equations:

$$\mathbf{r}' = \mathbf{r} + (\beta - 1)v^{-2}(\mathbf{v}\cdot\mathbf{r})\mathbf{v} - \beta t\mathbf{v}, \tag{5}$$

$$t' = \beta(t - \mathbf{v}\cdot\mathbf{r}/c^2), \tag{6}$$

where $\beta = (1 - v^2/c^2)^{-\frac{1}{2}}$, $\mathbf{v}$ being the velocity of the primed coordinate system relative to the unprimed. We must therefore show that if

$$\mathbf{j}'(\mathbf{r}', t') = \sum_s (e_s/c)\mathbf{u}_s'(t')\delta(\mathbf{r}' - \mathbf{r}_s'(t')) \tag{7}$$

and

$$\rho'(\mathbf{r}', t') = \sum_s e_s \delta(\mathbf{r}' - \mathbf{r}_s'(t')) \tag{8}$$

are the current and charge densities defined in the primed coordinate system, then, in an analogous manner to Eqs. (5) and (6),

$$\mathbf{j}'(\mathbf{r}', t') = \mathbf{j}(\mathbf{r}, t) + (\beta - 1)v^{-2}\mathbf{v}\cdot\mathbf{j}(\mathbf{r}, t)\mathbf{v} - \beta\mathbf{v}\rho(\mathbf{r}, t)/c \tag{9}$$

and

$$\rho(\mathbf{r}', t') = \beta[\rho(\mathbf{r}, t) - \mathbf{v}\cdot\mathbf{j}(\mathbf{r}, t)/c]. \tag{10}$$

More explicitly, we have to show that the equations

$$\mathbf{j}'(\mathbf{r}', t') = \sum_s (e_s/c)\{\mathbf{u}_s(t) + (\beta - 1)v^{-2}\mathbf{v}\cdot\mathbf{u}_s(t)\mathbf{v} - \beta\mathbf{v}\}\delta(\mathbf{r} - \mathbf{r}_s(t)) \tag{11}$$

and

$$\rho'(\mathbf{r}', t') = \sum_s e_s\beta\{1 - \mathbf{v}\cdot\mathbf{u}_s(t)/c^2\}\delta(\mathbf{r} - \mathbf{r}_s(t)), \tag{12}$$

obtained by substitution into Eqs. (9) and (10)

of the values of $\mathbf{j}$ and ρ from Eqs. (3) and (4), reduce to Eqs. (7) and (8).

In these equations, in which $\mathbf{r}$ and t are arbitrary position vector and time, and $\mathbf{r}'$ and t' the corresponding quantities connected with $\mathbf{r}$ and t by Eqs. (5) and (6), $\mathbf{r}_s(t)$ must be supposed to be some known or measurable functions of t, corresponding to the particle motion in the unprimed coordinate system, while $\mathbf{r}_s'(t')$ must give the same motion as seen in the primed system. A difficulty arises because of the fact that if, with t fixed, we apply Eqs. (5) and (6) to t and the corresponding $\mathbf{r}_s$, these will go over into t_s' and the corresponding $\mathbf{r}_s'$, with t_s' in general not equal to t'. In fact we obtain:

$$\mathbf{r}_s'(t_s') = \mathbf{r}_s(t) + (\beta - 1)v^{-2}\mathbf{v}\cdot\mathbf{r}_s(t)\mathbf{v} - \beta t\mathbf{v} \quad (13)$$

and

$$t_s' = \beta(t - \mathbf{v}\cdot\mathbf{r}_s(t)/c^2), \quad (14)$$

so that the transformed time t_s' varies from particle to particle and is equal to t' only when $\mathbf{r}_s(t) = \mathbf{r}$.

It appears, therefore, that we cannot express $\mathbf{r}_s'(t')$ explicitly in terms of $\mathbf{r}_s(t)$, $\mathbf{r}$, and t. Fortunately this also turns out to be unnecessary. To see this, we note that the only events $(\mathbf{r}, t)$ for which the right-hand members of Eqs. (11) and (12) do not vanish are those for which

$$\mathbf{r} = \mathbf{r}_s(t),$$

and that then

$$t_s' = t', \quad \text{and} \quad \mathbf{r}_s'(t_s') = \mathbf{r}_s'(t') = \mathbf{r}', \quad (15)$$

as can readily be seen by comparison of Eqs. (13) and (14) with Eqs. (5) and (6). These events are, therefore, to be found among the events $(\mathbf{r}', t')$ for which the right-hand members of Eqs. (7) and (8) do not vanish. The converse is also easily shown.

Thus the events for which the δ-functions in Eqs. (7) and (8) do not vanish are *the same events* for which the δ-functions in Eqs. (11) and (12) do not vanish.

It is therefore possible to establish a relation between $\delta(\mathbf{r}' - \mathbf{r}_s'(t'))$ and $\delta(\mathbf{r} - \mathbf{r}_s(t))$. This is done in the Appendix and gives:

$$\delta(\mathbf{r}' - \mathbf{r}_s'(t')) = \beta[1 - \mathbf{v}\cdot\mathbf{u}_s(t)/c^2]\delta(\mathbf{r} - \mathbf{r}_s(t)). \quad (16)$$

With this relation Eq. (11) obviously reduces to Eq. (7), while Eq. (12) becomes:

$$\mathbf{j}'(\mathbf{r}', t') = \sum_s (e_s/\beta c)\{\mathbf{u}_s(t) + (\beta - 1)v^{-2}\mathbf{v}\cdot\mathbf{u}_s(t) - \beta\mathbf{v}\} \times \frac{\delta(\mathbf{r}' - \mathbf{r}_s'(t))}{1 - \mathbf{v}\cdot\mathbf{u}_s(t)/c^2}. \quad (17)$$

This may be further simplified, however, by introducing $\mathbf{u}_s'(t')$. Thus, differentiation of Eqs. (13) and (14) gives:

$$d\mathbf{r}_s'(t_s') = d\mathbf{r}_s(t) + (\beta - 1)v^{-2}\mathbf{v}\cdot d\mathbf{r}_s(t)\mathbf{v} - \beta\mathbf{v}dt \quad (18)$$

and

$$dt_s' = \beta[dt - \mathbf{v}\cdot d\mathbf{r}_s(t)/c^2]. \quad (19)$$

Hence

$$\mathbf{u}_s'(t_s') = d\mathbf{r}_s'(t_s')/dt_s' = \frac{\mathbf{u}_s(t) + (\beta - 1)v^{-2}\mathbf{v}\cdot\mathbf{u}_s(t)\mathbf{v} - \mathbf{v}\beta}{\beta[1 - \mathbf{v}\cdot\mathbf{u}_s(t)/c^2]}. \quad (20)$$

Substituting this relation into Eq. (17) and making use of Eq. (15), we finally obtain Eq. (8).

APPENDIX

Let $F(\mathbf{r}')$ be any function of $\mathbf{r}'$, and let $\mathbf{r} - \mathbf{r}_s(t)$, regarded as a function of $\mathbf{r}'$ and t', be $\mathbf{R}$. Thus

$$\mathbf{R} = \mathbf{r} - \mathbf{r}_s(t) = \mathbf{R}(\mathbf{r}', t'). \quad (21)$$

Then

$$\int\int\int_{-\infty}^{\infty} F(\mathbf{r}')\delta(\mathbf{r} - \mathbf{r}_s(t))dx'dy'dz'$$

$$= \int\int\int_{-\infty}^{\infty} F(\mathbf{r}')\delta(\mathbf{R})dx'dy'dz'$$

$$= \int\int\int_{-\infty}^{\infty} F(\mathbf{r}')\frac{\partial(x', y', z')}{\partial(R_x, R_y, R_z)}\delta(\mathbf{R})dR_xdR_ydR_z$$

$$= \left[F(\mathbf{r}')\frac{\partial(x', y', z')}{\partial(R_x, R_y, R_z)}\right]_{\mathbf{R}=0}$$

$$= \left[F(\mathbf{r}')\frac{\partial(x', y', z')}{\partial(R_x, R_y, R_z)}\right]_{\mathbf{r}'=\mathbf{r}_s'(t')},$$

by Eq. (15). But, the last expression is also

equal to

$$\int\int\int_{-\infty}^{\infty} F(\mathbf{r}')\frac{\partial(x', y', z')}{\partial(R_x, R_y, R_z)}\delta(\mathbf{r}'-\mathbf{r}_s'(t'))dx'dy'dz'.$$

Therefore

$$\delta(\mathbf{r}-\mathbf{r}_s(t))=\frac{\partial(x', y', z')}{\partial(R_x, R_y, R_z)}\delta(\mathbf{r}'-\mathbf{r}_s'(t'))$$

$$=\delta(\mathbf{r}'-\mathbf{r}_s'(t'))/J, \quad (22)$$

where

$$J=\partial(R_x, R_y, R_z)/\partial(x', y', z').$$

In calculating derivatives of the components of $\mathbf{R}$ we must remember that $\mathbf{r}_s(t)$ are some given functions of t, specifying the motions of the particles in the unprimed coordinate system, while

$$\mathbf{r}=\mathbf{r}'+(\beta-1)v^{-2}(\mathbf{v}\cdot\mathbf{r}')\mathbf{v}+\beta t'\mathbf{v} \quad (23)$$

and

$$t=\beta(t'+\mathbf{v}\cdot\mathbf{r}'/c^2). \quad (24)$$

Thus, we have, for example,

$$R_x=x'+(\beta-1)v^{-2}(x'v_x+y'v_y+z'v_z)v_x+\beta t'v_x-x_s(t),$$

where x' and $x_s(t)$ are the x-components of $\mathbf{r}'$ and $\mathbf{r}_s(t)$, respectively. Therefore

$$\partial R_x/\partial x'=1+(\beta-1)v^{-2}v_x^2-(dx_s(t)/dt)\partial t/\partial x'$$

$$=1+(\beta-1)v^{-2}v_x^2-\dot{x}_s(t)\beta v_x/c^2,$$

the factor $\partial t/\partial x'$ being obtained from Eq. (24), while $\dot{x}_s(t)$ is the x-component of $\mathbf{u}_s(t)$.

In this way we obtain:

$$J=\beta[1-\mathbf{v}\cdot\mathbf{u}_s(t)/c^2]. \quad (25)$$

Combining Eqs. (22) and (25) we obtain Eq. (16).

PHYSICAL REVIEW VOLUME 72, NUMBER 7 OCTOBER 1, 1947

Recurrence Formulas for Coulomb Wave Functions

JOHN L. POWELL
University of Wisconsin, Madison, Wisconsin

(Received June 13, 1947)

Recurrence relations connecting Coulomb functions for different values of the angular momentum L and the same value of the nuclear radius parameter ρ are summarized, and their derivation is outlined.

THE Coulomb wave functions F_L and G_L, as defined by Yost, Wheeler, and Breit,[1] are solutions of the differential equation

$$\frac{d^2F}{d\rho^2}+\left\{1-\frac{2\eta}{\rho}-\frac{L(L+1)}{\rho^2}\right\}F=0 \quad (1)$$

which, for large ρ, have the asymptotic forms

$$F_L\sim\sin\left(\rho-\frac{L\pi}{2}-\eta\ln 2\rho+\sigma_L\right),$$

$$G_L\sim\cos\left(\rho-\frac{L\pi}{2}-\eta\ln 2\rho+\sigma_L\right),$$

where $\sigma_L=\arg\Gamma(L+1+i\eta)$.

[1] F. L. Yost, John A. Wheeler, and G. Breit, J. Terr. Mag. 40, 443 (1935); Phys. Rev. 49, 174 (1936).

F_L and G_L are the real and imaginary parts, respectively, of the function

$$Y_L=F_L+iG_L=\frac{\rho^{L+1}}{i(e^{2\pi\eta}-1)(2L+1)!C_L}$$

$$\times\int_D (z-i)^{L+i\eta}(z+i)^{L-i\eta}e^{z\rho}dz, \quad (2)$$

where

$$C_L^2=\frac{[1+(\eta^2/L^2)]\cdots[1+(\eta^2/1^2)]}{1^2\cdot 3^2\cdots(2L+1)^2}\frac{2\pi\eta}{(e^{2\pi\eta}-1)}, \quad (3)$$

and D is a contour in the complex z plane which starts at $(-\infty-i)$, encircles the point $-i$ once in the positive sense, and returns to the starting point. The expression (2) may be derived by

standard methods and is well-known among workers in the field.

The function Y_L (and therefore also F_L and G_L) satisfies the relations

$$(L+1)\{L^2+\eta^2\}^{\frac{1}{2}}Y_{L-1} - (2L+1)\left[\eta+\frac{L(L+1)}{\rho}\right]Y_L + L[(L+1)^2+\eta^2]^{\frac{1}{2}}Y_{L+1}=0, \quad (4)$$

$$(L+1)Y_L' - \left[\frac{(L+1)^2}{\rho}+\eta\right]Y_L + [(L+1)^2+\eta^2]^{\frac{1}{2}}Y_{L+1}=0, \quad (5)$$

$$LY_L' + \left(\frac{L^2}{\rho}+\eta\right)Y_L - (L^2+\eta^2)^{\frac{1}{2}}Y_{L-1}=0. \quad (6)$$

(The primes denote differentiation with respect to ρ.)

DERIVATION

Let I_L denote the integral

$$I_L=\int_D (z-i)^{L+i\eta}(z+i)^{L-i\eta}e^{z\rho}dz.$$

By integrating the expression

$$\{\rho(z^2+1)+2(L+1)z-2\eta\}(z-i)^{L+i\eta}(z+i)^{L-i\eta}e^{z\rho} = \frac{d}{dz}\{(z-i)^{L+1+i\eta}(z+i)^{L+1-i\eta}e^{z\rho}\},$$

with respect to z around the contour D, it is found that

$$2(L+1)I_L'-2\eta I_L+\rho I_{L+1}=0. \quad (7)$$

From (2) and (3) we have

$$Y_L=\frac{\rho^{L+1}}{i(e^{2\pi\eta}-1)(2L+1)!C_L}I_L,$$

and

$$C_{L+1}=\frac{2}{(2L+2)(2L+3)}[(L+1)^2+\eta^2]^{\frac{1}{2}}C_L,$$

and using these relationships in (7) we obtain formula (5). Equation (4) is obtained by differentiating (5) and using (1) (with F replaced by Y_L) to eliminate the second derivative. Equation (6) is an immediate consequence of (4) and (5).

By using (6) to eliminate the derivatives in the expression for the Wronskian

$$F_L'G_L-F_LG_L'=1,$$

one obtains

$$F_{L-1}G_L-F_LG_{L-1}=\frac{L}{(L^2+\eta^2)^{\frac{1}{2}}}.$$

The last two relationships are convenient forms for checking numerical tables.

The recurrence relations derived here for the regular function F_L have been previously published by Lowan and Horenstein.[2] The writer has also been informed that Mr. J. K. Tyson of the Department of Physics of the Massachusetts Institute of Technology has independently derived the relations presented here subsequent to the completion of this work.

ACKNOWLEDGMENT

Assistance of the Wisconsin Alumni Research Foundation and of Contract N6ori-97, Task I of the Office of Naval Research is gratefully acknowledged.

[2] A. N. Lowan and W. Horenstein, J. Math. and Phys. 21, 264 (1942).

Self-Energy and Interaction Energy in Podolsky's Generalized Electrodynamics

ALEX E. S. GREEN
Department of Physics, University of Cincinnati, Cincinnati, Ohio

(Received June 16, 1947)

Using a perturbation method, explicit expressions are derived for the electromagnetic self-energy and electromagnetic interaction energy of charged particles in Podolsky's generalized quantum electrodynamics. No infinities arise in the derivation, which is justified to the first order of approximation (i.e., to terms quadratic in the charges). Two noteworthy results follow from the calculations. (a) The self-energy is finite and negative. (b) The interaction energy contains no singularities.

I. INTRODUCTION

IN a series of papers [1–4] a generalized electrodynamics has been developed in which the Lagrangian contains derivatives of the field quantities. This has led to a theory in which an extraordinary field appears in combination with the usual Maxwell-Lorentz field. This extraordinary field is associated with a neutral particle of mass $m=\hbar/ac$, where a is a natural unit of length occurring in the theory. The quantization rules have been derived and the auxiliary conditions eliminated by methods which are generalizations of those used in the earlier basic work in relativistic quantum electrodynamics.

In GE III the auxiliary conditions are used to eliminate from the wave functional the ordinary scalar potential, the longitudinal component of the ordinary vector potential, the extraordinary scalar potential, and part of the longitudinal component of the extraordinary vector potential. The consequence of the transformations, which are exact, is the explicit appearance in the wave equation of terms which can be interpreted as the electrostatic self-energy and the electrostatic interaction. The present problem is to investigate the effect of the remainder of the ordinary and extraordinary vector potentials to obtain what can be interpreted as the "transverse" self-energy and the spin and retardation interactions.

II. CALCULATION OF THE PERTURBATION ENERGY

As a starting point we use some equations obtained in GE IV. In this paper a generalization of the functional formalism of Fock,[5] leads to the following set of ordinary wave equations in $\mathbf{k}$-space for a system of charged particles [GE IV Eqs. (2.25), (2.26), and (2.27), respectively].

$$(H-i\hbar\partial/\partial t)\psi_{00}=\sum_{j=1}^{3}\int d\mathbf{k}[G_0^*(\mathbf{k},j)\psi_{10}(\mathbf{k},j)+\bar{G}_0^*(\mathbf{k},j)\psi_{01}(\mathbf{k},j)], \tag{2.1}$$

$$(H+\hbar ck-i\hbar\partial/\partial t)\psi_{10}(\mathbf{k},j)=G_0(\mathbf{k},j)\psi_{00}, \tag{2.2}$$

$$(H+\hbar c\bar{k}-i\hbar\partial/\partial t)\psi_{01}(\mathbf{k},j)=-\bar{G}_0(\mathbf{k},j)\psi_{00}, \tag{2.3}$$

where[6]

$$H=\sum_{s=1}^{n}(\boldsymbol{\alpha}_s\cdot c\mathbf{p}_s+m_sc^2\beta_s)+(1/8\pi a)\textstyle\sum_s\epsilon_s^2+\sum_{s,u}'(\epsilon_s\epsilon_u/8\pi R)[1-\exp(-R/a)], \tag{2.4}$$

[1] B. Podolsky, Phys. Rev. 62, 68 (1942), to be referred to as GE I.
[2] B. Podolsky and C. Kikuchi, Phys. Rev. 65, 228 (1944), to be referred to as GE II.
[3] B. Podolsky and C. Kikuchi, Phys. Rev. 67, 184 (1945), to be referred to as GE III.
[4] D. J. Montgomery, Phys. Rev. 69, 117 (1946), to be referred to as GE IV.
[5] V. Fock, Physik. Zeits. Sowjetunion 6, 425 (1934).
[6] Note the typographical error in GE IV Eq. (2.16) which has a factor $\frac{1}{4}$ instead of a factor $\frac{1}{8}$ before the interaction term.

$$G_0^*(\mathbf{k}, j) = (1/2\pi)^{\frac{1}{2}}(ch/2k)^{\frac{1}{2}} \sum_s \epsilon_s \beta_j (1/k)\boldsymbol{\alpha}_s \cdot \mathbf{k}\times\mathbf{e}_j \exp(i\mathbf{k}\cdot\mathbf{r}_s), \tag{2.5}$$

$$\tilde{G}_0^*(\mathbf{k}, j) = (1/2\pi)^{\frac{1}{2}}(ch/2\tilde{k})^{\frac{1}{2}} \sum_s \epsilon_s \tilde{\beta}_j (1/a\tilde{k})(\boldsymbol{\alpha}_s \cdot a\mathbf{k}\times\mathbf{e}_j + \boldsymbol{\alpha}_s \cdot \mathbf{e}_j) \exp(i\mathbf{k}\cdot\mathbf{r}_s), \tag{2.6}$$

$$\mathbf{R} = \mathbf{r}_s - \mathbf{r}_u, \quad \tilde{k} = (1+a^2k^2)^{\frac{1}{2}}/a \quad \text{and} \quad \beta_j^2 = \tilde{\beta}_j^2 = 1.$$

In the derivation of Eqs. (2.1), (2.2), and (2.3) the series expansion of the wave functional was broken off after three terms, which corresponds to limiting the investigation to processes involving one ordinary quantum and one extraordinary quantum. As in GE IV we treat the term on the right of (2.1) as a perturbation of the unperturbed Hamiltonian. At this point we depart from the procedure of GE IV because we seek an explicit expression for the perturbation energy rather than the corresponding matrix element.

In order to eliminate ψ_{10} and ψ_{01} from (2.1) we assume that as a zero-order approximation

$$(H - ih\partial/\partial t)\psi_{10}(\mathbf{k}, j) = 0 \quad \text{and} \quad (H - ih\partial/\partial t)\psi_{01}(\mathbf{k}, j) = 0. \tag{2.7}$$

From (2.2) and (2.3) we have thus

$$\psi_{10}(\mathbf{k}, j) = G_0(\mathbf{k}, j)\psi_{00}/hck \quad \text{and} \quad \psi_{01}(\mathbf{k}, j) = -\tilde{G}_0(\mathbf{k}, j)\psi_{00}/hck. \tag{2.8}$$

Introducing these terms into the right side of (2.1) gives as a first-order approximation the perturbation energy

$$U = -\sum_j \int d\mathbf{k}[G_0^*(\mathbf{k}, j)G_0(\mathbf{k}, j)/hck - \tilde{G}_0^*(\mathbf{k}, j)\tilde{G}_0(\mathbf{k}, j)/hc\tilde{k}]. \tag{2.9}$$

This expression may be simplified by use of the following identities:

$$\sum_j \beta_j(1/k)\boldsymbol{\alpha}_s \cdot \mathbf{k}\times\mathbf{e}_j \exp(i\mathbf{k}\cdot\mathbf{r}_s)\beta_j(1/k)\boldsymbol{\alpha}_u \cdot \mathbf{k}\times\mathbf{e}_j \exp(-i\mathbf{k}\cdot\mathbf{r}_u)$$
$$= \sum_j (1/k^2)(\boldsymbol{\alpha}_s\times\mathbf{k}\cdot\mathbf{e}_j)(\boldsymbol{\alpha}_u\times\mathbf{k}\cdot\mathbf{e}_j) \exp(i\mathbf{k}\cdot\mathbf{R}) = (\boldsymbol{\alpha}_s\times\mathbf{k}/k)\cdot(\boldsymbol{\alpha}_u\times\mathbf{k}/k) \exp(i\mathbf{k}\cdot\mathbf{R}) \tag{2.10}$$

and

$$\sum_j \beta_j(1/a\tilde{k})(\boldsymbol{\alpha}_s \cdot a\mathbf{k}\times\mathbf{e}_j + \boldsymbol{\alpha}_s \cdot \mathbf{e}_j) \exp(i\mathbf{k}\cdot\mathbf{r}_s)\beta_j(1/a\tilde{k})(\boldsymbol{\alpha}_u \cdot a\mathbf{k}\times\mathbf{e}_j + \boldsymbol{\alpha}_u \cdot \mathbf{e}_j) \exp(-i\mathbf{k}\cdot\mathbf{r}_u)$$
$$= \sum_j (1/a^2\tilde{k}^2)(\boldsymbol{\alpha}_s\times a\mathbf{k} + \boldsymbol{\alpha}_s)\cdot\mathbf{e}_j(\boldsymbol{\alpha}_u\times a\mathbf{k} + \boldsymbol{\alpha}_u)\cdot\mathbf{e}_j \exp(i\mathbf{k}\cdot\mathbf{R})$$
$$= (1/a^2\tilde{k}^2)[a^2(\boldsymbol{\alpha}_s\times\mathbf{k})\cdot(\boldsymbol{\alpha}_u\times\mathbf{k}) + \boldsymbol{\alpha}_s\cdot\boldsymbol{\alpha}_u + a(\boldsymbol{\alpha}_s\times\mathbf{k}\cdot\boldsymbol{\alpha}_u + \boldsymbol{\alpha}_s\cdot\boldsymbol{\alpha}_u\times\mathbf{k})] \exp(i\mathbf{k}\cdot\mathbf{R})$$
$$= [(\boldsymbol{\alpha}_s\times\mathbf{k}/k)\cdot(\boldsymbol{\alpha}_u\times\mathbf{k}/k) + (1/a^2\tilde{k}^2)(\boldsymbol{\alpha}_s\cdot\mathbf{k}/k)(\boldsymbol{\alpha}_u\cdot\mathbf{k}/k)] \exp(i\mathbf{k}\cdot\mathbf{R}). \tag{2.11}$$

In arriving at the last expression we use the known properties of the triple scalar product and the vector equation

$$(\boldsymbol{\alpha}_s\times\mathbf{k}/k)\cdot(\boldsymbol{\alpha}_u\times\mathbf{k}/k) = \boldsymbol{\alpha}_s\cdot\boldsymbol{\alpha}_u - (\boldsymbol{\alpha}_s\cdot\mathbf{k}/k)(\boldsymbol{\alpha}_u\cdot\mathbf{k}/k). \tag{2.12}$$

The perturbation energy thus becomes

$$U = -\sum_{s,u}(\epsilon_s\epsilon_u/16\pi^3)\int d\mathbf{k} \exp(i\mathbf{k}\cdot\mathbf{R})[(\boldsymbol{\alpha}_s\times\mathbf{k}/k)\cdot(\boldsymbol{\alpha}_u\times\mathbf{k}/k)(1/k^2) - (\boldsymbol{\alpha}_s\times\mathbf{k}/k)\cdot(\boldsymbol{\alpha}_u\times\mathbf{k}/k)(1/\tilde{k}^2)$$
$$- (\boldsymbol{\alpha}_s\cdot\mathbf{k}/k)(\boldsymbol{\alpha}_u\cdot\mathbf{k}/k)(1/a^2\tilde{k}^4)]. \tag{2.13}$$

It can be shown[7] that the three terms have the following origins. The first term is the contribution of the transverse component of the ordinary field. It is the only term present in the usual electrodynamics, in which case it gives rise to an infinite self-energy. The second term is the contribution of the transverse component of the extraordinary field. The third term is the contribution of the longitudinal component of the extraordinary field. Its magnitude has been determined by the treatment of the auxiliary conditions in GE II and GE III.

[7] To do so requires a formalism in which all vector quantities are resolved into transverse and longitudinal components rather than the formalism of GE IV. Such a development has been carried out. It also leads to Eq. (2.13).

Using (2.12) and rearranging terms, it follows that

$$U=-\sum_{s,u}(\epsilon_s\epsilon_u/16\pi^3)\Big\{\int d\mathbf{k}\exp(i\mathbf{k}\cdot\mathbf{R})\boldsymbol{\alpha}_s\cdot\boldsymbol{\alpha}_u(1/k^2-1/\bar{k}^2)$$
$$-\int d\mathbf{k}\exp(i\mathbf{k}\cdot\mathbf{R})(\boldsymbol{\alpha}_s\cdot\mathbf{k}/k)(\boldsymbol{\alpha}_u\cdot\mathbf{k}/k)(1/k^2-1/\bar{k}^2)$$
$$-\int d\mathbf{k}\exp(i\mathbf{k}\cdot\mathbf{R})(\boldsymbol{\alpha}_s\cdot\mathbf{k}/k)(\boldsymbol{\alpha}_u\cdot\mathbf{k}/k)(1/a^2\bar{k}^4)\Big\}. \quad (2.14)$$

To evaluate the integrals we use polar coordinates in $\mathbf{k}$-space, taking $\mathbf{R}$ as the direction of the polar axis. The volume element is $k^2\sin\theta dkd\theta d\varphi$, where θ and φ are the polar and azimuth angles, respectively. As $\boldsymbol{\alpha}_s\cdot\boldsymbol{\alpha}_u$ is independent of $\mathbf{k}$, it is unaffected by the integrations. The factor $(\boldsymbol{\alpha}_s\cdot\mathbf{k}/k)\times(\boldsymbol{\alpha}_u\cdot\mathbf{k}/k)$ however, requires more careful attention. Introducing α_x, α_y, and α_z, the well-known Dirac matrices, and

$$k_x/k=\sin\theta\cos\varphi, \qquad k_y/k=\sin\theta\sin\varphi, \qquad k_z/k=\cos\theta$$

we have

$$(\boldsymbol{\alpha}_s\cdot\mathbf{k}/k)(\boldsymbol{\alpha}_u\cdot\mathbf{k}/k)=\alpha_{sx}\alpha_{ux}\sin^2\theta\cos^2\varphi+\alpha_{sy}\alpha_{uy}\sin^2\theta\sin^2\varphi+\alpha_{sz}\alpha_{uz}\cos^2\theta$$
$$+(\alpha_{sx}\alpha_{uy}+\alpha_{sy}\alpha_{ux})\sin^2\theta\sin\varphi\cos\varphi+(\alpha_{sy}\alpha_{uz}+\alpha_{sz}\alpha_{uy})\sin\theta\cos\theta\sin\varphi$$
$$+(\alpha_{sz}\alpha_{ux}+\alpha_{sx}\alpha_{uz})\sin\theta\cos\theta\cos\varphi. \quad (2.15)$$

Upon integration with respect to φ over the range $0-2\pi$ the cross products all vanish. Using

$$\alpha_{sx}\alpha_{ux}+\alpha_{sy}\alpha_{uy}+\alpha_{sz}\alpha_{uz}=\boldsymbol{\alpha}_s\cdot\boldsymbol{\alpha}_u \quad \text{and} \quad \alpha_{sz}\alpha_{uz}=(\boldsymbol{\alpha}_s\cdot\mathbf{R}/R)(\boldsymbol{\alpha}_u\cdot\mathbf{R}/R),$$

the remaining terms give

$$U=-\sum_{s,u}(\epsilon_s\epsilon_u/16\pi^2)[\boldsymbol{\alpha}_s\cdot\boldsymbol{\alpha}_u(2I_1-I_1+I_2-I_3+I_4)+(\boldsymbol{\alpha}_s\cdot\mathbf{R}/R)(\boldsymbol{\alpha}_u\cdot\mathbf{R}/R)(I_1-3I_2+I_3-3I_4)], \quad (2.16)$$

where

$$I_1=\int_0^\infty\int_0^\pi\frac{\exp(ikR\cos\theta)\sin\theta dkd\theta}{1+a^2k^2}, \quad (2.17)$$

$$I_2=\int_0^\infty\int_0^\pi\frac{\cos^2\theta\exp(ikR\cos\theta)\sin\theta dkd\theta}{1+a^2k^2}, \quad (2.18)$$

$$I_3=\int_0^\infty\int_0^\pi\frac{a^2k^2\exp(ikR\cos\theta)\sin\theta dkd\theta}{(1+a^2k^2)^2}, \quad (2.19)$$

$$I_4=\int_0^\infty\int_0^\pi\frac{a^2k^2\cos^2\theta\exp(ikR\cos\theta)\sin\theta dkd\theta}{(1+a^2k^2)^2}. \quad (2.20)$$

These integrals may be evaluated by standard methods. No special limiting processes are necessary. The results are

$$I_1=(\pi/R)[1-\exp(-R/a)], \quad (2.21)$$

$$I_2=-\pi\exp(-R/a)(1/R+2a/R^2+2a^2/R^3)+2\pi a^2/R^3, \quad (2.22)$$

$$I_3=(\pi/2a)\exp(-R/a), \quad (2.23)$$

$$I_4=(\pi/2a)\exp(-R/a)+\pi\exp(-R/a)(1/R+2a/R^2+2a^2/R^3)-2\pi a^2/R^3. \quad (2.24)$$

Introducing these expressions into (2.16) we observe that the effect of the terms which come from the residual longitudinal component of the extraordinary field is to cancel all the singularities which arise from the terms representing the effect of the transverse components of the ordinary and extraordinary fields. We obtain finally an amazingly simple expression for the perturbation of the Hamiltonian.

$$U=-\sum_{s,u}\frac{\epsilon_s\epsilon_u}{16\pi}\left\{\boldsymbol{\alpha}_s\cdot\boldsymbol{\alpha}_u\left[\frac{1-\exp(-R/a)}{R}\right]+(\boldsymbol{\alpha}_s\cdot\mathbf{R}/R)(\boldsymbol{\alpha}_u\cdot\mathbf{R}/R)\left[\frac{1-\exp(-R/a)}{R}-\frac{\exp(-R/a)}{a}\right]\right\}. \quad (2.25)$$

III. SELF-ENERGY OF CHARGED PARTICLES

To obtain the self-energy we consider only those terms in the summation corresponding to $s=u$ and let R go to zero. The second term in (2.25), which incidentally can be interpreted as the effect of retardation, vanishes. For a single particle we have left only[8]

$$U=-(\epsilon^2/16\pi a)\boldsymbol{\alpha}\cdot\boldsymbol{\alpha}=-\tfrac{3}{4}\epsilon^2/4\pi a. \quad (3.1)$$

Combining this with the electrostatic self-energy, we obtain for the total, electromagnetic self-energy of a charged particle

$$U_s=-\tfrac{1}{4}\epsilon^2/4\pi a \quad \text{(in Heaviside units)} \quad (3.2)$$

or

$$U_s=-\tfrac{1}{4}\epsilon^2/a \quad \text{(in electrostatic units)}. \quad (3.3)$$

Thus on this theory the electromagnetic self-energy of a charged particle is necessarily distinct from the mass energy.

The wave equation for an isolated charged particle is

$$(c\boldsymbol{\alpha}\cdot\mathbf{p}+mc^2\beta-\epsilon^2/4a-i\hbar\partial/\partial t)\psi=0. \quad (3.4)$$

IV. THE ELECTROMAGNETIC INTERACTION ENERGY

Omitting the self-energy terms in (2.25) and considering the electrostatic interaction, we have for the complete electromagnetic interaction energy the following equation:

$$U_i=\sum_{s,u}{}'\frac{\epsilon_s\epsilon_u}{8\pi}\left\{(1-\tfrac{1}{2}\boldsymbol{\alpha}_s\cdot\boldsymbol{\alpha}_u)\left[\frac{1-\exp(-R/a)}{R}\right]\right.$$

$$\left.-\tfrac{1}{2}(\boldsymbol{\alpha}_s\cdot\mathbf{R}/R)(\boldsymbol{\alpha}_u\cdot\mathbf{R}/R)\left[\frac{1-\exp(-R/a)}{R}-\frac{\exp(-R/a)}{a}\right]\right\}. \quad (4.1)$$

Note the appearance of the term $(1/a)\exp(-R/a)$ which is only effective at short ranges. If we let $a\to 0$, Eq. (4.1) reduces to Breit's formula.

The remarkable simplicity of the above result, as well as its freedom from singularities, has led the writer to the opinion that the theory upon which it is based has a deep-seated validity.

The author is indebted to Dr. Boris Podolsky for his guidance and encouragement.

[8] This result may be obtained more directly by letting $s=u$ and $R=0$ in Eq. (2.14). The integrations can then be carried out very simply.

Stellar Electromagnetic Fields

LEVERETT DAVIS, JR.
California Institute of Technology, Pasadena, California
(Received August 15, 1947)

CALCULATION shows that a magnetized rotating star will be surrounded by electrostatic fields in which the potential differences are of the order of 4×10^9 volts for the sun and may be 10^{14} volts for some stars. The presence of the electromagnetic field will produce an ion distribution in space that will considerably modify the electric and magnetic fields. A determination of the space charge and the resulting fields should have a bearing on problems in cosmic rays and astrophysics.

Suppose that all the material of a stellar model is confined within a sphere of radius a and rotates rigidly with angular velocity ω. Suppose the magnetic induction, B, to be constant throughout the region $r<b\leqslant a$ and that for $r>b$

$$\mathbf{B}=-B_p(a/r)^3(\mathbf{e}_r\cos\theta+\tfrac{1}{2}\mathbf{e}_\theta\sin\theta)\text{ gauss},\quad(1)$$

where B_p is the induction at the pole and r, θ, ϕ are the usual spherical coordinates, the polar axis coinciding with the axis of rotation. A uniformly magnetized core would produce this field and it is not inconsistent with the assumption that the field is due to the rotation. B_p is positive when the magnetization is antiparallel to the rotation as in the earth and sun.

The rotation of the star produces motion through this field[1,2] and thus electromotive forces. These are balanced within the star by the electrostatic field resulting from an appropriate charge distribution throughout the conducting sphere; thus the net force on any internal charge rotating with the star is zero. The field outside the star, as seen from a non-rotating inertial frame, consists of the magnetic induction (1) plus the quadrupole electrostatic field due to the charge. The corresponding potential for $r\geqslant a$ is

$$V=V_p(a/r)^3\tfrac{1}{2}(3\cos^2\theta-1)\text{ e.s.u.},\quad(2)$$

where $V_p=\omega B_p a^2/3c$ is the potential of the pole with respect to infinity, $-\frac{1}{2}V_p$ is the potential of the equator, c is the velocity of light, and it is assumed that the star has no net charge. The correctness of the general procedure used is indicated by the agreement of (2) with Swann's[3] result for the case in which $b=a$. Alfvén[4] obtains a different result, and different motions of the ions in the equatorial plane, but his assumption that the lines of induction rotate with the star appears to be incorrect. The electrostatic field for $r>a$ is

$$\mathbf{E}=E_p(a/r)^4[\mathbf{e}_r\tfrac{1}{2}(3\cos^2\theta-1)+\mathbf{e}_\theta\cos\theta\sin\theta]\text{ e.s.u.},\quad(3)$$

where $E_p=\omega B_p a/c$ is the field strength at the pole. The magnetic field produced by the motion of the charges that produce $\mathbf{E}$ is negligible, being of the order of $(\omega a/c)^2B_p$.

The order of magnitude of the various quantities is given in Table I for the earth, sun, and two stars, together with the data[5-7] used in the calculations. In accordance with the discussions of Blackett[8] and Babcock,[9] the angular velocities of the stars are chosen so that the ratio of magnetic moment to angular momentum is the same as for the sun; the resulting values appear possible.

TABLE I. Polar potentials and field strengths.

	Earth	Sun	78 Vir	BD-18°3789
a, radius, cm	6.4×10^8	7.0×10^{10}	1.6×10^{11}	1.6×10^{11}
M, mass, g	6×10^{27}	2×10^{33}	5×10^{33}	5×10^{33}
ω, ang. vel., rad/sec.	7.3×10^{-5}	3×10^{-6}	7×10^{-5}	2×10^{-4}
B_p, induction at pole, gauss	0.61	53	1500	5500
V_p, potential at pole, volts	6.0×10^4	2.6×10^9	9×10^{12}	9×10^{12}
E_p, elec. field at pole, volt/cm	2.6×10^{-4}	1.1×10^{-1}	170	1700

[1] J. T. Tate, Bull. Nat. Research Council **4**, Part 6, 75 (1922).
[2] W. V. Houston, Am. J. Phys. **7**, 373 (1939).
[3] W. F. G. Swann, Phys. Rev. **15**, 365 (1920).
[4] H. Alfvén, Arkiv f. Mat. Astr. och Fysic **28A**, 1 (1942).
[5] H. W. Babcock, Ap. J. **105**, 105 (1947).
[6] H. W. Babcock, Phys. Rev. **72**, 83 (1947).
[7] W. Becker, *Sterne und Sternsystem* (Dresden, 1942), p. 64.
[8] P. M. S. Blackett, Nature **159**, 658 (1947).
[9] H. W. Babcock, Pub. Astro. Soc. Pac. **59**, 112 (1947).

Evidently few observable effects are to be expected for the earth, especially since the field would appear only above the zone where the atmosphere can be regarded as rotating with the earth and since (3) gives the field for a non-rotating observer. In the case of the sun and stars, if the above fields were not altered by nearby ions, cosmic rays should be ejected with energy eV_p along the polar axis where the electric and magnetic fields are parallel. The source of energy is the rotational kinetic energy, which loses the energy eV_p per ion because of the motion of the induced surface charge in the magnetic field. The necessary angular momentum goes into the electromagnetic field. The observed cosmic-ray density reported by Millikan[10] could not be produced in this way because the stars do not have enough rotational energy. There is enough rotational energy to produce a few of the highest energy particles, leaving the bulk of the cosmic-ray energy to be accounted for by other means, perhaps annihilation of atoms.

If the sun produced cosmic rays in this way, the decelerating torque would be applied mainly near the poles. This would explain the observed slow rotation of the polar regions of the sun in spite of the very significant damping of any non-uniform rotation that must be produced by the electrical eddy currents produced by non-uniform rotation in a magnetic field of the order of 50 gausses.

Consideration of the behavior of ions that do not move along the polar axis indicates that a space charge should accumulate that will invalidate the model considered above. Ions in the equatorial plane are not accelerated into cosmic rays by the radial electric field, appreciable radial motion being prevented by the magnetic field. Such ions move in small circles, the center of the circle drifting with the velocity $\mathbf{e}_\phi\omega a^2/r$. In general, a positive ion will accelerate along a line of induction and move toward the equatorial plane. A negative ion accelerates in the opposite direction until it strikes the star. Thus a positive space charge is built up in the equatorial plane while the star acquires a negative surface charge. The magnetic field inhibits the mechanism described by Evans[11] since it prevents ions from moving from infinity to the star except along the polar axis. Hence the entire polar axis comes to have zero potential, and the potential of the surface of the star must be $-\frac{3}{2}V_p\sin^2\theta$. It appears that in the equilibrium condition, if one is possible for this model, the space charge is sufficient so that the electrostatic equipotentials outside the star are obtained by rotating the lines of induction about the polar axis, the value of the potential being given by the specified potential at the surface. The ions move with average velocity $c\mathbf{E}\times\mathbf{B}/B^2$. The resulting currents affect the magnetic induction so that (1) is completely invalid at large r. Thus the determination of the fields and the charge distribution is complicated, but it appears that potential differences and fields of the order of those in the table must exist in the neighborhood of rotating magnetized stars, that the electric fields should extend as far into space as do the magnetic fields, and that the magnetic field cannot be purely a dipole field.

A more detailed and extensive treatment should be completed soon.

The author is indebted to many members of the faculty of the California Institute of Technology for profitable discussions; he is particularly indebted to Drs. P. S. Epstein, W. R. Smythe, and O. R. Wulf of this Institute and to Dr. H. W. Babcock of the Mount Wilson Observatory.

[10] R. A. Millikan, *Electrons (+ and −)* (University of Chicago Press, Chicago, Illinois, 1947), p. 309.

[11] F. Evans, Phys. Rev. **59**, 1 (1942).

Interaction of Neutrons with Electrons in Lead*

W. W. HAVENS, JR., I. I. RABI, AND L. J. RAINWATER
Department of Physics, Columbia University, New York, New York

(Received August 11, 1947)

ABOUT ten years ago Condon[1] showed that Dee's[2] estimate of the upper limit for the neutron-electron interaction could be greatly reduced by considering the interaction of slow neutrons with atoms.

These considerations can be greatly extended by considering the interference of the wave scattered by the nucleus with the wave scattered by all of the electrons in the atom as first introduced by Bloch[3] in connection with the magnetic scattering of neutrons. In this case the scattered amplitude consists of the sum of terms due to the nucleus and to the electron

$$\psi=\psi_N+\psi_e+\cdots, \tag{1}$$

and the atomic cross section becomes, to a close approximation,

$$\sigma=\sigma_N+2Z\bar{f}(\sigma_e\cdot\sigma_N)^{\frac{1}{2}}+Z^2(f^2)_{Av}\sigma_e, \tag{2}$$

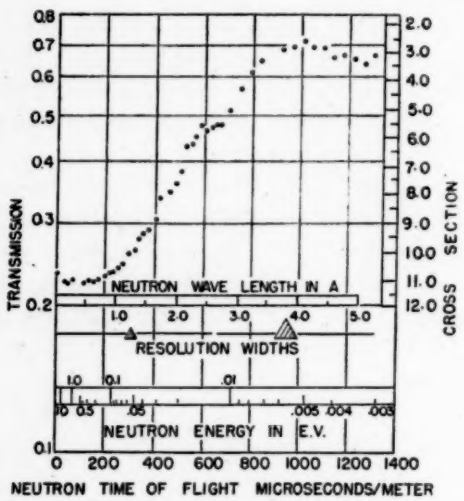

FIG. 1. The slow-neutron transmission of 46.51 g/cm² of solid lead.

where σ_N is the nuclear cross section, σ_e is the cross section per bound electron, $\bar{f}$ is the integrated form factor for the amplitude, and $(f^2)_{Av}$ for the square of the amplitude of the wave scattered by the bound electrons. For $\sigma_e\ll\sigma_N$ the main contribution to $\Delta\sigma\equiv(\sigma-\sigma_N)$ is from the cross term $2Z\bar{f}(\sigma_N\sigma_e)^{\frac{1}{2}}$. For $Z\bar{f}\sim40$ it is seen that $\sigma_e=6\times10^{-3}\sigma_N$ will give a 2 percent shift in the total cross section. The last term in Eq. (2) can be neglected for subsequent considerations.

The effect here described is not a spin-spin interaction since the total electronic spin of the atom is zero and the effect is thus different from the paramagnetic and ferromagnetic scattering of neutrons.

To study this effect we have measured the total cross section of solid and molten lead as a function of the wave-length of the incident neutrons using the neutron spectrometer.[4] Lead was chosen because of its large value of $Z(Z=82)$ and its small absorption for slow neutrons ($\sigma=0.1\lambda$ in units of 10^{-24} cm²/atom where λ is given in angstrom units). The change of the atomic form factor $\bar{f}$ for the electrons as λ changes from 0.2A to 1.7A, is used for the observation of the effect. The nuclear form factor remains constant and equal to unity since the nuclear scattering is isotropic. The atomic form factor is given sufficiently well for this purpose by the Fermi-Thomas atom model.

The experimental points are given in Figs. 1 and 2. Figure 1 is for the solid and shows the characteristic increase in transparency with λ as is expected for crystalline materials. Figure 2 shows the results for liquid lead at about 350°C and 500°C. A disk of lead metal was used for the solid sample. A sample holder, in which the lead could be poured in and out of the sample position without altering the position of the container in the beam, was used for the liquid sample. The thicknesses (g/cm²) of the liquid samples were

* This document is based on work performed under Contract AT-30-1-GEN-72 with the Atomic Energy Commission at Columbia University.

[1] E. U. Condon, Phys. Rev. **49**, 459 (1936).
[2] P. I. Dee, Proc. Roy. Soc. **A136**, 727 (1932).
[3] F. Bloch, Phys. Rev. **50**, 529 (1936).
[4] Rainwater, Havens, Wu, and Dunning, Phys. Rev. **71**, 65 (1947).

not known accurately so the cross sections were adjusted to be equal to that of the solid in the region above thermal energies. In any event, it is the *shape* rather than the absolute value of the curve which is of greatest importance. A minimum of uncertainty in the shape of the curve was obtained by the fact that all 16 points on a given curve were taken simultaneously.

The general flatness of the curve shows that the diffraction effects due to the liquid structure are not very important at these neutron wave-lengths. Nevertheless, a correction can be made for this effect by the use of the theory of liquid scattering.[5]

From this theory the contribution to $\Delta\sigma$ due to the liquid molecular structure is $(\lambda^2/\lambda_0^2)\Delta\sigma(\lambda_0)$, when λ_0 is taken at some point where the liquid form factor deviates imperceptibly from the atomic form factor. X-ray results indicate that this is true for most monatomic liquids at $\lambda \sim 1.6$A. Since the nuclear scattering is isotropic, the nuclear form factor is always unity, therefore the cross section would be constant with respect to λ in the energy region investigated except for a small correction for the temperature agitation. This correction is under 1 percent in the region in which we are interested from 0.2A to 1.7A and is parabolic in form, therefore this correction can be lumped with the parabolic correction for the liquid-diffraction effect.

In our analysis we have assumed that all of the isotopes of lead scatter with the same phase and approximately the same amplitude, because the capture cross section is small and the scattering cross section is very nearly $4\pi R^2$.[6] However, the recent results of Fermi and Marshall[7] suggest that one isotope has opposite phase and therefore the effective scattering length of lead of normal isotopic composition is about $\frac{1}{2}$ of the expected value. This would reduce the sensitivity of our measurement of the electron-interaction amplitude by a factor of two.

To obtain the true variation of the total atomic scattering (nuclear+electron), we have to subtract the liquid interference effect together with

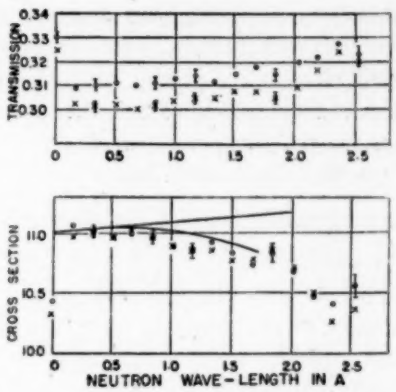

FIG. 2. The slow-neutron transmission and cross section of molten lead as a function of the neutron wave-length. ○—temperature ~500°C, ×—temperature ~350°C.

the 1/v change in cross section which is due to absorption.

In addition it should be noted that we assume the incoherent scattering to be constant and small over the region because of the great mass of the lead atom and because the temperature of the lead is from 7 to 9 times the characteristic temperature Θ which is 88°K for solid lead; furthermore, the two curves agree closely although one is close to the melting point and the other is about 150°C higher, indicating no great effect because of liquid aggregation. We also neglect spin-orbit interaction which gives an effect which is orders of magnitude less than observable in our experiment.

The net result is given in Fig. 3. The 1/v capture line and the parabolic correction are indicated in Fig. 2. The values of the ordinates of the points in Fig. 3 correspond to the distance of the points from the correction curve in Fig. 2. The magnitude of the parabolic correction is closely

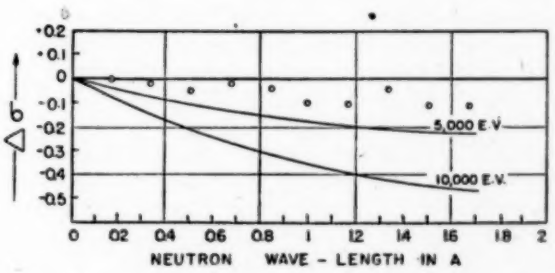

FIG. 3. Comparison of the corrected experimental points with the theoretical electron-neutron interaction curve for two different interaction potentials.

[5] N. S. Gingrich, Rev. Mod. Phys. 15, 90 (1943).
[6] H. Feshbach, D. Peaslee, and V. F. Weisskopf, Phys. Rev. 71, 145 (1947).
[7] E. Fermi and L. Marshall, Phys. Rev. 71, 666 (1947).

determined by comparing the *shape* of the first part of the curve (0.2 to 1A) and the total deviation of the latter part of the curve near 1.7A. The points shown in Fig. 3 are the averages of the values for the two temperatures.

From the Born approximation

$$\Delta\sigma = 2\pi^{\frac{1}{2}}(2M/\hbar^2)(KZ/4\pi)\tilde{f}(4\pi/\lambda). \qquad (3)$$

K is the interaction function which we take as $4/3\pi a^3 V$ where a is the electron radius e^2/mc, M is the mass of the neutron, and $\tilde{f}(4\pi/\lambda)$ is the integrated atomic form factor for the given wave-length which can be evaluated from the curve on page 148 of Compton and Allison.[8]

The two solid lines show what form this curve would take for a potential well of 10,000 ev and of 5000 ev. It is clear that the experimental points are well within the 5000-ev curve which can be taken as a fairly safe upper limit. Perhaps 2500 ev would be a closer fit to the present status of this experiment. At 5000 ev σ_s per bound electron is 4×10^{-31} cm^2. If the effective scattering length of lead is $\frac{1}{2}$ the assumed value,[7] the magnitude of all the interaction potentials given here should be doubled.

The experimental results seem to indicate that the electronic interaction causes a diminution of the scattering cross section. This would mean that the interaction is that of an attraction rather than a repulsion. If, as is supposed in some meson theories of neutron structure, the neutron is part of the time a proton plus a negative meson at a distance of the Compton wave-length of the meson, this would correspond to an attraction.

Experiments of this type can yield exact information which should provide a severe test of the validity of such theories of the structure of the elementary nuclear particles.

[8] A. H. Compton and S. K. Allison, *X-rays in Theory and Experiment* (D. Van Nostrand and Company, Inc., New York, 1935).

Letters to the Editor

PUBLICATION of brief reports of important discoveries in physics may be secured by addressing them to this department. The closing date for this department is five weeks prior to the date of issue. No proof will be sent to the authors. The Board of Editors does not hold itself responsible for the opinions expressed by the correspondents. Communications should not exceed 600 words in length.

The Magnetic Moment of Tl^{205} *

H. L. Poss
Research Laboratory of Electronics, Massachusetts Institute of Technology, Cambridge, Massachusetts
August 20, 1947

NUCLEAR magnetic resonances arising from the isotopes of thallium (Tl^{203} and Tl^{205}) have been observed. The ratio of the resonant frequencies of Tl^{205} and H^1 was measured.

Thallium in solution was used for a sample in order to obtain the narrow resonance lines characteristic of liquids. Two r-f coils, $\frac{1}{2}$ inch long and $\frac{7}{16}$ inch in diameter, were wound on a glass coil form containing a saturated solution of thallium acetate, the most soluble of the thallium compounds available. Each coil was part of a circuit similar to one which has been described elsewhere.[1] A $\frac{1}{2}$-inch separation between coils reduced the coupling between them sufficiently so that adjustment of one circuit did not appreciably disturb the other. The M.I.T. cyclotron magnet provided the magnetic field.

Proton resonances were observed in one circuit at about 30.5 Mc/sec. In the other circuit, operated at a frequency calculated from spectroscopic values[2] [spin: $\frac{1}{2}$; magnetic moment: 1.45 μ_N (nuclear magnetons); $\mu_{205}/\mu_{203}=1.00966$] to give thallium resonances for the same magnetic field, two resonances separated by a one percent difference in field were observed for a field about 10 percent less than expected. The stronger resonance occurred at the lower magnetic field and was identified as caused by Tl^{205}, since the ratio of its abundance[3] to Tl^{203} is 2.5 and their spins are the same. Also, from the resonance condition, $h\nu=g\mu_N H$, it is seen that at a given frequency, resonance will occur for the larger moment in a smaller field. The spectroscopic value of the moments is thus shown to be about 10 percent too low, while the value of their ratio is roughly confirmed.

With the thallium circuit operating in the vicinity of 17.5 Mc/sec. both proton and thallium resonances could be observed simultaneously, using an electronic switch to display the output of the receiver in each circuit on the same oscilloscope. The Tl^{205} and proton resonances were aligned, and measurements were made of the ratio of resonant frequencies for slightly differing oscillator frequencies. Another run was made on a subsequent occasion and gave results in close agreement with those of the first run. The signal-to-noise ratio for the weak Tl^{203} resonance was unfortunately too low at this time to permit an accurate check of the ratio of the moments of the two isotopes.

Frequencies were measured with a General Radio 620A frequency meter. The crystal oscillator in the meter was check against that in a Signal Corps BC-221 frequency meter. The agreement was exact as far as could be measured. Systematic errors that might arise from inhomogeneities in the steady magnetic field or modulating field over the length of the coil form, or from differences in phase shift in the audio stages of the receivers used were studied, the indications being that errors from these effects did not exceed those in the frequency measurements.

The result of the measurements gives for the ratio of resonant frequencies

$$\nu(Tl^{205})/\nu(H^1)=0.577135\pm.00005.$$

To compute the magnetic moment of Tl^{205}, a correction must be made to take into account the fact that the field at a nucleus of atomic number Z is less than the applied field, H, by an amount $\bar{H}$. An expression[4] for $\bar{H}/H$ is $3.20\times10^{-6}Z^{4/3}$. Taking the proton moment to be[5] 2.7896 ±0.0008 μ_N and making this correction gives the result

$$\mu(Tl^{205})=1.628\ \mu_N.$$

I am indebted to Professor F. Bitter for suggesting this experiment and to him and the other members of our group for rendering valuable assistance throughout.

* This research has been supported in part through the Joint Service Contract No. W-36-039 sc-32037.

[1] W. R. Arnold and A. Roberts, Phys. Rev. **71**, 878 (1947).
[2] Spin: H. Schüler and J. E. Keyston, Zeits. f. Physik **70**, 1 (1931); magnetic moment: H. Schüler and T. Schmidt, Zeits. f. Physik **104**, 468 (1937); H. Schüler and H. Korsching, Zeits. f. Physik **105**, 168 (1937).
[3] A. O. Nier, Phys. Rev. **54**, 275 (1938).
[4] P. Kusch, S. Millman, and I. I. Rabi, Phys. Rev. **55**, 1176 (1939).
[5] S. Millman and P. Kusch, Phys. Rev. **60**, 91 (1941).

Studies of the Solid State by Means of Nuclear Magnetism*

N. L. Alpert
Research Laboratory of Electronics, Massachusetts Institute of Technology, Cambridge, Massachusetts
August 20, 1947

FURTHER exploratory application of nuclear magnetic resonance absorption to the study of the solid state has recently led to new results in investigations of deuterated methane (CH_2D), hydrogen chloride, and rubber.

Although normal methane (CH_4) shows a λ-point transition in the solid at 20.4°K, the deuterated methane has two λ-point transitions in the solid state, at 15.5°K and at 22.6°K. In an earlier communication[1] a narrow resonance in methane above its λ-point and a broad resonance below this temperature were reported and interpreted as a transition from free molecular rotation to hindered rotation. This indicated that one of the transitions in deuterated methane might also be identified with a rotational transformation. A behavior of the proton resonance analogous to that found in solid methane was observed in deuterated methane just above liquid hydrogen temperatures (20.4°K). Below this transition a resonance of the order of 5 gausses wide was observed, while above the transition line widths of the order of 0.5 gauss were found. That is, deuterated methane apparently undergoes a transition from free to hindered rotations at the upper λ-point.

Hydrogen chloride exhibits a transition of the first order at 98.4°K, which has been alternately interpreted either as a transition from hindered to free molecular rotation, or as a transition between ordered and disordered arrays of dipoles.[2] These experiments eliminate the former explanation in favor of the latter. Following the proton resonance from about 80°K to the melting point of hydrogen chloride at 159°K, a line width of roughly 10 gausses was observed. There was no appreciable change in this width at the transition point. A narrow line was observed only after the sample had melted.

In the case of natural rubber, samples of pale crepe, unloaded and unvulcanized, and a vulcanized sample, unloaded, gave proton resonance widths of 0.3 gauss at a resonant frequency of 30.5 Mc/sec. and at room temperature. Such narrow resonances have been identified with molecular rotation in liquids and in a few solids (e.g., CH_4). In view of the chain-like structure of the rubber molecule the interpretation of the narrow lines cannot be so direct. The effect is probably due to internal rotation of parts of the chain, i.e., hydrogen bonds, side methyl groups, or radicals.

The pale crepe natural rubber, unvulcanized and unloaded, was studied over a temperature range from 24°C to −75°C. Contrary to what might be expected, there was little or no apparent hindering of the internal free rotations at lower temperatures. That is, no change in the width or damping properties of the resonance was noted in the above temperature range. However, there was a drastic change in the amplitude of the resonance which decreased by about a factor of 10 over this range. The greatest change in amplitude occurred in the temperature interval from 24°C to 0°C. At liquid nitrogen temperature the narrow resonance was not visible. This behavior might indicate that at the lower temperatures there is a decrease in the number of atoms which are rotating, and as a result fewer nuclei find themselves in high frequency internuclear fields which essentially average out to zero.

The observation that this effect occurred gradually over the entire temperature range and was not yet complete at −75°C is surprising in view of dynamic Young's modulus measurements[3] on this same material by A. W. Nolle of the Acoustics Laboratory, M.I.T. Nolle found a relatively rapid transition in this quantity near −50°C. Also, the transition of rubber to its rigid form is generally assumed to be complete by −70°C.

A single sample of carbon-loaded natural rubber, unvulcanized, was investigated. The resulting resonance was more rapidly damped and slightly wider than for the unloaded sample, indicating the more hindered nature of the internal rotations in the loaded rubber. In addition, one unloaded sample and one carbon-loaded sample of Buna-N synthetic rubber showed broad resonances greater than 5 gausses in width. It may be remarked in this connection that the mechanical relaxation phenomena in Buna-N rubbers are appreciably slower than those in natural rubber.

The author wishes to thank Professor F. Bitter for his advice and encouragement in the direction of this research. He is also indebted to Professor L. Tisza for many suggestions and to C. G. Lehr, S. T. Lin, and H. L. Poss of the nuclear magnetism group for their invaluable aid in these experiments.

* This research has been supported in part through the Joint Service Contract No. W-36-039 sc-32037.

[1] F. Bitter, N. L. Alpert, H. L. Poss, C. G. Lehr, and S. T. Lin, Phys. Rev. 71, 738 (1947).
[2] L. Tisza, Phys. Rev. 72, 161A (1947).
[3] Private communication.

Saturation Effect in Microwave Spectrum of Ammonia*

WILLIAM V. SMITH AND R. L. CARTER
Physics Department, Duke University, Durham, North Carolina
August 1, 1947

TOWNES[1] has reported the existence of a saturation effect in the microwave spectrum of ammonia. He observed that at low pressures the peak attenuation, γ, of the 3,3 line decreased with increase in power while the width of the line increased. Gordy and Kessler[2] have failed to confirm the broadening of the line. The present observations find no broadening of the line, but agree in magnitude of intensity saturation with Townes' results.

The total power absorbed at the center of the line was examined as a function of the power, P, fed into a 3.5-meter guide of 10.7×4.3-mm cross section. Starting with low powers, this peak absorbed power γP was observed first to increase linearly with input power (region of constant attenuation γ_0), then to increase more slowly (onset of saturation), and finally to approach a constant asymptote. At a line width of $2\Delta\nu=350$ kc, γP was observed to be constant within ±20 percent over a power range of 600 to 6000 microwatts, the high power limit of our observations. Similar plateaus were observed at other pressures, the low power end of the plateau varying in proportion to the pressure. Over each run at constant pressure the line width was observed to be independent of the input power within ±20 percent. The detectors were calibrated crystals, used in their approximately square-law range to minimize corrections.

If t is the average time between collisions, I the power in quanta per second per cm², and n_0 the number of molecules per cm³ in the ground state at thermal equilibrium, it may be shown that, if the line shape is constant,

$$I\gamma=(1-\gamma/\gamma_0)(n_0h\nu/2kTt).$$

At low powers γ approaches γ_0 while at high powers, where γ approaches zero, $I\gamma$ becomes constant in agreement with our observations. Our value of t measured near $\gamma/\gamma_0=\frac{1}{2}$ agrees with the value deduced from pressure broadening within 50 percent, the accuracy of the experiment. This observation is in agreement with Townes' conclusions.

In his theory, Townes apparently identified the rate, n_0, at which molecules make transitions because of the radiation present, with BI, where B is the Einstein coefficient of induced radiation, rather than with $BI(1-m/n)$, where m and n are the probabilities of the molecule in the upper and lower state, respectively. The latter identification leads to a time between radiative absorptions that approaches

a constant minimum value of the order of magnitude of $t(1+kT/h\nu)$, which is much greater than t and hence does not lead to a broadening of the line.

Irrespective of the details of the theory, it would seem that induced radiative transitions should not greatly broaden the line, as the time allowed for a measurement of the energy E of the system of (atom+radiation field of definite frequency) is the time t between molecular collisions and $\Delta E \cdot t = h$, according to the Heisenberg uncertainty principle. At the time of measurement, the molecule may be in either an upper or lower state, differing by the definite amount $h\nu$, but either state uncertain in energy only to an amount h/t. The line width, therefore, should not differ greatly from that given by theories of collision broadening.

The authors wish to acknowledge several helpful discussions with Professors W. O. Gordy and W. M. Nielsen.

* The research described in this report was supported by contract No. W-28-099-ac-125 with the Army Air Forces, Watson Laboratories, Air Materiel Command.

[1] C. H. Townes, Phys. Rev. **70**, 665 (1946).
[2] W. Gordy and M. Kessler, Phys. Rev. **71**, 640 (1947).

Radiations from K^{38}

MARGARET M. RAMSEY, J. LAWRENCE MEEM, JR., AND ALLAN C. G. MITCHELL
Indiana University, Bloomington, Indiana
August 18, 1947

WE have made a preliminary investigation of the beta- and gamma-radiations emitted from K^{38}. Radioactive K^{38} has been investigated by Hurst and Walke[1]; Pool, Cork, and Thornton[2]; and Ridenour and Henderson.[3] Hurst and Walke, Ridenour and Henderson produced this activity by the action of alpha-particles on chlorine, while Pool, Cork, and Thornton produced it by fast neutrons. The period was found to be 7.5–7.6 minutes. Walke and Hurst found a beta-ray end point of 2.0 Mev, while Ridenour and Henderson found 2.3 Mev.

We have studied the radiations from K^{38} with a view to correlating the energy levels of A^{38} formed by positron emission with those of the same element formed by the negatron emission from Cl^{38}, as reported by Hole and Siegbahn.[4]

K^{38} was formed by bombarding LiCl with 23-Mev helium ions from the cyclotron. This was separated chemically by adding KNO_3 carrier and bringing down the potassium as potassium cobaltinitrite. The absorption of the positrons in aluminum was measured, and the range was found to be 1.20 g/cm², corresponding to an end point of 2.53 Mev. The period was found to be 7.5 min.

The substance was shown to emit gamma-rays. The absorption of the gamma-rays in lead showed a highly absorbable component corresponding to an energy of about 0.5 Mev, no doubt caused by annihilation radiation, and a more penetrating component, corresponding to an energy of 1.5–2.0 Mev. Since the lead absorption coefficient varies only slowly with energy in this region, we determined the energy of the most energetic gamma-ray by measuring the range of the Compton electrons from an aluminum radiator with the help of a coincidence counting set.[5] The range of the Compton secondaries corresponds to a gamma-ray whose energy lies between 2.0 and 2.15 Mev.

Hole and Siegbahn[4] have measured the gamma-rays associated with Cl^{38} which come from excited levels of A^{38}. These have been found to be 1.60 Mev and 2.15 Mev, and are in cascade, the 2.15-Mev ray coming from the first excited state to the ground state of A^{38}. Our measurement of the gamma-ray at 2.15 Mev associated with K^{38} shows that the 2.15-Mev state of A^{38} is excited by positron emission from K^{38} as well as by negatron emission from Cl^{38}. Work is continuing with a view to obtaining the complete disintegration scheme of K^{38}.

This work was supported by the Office of Naval Research.

[1] D. G. Hurst and H. Walke, Phys. Rev. **51**, 1033 (1937).
[2] M. L. Pool, J. M. Cork, and R. L. Thornton, Phys. Rev. **52**, 239 (1937).
[3] L. N. Ridenour and W. J. Henderson, Phys. Rev. **52**, 889 (1937).
[4] N. Hole and K. Siegbahn, Arkiv f. Mat, Astr. och Fysik, **33**, 1 (1946).
[5] A. C. G. Mitchell, L. M. Langer, and P. W. McDaniel, Phys. Rev. **57**, 1107 (1940).

On the Positively Charged Particles Accompanying the Beta-Rays of P^{32}

T. H. PI* AND C. Y. CHAO*
National Central University, Nanking, China
August 20, 1947

IN the cloud chamber pictures of beta-ray tracks from radioactive sources such as Ra($B+C$), Th($C+C'+C''$), RaE, P^{32}, etc., a few tracks are often present because of positively charged particles.[1,2] The ratio of the number of positive particles to that of the ordinary decay electrons which has been found in this way by others ranges from 0.2×10^{-2} to 1×10^{-2}. But with the beta-ray spectrometer[3,4] this ratio was found only to be of the order of 10^{-4}.

We have recently taken about a thousand cloud chamber pictures of the beta-ray tracks of P^{32}. P^{32} was chosen in order to avoid the effect of gamma-rays. Since positive particles might be emitted by the source itself or created by the beta-rays, we took three series of pictures with the beta-rays filtered through materials of different thicknesses. In the first series the source was put in a thin-walled glass tube of thickness 0.01 g/cm², in the second we surrounded the thin-walled tube with an Al filter of thickness 0.11 g/cm², and in the third we used a source in a glass tube of thickness 0.09 g/cm². We chose filters of light elements in order to avoid the gamma-ray effect. The cloud chamber had a diameter of 8 inches. Air and ethyl alcohol vapor were used. The thin glass tube had a diameter of 1.1 mm and the thicker one and the Al filter had the same outer diameter of 2.1 mm, the length being about 4 cm. The radio-phosphorus in Na_2HPO_4 was deposited on the middle portion of the inner wall of the tubes, and the tube in each case was attached to the covering glass of the chamber. The magnetic field was about 360 gausses, and stereoscopic pictures were obtained by using two mirrors.

The result of our experiment is given in Table I.

Since tracks caused by negative particles moving towards the source might be mistaken for those of positive particles, the pictures are analyzed in the following way. (a) Both

TABLE I. Positive particles accompanying the beta-rays of P^{32}.

Filter	Thickness (g/cm^2)	Number of pictures	Number of negatives N^-	Number of good positives N^+	N^+/N^- (percent)	Number of doubtful positives M^+	$(N^++M^+)/N^-$ (percent)
Glass	0.01	366	8224	1	0.01	3	0.05
Al	0.11	485	4983	6	0.12	2	0.16
Glass	0.09	389	8423	5	0.06	5	0.12

negative and positive tracks under 4 cm in length are rejected in order to eliminate, as far as possible, the reflected electrons from either the top or the bottom of the chamber. (b) Certain positive tracks which were either partially superposed by other tracks or became very faint in the neighborhood of the source are listed in the column of doubtful positives. The sum of the good and doubtful positives divided by the negatives gives the upper limit of the ratio of the positive to negative particles. (c) Among the good positives given in the table, there might still be tracks caused by reflected or scattered electrons which just hit the source. The chance of having a false positive due to this cause can be estimated from the total number of such reflected or scattered tracks and the ratio of the apparent diameter of the source to that of the chamber,[1] and is found to be about 0.03 percent of the number of negatives. Hence, the number of positive particles which we found with an almost bare source lies within our experimental error. With a filter of light substance, such as Al or glass, of thickness 0.1 g/cm^2, the ratio of the positive to negative particles is about 0.05 percent after taking due consideration of the reflected electrons. This gives evidence that positive particles are produced by beta-rays during their passage through matter. Though the ratio of the positive to negative particles we found is much smaller than those found by others with the same method, it is more in conformity with the values obtained by the beta-ray spectrometer. It is, therefore, very desirable to make measurements with different filtrations using a beta-ray spectrometer.

The authors are grateful to Dr. D. B. Cowie, Dr. N. P. Heydenburg, and Dr. A. T. Ness for their help.

* Now at Department of Terrestrial Magnetism, Carnegie Institution of Washington.

[1] H. Bradt, H. G. Heine, and P. Scherrer, Helv. Phys. Acta. 16, 491 (1943).
[2] L. Smith and G. Groetzinger, Phys. Rev. 70, 96 (1946).
[3] A. I. Alichanow, A. I. Alichanian, and M. S. Kosodaew, J. Phys. U.S.S.R. 7, 163 (1936).
[4] H. Bradt, J. Halter, H. G. Heine, and P. Scherrer, Helv. Phys. Acta. 19, 431 (1946).

On the Gamma-Rays of K^{40}

E. GLEDITSCH AND T. GRÅF
Department of Chemistry and Physics, University of Oslo, Oslo, Norway
August 11, 1947

IN the course of some work on the radioactivity of potassium, so far only partly published[1] owing to war conditions, we found a gamma-ray intensity several times larger than that published by Gray and Tarrant.[2] On account of the geophysical significance of this question[3] we feel that a preliminary account of our results may be of interest.[4]

The number of counts of a Geiger-Müller counter, first surrounded by pure K_2SO_4 salt disposed as a cylinder of 4.9-cm inner diameter and of 1.45-cm thickness, was compared with that given by a cylinder of cleveite of 5.75-cm inner diameter and of 0.21-cm thickness. According to previous determinations by the emanation method, the cleveite contained 0.345 g of uranium per gram, and no thorium. The counter was of aluminium 0.02 cm thick, and had a diameter of 2.2 cm. The length of both the counter and the K_2SO_4 cylinder was 5 cm, that of the cleveite cylinder only 0.8 cm. The counter was directly surrounded by a coaxial lead cylinder of 0.75-cm thickness, which stopped the beta-rays and also the softer gamma-rays of UX_2 and of radium $(B+C)$.

Special absorption measurements were carried out with 0.1 mg of radium. By the use of the correction factor deduced from these measurements, a corrected absorption coefficient of 0.58 cm^{-1} was obtained for the gamma-rays of potassium. This value agrees well with previous determinations.[5,6] We found no experimental evidence for softer components in the gamma-radiation of potassium. The intensities were reduced to values corresponding to zero absorber thickness, and corrected for absorption in the source itself, by the use of the absorption coefficients obtained with the same experimental arrangement. After applying minor corrections to account for differences in the geometrical conditions, we found that the gamma-rays of one gram of potassium produce the same number of counts as the hard gamma-ray components of $(1.06\pm0.12)\times10^{-10}$ g of radium. The known relation between absorption coefficient and energy yields for the gamma-rays of potassium an energy of 1.55 ± 0.05 Mev,[7] instead of 2 Mev, the value generally adopted following Gray and Tarrant.[2] By correcting for differences in the counter efficiency for the gamma-rays of potassium and of RaC, we obtain the final result that one gram of potassium emits the same number of quanta per second as $(1.23\pm0.15)\times10^{-10}$ g of radium, when only the hard components of RaC are considered. From data published by Ellis and Aston[8] and by Roberts,[9] we conclude that 80 ± 15 hard gamma-quanta are emitted per 100 disintegrating radium C atoms. For one gram of potassium we thus deduce 3.6 ± 0.8 emitted gamma-quanta per second. If we assume $(7\pm1)\times10^8$ years[10] as the most probable period for the beta-decay of K^{40}, we obtain 7 ± 1.5 gamma-quanta per 100 beta-rays of K^{40}. It is most likely that these rays are emitted by A^{40} atoms left in an excited state after the disintegration of K^{40} by the capture of a K-electron.[7,11] Figure 1 shows the disintegration scheme of K^{40}, with the intensities of the branching ratios for which 1.9 capture processes per beta-decay are assumed, following Bleuler and Gabriel.[10] The equivalence of the gamma-rays of one gram of potassium to those of 1.3×10^{-10} g of radium in equilibrium, found by Běhounek,[6] is in good agreement with our result. Gray and Tarrant[2] also state that their corresponding result of 1.6×10^{-11} g, from which they deduce 3 gamma-quanta per 100 beta-rays, agrees well with

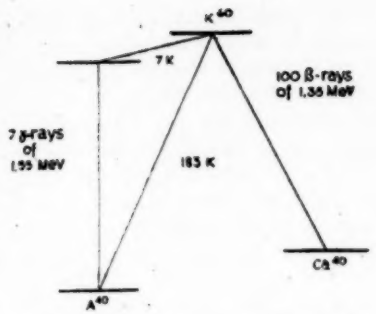

FIG. 1. Disintegration scheme for the decay of K^{40} with relative branching intensities.

the value of Běhounek. However, they cite this latter value erroneously as 1.3×10^{-11}. This fact renders it extremely likely that their own value also was taken too low by a factor ten.

[1] E. Gleditsch and T. Gráf, Arch. f. Math. og Naturvid. **44**, 63, 145 (1941).
[2] L. H. Gray and G. T. P. Tarrant, Proc. Roy. Soc. **A143**, 681 (1934).
[3] E. Gleditsch and T. Gráf, Phys. Rev. **72**, 641 (1947).
[4] A more detailed account will appear in Ark. f. Mat. Astr. och Fysik.
[5] W. Mühlhoff, Ann. d. Physik **7**, 205 (1930).
[6] F. Běhounek, Zeits. f. Physik **69**, 654 (1941).
[7] O. Hirzel and H. Wäffler, Helv. Phys. Acta **19**, 216 (1946).
[8] C. D. Ellis and G. H. Aston, Proc. Roy. Soc. **A129**, 180 (1930).
[9] J. E. Roberts, Proc. Roy. Soc. **A183**, 338 (1945).
[10] E. Bleuler and M. Gabriel, Helv. Phys. Acta **20**, 67 (1947).
[11] H. A. Meyer, G. Schwachheim, and M. D. de Souza Santos, Phys. Rev. **71**, 908 (1947).

Significance of the Radioactivity of Potassium in Geophysics

E. GLEDITSCH AND T. GRÁF
Department of Chemistry and Physics, University of Oslo, Oslo, Norway
August 11, 1947

CONSIDERING recent data on the radioactivity of K^{40}, such as greater gamma-ray intensity,[1] higher beta-ray energy,[2] as well as a shorter half-value period[3] than previously admitted, some interesting consequences in geophysics are apparent to us. We should like to point out two of these consequences, the first concerning the ionization balance of the atmosphere, the second the radioactive heat production of K^{40} in rocks and, more generally, in the earth's crust. Recent measurements by V. F. Hess[4] with a thick-walled ionization chamber disclose a large discrepancy between the value of the ionization in air, produced by the gamma-rays of the different radioactive substances contained in Quincy granite, and that computed from the concentrations of these substances known by the measurements of Evans and Goodman.[5] Assuming, according to Gray and Tarrant,[6] that one gram of potassium is equivalent in its gamma-ray effect to 1.6×10^{-11} g of radium, Hess computes the value of 0.50 I (where I is a symbol for "ion pairs per cm³ per sec.") for the ionization of the air due to the potassium contained in Quincy granite. Uranium and thorium will produce in the same case 0.64 I and 0.92 I, respectively. The total of 2.06 I, computed for a point above an infinite layer of rock, compares with the measured value of 5.18 I obtained on a ground of crushed granite. With the use of our recent value[1] for the gamma-ray intensity of K^{40}, for potassium alone we obtain 2.6 I, which gives a total of 4.16 ± 1.25 I, in satisfactory agreement with the experimental result. Thus, in the case of granites, the gamma-rays of potassium play a more important part in the ionization of the air than those of the uranium and thorium families together.

For the radioactive-heat production of potassium, Evans and Goodman[5] compute the value of $(5\pm2)\times10^{-6}$ cal. per year per gram. If we admit $(7\pm1)\times10^{9}$ years for the period of the beta-decay of K^{40}, we find 52.5 beta-rays per second for one gram of potassium. Their average energy[2] being 0.49 ± 0.06 Mev we compute for the beta-rays alone a heat production of $3.15\times10^{7}\times52.5\times0.49\times0.382\times10^{-13}=(31\pm6)\times10^{-6}$ cal per year per gram of potassium (1 year $=3.15\times10^{7}$ sec.). For 3.6 ± 0.8 gamma-quanta[1] of 1.55 ± 0.05 Mev, the heat production amounts to $3.15\times10^{7}\times3.6\times1.55\times0.382\times10^{-13}=(7\pm2)\times10^{-6}$ cal. per year per gram of potassium. We thus arrive at a total heat output of $(38\pm7)\times10^{-6}$ cal. per year per gram of potassium. In the case of acidic igneous rocks, Evans and Goodman[5] compute, for average uranium, thorium, and potassium contents, the respective values of $(2.2\pm0.2)\times10^{-6}$, $(2.6\pm0.4)\times10^{-6}$, and $(0.14\pm0.06)\times10^{-6}$ cal per year per gram of rock. We obtain in the same case for potassium alone $(1.1\pm0.2)\times10^{-6}$ cal per year per gram of rock. This is about 20 percent of the total heat production in acidic igneous rocks. Much more important must have been the role played by potassium in the early history of the earth. Considering the total period of K^{40}, only $(2.4\pm0.5)\times10^{9}$ years[3] as a result of its dual decay, it is easy to see that 2.4×10^{9} years ago, for example, a time which corresponds to 10 periods of K^{40} and leads us back to the beginning of the earth's history, $2^{10}=1024$ times more K^{40} was present than today. The heat produced by K^{40} alone was about 200 times that generated at present by all the radioactive elements in the earth together. Of course, the heat output due to uranium and thorium then was also larger than now, but the difference did not exceed 50 percent of the present value. The tremendous source of energy, constituted by the active isotope of potassium, was diminishing continuously, but even 1.2×10^{9} years ago was still about 6 times larger than the present disintegration energy of all radioactive elements in the earth's crust.

[1] E. Gleditsch and T. Gráf, Phys. Rev. **72**, 640 (1947).
[2] L. D. Marinelli, R. T. Brinckerhoff and G. J. Hine, Rev. Mod. Phys. **19**, 25 (1947).
[3] E. Bleuler and M. Gabriel, Helv. Phys. Acta **20**, 67 (1947).
[4] V. F. Hess, Norsk Geologisk tidsskrift **27**, 1 (1947).
[5] R. D. Evans and C. Goodman, Bull. Geol. Soc. Am. **52**, 459 (1941).
[6] L. H. Gray and G. T. P. Tarrant, Proc. Roy. Soc. **A143**, 681 (1934).

Excess-Defect Semiconductor Contacts

L. SOSNOWSKI
Admiralty Research Laboratory, Teddington, Middlesex, England
August 22, 1947

TWO recent papers[1,2] have dealt with the theoretical aspects of silicon-germanium rectifiers. Impurity centers giving rise to both excess and defect conductivity are shown to exist with corresponding energy levels only

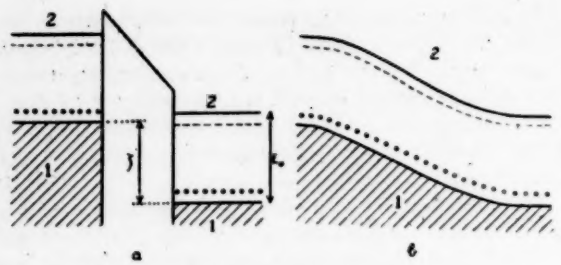

FIG. 1. Potential barriers at the contact between excess and defect semiconductors.

slightly removed from the ground or conduction bands. It may be of interest to note that lead sulfide shows an analogous distribution of levels, the metallic centers being connected with excess lead and the electronegative centers with oxygen impurity. In the course of work on the photo-effects in lead sulfide[3] it was found at this establishment that a thin layer of the material could exhibit photo-voltaic and rectifying properties that are not associated with a contact with metallic electrodes.[4,5] A theory of the contact between excess and defect semiconductors has been developed to account for these phenomena.[6] In particular, the case of the rectifying effect appears to be worth brief mention here.

Figure 1 gives the energy-level distribution at the boundary between regions of excess and defect conductivity. Case (a) corresponds to imperfect contact between, for example, two crystals, while case (b) would correspond to a continuous variation of impurity concentration. The width of the transition region in case (b) will be given by $(\epsilon\zeta/\pi Ne^2)^{\frac{1}{2}}$ where ϵ is the dielectric constant and ζ is the displacement of the levels. As long as the width of this region is comparable with the mean free path of the electrons (about 100A in lead sulfide), both cases can be subjected to the same mathematical treatment. In fact experimental results indicate a value of about 30A.

There are three contributions to the current across the boundary, the flow of electrons between conduction bands, J_{22}, between ground bands, J_{11}, and between the top of the ground band on the left of the boundary and the conduction band on the right, J_{12}. The latter component is present only when the applied voltage is sufficient for the appropriate bands to overlap. The following approximations can be obtained for the three components of current density:

$$J_{11}=(kTe^2/2\pi m)^{\frac{1}{2}}n_A D_{11}e^{-\zeta/kT}(1-e^{-eV/kT}),$$
$$J_{22}=(kTe^2/2\pi m)^{\frac{1}{2}}n_e D_{22}e^{-\zeta/kT}(1-e^{-eV/kT}),$$
$$J_{12}=(2\pi em/h^3)D_{12}(\zeta-E_0-eV)^2;\quad J_{12}=0\quad \text{for}\quad V<0.$$

n_A is the concentration of holes on the left of the boundary and n_e the concentration of electrons on the right. D_{11}, D_{22}, and D_{12} are the appropriate penetration probabilities.

Figure 2 shows the theoretical rectifying curves at room temperature and −80°C based on these formulae, together with experimental points. The broken curves apply to a cell containing five elements in series.

In view of the similarity in energy-level distribution between lead sulfide and silicon-germanium, it should be possible to apply the theory advanced for lead sulfide to the latter materials, and also, if sufficiently close contact could be made between N- and P-type samples of, say, silicon, to observe rectifying and photo-voltaic effects. The results briefly reported by Brattain[7] seem to indicate that such effects do occur.

[1] J. Bardeen, Phys. Rev. 71, 717 (1947).
[2] W. E. Meyerhof, Phys. Rev. 71, 727 (1947).
[3] J. Starkiewicz, L. Sosnowski, and O. Simpson, Nature 158, 28 (1946).
[4] L. Sosnowski, J. Starkiewicz, and O. Simpson, Nature 159, 818 (1947).
[5] A.R.L. Report: ARL/R8/E320, to be published.
[6] A.R.L. Report: ARL/R9/E320, to be published.
[7] W. H. Brattain, Phys. Rev. 69, 628 (1946).

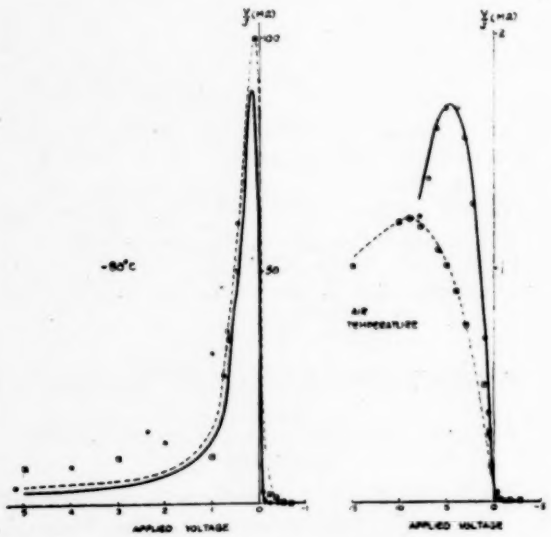

FIG. 2. Theoretical rectifying curves at air temperature and −80°C with experimental points added.

Determination of the Molecular Law of Force from Self-Diffusion Coefficients

I. AMDUR
Department of Chemistry, Massachusetts Institute of Technology, Cambridge, Massachusetts
August 8, 1947

EXPERIMENTAL results have recently appeared for the room temperature self-diffusion coefficients of uranium hexafluoride[1] and methane.[2] In both cases, the authors relate the molecular-force law to the ratio $\rho D/\eta$, where ρ is the density, D the self-diffusion coefficient, and η the coefficient of viscosity. It seems desirable to point out that force laws based on values of the above ratio are likely to be incorrect.

If the molecules of a gas are considered to be point centers repelling with a force C/r^ν, where C and ν are constants and r is the separation distance between two molecules, $\rho D/\eta$ may be evaluated for certain values of ν from tables given by Chapman and Cowling.[3] For example, for $\nu=5$, $\rho D/\eta=1.551$; for $\nu=\infty$, $\rho D/\eta=1.204$; and for intermediate ν values, the ratio lies between the above

values. There are several reasons, however, why such information is of little use. First, at laboratory temperatures, the transport properties of gases depend upon molecular interactions which must be represented as a *combination* of attractive and repulsive forces. Second, it is possible to obtain essentially the same $\rho D/\eta$ values for different molecular-force models which are not demonstrably equivalent. This is illustrated by recent calculations of low temperature transport properties of gaseous helium by use of an interaction potential consisting of two repulsive and three attractive terms.[4] These calculations predict a value of 1.18 for $\rho D/\eta$ at 300°K in close agreement with the value of 1.20 for classical hard spheres. And yet, a classical hard-sphere model has on many occasions been shown to be incapable of representing the transport properties of gaseous helium as a function of temperature, in agreement with quantum-mechanical calculations which show the need for both repulsive and attractive terms in the interaction potential.

Table I, from a paper on the self-diffusion coefficient of neon by Groth and Sussner,[5] shows that other gases besides helium have $\rho D/\eta$ values which lead to incorrect laws of force if interpreted on the basis of point-repelling molecules, since hydrogen has the "hardest" and xenon the "softest" force field of the group.

TABLE I.

Gas	$\rho D/\eta$ at 20°C
H_2	$1.37_0 \pm 0.003$
Ne	$1.27_8 \pm 0.006$
Kr	1.30 ± 0.06
Xe	1.24 ± 0.06

It should be pointed out that, for the reasons already given, the temperature variation of the coefficient of viscosity ($\eta \propto T^{\frac{1}{2}+2/(\nu-1)}$ for point-repelling molecules) provides no better information about the law of force than the ratio $\rho D/\eta$ or the temperature dependence of D if it were known. Chapman and Cowling[6] summarize the difficulty with respect to both D and η in their statement that "viscosity data throw light on the appropriateness of a formula for the molecular field derived by other means, but by themselves they do not give unambiguous information as to the field."

[1] E. P. Ney and F. C. Armistead, Phys. Rev. **71**, 14 (1947).
[2] E. B. Winn and E. P. Ney, Phys. Rev. **72**, 77 (1947).
[3] S. Chapman and T. G. Cowling, *Mathematical Theory of Non-Uniform Gases* (Cambridge University Press, Teddington, England, 1939), pp. 172 and 198.
[4] I. Amdur, J. Chem. Phys. **15**, 482 (1947).
[5] W. Groth and E. Sussner, Zeits. f. physik. Chemie **193**, 296 (1944).
[6] Reference 3, p. 229.

Diamond as a Gamma-Ray Counter

L. F. CURTISS AND B. W. BROWN
National Bureau of Standards, Washington, D. C.
August 15, 1947

CONSIDERABLE interest has been evinced in the use of crystals as counters for nuclear radiations since the report by van Heerden[1] in 1945 on the successful use of silver chloride crystals for this purpose. Silver chloride crystals suffer the serious disadvantage that they must be cooled to liquid-air temperatures to reduce the spontaneous random conduction in these crystals at room temperatures.

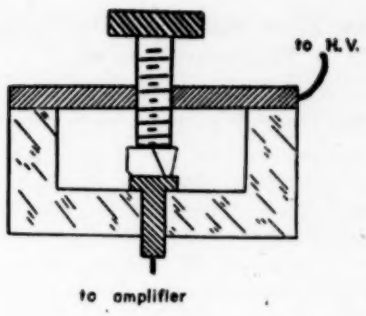

FIG. 1.

Although van Heerden tried a single specimen of diamond he was unsuccessful in obtaining counting. However Woolridge, Ahearn, and Burton[2] have subsequently found that diamonds will count alpha-particles when electrodes are applied to a surface with a small separation. This counting effect, of course, arises in the surface layer of the crystal.

Diamond does not require cooling to operate as a counter and therefore it can well prove to be a convenient detector. It is of considerable interest to determine whether it responds to gamma-rays. Since the absorption per unit volume for this type of radiation is much greater in diamond than in a Geiger-Müller counter, considerable increase in volume sensitivity for gamma-rays can be anticipated. To survey the possibilities of diamonds as gamma-ray counters approximately 100 industrial diamonds of roughly ¼-carat size have been tested. These diamonds were in their natural state. They were held in a simple compression mounting shown schematically in Fig. 1 in which the high voltage electrode pressed against one side of the crystal and the electrode leading to the grid of the first amplifier tube was in contact with the opposite face. From the total number tested two were found to give excellent response to radium gamma-rays and several others showed some response. The diamonds which gave good response were single crystals free from obvious flaws and water-white. This substantiates the general ideas of crystal conduction and those regarding properties required for counting.

The pulses delivered by the diamond are quite small, requiring considerable amplification for convenient observation. However many of the pulses are at least 10 times the background noise of the crystal plus that of the amplifying system so that no difficulty is encountered in recording them. The variation in pulse size indicates that they originate at random throughout the effective volume of the crystal.

[1] van Heerden, N. V. Noord-Hollandsche Uitgevers Maatschappij (1945).
[2] E. D. Woolridge, A. J. Ahearn, and J. A. Burton, Phys. Rev. **71**, 913 (1947).

A New Electronic System for Detecting Microwave Spectra*

WALTER GORDY AND MYER KESSLER
Department of Physics, Duke University, Durham, North Carolina
August 11, 1947

IN an earlier report[1] we described a single-crystal detecting system for microwave spectroscopy which employs a low frequency cut-off filter to eliminate the contour of the oscillator mode and the spurious signals caused by reflections in the microwave line. We have now improved the sensitivity of our system by a modulation technique which allows the signal to be amplified at higher frequencies.

Upon the slowly varying sawtooth voltage used to sweep the microwave oscillator over its mode we superimpose a radiofrequency voltage (≈ 100 kc) of low amplitude which causes the oscillator to be frequency modulated over a small range of frequencies, at a rate determined by the superimposed radiofrequency. An absorption line of a gas then acts as a discriminator to produce intensity modulation of the output radiation at a frequency corresponding to that of the modulating voltage. A single-crystal detector is used with an amplifier tuned to the modulating frequency. After pre-amplification at this frequency a second detector is employed followed by the filter mentioned above and by an audio amplifier. The filter we find effective against reflections. There are sharp, strong signals caused by the abrupt beginning and ending of the mode which are not eliminated by the filter. These are easily identified and are useful as indicators for crystal tuning and as markers to define the limits of tube oscillation.

Using the method described here with a 3.6-meter *K*-band wave-guide cell we easily detected the stronger lines of $N^{15}H_3$ in its naturally occurring concentrations of 0.3 percent in ordinary NH_3. A photograph of the 3,3 line of $N^{15}H_3$ thus obtained is shown in Fig. 1. The photograph of the 3,3 line of $N^{14}H_3$ in Fig. 2 demonstrates that good resolution can also be obtained. The distortions apparent in these photographs are not caused by the modulation but by the narrow band pass of the receiver used. Objectionable distortions can, of course, be produced by an incorrect modulation, but the adjustment of the modulation voltage is not critical.

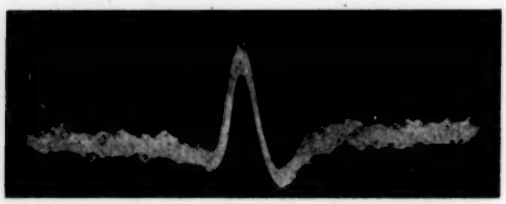

FIG. 1. Cathode-ray scope display of the 3,3 line of $N^{15}H_3$ at natural concentrations of 0.3 percent in normal ammonia. Cell length, 3.6 meters. Pressure, 2×10^{-4} mm of Hg. Modulation frequency 100 kc.

FIG. 2. Cathode-ray scope display of the 3,3 line $N^{14}H_3$ showing satellite structure. Cell length, 3.6 meters. Pressure, 4×10^{-4}. Modulation frequency 100 kc.

No greater sensitivity can be claimed for the system described above than for the Stark-effect modulation method of Hughes and Wilson.[2] In both systems the reception depends upon an intensity modulation produced by a high frequency motion of the signal in time (or components of the signal in the Stark-effect case). The present method has the advantage of being convenient to use with a cell of indefinite length. It is in general easier to modulate the oscillator than the molecules. The Hughes-Wilson method has the advantage of not requiring a filter to eliminate reflections.

A more complete description of the system will be reported elsewhere.

* This research was supported by a Frederick Gardner Cottrell Special Grant from the Research Corporation and by a loan of equipment from the Office of Naval Research.

[1] W. Gordy and M. Kessler, Phys. Rev. 71, 540 (1947).
[2] R. H. Hughes and E. B. Wilson, Jr., Phys. Rev. 71, 562 (1947).

New Atomic Lines in the Infra-Red Solar Spectrum

ROBERT R. MCMATH, ARTHUR ADEL, LEO GOLDBERG, AND ORREN C. MOHLER
McMath-Hulbert Observatory of the University of Michigan Lake Angelus, Pontiac, Michigan
August 20, 1947

THE infra-red region of the solar spectrum offers a rich and unique field for astrophysical study, for it is here that one is most likely to encounter atomic lines of high excitation potential. Studies of infra-red lines may be expected to yield important information on the extent to which the solar atmosphere departs from thermodynamic equilibrium. They may also serve to provide a check on current theories of the solar continuous absorption coefficient, and can furnish valuable supplementary data for the laboratory analysis of spectra.

During the past two months, a Cashman lead-sulfide photo-conductive cell has been employed in conjunction with the McGregor tower and spectrograph of the McMath-Hulbert Observatory to map the solar spectrum in the region 1 to 2μ. The spectrograph is of the Littrow type, consisting of a 15,000-line plane grating and 25-foot lens collimator, the dispersion being 2.1A/mm in the first order. The spectrum was traced on a Speedomax recorder, the dispersion on the record being 1.63 mm/A. The limiting resolution on the tracings was determined by the widths of the entrance and exit slits, 0.25 mm, which corresponds to about $\frac{1}{2}$A in the focal plane of the spectrograph. The resolution appears adequate to register clearly faint Fraunhofer lines with equivalent widths as low as 0.01A.

The search for atomic lines was hampered by the absence of accurate laboratory wave-length standards beyond the photographic limit at about 13,500A. Approximate standards (within about 2–3A) were first established by the method of overlapping grating orders, with the expectation that the standards would be refined through the use of wave-lengths computed for atomic lines from accurate laboratory term values. Since the FeI atom is the most prolific source of lines in the photographic region of the solar spectrum, a search was first made in the extensive compilation of term values by Russell and Moore,[1] for lines in the region between about 15,000A and 16,500A. In this region only three multiplets permitted by *LS* coupling were found in the tables, the triad $3d^64s(a^6D)5s\ e^5D - 3d^64s(a^6D)5p u^5F^\circ i^5D^\circ u^5P^\circ$. Of the 33 possible lines in these multiplets, nineteen have been identified with practical certainty on tracings of the solar spectrum, while the remaining fourteen are too badly blended, usually with strong telluric lines of water vapor, to permit conclusive identifications.

With the aid of the accurate wave-length calibration established by the identification of the e^5D triad of FeI, many additional atomic lines have been identified, including more than 20 intersystem and interlimit combinations of FeI, 12 lines of SiI, 10 lines of CI, and several faint lines of TiI and VI. Many other lines of CI appear to be present, but the inaccuracies of the calculated wave numbers make the assignments precarious. The SiI identification includes most of the lines of the multiplets $4p\ ^1P - 3d\ ^1P^\circ$, $4p\ ^1D - 4d\ ^1D^\circ$, $4p\ ^3D - 5s\ ^3P^\circ$, and $4p\ ^3D - 4d\ ^3D^\circ$.

Approximate measures of intensity have been made for the e^5D triad of FeI. The equivalent widths of the strongest lines average about 0.25A, which is surprisingly high, in view of the high excitation potential (5.6 volts) of the e^5D term. A preliminary calculation indicates that the populations of the e^5D levels (as compared with the ground state) are at least 50 times greater than would be expected from a Boltzmann distribution at a temperature of 4800°K.

A full account of the present investigation will appear in the *Astrophysical Journal*.

[1] H. N. Russell and C. E. Moore, Trans. Am. Phil. Soc. **34**, Part 2 (1944).

Conversion of Ordinary Sound into Second Sound

WILLIAM M. FAIRBANK, HENRY A. FAIRBANK, AND C. T. LANE
Sloane Physics Laboratory, Yale University, New Haven, Connecticut*
August 15, 1947

IN 1938 L. Tisza[1] predicted theoretically that temperature fluctuation in liquid helium *II* should be propagated through the liquid as an undamped wave with a characteristic temperature dependent velocity. V. Peshkov[2] experimentally confirmed this prediction in 1944. He generated the second-sound waves by means of a resistance coil immersed in the fluid whose temperature was made to fluctuate by passing an alternating current of known frequency through it. This method of generating second sound was used in his later measurements[3] and also by us.[4,5] Up to this time no successful experiments have been reported using other methods of generating second sound. The problem is one of creating a periodic change in the normal and superfluid components of the liquid. For example, a non-porous diaphragm vibrating perpendicular to its plane

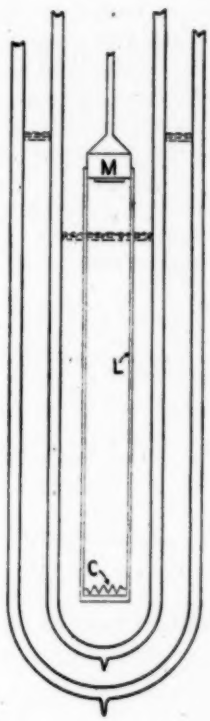

FIG. 1. Schematic diagram of the apparatus.

would not be expected to accomplish this purpose, but a diaphragm vibrating parallel to its plane should accomplish this phase separation, since the normal component has a non-zero viscosity. E. Lifshitz[6] has handled the above cases theoretically and also discussed the second-sound radiation from a surface whose temperature fluctuates periodically in time.

It occurred to us that it might be possible to generate second sound at a liquid vapor interface by allowing normal sound generated in the vapor to be reflected from the liquid surface. The consequent pressure fluctuations at this surface would be accompanied by corresponding temperature fluctuations giving rise to second-sound waves in the liquid column. Figure 1 is a schematic diagram of the apparatus. In the inner Dewar flask is placed a Lucite tube (*L*) closed at one end by a magnetic-type microphone (*M*) and at the

other end by a carbon-strip resistance thermometer detector (C).[7] Normal sound at a frequency of 1000 cycles was generated in the vapor by the transmitter (M). The temperature was now set at about 1.7°K and allowed to rise slowly beyond the λ-point. A series of second-sound resonances at 1000 cycles was detected by C, the output of which was amplified, rectified, and recorded on a recording potentiometer. The length of the liquid column remained substantially constant during this temperature sweep, and a resonance peak occurred whenever the velocity was such that the liquid column was an integral number of half-wave lengths. As was to be expected, we found that the resonances came successively closer together and finally disappeared at the λ-point. This allowed calculation of the velocity of second sound at a series of temperatures, and the results are in substantial agreement with our previous measurements and also those of Peshkov.

It appears possible that this method of generating second sound might be useful for extending the velocity measurements to lower temperatures, inasmuch as the heat generated in the liquid is much smaller than in the case of generation by a resistance heater.

* Assisted by the Office of Naval Research under Contract N6ori-44.
[1] L. Tisza, C. R. Acad. Sci. 207, 1035, 1186 (1938).
[2] V. Peshkov, J. Phys. U.S.S.R. 8, 381 (1944).
[3] V. Peshkov, J. Phys. U.S.S.R. 10, 389 (1946).
[4] C. T. Lane, H. A. Fairbank, H. L. Schultz, and W. M. Fairbank, Phys. Rev. 70, 431 (1946).
[5] C. T. Lane, H. A. Fairbank, and W. M. Fairbank, Phys. Rev. 71, 600 (1947).
[6] E. Lifshitz, J. Phys. U.S.S.R. 8, 110 (1944).
[7] H. A. Fairbank and C. T. Lane, Rev. Sci. Inst. 18, 525 (1947).

Formation and Properties of Radioactive Lithium*

D. J. Hughes, D. Hall, C. Eggler, and E. Goldfarb
Argonne National Laboratory, Chicago, Illinois
August 12, 1947

THE short-lived Li^8 (half-life about 1 sec.) was first produced[1] by the (d, p) reaction on Li^7. Knol and Veldkamp[2] found evidence for the formation of this activity by neutron irradiation of lithium. Bethe[3] concluded that the activity found by Knol and Veldkamp was really He^6 formed by the reaction $Li^6(n, p)He^6$ because He^6 was known to have approximately the same half-life as Li^8 and formation of the latter by an (n, γ) reaction would be unlikely for such a light element. Rumbaugh[4] looked for the capture reaction in Li^7 also, but was unable to find it and fixed the upper limit for the cross section at about 10^{-3} barn. As this value of the cross section was smaller than that necessary to give the results observed by Knol and Veldkamp, it appeared as though the reaction they had observed was really the $Li(n, p)$ reaction. Recently Poole and Paul[5] reported that Li^8 is formed by the (n, γ) reaction with a cross section about 10^{-3} barn. In view of the uncertainty concerning this reaction, it seems well to publish some results which were obtained using the deuterium-moderated pile at the Argonne Laboratory during the spring of 1945.

Several grams of Li_2O were placed in a lusteroid tube and irradiated for several seconds inside the pile shield. The sample was transferred from the pile through an aluminum tube to a position where a G.M. counter was placed just outside the tube. A short life of intensity sufficient to block the scaler for about 10 sec. was observed in spite of the 1 g/cm² absorber equivalent of the aluminum tube. Figure 1 shows the decay over many half-lives of this activity

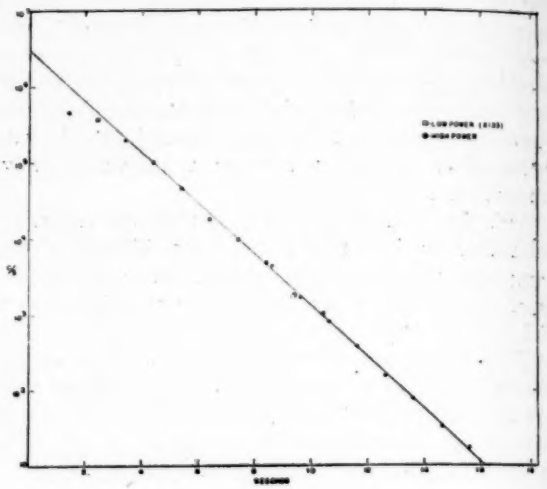

FIG. 1. Decay curve of irradiated sample.

made up of runs at two power levels. The half-life of 0.89 ± 0.02 sec. agrees with the previous value[1] of 0.88 ± 0.1 sec. for Li^8 obtained from the (d, p) reaction.

When the sample is covered with Cd the activity drops to 2 percent of its no-Cd value, thus showing that the activation is thermal. A rough absorption curve in Al was obtained and its end point (about 6 g/cm²) indicates an energy of at least 11 Mev. The cross section was estimated by measuring the value of $n\bar{v}$ with a standard gold foil, calculating the geometrical counter efficiency, and correcting the absorption curve to zero absorber, the last correction being difficult to make accurately. The value obtained was 0.049 barn which is surprisingly high, being at least ten times greater than Rumbaugh's upper limit and 50 times greater than an estimated upper limit of Wigner's.[6] The cross section was measured more accurately by irradiating LiF, comparing the relative amounts of 0.89-sec. Li^8 and 12-sec. F^{20} and assuming $\sigma(F)=0.01$ barn. Here it is necessary to measure an absorption curve for F and also to correct the F activation to zero absorber. The value resulting from this method is 0.033 ± 0.005 barn (kT value) a much more accurate value than the above result. We considered the possibility that the Li^8 might be formed from the high H^3 bombardment of Li, resulting from the

Li(n, α)H^3 reaction. This was investigated by measuring the Li^8 activation as a function of thickness of Li sample for small thicknesses (less than H^3 range). The results showed a definite linear relationship between Li^8 produced and thickness of sample, thus disproving any H^3 effect which would result in a quadratic increase of activation.

In order to rule out the possibility that the activity was He^6, the energy of the short-lived β-activity obtained from Li was also measured by allowing the higher energy β's from the sample to enter a cloud chamber in a 500-gauss magnetic field. Only the high energy β's were measured and the highest of these were in the range 10–11 Mev. No effort was made to determine the end point more carefully, for the occurrence of β's above 10 Mev shows that the activity cannot be He^6 (which has a 6-Mev end point).

The isotopic assignment of the activity to Li^8 was substantiated recently (November 1946) by the use of enriched isotopes. A sample containing only 0.1 percent Li^6 instead of the normal 8 percent was irradiated and the amount of the short-lived activity produced was determined. The amount produced was very closely the same as that produced from an equal sample of normal Li, showing that the activity was that of Li^8. If the activity had been formed in Li^6, the 80-fold change in its abundance would have given a much different result.

The results reported here show quite definitely that the 0.89-sec. activity is Li^8 formed by the Li$^7(n, \gamma)$ reaction. The cross section we observe is much larger than that of Poole and Paul. A possible explanation is that they used In for a cross-section comparison and any resonance neutrons present would lower the apparent value of the Li cross section.

* This document is based on work performed under Contract No-W-31-109-end-38 for the Atomic Energy Project at the Argonne National Laboratory. It was submitted for declassification April 10, 1947

[1] D. S. Bayley and H. R. Crane, Phys. Rev. **52**, 604 (1937); W. B Lewis, W. E. Burchain, and W. Y. Chang, Nature **139**, 24 (1937).
[2] K. S. Knol and J. Veldkamp, Physica **3**, 145 (1936).
[3] H. A. Bethe, Rev. Mod. Phys. **9**, 344 (1937).
[4] L. H. Rumbaugh and L. R. Hafstad, Phys. Rev. **54**, 657 (1938).
[5] M. J. Poole and E. B. Paul, Nature **158**, 482 (1946).
[6] E. P. Wigner, private communication.